Nonstandard Representation of Correlated-Fermion Models and its Application to Description of Magnetism and Unconventional Superconductivity

Rozprawa doktorska

Marcin Abram

Promotor: Prof. dr hab. Józef Spałek
Promotor pomocniczy: Dr inż. Michał Zegrodnik

Zakład Teorii Materii Skondensowanej i Nanofizyki
Instytut Fizyki im. Mariana Smoluchowskiego
Uniwersytet Jagielloński
ul. Łojasiewicza 11, 30-348 Kraków, Poland

Kraków, 2016

Special thanks to Allison H. and Regina A.

Oświadczenie

Ja niżej podpisany, Marcin Abram (nr indeksu: 1014598), doktorant Wydziału Fizyki, Astronomii i Informatyki Stosowanej Uniwersytetu Jagiellońskiego oświadczam, że przedłożona przeze mnie rozprawa doktorska pt. *„Nonstandard Representation of Correlated-Fermion Models and its Application to Description of Magnetism and Unconventional Superconductivity"* jest oryginalna i przedstawia wyniki badań wykonanych przeze mnie osobiście, pod kierunkiem prof. dr. hab. Józefa Spałka. Pracę napisałem samodzielnie.

Oświadczam, że moja rozprawa doktorska została opracowana zgodnie z Ustawą o prawie autorskim i prawach pokrewnych z dnia 4 lutego 1994 r. (Dziennik Ustaw 1994 nr 24 poz. 83 wraz z późniejszymi zmianami).

Jestem świadom, że niezgodność niniejszego oświadczenia z prawdą ujawniona w dowolnym czasie, niezależnie od skutków prawnych wynikających z ww. ustawy, może spowodować unieważnienie stopnia nabytego na podstawie tej rozprawy.

Kraków, dnia 27 lipca 2016 r.

\- - - - - - - - - - - - - - - -

(podpis doktoranta)

Contents

Oświadczenie (legal statement) **iii**

Abstract **1**

Abstrakt (abstract in Polish) **3**

Acknowledgments **5**

List of abbreviations and symbols **7**

Additional adopted conventions **11**

I Models and Methods **13**

1 Hubbard and related models of correlated electrons used in the Thesis **15**
1.1 Introductory remarks: the general approach used in the Thesis 15
1.2 Hubbard model 17
1.3 General properties of high-temperature superconductors 18
1.4 Derivation of t–J model from the Hubbard model 22
1.5 Extension 1: t–J–U model 29
1.6 Extension 2: t–J–U–V model 31
1.7 Charge density wave: a brief literature survey 31

2 Methods used in the Thesis **35**
2.1 The Gutzwiller Approach 35
2.1.1 Example 1: renormalization factor for hopping term 36
2.1.2 Example 2: the renormalization factor for spin exchange term . . 37
2.2 Two ways of defining the Gutzwiller factor in the presence of extra symmetries 38
2.3 Statistically-consistent Gutzwiller approach (SGA) 41

3 Heavy fermions and Anderson lattice model **45**
3.1 Introductory remark: heavy fermion materials 45
3.2 Anderson Lattice model (ALM) 46

A Three-site corrections for t–J model **49**

B Another example of Gutzwiller factor derivation **51**

C Another example of Gutzwiller factors derivation ambiguity **53**

Bibliography **53**

II Research Papers **61**

Article 1: d-wave superconductivity and its coexistence with antiferromagnetism in the t–J–U model: Statistically consistent Gutzwiller approach **65**

Article 2: t–t'–J–U Model in Mean-Field Approximation: Coexistence of Superconductivity and Antiferromagnetism **77**

Article 3: Ferromagnetism in UGe_2: A microscopic model **85**

Article 4: Criticalities in the itinerant ferromagnet UGe_2 **93**

Article 5: Tricritical wings in UGe_2: A microscopic interpretation **101**

Article 6: Antiferromagnetism, charge density wave and d-wave superconductivity in the t–J–U–V model of correlated electrons **107**

Article 7: Model of hard spheroplatelets near a hard wall **123**

III Brief summary and conclusions **135**

Abstract

The principal aim of this Thesis is to apply the methods of the statistically consistent Gutzwiller approximation (SGA) to the description of selected magnetic and superconducting properties of strongly correlated systems. This is analyzed within two models: the extended t–J model (the t–J–U and t–J–U–V models) and the two-orbital Anderson lattice model (ALM). The first model is used to describe both the appearance of antiferromagnetic (AF) and charge-density-wave (CDW) states, as well as their coexistence/competition with high-temperature superconducting (HTS) states. The second model describes the magnetism of UGe_2 compound, as well as its classical and quantum critical behaviour. In both of these models we obtain results which are compared semi-quantitatively (in the case of the extended t–J models) and quantitatively (for ALM model) with experimental results.

The general structure of the Thesis is as follows. In Part I we introduce the theoretical models that constitute the methodological approach of this Thesis and we present the use of SGA method, that modifies the standard renormalized mean-field Gutzwiller approach (RMFT) to strongly correlated systems. We also show how to derive the Gutzwiller renormalization factors and we discuss some subtle differences in the final form of those factors that may occur when either AF or CDW order is considered. This part ends with Appendix containing details of selected calculations. Part II presents our original articles relevant to the material discussed in this Thesis.[1] Each article is preceded by brief overview.

[1] According to current Polish law, the PhD Thesis should be a composition of the reviewed articles published in recognizable journals with a short introduction of the topic made by the author.

Abstrakt

Głównym celem tej pracy doktorskiej jest opisanie wybranych właściwości magnetycznych i nadprzewodzących silnie skorelowanych układów przy pomocy dwóch modeli teoretycznych: rozszerzonego modelu t–J (a dokładniej modeli t–J–U oraz t–J–U–V) oraz dwuorbitalowego, sieciowego modelu Andersona (ALM). W tym celu użyto statystycznie konsystentnego przybliżenia Gutzwillera (SGA), które rozszerza standardową teorię renormalizacji pola średniego (RMFT). Pierwszy z modeli (rozrzerzony model t–J) został użyty do zbadania stabilności faz antyferromagnetycznej (AF) oraz fali gęstości ładunku (CDW), a także do rozważenia ich współzawodnictwa lub współistnienia ze stanami wysokotemperaturowego nadprzewodnictwa (HTS). Drugi model (ALM) posłużył do opisu magnetyzmu w związku UGe_2 oraz do wyjaśnienia klasycznych oraz kwantowych zjawisk krytycznych w tym układzie. W obu przypadkach uzyskano zgodność z wynikami eksperymentalnymi (dla modelu t–J jakościową, a dla ALM ilościową).

Niniejsza praca doktorska podzielona jest na dwie części. W pierwszej zawarte jest wprowadzenie do tematu pracy, pokazane jest wyprowadzenie użytych modeli oraz przedstawione są metody użyte do ich rozwiązywania. W części tej pokazane jest też w jaki sposób wyprowadzić współczynniki renormalizacyjne Gutzwillera, a także omówiona jest pewna dwuznaczność tego wyprowadzenia gdy układ posiada dodatkowe symmetrie (przykładowo AF lub CDW). Pokazana jest przyczyna takich rozbieżności oraz ich możliwy wpływ na uzyskiwane wyniki. Część ta zakończona jest dodatkiem, w którym umieszczone zostały niektóre szczegółowe rachunki. W części drugiej zgromadzone są oryginalne publikacje, które stanową główną treść tej rozprawy. Każdy z artykułów poprzedzony jest krótkim wprowadzeniem.

Acknowledgments

I would like to express my thanks to my Thesis supervisor Prof. Józef Spałek for selecting my research topic as well as his multiple critical readings of this and many other manuscripts. I also thank him for his guidance and support during my years spent at Jagiellonian University.

I would also like to thank Dr Marcin Wysokiński, Dr Andrzej Kapanowski, Dr Jan Kaczmarczyk, Dr Jakub Jędrak, and Dr Michał Zegrodnik for fruitful collaborations and inspiring discussions. I have special gratitude to my family for their constant support and to my wife, Allison Hartnett, for her endless belief in me and inexhaustible patience during my PhD studies.

During the years I have spent at Jagiellonian University I was lucky to meet great colleagues and physicists, among others, Marek Nikiel, Dr Andrzej Kądzielawa, Ewa Kądzielawa-Major, Jan Major, Piotr Czarnik, Dr Grzegorz Rut.

Last but not least, I would like to acknowledge the help of Dr Danuta Goc-Jagło who made my life as a PhD student at the University much easier, as well as to recognize the invaluable friendship of Paweł Witanowski, Paweł Drożdż, Kamil Nowosad, Elizabeth Perry and Julia Stadler. My life is better for knowing you.

Funding

I would like to acknowledge the partial financial support both from the Foundation for Polish Science (FNP) within the project TEAM/2010-6/7, carried out within the TEAM program, co-financed by the European Union under the European Regional Development Fund, and from the Grant MAESTRO, No. DEC-2012/04/A/ST3/00342 from the National Science Centre (NCN) of Poland.

List of abbreviations and symbols

symbol	explanation
t–J model	minimal mathematical model of superconductivity in cuprates (materials with a quasi-two-dimensional layers of CuO_2 such as $La_{2-x}Sr_xCuO_4$ or $YBa_2Cu_3O_7$). This model can be derived from the Hubbard model or, as an effective model, from the three-band p-d model.
t–J–U model	extension of the t–J model. An additional term, $\sim U$, is introduced, accounting for the on-site Coulomb repulsion between electrons.
t–J–U–V model	extension of the t–J–U model. An additional term, $\sim V$, is introduced, accounting for the inter-site Coulomb repulsion of particles located on neighboring sites.
ALM (PAM)	Anderson Lattice Model (or Periodic Anderson Model). ALM (PAM) represents a two-band model, modeling the physics of heavy fermion compounds. In this Thesis this model was used to describe magnetism of UGe_2.
AF	antiferromagnetism or antiferromagnetic phase.
BCS	Bardeen–Cooper–Schrieffer theory, the first microscopic theory of (low-temperature) superconductivity.
CDW (SDW)	charge-density (or spin-density) wave state/phase.
CEP	critical ending point.
DE-GWF	diagrammatic expansion for the Gutzwiller wave function.
DOS	density of states (the number of states per interval of energy).
FM1	in the context of the Periodic Anderson Model, the name of the phase with weak ferromagnetic order, having a half-metallic character.
FM2	in the context of the Periodic Anderson Model, the name of the phase with strong ferromagnetic order.
GA	(original) Gutzwiller Approximation.

symbol	explanation
HSC	high-temperature superconductivity (or high-temperature superconductors).
QCEP	quantum critical ending point.
SC	superconductivity or superconducting phase.
SGA	statistically-consistent Gutzwiller approximation.
TCP	tricritical point.
t, t', t''	the amplitudes of hopping of electrons between the first, second, and third next nearest neighbors respectively.
J	the spin-exchange integral.
U	the on-site Coulomb (Hubbard) interaction.
V	1) the inter-site Coulomb repulsion (in of t–J–U–V model) or 2) the hybridization between c and f electrons (in ALM model).
ϵ_f	atomic level of f-electrons.
μ	chemical potential.
Λ	the number of sites in the lattice.
$\hat{c}_{i\sigma}$ $(\hat{c}^\dagger_{i\sigma})$	fermionic annihilation (creation) operator for electron with spin σ located on site i, The operators fulfill the usual fermion anticommutation relations $\{\hat{a}_{i\sigma}, \hat{a}^\dagger_{j\sigma'}\} = \delta_{ij}\delta_{\sigma\sigma'}$, and $\{\hat{a}^\dagger_{i\sigma}, \hat{a}^\dagger_{j\sigma'}\} = \{\hat{a}_{i\sigma}, \hat{a}_{j\sigma'}\} = 0$.
$\hat{n}_{i\sigma} \equiv \hat{a}^\dagger_{i\sigma}\hat{a}_{i\sigma}$	particle-number operator.
$\hat{f}_{i\sigma}$ $(\hat{f}^\dagger_{i\sigma})$	annihilation (creation) operator for f-electrons in the Periodic Anderson Model.
$\hat{n}^f_{i\sigma} \equiv \hat{f}^\dagger_{i\sigma}\hat{f}_{i\sigma}$	f-electrons number operator (for the Periodic Anderson Model).
$\hat{b}_{i\sigma}$ $(\hat{b}^\dagger_{i\sigma})$	projected fermion operator annihilating (creating) an electron with spin σ on site i with the restrictions that there is no electron with opposite spin on that site, $\hat{b}_{i\sigma} \equiv \hat{c}_{i\sigma}(1 - \hat{n}_{i\bar{\sigma}})$. The operators $\hat{b}_{i\sigma}$ and $\hat{b}^\dagger_{i\sigma}$ do not fulfill the anticommutation relations, instead $\{\hat{b}_{i\sigma}, \hat{b}^\dagger_{j\sigma'}\} = \delta_{ij}\left[(1 - \hat{n}_{i\bar{\sigma}})\delta_{\sigma\sigma'} + S^{\bar{\sigma}}_i\delta_{\bar{\sigma}\sigma'}\right]$.
$\hat{\nu}_{i\sigma} \equiv \hat{b}^\dagger_{i\sigma}\hat{b}_{i\sigma}$	projected-particle number operator, $\hat{\nu}_{i\sigma} = \hat{n}_{i\sigma}(1 - \hat{n}_{i\bar{\sigma}})$.
$\hat{\mathbf{S}}_i = (\hat{S}^x_i, \hat{S}^y_i, \hat{S}^z_i)$	spin angular momentum operator.
$\hat{S}^\sigma_i \equiv \hat{S}^x_i + i\hat{S}^y_i = \hat{a}^\dagger_{i\sigma}\hat{a}_{i\bar{\sigma}}$	circular component of the spin operator flipping the electron $\bar{\sigma} \to \sigma$ on site i in the fermionic representation.

symbol	explanation
$\hat{S}_i^z \equiv \frac{1}{2}(\hat{n}_{i\uparrow} - \hat{n}_{i\downarrow})$	z-component of the spin operator in the fermionic representation.
$\hat{n}_{i\sigma}^{HF} = \hat{n}_{i\sigma} - \langle \hat{n}_{i\sigma} \rangle_0$	in some cases, using the relative occupancy $\hat{n}_{i\sigma}^{HF}$, instead of $\hat{n}_{i\sigma}$, can simplifies the notation (for example in calculations within the DE-GWF approach or in the derivation of the Gutzwiller renormalization factors).
$\hat{\mathcal{P}} = \prod_i (1 - \hat{n}_{i\uparrow}\hat{n}_{i\downarrow})$	Gutzwiller projection operator in the limit, eliminating entirely the double occupied-site configurations.
$\hat{\mathcal{P}}_{i\sigma} = 1 + x\, \hat{n}_{i\sigma}^{HF}\hat{n}_{i\sigma}^{HF}$	local projector used to determining the optimal double occupancy probability (d^2).
$\langle \ldots \rangle \equiv \langle \Psi \vert \ldots \vert \Psi \rangle$	short notation for an average of some operators (marked here as "$\ldots$"), calculated with respect to the the correlated (projected) wave function $\vert \Psi \rangle$.
$\langle \ldots \rangle_0 \equiv \langle \Psi_0 \vert \ldots \vert \Psi_0 \rangle$	short notation for an average of some operators (marked here as "$\ldots$"), calculated with respect to the the uncorrelated (unprojected) wave function $\vert \Psi \rangle_0$.
$n_\sigma \equiv \langle \hat{c}_{i\sigma}^\dagger \hat{c}_{i\sigma} \rangle_0$	average number of particles (electrons) per site with spin σ.
$n = n_\uparrow + n_\downarrow$	number of electrons in the band counted per site.
$\delta = 1 - n$	number of holes per Cu site (the hole doping).
d^2	probability of the double occupancy (per site).
$\chi_{ij\sigma} \equiv \langle \hat{c}_{i\sigma}^\dagger \hat{c}_{j\sigma} \rangle_0$	average probability of electron hopping with the spin σ between the sites i and j.
$\Delta_{ij\sigma} \equiv \langle \hat{c}_{i\sigma} \hat{c}_{j\bar{\sigma}} \rangle_0$	superconducting gap parameter of paired electrons in real space located at sites i and j, with opposite spins.

Additional adopted conventions

In addition to the listed symbols and abbreviations, the following convention of notation were adopted,

- All operators in the Fock space are designated by Latin letters with "hats", eg. $\hat{c}_{i\sigma}$ or $\hat{S}_i^{\pm}$, etc.
- All averages of operators are designated by Latin letters without "hats", eg. $n_\sigma \equiv \langle \hat{c}_{i\sigma}^\dagger \hat{c}_{i\sigma} \rangle_0$.
- All vectors, except one instance, are designated by bold letters, eg. $\mathbf{R}_i$ is the vector indicating the position of site i in the lattice, and $\hat{\mathbf{S}}_i$ is the vector composed of the operators $(\hat{S}_i^x,\ \hat{S}_i^y,\ \hat{S}_i^z)$. There is one exception from this notation. The unit-length basis vectors are marked differently, by "hats", eg. the unit vector indicating OX direction in the Cartesian coordinate system is $\hat{x}$, etc.
- Spin states of electron ($S = \frac{1}{2}$) are labeled as $\sigma = \pm 1$ or as $\uparrow$ $(+1)$ and $\downarrow$ (-1).
- All matrixes are designated by dual font, eg. $\mathbb{1}$ indicates the identity matrix.
- Summation over all:
  - sites of a lattice is marked as $\sum_i$,
  - possible pairs, with (i, j) and (j, i) being counted separately, as $\sum_{i,j}$,
  - possible pairs i and j, except those for which $i = j$, as $\sum'_{i,j}$ (note the prime) or as $\sum_{i \neq j}$,
  - nearest neighbors with each pair being counted only once (e.g. when (i, j) is counted, then (j, i) is not) as $\sum_{\langle i,j \rangle}$,
  - second nearest neighbors with each pair being counted only once as $\sum_{\langle\langle i,j \rangle\rangle}$, etc.
- Fourier transform operator to reciprocal ($\mathbf{k}$) space has form,

$$\begin{cases} \hat{c}_{\mathbf{k}\sigma} = \frac{1}{\sqrt{N}} \sum_i e^{-i\mathbf{k}\cdot\mathbf{R}_i} \hat{c}_{i\sigma}, \\ \hat{c}_{i\sigma} = \frac{1}{\sqrt{N}} \sum_{\mathbf{k}} e^{i\mathbf{k}\cdot\mathbf{R}_i} \hat{c}_{\mathbf{k}\sigma}. \end{cases}$$

- Summation over all points in reciprocal space means summation over $\mathbf{k}$ in the first Brillouin zone (RBZ). However, when the AF order is considered, the summation is over half of the original RBZ of the paramagnetic state.

Part I

Models and Methods

Chapter 1

Hubbard and related models of correlated electrons used in the Thesis

1.1 Introductory remarks: the general approach used in the Thesis

We start from the question of how to model electronic properties of correlated solid state systems such as metals or insulators. There are many ways how to approach this problem, depending on whether we are interested in a precise description of a specific system or if we rather seek general answers (e.g., explaining why certain phenomena occur, what is the microscopic description of such processes or what are the essential conditions for them to appear). To illustrate it,[1] Vanadium(III) Oxide, V_2O_3, at sufficiently low temperature (below 155 K) is an antiferromagnetic insulator [1–3]. With increasing temperature or pressure, or with V^{+3} atoms being increasingly substituted by Ti^{+3}, a very sharp transition to the metallic state is observed.[2] Having an interest in modeling this very specific transition, we can use e.g., various *ab initio* methods adapted to this situation. However, we can also ask general questions, namely: *(i)* What is the microscopic mechanism responsible for such a transition? *(ii)* Why without changing the number of valence electrons in the system we can have in one situation an insulator and in another a metal? *(iii)* Is it essential for the insulator to be antiferromagnetic to observe such a transition?

To answer those questions and develop an intuition about the underlying microscopic processes that make the system to change its macroscopic properties (for example, the conductivity), it can be useful to find a minimal mathematical model to quantitatively describe such a transition. Such a model should include the necessary features for the phenomenon to occur, but neglect all details which might have only *quantitative*, but not *qualitative* impact on the final results. The reason for creating

[1] The problem of metal–insulator transition is not the main topic of this Thesis. This example serves its purpose only to illustrate the main approach that is used in the Thesis, namely the importance of finding a minimal model that can describe certain phenomena.

[2] For a long time it was believed that by changing pressure, doping or temperature in V_2O_3 one can reach the same metallic phase, regardless of the specific "path" that was taken on the phase diagram. However, recently such a belief has been questioned. Using high-resolution x-ray absorption spectroscopy it was found that the metallic phase reached by increasing the pressure might differ from that obtained by changing the doping or temperature, cf. Refs. [4, 5]. Nevertheless, it is a detail and it does not depreciate our reasoning.

such a simplistic model is that it can be solved easier and understood in greater detail than a more realistic one, giving a cleaner understanding of the key mechanism leading to the observed behavior. Thus, it represents an essential step in building realistic models.

In the discussed case of V_2O_3, the minimal model should include the following features and simplifications: *(i)* we assume that our metal is composed of a number of ions which form a crystal,[3] and *(ii)* the physics is determined by the certain number of valence electrons which are localized on parent ions. In other words, we construct a model of an infinite lattice (or net), where each site (or node) can be in one of the four states, being non-occupied, occupied by one electron with certain spin (here, only $+1/2$ or $-1/2$, marked also as $\uparrow$ and $\downarrow$, representatively), or occupied by two electrons ($\uparrow$ and $\downarrow$). At each moment, the electrons can "hop" between sites with certain probability that respect the Pauli exclusion principle and the distance between the sites (further hops are less likely; also the hops in specific directions might be more probable than in others).

In the model described above, we can take two opposite limits. In the first one, we can assume, that electrons with opposite spins do not interact with each other. In the second limit, we can assume that the electrons interact strongly (and repulsively), especially if they occupy the same site. Let us now assume that there is exactly one electron per site and that exactly half of the electrons population have spin up, and the second half have spin down. In the first limit, the solution can be exact and describes the free-electron gas limit. In such a case, when the electric field is applied, the electrons can move freely. In this way, the system is characterized as a simple metal. In the second limit, when the onsite interaction between electrons with opposite spins is large, in the ground state each site is single-occupied. Even if electric field is applied, electrons cannot move, either due to the Pauli exclusion principle or due to the large onsite interaction of electrons with opposite spins. In such a case, the system is characterized as an insulator with one particle per site. This is the classic case of the Mott insulator.

Obviously, such a simple model cannot explain the complexity of the V_2O_3 system, but it can give us a glimpse into the problem of why the transition between metallic and insulating states occur and suggests that such transitions may originate from the electron–electron Coulomb interaction.

In brief, my personal project in this respect was: (1) to analyze selected theoretical models; (2) to test which of them can be regarded as the minimal model that explains the occurrences of superconductivity, antiferromagnetism or the charge-density-wave state; (3) to relate the obtained theoretical results to experiments; and (4) to discuss which microscopic process might be responsible for the observed phenomena.

We overview next the canonical model of the correlated electrons, the single-band Hubbard model, as well as the related models of strongly correlated electrons: t–J, t–J–U, and t–J–U–V models. Those models will be applied to selected topic related to high temperature superconductivity.

[3]Since the metal–insulator transition occurs at low temperature, we neglect here the phonon excitations of the ions, assuming that they are truly locked in the space and the physics of the system is determined only by the single-electron dynamics and interactions between electrons.

1.2 Hubbard model

The basic model described in the foregoing Section was in fact the Hubbard model [6,7], characterized by the Hamiltonian,

$$\hat{\mathcal{H}}_{tU} = \hat{\mathcal{H}}_{kin} + \hat{\mathcal{H}}_{int} = \sum_{i \neq j,\, \sigma} t_{ij} \hat{c}^{\dagger}_{i\sigma} \hat{c}_{j\sigma} + U \sum_{i} \hat{n}_{i\uparrow} \hat{n}_{i\downarrow},, \tag{1.1}$$

where i and j label sites, σ spin $\uparrow$ or $\downarrow$, t_{ij} is the hopping integral between sites i and j, and U is the electron–electron onsite Coulomb repulsion magnitude. In the limit $U \to 0$, the Hubbard Hamiltonian reduces to the free-electron Hamiltonian, that is easy to diagonalize by taking the Fourier transformation to the the reciprocal lattice,

$$\hat{\mathcal{H}}_{tU} \xrightarrow{U \to 0} \tilde{\mathcal{H}}_{kin} = \sum_{\mathbf{k},\, \sigma} \epsilon_{\mathbf{k}}\, \hat{c}^{\dagger}_{\mathbf{k}\sigma} \hat{c}_{\mathbf{k}\sigma}, \quad \text{with} \quad \epsilon_{\mathbf{k}} = \frac{1}{\Lambda} \sum_{i \neq j} t_{ij} e^{i\mathbf{k}(\mathbf{R}_i - \mathbf{R}_j)}, \tag{1.2}$$

where Λ is the number of sites and $\mathbf{R}_i$ is a vector indicating the position of the site i. The exact value of $\epsilon_{\mathbf{k}}$ depends on geometry of the system. For example, for two-dimensional square lattice,

$$\epsilon_{\mathbf{k}} = 2t \left(\cos(k_x a) + \cos(k_y a)\right) + 4t' \cos(k_x a) \cos(k_y a) + \ldots, \tag{1.3}$$

where t is the hopping integral between the nearest neighbor sites, t' is that between the second nearest neighbor systems, etc. In general, $t < 0$ (due to the Coulomb interaction between the electrons and the ions)[4] and $|t_{n+1}| \ll |t_n|$ (since the overlap of the wave function decrease rapidly with the increasing distance). Therefore, there is energy gain if electrons are mobile (when they can propagate through the system, i.e. hop from one site to another).

On the other hand, in the limit $U \to \infty$ the doubly occupied sites increase essentially the system energy. If we have one electron per site, hopping of electrons is restricted because each such hopping would involve the creation of a double occupancy. Therefore, the system becomes an insulator, with electrons localized on their parent atoms. More careful calculations (that include the virtual hopping of electrons between the neighboring sites, cf. Ref. [8, 9]) show, that for the square or cubic lattices, the electron spins organize themselves in an alternating up–down manner, creating an antiferromagnetic insulator (for example, into the Néel state, cf. Fig. 1.1). All of this is not a trivial result, since from the point of view of the electronic band theory one needs to have two electrons per site to reach the band-insulator state. However, in the described case, the insulator state was reached with one electron per site (such phenomena is called the Mott metal–insulator transition, cf. Refs. [10–12]).

We have just suggested that for the Hubbard model and for square or cubic system, two solutions are possible: a metal and an antiferromagnetic insulator. The solution depends on the value of $|t|/U$, which can be changed either by modifying the value

[4] Formally the hopping term is expressed as

$$t_{ij} = \int_{\mathbf{r}} d\mathbf{r}\, \phi(\mathbf{r}_i) \left(-\frac{\hbar^2}{2m} \nabla^2 + V(\mathbf{r}) \right) \phi(\mathbf{r}_j),$$

where $\phi(\mathbf{r}_i)$ is the Wannier orbital for i-th ion and $V(\mathbf{r})$ is the periodic potential energy of the lattice. Due to the Coulomb attraction of electrons to the ions, $V(\mathbf{r})$ is negative. In the described model, all electrons are described by bound states, therefore the hopping term between the nearest neighbors is negative.

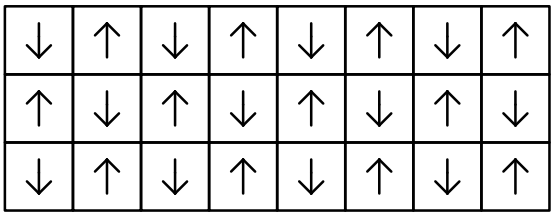

Figure 1.1: *Schematic representation of the Néel state for a crystal described by two-dimensional (square) lattice. Spins $+1/2$ and $-1/2$ are represented by the $\uparrow$ and $\downarrow$ arrows respectively.*

of U, which can be difficult to accomplish, or by increasing/decreasing the value of $|t|$, what can be realized by applying positive/negative pressure, or in other words, by bringing the atoms closer or further apart. This is an analogous situation to the case of V_2O_3 we described in the previous section. Therefore, even if the description by using the Hubbard model is extremely simplistic and provides only a qualitative agreement with the experimental results, it can give an idea about the microscopic effects responsible for such metal–insulator transitions. There are still questions to be answered, for example whether the Hubbard model with exactly one electron per site actually describes the V_2O_3 case in a realistic manner, especially since V^{+3} ion possesses two valence electrons. Is there any other mechanism leading to the metal–insulator transition which may be equally basic? Without answering such questions we cannot be sure that the intuition we have when solving the Hubbard model is correct in this very specific situation. Nevertheless, such simple analyzes let us formulate some interesting hypotheses that can be tested further.

1.3 General properties of high-temperature superconductors

Superconducting properties were first measured for clean samples of elemental superconductors such as Hg, then Pb, Nb, and simple compounds such as NbN, Nb_3Sn, V_3Si, with the critical temperature T_c lower than 25 K. Formulation of Bardeen–Cooper–Schrieffer (BCS) theory in 1957 [13] quantitatively explained the unusual behavior of those (and similar) materials at low temperature, namely its vanishing resistance, the Meissner effect, and the exponential behavior of the heat capacity at low temperature $T < T_c$ (cf. Fig. 1.2). The main idea was that the superconductivity was an effect of electrons pairing up (creation of Cooper pairs), induced by the interaction of electrons with phonons. Since there is an energy gain (energy gap) associated with such a pair binding, to break the pairs extra energy is required (it explains the increase in heat capacity). Furthermore, at low temperature, scattering of electrons from impurities cannot occur (electrons do not have enough energy to break the pairing), therefore the resistance drops to zero at $T_c > 0$.

The BCS theory was a great success and was awarded the Nobel Price in 1972. However, in 1986 a new challenge for theorists was presented when Bednorz and Müller discovered in $La_{2-x}Ba_xCuO_4$ a new type of superconductivity (with $T_c \approx 30$ K, cf. [25,26]), that displayed a number of phenomena that were not described by the BCS theory. Namely, the superconducting gap without s- but with d-wave symmetry, and a state with magnetic vortices that occurs in in relatively small applied field $H > H_{c1}$

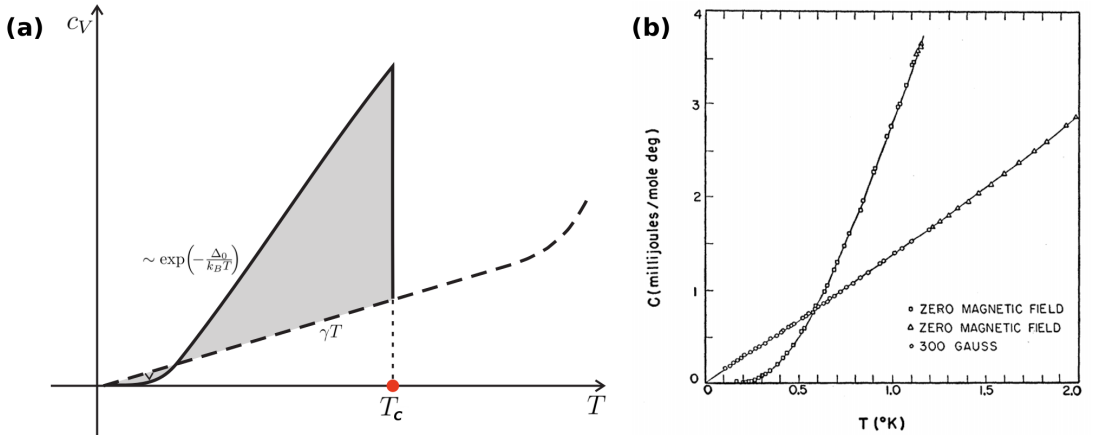

Figure 1.2: **(a)** *Temperature dependence of heat capacity from the BCS theory (solid line) and for the normal state (dashed line), cf. Ref. [14]. T_c stands for the critical temperature at which a transition from superconducting state to normal state occurs (Figure adapted from [15]).* **(b)** *Measured heat capacity for Al in superconducting state (curved line) and the normal state (straight line) (Figure taken from Ref. [16]).*

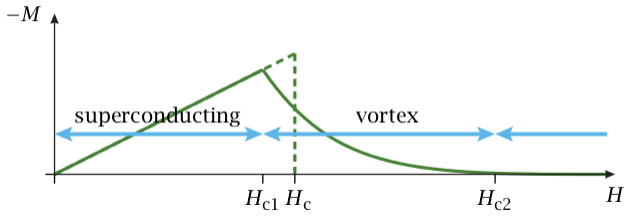

Figure 1.3: *Magnetization M as a function of the applied magnetic field H. Magnetization is negative due to the supercurrent screening the field (the Meissner effect). For the type I superconductors there is a critical value of the magnetic field at which the magnetization disappears (first order transition, cf. dotted line). For type II superconductors (e.g., the high-T_c SC) at $H = H_{c1}$ lattice of vortices with quantum magnetic flux are created. The vortices disappear for much higher values of magnetic field H_{c2} (Figure taken from Ref. [17]).*

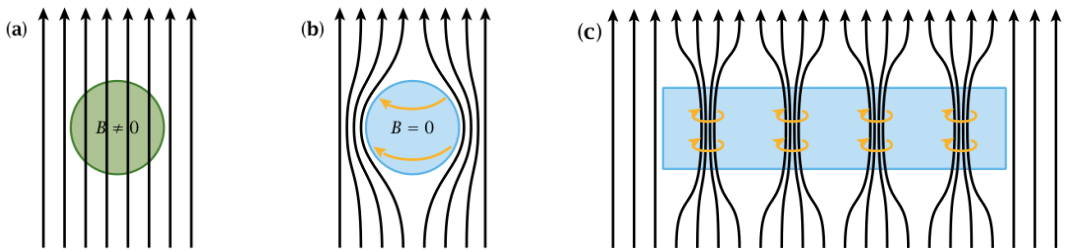

Figure 1.4: **(a)** *Illustration of the applied magnetic field penetrating normal metal.* **(b)** *Meissner effect for type I superconductor.* **(c)** *Meissner effect for type II superconductor. Vortices are created for magnetic field $H_{c1} < H < H_{c2}$. The yellow arrows illustrate the shielding supercurrent (Figures taken from Ref. [17]).*

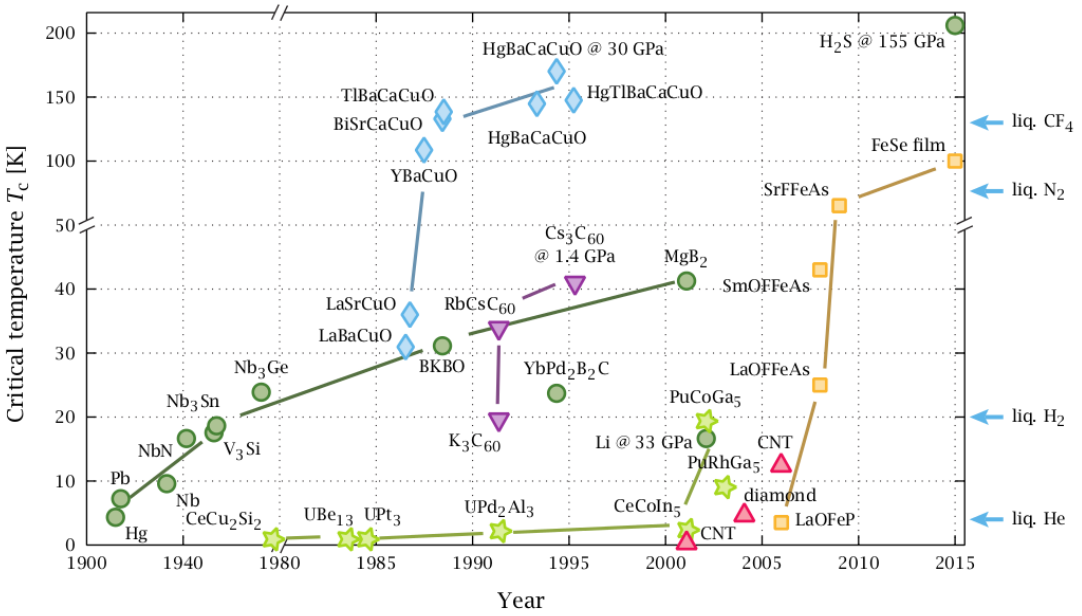

Figure 1.5: *Schematic chronology of superconductivity discoveries. On the vertical axis, the critical temperature is marked. Different colors indicate different classes of materials, for example, the green dots stand for pure elements and simple compounds, the blue diamonds are for the cuprates, and the yellow squares for the iron pnictides (Figure taken from Ref. [17]).*

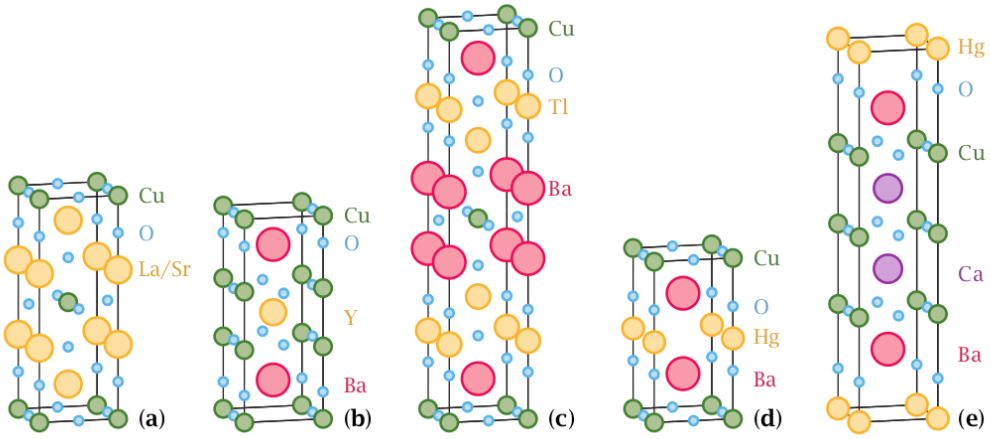

Figure 1.6: *Structure of selected cuprates:* **(a)** $La_{2-x}Sr_xCuO_4$ *with the critical temperature* $T_c = 39$ *K [18],* **(b)** $YBa_2Cu_3O_{7-\delta}$, *with* $T_c = 93$ *K [19]* **(c)** $Tl_2Ba_2CuO_{6+x}$, *with* $T_c = 81$ *K [20]* **(d)** $HgBa_2CuO_4$, *with* $T_c = 94$ *K [21]* **(e)** $HgBa_2Ca_2Cu_3O_8$, *with* $T_c = 135$ *K [22, 23] (and* 153 *K at* 23 *GPa) [24] (Figure taken from Ref. [17]).*

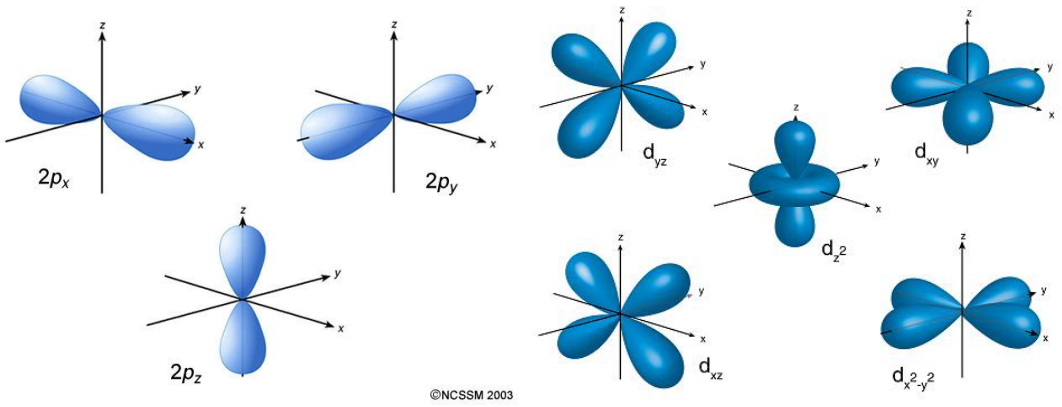

Figure 1.7: *Schematic shape of electronic wave functions for p (left) and d orbitals (right) in real-number representation (Figures are taken from Refs. [29, 30]).*

(cf. Figs. 1.3 and 1.4). Soon other compounds were discovered, that have similar, unusual behavior (cf. Fig. 1.5).[5] Additionally, unlike the "classical" superconductivity, that was observed mostly in pure elements or in simple compounds, the new type of superconductivity was discovered in compounds in which atoms (mostly Cu and Fe) are arranged in layers (cf. Fig. 1.6).

We focus here only on the compounds with the Cu layers (cuprates). For such materials, the full theoretical model of superconductivity should include the electronic structure of both Cu^{2+} ($[Ar]\,3d^9 4s^0$) and and O^{2-} ions ($[He]\,2s^2 2p^6$). In the first approximation, Cu and O atoms form ionic bonds, resulting in the formulation of ions Cu^{2+} (with total 9 electrons on the d orbitals) and O^{2-} (with total 6 electrons on p orbital). However, according to the crystal-field theory, due to the static electric field from the anion neighbors (O^{-2}) that surrounds every Cu^{2+} ion, the energy of both $3d^9$ and $2p^6$ configurations should be split [31,32]. There are 5 different symmetries of the electronic wave function possible for $3d$ and 3 for $2p$ orbitals (cf. Fig. 1.7). If we take compounds such as $La_{2-x}Sr_xCuO_4$, $Tl_2Ba_2CuO_6$, $HgBa_2CuO_4$, and $HgBa_2Ca_2Cu_3O_8$ (cf. again Fig. 1.6), we see that Cu^{2+} ion is surrounded by six O^{2-} ions, which form an octahedron. However, due to the strong Jahn-Teller effect [31, 32], such symmetry is broken into a tetragonal one; the CuO_6 cluster structure is stretched along the z-axis (e.g. for $La_{2-x}Sr_xCuO_4$, from the initial distance 1.9 Å to 2.4 Å). This results in a further splitting of the orbitals' energy (cf. Fig. 1.8). It happens that the strongest hybridization takes place between the $3d$ states of $x^2 - y^2$ symmetry and the $2p^6$ states of in-plane σ symmetry (creating bonding (B) and anti-bonding (AB) hybridized p_σ–d states). The remaining oxygen orbitals do not couple with the cooper orbitals and create a separate, narrow non-bonding band [31].

In other words, the model of cuprates could have up to 17 bands (five orbital 3d states from Cu and three 2p states from each of the four O atom surrounding Cu), however, it is justified to consider only the $pd\sigma$ band [33, 34] It is also visible on the energy band diagram (cf. Fig. 1.9 (a) or Ref. [35]). We can see that most of the bands are placed deeply below (or above) the Fermi energy level ϵ_F and thus their contribution can be neglected. Separating the impact to the total density of states to Cu, O in plane

[5] The Figure 1.5 shows the situation for 2015. As a side note, there is a controversy about the value of $HgBa_2Ca_2Cu_3O_{8+\delta}$ (Hg1223). First papers showed that the critical temperature is $T_c = 166$ K [27,28], however, recently a paper published in Nature Communications, confirming only $T_c = 153$ K, cf. Ref. [24].

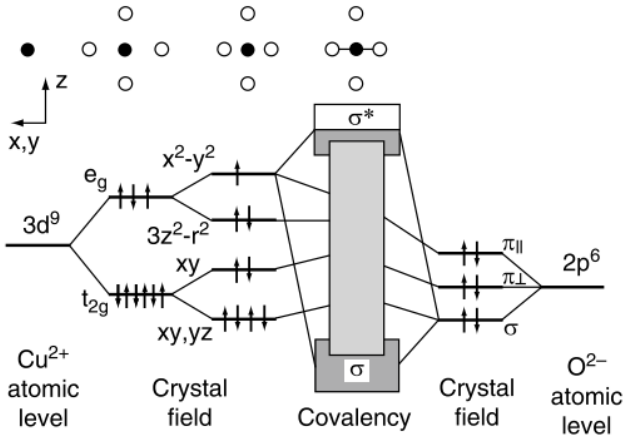

Figure 1.8: *Splitting of the electron configuration $3d^9$ (left) and $2p^6$ (right) due to the crystal field and Jahn-Teller effects. Only in-plane σ-type states from oxygen and x^2-y^2 states from copper form strong covalent bonds. Therefore, the metallic conduction occurs only in the x-y plane and theoretical models of superconductivity in cuprates are two dimensional (Figure taken from [31]).*

(x- and y-direction) and O out of plane (z-direction) (cf. Fig. 1.9 (b)), we have another proof that Cu-O_z adds very little (if at all) to the density of states around the Fermi level. Therefore, it is safe to assume that the physics of the cuprates is determined just by the Cu-O plane that can be regarded as sufficient to describe all relevant phenomena, including the superconductivity.

In summary, for pristine undoped cuprates the electronic structure should comprise broad bonding and anti-bonding bands (σ and σ^* in Fig. 1.8) and a narrow non-bonding oxygen band. All the bands are filled except the anti-bonding (AB) band that has the highest energy and is half-filled (cf. Fig. 1.10 (a)). According to such a conceptualization, undoped cuprates should be metallic. However, experiments show that they are in fact antiferromagnetic (AF) insulators. The process responsible for AF configuration is the kinetic exchange induced by the virtual d–p–d hopping processes. As a result, a $3d^{10}$–$2p^5$ configuration is created in the intermediate state. Extra electrons in the d shell experience a strong onsite Coulomb repulsion, typically $U \sim 8$–10 eV, whereas the width of the bare (uncorrelated) $pd\sigma$ band is $W \sim 3$ eV [31]. The Coulomb interaction splits the anti-bonding band into two, with and without the double occupancies, separated by the energy $\sim (U-W)$ (cf. Fig. 1.10 (b)). In effect, the ground state is not metallic but insulating.

1.4 Derivation of t–J model from the Hubbard model

Experiments show that cuprates are very sensitive to an admixture of different elements. By substituting certain atoms we can alter the number of electrons in the system. For example, if in $La_{2-x}Sr_xCuO_4$ we substitute Sr^{2+} ion for La^{3+} ion, then the number of electrons in Cu-O plane decreases by one.[6] It turns out that a minimal model that takes into account a single-band split by the onsite Coulomb repulsion and displays the main features of cuprates (an antiferromagnetic insulator for the half-filled band, superconducting dome when system is doped) can be directly derived from the Hubbard

[6] Taking electrons off is like adding holes to the system.

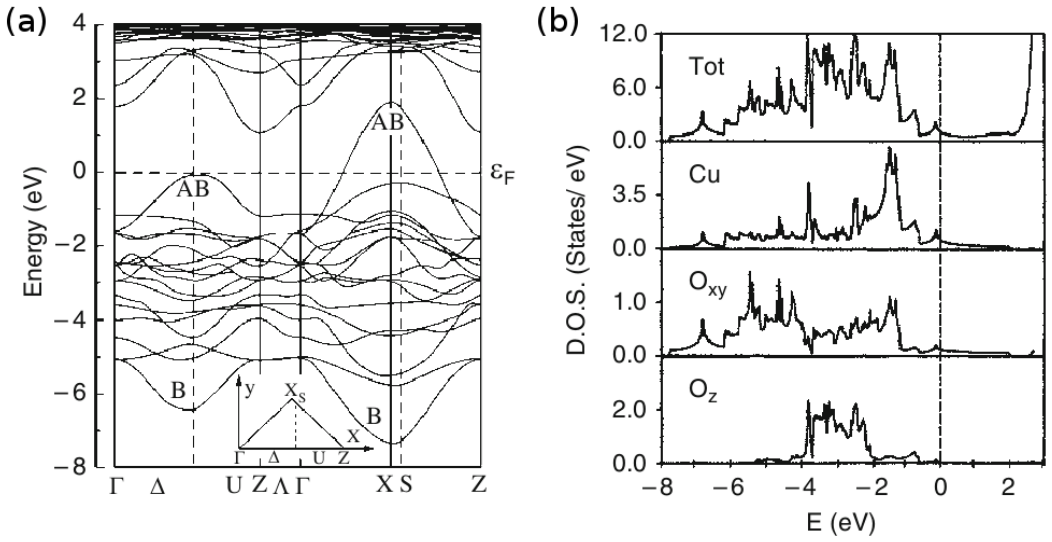

Figure 1.9: **(a)** *Energy of the band structure for La_2CuO_4 is calculated using density functional theory (DFT method; Figure from Ref. [35]). B and AB stand respectively for bonding and antibonding states.* **(b)** *Total (Tot) and projected density of states (DOS) for La_2CuO_4 (Figure taken from Ref. [36]). Note, that there is no contribution of electrons from the O_z orbitals to the total density of electron states around the Fermi level, $\epsilon_F = 0$.*

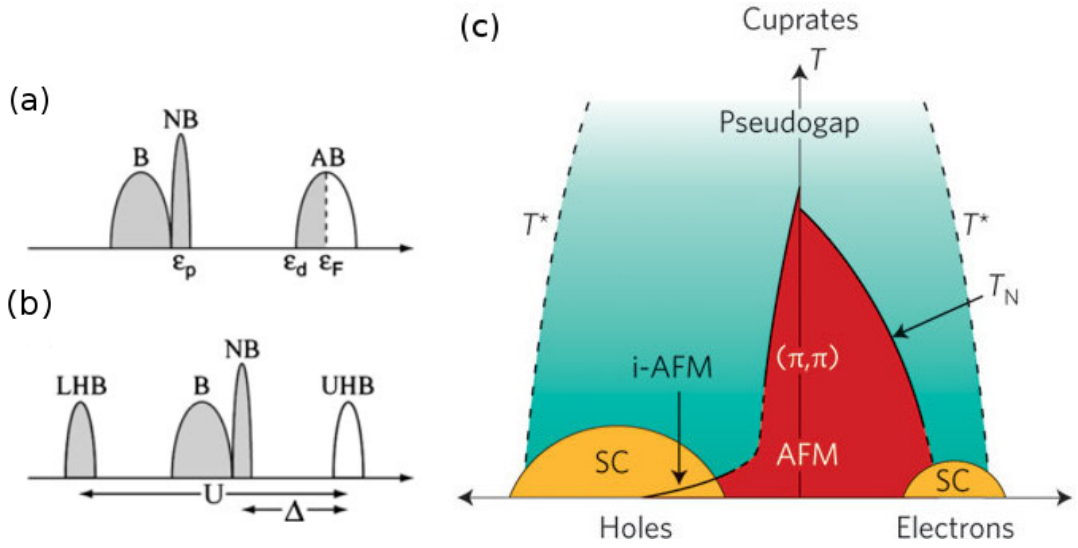

Figure 1.10: **(a)** *Illustration of the p–d electronic band for the case with the onsite electron repulsion $U = 0$.* **(b)** *p–d electronic band for U larger than the energy of an anion-cation charge transfer, Δ. Labels B, NB, AB stand respectively for the bonding, not-bonding, and anti-bonding bands. LHB and UHB designate the lower and the upper Hubbard subbands. The lower band is filled by electrons. Upper band represents the double-occupied states (Figure taken from Ref. [37]).* **(c)** *Schematic phase diagram for the cuprates, both doped by electrons and holes. T_N stands for the Neél temperature and T* for the pseudo-gap characteristic temperature (Figure taken from Ref. [38])*

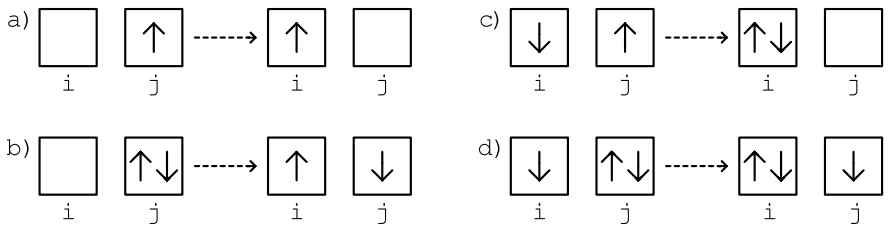

Figure 1.11: *Schematic representation of the hopping processes described by Eqs. (1.5a)–(1.5d), respectively.*

model to the limit of large U (cf. original papers, Refs. [39–43]). Here we show the derivation of that model (called t–J), following Refs. [9, 44].[7]

In the first step, we shall first define the following projection operators, $\hat{P}_N = \mathbb{1} - \hat{P}_0$, where $\hat{P}_0 = \prod_i (1 - \hat{n}_{i\uparrow}\hat{n}_{i\downarrow})$, and $\hat{n}_{i\sigma} = \hat{c}^\dagger_{i\sigma}\hat{c}_{i\sigma}$ is the particle number operator with spin σ at site i. $\hat{P}_0$ operator projects wave functions in Fock space onto its subspace, where the site double occupancies are eliminated. Conversely, the operator $\hat{P}_N$ projects the wave function to the sub-space with the double occupations present.

Note, that the following identities are satisfied: $\hat{P}_0 + \hat{P}_N = \mathbb{1}$, $\hat{P}_0\hat{P}_N = 0$, and $\hat{P}^2_\alpha = \hat{P}_\alpha$, for $\alpha \in \{0, N\}$. Therefore, one can rewrite Hubbard Hamiltonian (1.1) in the form,

$$\hat{\mathcal{H}} \equiv (\hat{P}_0 + \hat{P}_N)\hat{\mathcal{H}}(\hat{P}_0 + \hat{P}_N) = \hat{P}_0\hat{\mathcal{H}}\hat{P}_0 + \hat{P}_0\hat{\mathcal{H}}\hat{P}_N + \hat{P}_N\hat{\mathcal{H}}\hat{P}_0 + \hat{P}_N\hat{\mathcal{H}}\hat{P}_N, \tag{1.4}$$

where in the leading orders,

$$\hat{P}_0\hat{\mathcal{H}}\hat{P}_0 = \sum_{i\neq j,\,\sigma} t_{ij}\hat{c}^\dagger_{i\sigma}(1-\hat{n}_{i\bar{\sigma}})\hat{c}_{j\sigma}(1-\hat{n}_{j\bar{\sigma}}), \tag{1.5a}$$

$$\hat{P}_0\hat{\mathcal{H}}\hat{P}_N = \left(\hat{P}_N\hat{\mathcal{H}}\hat{P}_0\right)^\dagger = \sum_{i\neq j,\,\sigma} t_{ij}\hat{c}^\dagger_{i\sigma}(1-\hat{n}_{i\bar{\sigma}})\hat{c}_{j\sigma}\hat{n}_{j\bar{\sigma}}, \tag{1.5b}$$

$$\hat{P}_N\hat{\mathcal{H}}\hat{P}_0 = \left(\hat{P}_0\hat{\mathcal{H}}\hat{P}_N\right)^\dagger = \sum_{i\neq j,\,\sigma} t_{ij}\hat{c}^\dagger_{i\sigma}\hat{n}_{i\bar{\sigma}}\hat{c}_{j\sigma}(1-\hat{n}_{j\bar{\sigma}}), \tag{1.5c}$$

$$\hat{P}_N\hat{\mathcal{H}}\hat{P}_N = \sum_{i\neq j,\,\sigma} t_{ij}\hat{c}^\dagger_{i\sigma}\hat{n}_{i\bar{\sigma}}\hat{c}_{j\sigma}\hat{n}_{j\bar{\sigma}} + U\sum_i \hat{n}_{i\uparrow}\hat{n}_{i\downarrow}. \tag{1.5d}$$

Using the $\hat{P}_0$ and $\hat{P}_N$ operators, the Hamiltonian has been separated into the parts which describe respectively the hopping of a single electron:

a) from a singly occupied site to an empty site,

b) from a doubly occupied site to an empty site,

c) from a single occupied site to a site containing an electron of opposite spin (creation of a doubly occupied state but also creation of an empty state),

d) from a doubly occupied site to a site containing an electron of opposite spin (annihilation and then creation of a doubly occupied site),

as illustrated in Fig. 1.11..

[7] Another approach to derive t-J model, not from the single-band Hubbard model but from an extended (three band) Hubbard model (called also as the d–p model) presented in Ref. [45].

We introduce an auxiliary Hamiltonian,

$$\hat{\mathcal{H}}_\varepsilon = \underbrace{\hat{P}_0\hat{\mathcal{H}}\hat{P}_0 + \hat{P}_N\hat{\mathcal{H}}\hat{P}_N}_{\hat{\mathcal{H}}_0} + \varepsilon \underbrace{\left(\hat{P}_0\hat{\mathcal{H}}\hat{P}_N + \hat{P}_N\hat{\mathcal{H}}\hat{P}_0\right)}_{\hat{\mathcal{H}}_1}. \tag{1.6}$$

Note, that for $\varepsilon = 1$, we obtain the Hubbard Hamiltonian, i.e. $\hat{\mathcal{H}}_{\varepsilon=1} = \hat{\mathcal{H}}$. Such notation allows us to transform the Hamiltonian in the following manner,

$$\begin{aligned}\tilde{\mathcal{H}}_\varepsilon &= e^{-i\varepsilon\hat{S}}\hat{\mathcal{H}}e^{i\varepsilon\hat{S}} = \\ &= \hat{\mathcal{H}}_0 + \varepsilon(\hat{\mathcal{H}}_1 + i[\hat{\mathcal{H}}_0,\ \hat{S}]) + \frac{1}{2}\varepsilon^2\left(2i[\hat{\mathcal{H}}_1,\ \hat{S}] - [[\hat{\mathcal{H}}_0,\ \hat{S}],\ \hat{S}]\right) + O(\varepsilon^3),\end{aligned} \tag{1.7}$$

where $[\hat{A},\ \hat{B}] \equiv \hat{A}\hat{B} - \hat{B}\hat{A}$ is the commutator, and $\hat{S} = \hat{S}^\dagger$ is certain (not explicitly known) Hermitian operator of unitary transformation on $\mathcal{H}$. The $e^{i\varepsilon\hat{S}}$ term can be understood as a polynomial function of $\hat{S}$ (when is expanded in the Taylor series). All terms above were grouped according to the power of ε. All terms proportional to ε^n with $n \geqslant 3$ are neglected, as it is marked by $O(\varepsilon^3)$ (cf. the standard *big O* notation). Next, we choose $\hat{S}$ so that $\hat{\mathcal{H}}_1 + i[\hat{\mathcal{H}}_0,\ \hat{S}] \equiv 0$. This condition can be rewritten, using the $\hat{P}_0$ and $\hat{P}_N$ projectors, as a set of four equations,[8]

$$\hat{P}_0[\hat{\mathcal{H}}_0,\ \hat{S}]\hat{P}_0 = 0, \tag{1.8a}$$
$$\hat{P}_0\hat{\mathcal{H}}_1\hat{P}_N + i\hat{P}_0[\hat{\mathcal{H}}_0,\ \hat{S}]\hat{P}_N = 0, \tag{1.8b}$$
$$\hat{P}_N\hat{\mathcal{H}}_1\hat{P}_0 + i\hat{P}_N[\hat{\mathcal{H}}_0,\ \hat{S}]\hat{P}_0 = 0, \tag{1.8c}$$
$$\hat{P}_N[\hat{\mathcal{H}}_0,\ \hat{S}]\hat{P}_N = 0. \tag{1.8d}$$

Since the second and third equations are connected by the Hermitian conjugation, there are only three unique conditions for the $\hat{S}$ operator to be fulfilled. Because $\hat{P}_\alpha\hat{\mathcal{H}}_0\hat{P}_\beta = \delta_{\alpha\beta}\hat{P}_\alpha\hat{\mathcal{H}}_0\hat{P}_\alpha$, $\mathbb{1} = \hat{P}_0 + \hat{P}_N$ and $P_\alpha^2 = P_\alpha$ (everywhere $\alpha \in \{0,\ N\}$), one can write that,

$$\hat{P}_\alpha\hat{\mathcal{H}}_0\hat{S}\hat{P}_\beta = \hat{P}_\alpha\hat{\mathcal{H}}_0(\hat{P}_0 + \hat{P}_N)\hat{S}\hat{P}_\beta = (\hat{P}_\alpha\hat{\mathcal{H}}_0\hat{P}_\alpha)(\hat{P}_\alpha\hat{S}\hat{P}_\beta), \tag{1.9}$$

and consequently the three conditions for $\hat{S}$ are,[9]

$$(\hat{P}_\alpha\hat{\mathcal{H}}_0\hat{P}_\alpha)(\hat{P}_\alpha\hat{S}\hat{P}_\alpha) = (\hat{P}_\alpha\hat{S}\hat{P}_\alpha)(\hat{P}_\alpha\hat{\mathcal{H}}_0\hat{P}_\alpha), \quad \text{with } \alpha \in \{0,\ N\} \tag{1.10a}$$
$$\hat{P}_0\hat{\mathcal{H}}_1\hat{P}_N + i(\hat{P}_0\hat{\mathcal{H}}_0\hat{P}_0)(\hat{P}_0\hat{S}\hat{P}_N) - i(\hat{P}_0\hat{S}\hat{P}_N)(\hat{P}_N\hat{\mathcal{H}}_0\hat{P}_N) = 0. \tag{1.10b}$$

Eq. (1.10a) means that $\hat{P}_\alpha\hat{S}\hat{P}_\alpha$ need to be a function of operators that commute with $\hat{P}_\alpha\hat{\mathcal{H}}_0\hat{P}_\alpha$. Note, that such function has to have the form $\hat{P}_\alpha\hat{S}\hat{P}_\alpha = f(\hat{P}_\alpha) = a\mathbb{1} + b\hat{P}_\alpha$. From (1.10b), as long as the inverse operator of $\hat{P}_N\hat{\mathcal{H}}_0\hat{P}_N$ exists, we have that,

$$\hat{P}_0\hat{S}\hat{P}_N = \left(-i\hat{P}_0\hat{\mathcal{H}}_1\hat{P}_N + (\hat{P}_0\hat{\mathcal{H}}_0\hat{P}_0)(\hat{P}_0\hat{S}\hat{P}_N)\right)(\hat{P}_N\hat{\mathcal{H}}_0\hat{P}_N)^{-1}. \tag{1.11}$$

[8] Note, that in Eqs. (1.8a) and (1.8d) we used the fact that $\hat{P}_\alpha\hat{\mathcal{H}}_1\hat{P}_\alpha \equiv 0$ for $\alpha \in \{0,\ N\}$

[9] Note, that the first equations stand for two conditions. So in total we have three of them.

It it can be solved iteratively,[10]

$$\begin{cases} (\hat{P}_0\hat{S}^{(1)}\hat{P}_N) = -i(\hat{P}_0\hat{\mathcal{H}}_1\hat{P}_N)(\hat{P}_N\hat{\mathcal{H}}_0\hat{P}_N)^{-1}, \\ (\hat{P}_0\hat{S}^{(n)}\hat{P}_N) = \left(-i\hat{P}_0\hat{\mathcal{H}}_1\hat{P}_N + (\hat{P}_0\hat{\mathcal{H}}_0\hat{P}_0)(\hat{P}_0\hat{S}^{(n-1)}\hat{P}_N)\right)(\hat{P}_N\hat{\mathcal{H}}_0\hat{P}_N)^{-1}, \text{ for } n>1. \end{cases} \tag{1.12}$$

$\hat{S}^{(n\to+\infty)} = \hat{S}$ can be evaluated, as[11]

$$\hat{P}_0\hat{S}\hat{P}_N = -i\frac{\hat{P}_0\hat{\mathcal{H}}_1\hat{P}_N}{\hat{P}_N\hat{\mathcal{H}}_0\hat{P}_N}\left(1+x+x^2+\ldots\right) = -i\frac{\hat{P}_0\hat{\mathcal{H}}_1\hat{P}_N}{\hat{P}_N\hat{\mathcal{H}}_0\hat{P}_N - \hat{P}_0\hat{\mathcal{H}}_0\hat{P}_0} \approx -\frac{i}{U}\hat{P}_0\hat{\mathcal{H}}_1\hat{P}_N, \tag{1.13}$$

with $x = (\hat{P}_0\hat{\mathcal{H}}_0\hat{P}_0)(\hat{P}_N\hat{\mathcal{H}}_0\hat{P}_N)^{-1}$. In the last step, we have noticed that $\hat{P}_N\hat{\mathcal{H}}_0\hat{P}_N$ and $\hat{P}_0\hat{\mathcal{H}}_0\hat{P}_0$ describe the states in the upper and lower subbands of the original model, and are (on energy scale) separated roughly by U. Replacing operators with a scalar value is an approximation, valid rigorously only up to the second order in t/U [9, 41].

Taking $\varepsilon = 1$, the effective $\tilde{\mathcal{H}}$ up to the second order in t/U takes the explicit form,

$$\begin{aligned} \tilde{\mathcal{H}}_{\varepsilon=1} \equiv \hat{\mathcal{H}} &= (\hat{P}_0+\hat{P}_N)(H_0 + \frac{1}{2}i[\hat{\mathcal{H}}_1,\ \hat{S}])(\hat{P}_0+\hat{P}_N) = \\ &= \hat{P}_0\hat{\mathcal{H}}_0\hat{P}_0 + \hat{P}_N\hat{\mathcal{H}}_0\hat{P}_N - \frac{1}{U}\hat{P}_0\hat{\mathcal{H}}_1\hat{P}_N\hat{\mathcal{H}}_1\hat{P}_0 + \frac{1}{U}\hat{P}_N\hat{\mathcal{H}}_1\hat{P}_0\hat{\mathcal{H}}_1\hat{P}_N + O\left(\frac{t^3}{U^2}\right), \end{aligned} \tag{1.14}$$

where we neglected the terms proportional to ε^n with $n \geqslant 3$, since they describe multiple hops that lead to higher-order contributions in t/U. In the explicit form, the four terms of (1.14) are,

$$\hat{P}_0\hat{\mathcal{H}}_0\hat{P}_0 = \sum_{i\neq j,\,\sigma} t_{ij}\hat{c}^\dagger_{i\sigma}(1-\hat{n}_{i\bar{\sigma}})\hat{c}_{j\sigma}(1-\hat{n}_{j\bar{\sigma}}), \tag{1.15a}$$

$$\hat{P}_N\hat{\mathcal{H}}_0\hat{P}_N = \sum_{i\neq j,\,\sigma} t_{ij}\hat{c}^\dagger_{i\sigma}\hat{n}_{i\bar{\sigma}}\hat{c}_{j\sigma}\hat{n}_{j\bar{\sigma}} + U\sum_i \hat{n}_{i\uparrow}\hat{n}_{i\downarrow}, \tag{1.15b}$$

$$\begin{aligned} -\frac{1}{U}\hat{P}_0\hat{\mathcal{H}}_1\hat{P}_N\hat{\mathcal{H}}_1\hat{P}_0 = &-\frac{1}{U}\hat{P}_0\left(\sum_{i\neq j,\,\sigma} t_{ij}\hat{c}^\dagger_{i\sigma}(1-\hat{n}_{i\bar{\sigma}})\hat{c}_{j\sigma}\hat{n}_{i\bar{\sigma}}\right)\times \\ &\times\left(\sum_{k\neq l,\,\sigma'} t_{kl}\hat{c}^\dagger_{k\sigma'}\hat{n}_{k\bar{\sigma}'}\hat{c}_{l\sigma'}(1-\hat{n}_{l\bar{\sigma}'})\right)\hat{P}_0, \end{aligned} \tag{1.15c}$$

$$\begin{aligned} \frac{1}{U}\hat{P}_N\hat{\mathcal{H}}_1\hat{P}_0\hat{\mathcal{H}}_1\hat{P}_N = &\frac{1}{U}\hat{P}_N\left(\sum_{i\neq j,\,\sigma} t_{ij}\hat{c}^\dagger_{i\sigma}\hat{n}_{i\bar{\sigma}}\hat{c}_{j\sigma}(1-\hat{n}_{i\bar{\sigma}})\right)\times \\ &\times\left(\sum_{k\neq l,\,\sigma'} t_{kl}\hat{c}^\dagger_{k\sigma'}(1-\hat{n}_{k\bar{\sigma}'})\hat{c}_{l\sigma'}\hat{n}_{l\bar{\sigma}'}\right)\hat{P}_N. \end{aligned} \tag{1.15d}$$

[10] It is not obvious at first if this iterative procedure is divergent. However, each of the terms $\hat{P}_0\hat{\mathcal{H}}_1\hat{P}_N$, $\hat{P}_N\hat{\mathcal{H}}_0\hat{P}_N$ or $\hat{P}_0\hat{\mathcal{H}}_0\hat{P}_0$ describes a hopping of electrons between sites, as it is shown in Fig. 1.11. Probability of such hops is finite and the probability of multiple hops goes to zero with the increasing number of hops. Therefore, we can assume that there exists an unique solution for $\hat{S}^{(n\to+\infty)} \equiv \hat{S}$.

[11] Since the operators $\hat{A}$ and $\hat{B}^{-1}$ might not commute, $\frac{\hat{A}}{\hat{B}}$ notation might be confusing, since it can be understood either as $(\hat{B})^{-1}\hat{A}$ or $\hat{A}(\hat{B})^{-1}$. Here, such notation stands for $\hat{A}(\hat{B})^{-1}$.

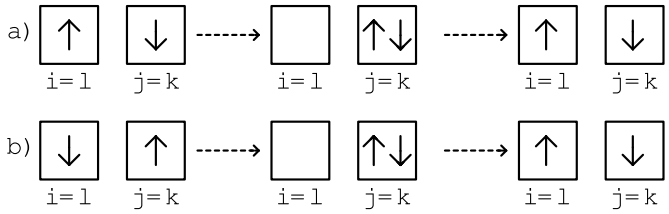

Figure 1.12: *Hopping in the second order between two sites described by Eq. (1.15c) or by Eq. (1.16a) (processes involving three different sites are neglected).*

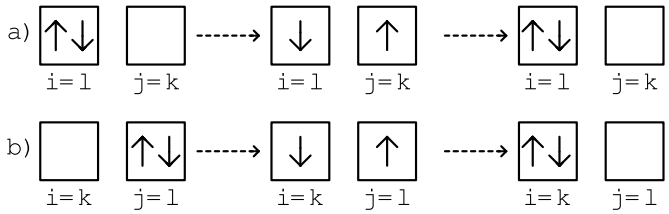

Figure 1.13: *Hopping between two sites described by Eq. (1.15d) or by Eq. (1.16b) (processes involving three different sites are neglected).*

The Eqs. (1.15a)–(1.15d) describes:

a) a hopping of single electron between a singly occupied site and an empty site,

b) a hopping of single electron between a doubly occupied site and a singly occupied,

c) a spin exchange between two sites, with the creation of intermediate doubly occupied state,

d) a transfer of doubly occupied state, with the intermediate creation of two singly occupied states.

Note, that the process in which three different sites are involved is less likely than a process that involves only two sites. Furthermore, as we already discussed, among all two-sites processes, a hopping between the nearest neighbors (n.n.) provides the largest contribution. Therefore, the Eqs. (1.15c) and (1.15d) can often be replaced by the leading n.n. term,[12]

$$-\frac{1}{U}\hat{P}_0\hat{\mathcal{H}}_1\hat{P}_N\hat{\mathcal{H}}_1\hat{P}_0 \approx -\sum_{i\neq j,\,\sigma}\frac{t_{ij}^2}{U}\left(\hat{n}_{i\sigma}(1-\hat{n}_{i\bar{\sigma}})\hat{n}_{j\bar{\sigma}}(1-\hat{n}_{j\sigma}) - \hat{c}^\dagger_{i\sigma}\hat{c}_{i\bar{\sigma}}\hat{c}^\dagger_{j\bar{\sigma}}\hat{c}_{j\sigma}\right), \quad (1.16a)$$

$$\frac{1}{U}\hat{P}_N\hat{\mathcal{H}}_1\hat{P}_0\hat{\mathcal{H}}_1\hat{P}_N \approx \sum_{i\neq j,\,\sigma}\frac{t_{ij}^2}{U}\left(\hat{n}_{i\sigma}\hat{n}_{i\bar{\sigma}}(1-\hat{n}_{j\sigma})(1-\hat{n}_{j\bar{\sigma}}) - \hat{c}^\dagger_{i\sigma}\hat{c}^\dagger_{i\bar{\sigma}}\hat{c}_{j\sigma}\hat{c}_{j\bar{\sigma}}\right), \quad (1.16b)$$

where the sum is over all pairs of neighboring sites. The first equation is written for $\{i = l \ \wedge \ j = k\}$ (cf. Eq. (1.15c) and Fig. 1.12), while the second for $\{i = l \ \wedge \ j = k\}$ when $\sigma = \sigma'$ and $\{i = k \ \wedge \ j = l\}$ when $\sigma = \bar{\sigma}'$ (cf. Eq. (1.15d) and Fig. 1.13).

[12] We assumed here also, that $t_{ij} = t_{ji}$, as t_{ij} parameters are assumed to be real.

In sum, we have shown so far, that Hubbard Hamiltonian can be rewritten as,[13]

$$\begin{aligned}\hat{\mathcal{H}}^{2\text{-site}} &\approx \hat{P}_0\hat{\mathcal{H}}_0\hat{P}_0 + \hat{P}_N\hat{\mathcal{H}}_0\hat{P}_N - \frac{1}{U}\hat{P}_0\hat{\mathcal{H}}_1\hat{P}_N\hat{\mathcal{H}}_1\hat{P}_0 + \frac{1}{U}\hat{P}_N\hat{\mathcal{H}}_1\hat{P}_0\hat{\mathcal{H}}_1\hat{P}_N \approx \\ &\approx \sum_{i\neq j,\,\sigma} t_{ij}\hat{c}^\dagger_{i\sigma}(1-\hat{n}_{i\bar{\sigma}})\hat{c}_{j\sigma}(1-\hat{n}_{j\bar{\sigma}}) + \sum_{i\neq j,\,\sigma} t_{ij}\hat{c}^\dagger_{i\sigma}\hat{n}_{i\bar{\sigma}}\hat{c}_{j\sigma}\hat{n}_{j\bar{\sigma}} + U\sum_i \hat{n}_{i\uparrow}\hat{n}_{i\downarrow} + \\ &\quad - \sum_{i\neq j,\,\sigma}\frac{t_{ij}^2}{U}\left(\hat{n}_{i\sigma}(1-\hat{n}_{i\bar{\sigma}})\hat{n}_{j\bar{\sigma}}(1-\hat{n}_{j\sigma}) - \hat{c}^\dagger_{i\sigma}\hat{c}_{i\bar{\sigma}}\hat{c}^\dagger_{j\bar{\sigma}}\hat{c}_{j\sigma}\right) + \\ &\quad + \sum_{i\neq j,\,\sigma}\frac{t_{ij}^2}{U}\left(\hat{n}_{i\sigma}\hat{n}_{i\bar{\sigma}}(1-\hat{n}_{j\sigma})(1-\hat{n}_{j\bar{\sigma}}) - \hat{c}^\dagger_{i\sigma}\hat{c}^\dagger_{i\bar{\sigma}}\hat{c}_{j\sigma}\hat{c}_{j\bar{\sigma}}\right),\end{aligned} \tag{1.17}$$

where we neglected terms describing hopping between the sites that are not the nearest neighbors of each other, multiple hopping (except those described in Figs. 1.12 and 1.13), and processes where more than two sites are involved. Such omission is justified only if $|t|/U \ll 1$, since the probability of a process describing n correlated electron hops is proportional to $(t/U)^n$ (cf. Appendix A for the three-site corrections).

We can rewrite the above Hamiltonian for the lowest Hubbard subband, introducing the following projected operators:

$$\hat{b}^\dagger_{i\sigma} \equiv \hat{c}^\dagger_{i\sigma}(1-\hat{n}_{i\bar{\sigma}}), \tag{1.18a}$$
$$\hat{b}_{i\sigma} \equiv \hat{c}_{i\sigma}(1-\hat{n}_{i\bar{\sigma}}), \tag{1.18b}$$
$$\hat{\nu}_{i\sigma} \equiv \hat{b}^\dagger_{i\sigma}\hat{b}_{i\sigma} = \hat{n}_{i\sigma}(1-\hat{n}_{i\bar{\sigma}}), \tag{1.18c}$$

that describe the creation of a single occupied state with spin σ at site i, the annihilation of such a state, and projected particle number operator for site i and spin σ, respectively. Note, that those operators do not anticommute, i.e.,

$$\left\{\hat{b}_{i\sigma},\ \hat{b}^\dagger_{j\sigma'}\right\} = \delta_{ij}\left((1-\hat{n}_{i\bar{\sigma}})\delta_{\sigma\sigma'} + \hat{S}^{\bar{\sigma}}_i\delta_{\bar{\sigma}\sigma'}\right), \tag{1.19a}$$
$$\left\{\hat{b}^\dagger_{i\sigma},\ \hat{b}^\dagger_{j\sigma'}\right\} = \left\{\hat{b}_{i\sigma},\ \hat{b}_{j\sigma'}\right\} = 0. \tag{1.19b}$$

Using this notation, the spin operator $\hat{\mathbf{S}}_i = \left(\hat{S}^x_i,\ \hat{S}^y_i,\ \hat{S}^z_i\right)^T$ can now be written as,

$$\hat{S}^+_i \equiv \hat{S}^x_i + i\hat{S}^y_i \equiv \hat{c}^\dagger_{i\uparrow}\hat{c}_{i\downarrow} \equiv \hat{b}^\dagger_{i\uparrow}\hat{b}_{i\downarrow}, \tag{1.20a}$$
$$\hat{S}^-_i \equiv \hat{S}^x_i - i\hat{S}^y_i \equiv \hat{c}^\dagger_{i\downarrow}\hat{c}_{i\uparrow} \equiv \hat{b}^\dagger_{i\downarrow}\hat{b}_{i\uparrow}, \tag{1.20b}$$
$$\hat{S}^z_i \equiv \frac{1}{2}(\hat{n}_{i\uparrow} - \hat{n}_{i\downarrow}) \equiv \frac{1}{2}(\hat{\nu}_{i\uparrow} - \hat{\nu}_{i\downarrow}), \tag{1.20c}$$

where $\hat{S}^+_i$ is the spin raising operator (it changes spin $\downarrow$ to $\uparrow$), $\hat{S}^-_i$ is the spin lowering operator (it changes spin $\uparrow$ to $\downarrow$), and $\hat{S}^z_i$ expresses the magnetic moment on one site i.[14]

[13] For those who wish to see the three-sites corrections, check Refs. [41,46]. For some critical remarks concerning the importance of the three-site term, cf. Refs. [47,48]

[14] Note, that the expressions for the spin component are identical in the original and projected representations. This is because in such an operation only single-occupied sites are involved.

As a result, Eq. (1.21) can be written to the form,

$$-\frac{1}{U}\hat{P}_0\hat{\mathcal{H}}_1\hat{P}_N\hat{\mathcal{H}}_1\hat{P}_0 = -\sum_{\langle i,\,j\rangle,\,\sigma}\frac{2t_{ij}^2}{U}\left(\hat{\nu}_{i\sigma}\hat{\nu}_{j\bar{\sigma}} - \hat{S}_i^{\sigma}\hat{S}_j^{\bar{\sigma}}\right) = \sum_{\langle i,\,j\rangle}\frac{4t_{ij}^2}{U}\left(\hat{\mathbf{S}}_i\cdot\hat{\mathbf{S}}_j - \frac{1}{4}\hat{\nu}_i\hat{\nu}_j\right), \tag{1.21}$$

where $\hat{\nu}_i = \hat{\nu}_{i\uparrow} + \hat{\nu}_{i\downarrow}$. Note, that $\sum_{\langle i,\,j\rangle}$ denotes summation over all nearest neighbors with each pair being counted only once (i.e., when $(i,\,j)$ is counted, then $(j,\,i)$ is not).[15] Thus, the $\hat{\mathcal{H}}^{2\text{-}site}$ Hamiltonian is,

$$\begin{aligned}\hat{\mathcal{H}}_{t-J}^{2\text{-}site} &\approx \hat{P}_0\hat{\mathcal{H}}_0\hat{P}_0 - \frac{1}{U}\hat{P}_0\hat{\mathcal{H}}_1\hat{P}_N\hat{\mathcal{H}}_1\hat{P}_0 \approx \\ &\approx \hat{P}_0\left(t\sum_{\langle i,\,j\rangle\,\sigma}\left(\hat{c}_{i\sigma}^{\dagger}\hat{c}_{j\sigma} + \text{H.c.}\right) + J\sum_{\langle i,\,j\rangle}\left(\hat{\mathbf{S}}_i\cdot\hat{\mathbf{S}}_j - \frac{1}{4}\hat{n}_i\hat{n}_j\right)\right)\hat{P}_0,\end{aligned} \tag{1.22}$$

where we neglected $\frac{1}{U}\hat{P}_N\hat{\mathcal{H}}\hat{P}_N$ part, since we assumed, that we have $|t| \ll U$ and $n \leqslant 1$.

The expression (1.22) is what is known in the literature as the t–J model. Sometimes the part $\sim \frac{1}{4}\hat{n}_i\hat{n}_j$ is disregarded (cf. Ref. [49] covering the importance of that term) or the hopping between further neighbors is included (cf. Ref. [50, 51] discussing the impact of such processes). However, in most cases modifications change the results only to a slight extent.[16]

1.5 Extension 1: t–J–U model

In the t–J model, derived above, the kinetic exchange integral is related to the values of the hopping and the onsite Coulomb repulsion, namely $J \equiv 4t^2/U$. However, if we use the t–J model to describe the Cu–O structure in cuprates, the above relationship may be not hold in such a case. Motivated by the microscopic electronic structure of the cuprates, we could expect that a full model should incorporate the hybridization processes between the $3d$ and $2p$ electronic states. The t–J model does not, and therefore it can be regarded only as an effective model for the cuprates. The parameter t can be related to the hopping integral between neighboring Cu ions, U to the onsite Coulomb repulsion interaction of two electrons located in the same $3d$ shell of the Cu ion, and J to the exchange interaction between two electrons from the nearest-neighboring $3d$ sites. Therefore, there is no reason to expect, that $J \equiv 4t^2/U$ any more. Instead, the quantities t, J, and U should be understood as *independent* parameters,[17] as they are expressed in terms of the $3d$ level position (ϵ_d) relative to that of $2p$ level (ϵ_p), the p–d hybridization amplitude V_{pd}, as well as the magnitude of U for d electrons relative to that for p electrons (U_{pp}).

When the t–J model is derived from the Hubbard model, it is done with the assumption of large U. In effect, no double occupancies are possible in this model. However, the value of U measured in real systems might be not large enough to assume,

[15] In other words, $\sum_{i\neq j} 1 = 2\sum_{\langle i,\,j\rangle} 1$, cf. page 11.

[16] One example, where t' is necessary, is the topology of the Fermi surface. To get realistic results t' term needs to be included, ($t' \approx -t/4$).

[17] The value of J can be found either experimentally or from *ab initio* simulations, cf. e.g. Ref. [31], specifically Table 7.2, according to which J for cuprates has a value of about 0.15–0.24 eV. Similarly, it can be found that U has a value of about 6–8 eV (cf. e.g. Ref. [52]) and t about 0.22–0.5 eV. Note that in calculations, to make it simpler, we define our energy scale with taking $|t| = 1$. Then both U and J are measured not in eV but in units of $|t|$.

that all double occupancies are excluded. To include such a possibility in our model, we can directly add a term that regulates the number of double occupancies, $U\sum_i \hat{n}_{i\uparrow}\hat{n}_{i\downarrow}$, to the t–J Hamiltonian. Such a model is known as t–J–U model,[18]

$$\hat{\mathcal{H}}_{t\text{–}J\text{–}U} = t\sum_{\langle i,j\rangle,\sigma}\left(\hat{c}^{\dagger}_{i\sigma}\hat{c}_{j\sigma} + H.c.\right) + J\sum_{\langle i,j\rangle}\left(\hat{\mathbf{S}}_i\cdot\hat{\mathbf{S}}_j - \frac{1}{4}\hat{n}_i\hat{n}_j\right) + U\sum_i \hat{n}_{i\uparrow}\hat{n}_{i\downarrow}, \quad (1.23)$$

where pairs in $\sum_{\langle i,j\rangle}$ are counted only once (cf. page 11). Note that in such a form we are neglecting the part $\sim t^2/U$ in $\hat{P}_N\hat{\mathcal{H}}\hat{P}_N$ (cf. Eq. (1.15b)), as it is regarded as a decisively smaller contribution than that coming from the term $\sim U$. In particular, for $U\to+\infty$, we restore the original t–J model, since the creation of even a single double occupancy would cost infinitely large energy; setting $U=0$ and $t=0$, the Heisenberg model is restored, with $J=0$ a Hubbard model, and with $J=0$ and $U=0$ a free electron gas model. Therefore, the t–J–U model effectively combines the physics coming from both the Hubbard and t–J models and is particularly useful when U and the width of the energy band (W) are the same order of magnitude.

For sake of simplicity, the term $-\frac{1}{4}\sum_{\langle i,j\rangle,\sigma} J\,\hat{n}_i\hat{n}_j$ is often neglected (for a critical study, cf. Ref. [49]). However, as we will see, this term is directly connected to the role of the intersite Coulomb repulsion, as discussed in the next Section.

The t–J–U model is analyzed in greater details in our paper (cf. Ref. [53]), that is also included in the second part of this Thesis.

A natural extension of the model (1.23) is to allow for a direct hopping of electrons between the second and the third nearest neighbors,

$$\hat{\mathcal{H}}_{t\text{–}t'\text{–}t''\text{–}J\text{–}U} = \hat{\mathcal{H}}_{t\text{–}J\text{–}U} + t'\sum_{\langle\langle i,j\rangle\rangle,\sigma}\left(\hat{c}^{\dagger}_{i\sigma}\hat{c}_{j\sigma} + H.c.\right) + t''\sum_{\langle\langle\langle i,j\rangle\rangle\rangle,\sigma}\left(\hat{c}^{\dagger}_{i\sigma}\hat{c}_{j\sigma} + H.c.\right), \quad (1.24)$$

where pairs in $\sum_{\langle\langle i,j\rangle\rangle}$ and in $\sum_{\langle\langle\langle i,j\rangle\rangle\rangle}$ are counted only once (cf. page 11). Note that considering the antiferromagnetic order (with $Q=(\pi,\pi)$) on a square lattice, the t' and t'' terms represent hopping within the same antiferromagnetic sublattice. Therefore, we can expect that introducing t' and t'' terms should not alter the AF stability, but since those terms contribute directly to electrons' (hole) motion, they should have an influence on the quasiparticle dispersion. On the other hand, if we have system with a short magnetic order (shorter than the range of the hopping) then the transfer process of electrons due to the t' and t'' terms may create spin excitations which contribute to the coherent hole motion (cf. Ref. [54]). It was also found that those additional hopping terms lead to a better agrement with the ARPES experiments.[19]

The importance of the additional hopping terms is discussed in greater detail in our paper (cf. Ref. [51]), that is also included in the second part of this Thesis.

[18] Note, that for the t–J model, each term contains a $\hat{\mathcal{P}}_0$ projector, that suppresses the double occupancies, d^2. For the t–J–U model, those projectors are not needed, since we can directly control the ratio of double occupied sites by setting U.

[19] For the importance of t', cf. Ref. [55]; for the importance of t'', cf. Ref. [56–60], and for a review cf. Ref. [37]). Finally, for the sake of simplicity, one can ask what is the impact of including the exchange term for more distant neighbors. This question was analyzed. First, the estimated value of J' in a real system would be rather small [61]; Second, even if J' was significant, for $J'/J < 0.65$ introducing J' does not qualitatively change the obtained results [50].

1.6 Extension 2: t–J–U–V model

A natural extension of the t–J–U model is the model where we include direct intersite Coulomb repulsion between the electrons on the neighboring sites. The Hamiltonian is then of the form,

$$\hat{\mathcal{H}}_{t-J-U-V} = t \sum_{\langle i,j\rangle,\sigma} \left(\hat{c}^{\dagger}_{i\sigma}\hat{c}_{j\sigma} + H.c.\right) + t' \sum_{\langle\langle i,j\rangle\rangle,\sigma} \left(\hat{c}^{\dagger}_{i\sigma}\hat{c}_{j\sigma} + H.c.\right) + \ldots$$
$$+ J \sum_{\langle i,j\rangle} \hat{\mathbf{S}}_i \cdot \hat{\mathbf{S}}_j + U \sum_i \hat{n}_{i\uparrow}\hat{n}_{i\downarrow} + \left(\tilde{V} - \frac{1}{4}J\right) \sum_{\langle i,j\rangle,\sigma,\sigma'} \hat{n}_{i\sigma}\hat{n}_{j\sigma'} \quad (1.25)$$

where where pairs in $\sum_{\langle i,j\rangle}$ and in $\sum_{\langle\langle i,j\rangle\rangle}$ are counted only once (cf. page 11), and where for simplicity we can denote, $V \equiv \tilde{V} - \frac{1}{4}J$. The inter-Coulomb repulsion $\tilde{V}$ is usually substantially smaller than the intersite repulsion U and can be similar order to J. Thus, V can in principle be either negative of positive. In the first approximation, we could assume that $\tilde{V} \approx J/4$, and therefore make the term $\sim n_i n_j$ negligible.

There is another way to justify the t–J–U–V model, not as an extension of t–J–U model, but rather as a simplification of the d–p model (a three-band model, that represents the Cu–O plane in cuprates, cf. Refs. [31,62]). The d–p model can be reduced using the cell-partubation theory to an effective, one band t-J-V model (cf. Ref. [45]). We can also argue, that the extension of t–J model to the t–J–U (or t–J–U–V) form can be also viewed from the physical point of view. Namely, the effective one band model of correlated fermions contains the general form of narrow d-band Hamiltonian (cf. Ref. [15], Appendix B), but the parameters are renormalized by interband processes or are taken in the form discussed above. In particular, the value of exchange integral comes from superexchange processes [34, 63].

1.7 Charge density wave: a brief literature survey

The first time the long-range charge order (CO) was observed was in 1939 in Fe_3O_4 [64, 65]. Later, CO was found in many transition metal oxides [66]. The interest in this field grew again, when the charge density wave (CDW) was found in cuprates [67, 68]. However, despite the growing evidence that the CDW state is a common feature (cf. Refs. [69–74]), and the theoretical work regarding stability of the CDW (cf. Refs. [75–79]), we are still very far from a consensus about the nature of that state.

It is observed [72], that CDW in cuprates appears frequently in the proximity of the superconductivity (SC) phase. This is the case for $YBa_2Cu_3O_{6.67}$ (YBCO) [69, 72–74], $La_{2-x-y}Nd_ySr_xCuO_4$ (Nd-LSCO), $La_{2-x}Ba_xCuO_4$ (LBCO), and $Bi_2Sr_{2-x}La_xCuO_{6+x}$ [70, 71]. In all those cases CDW appears for the hole doping around $\delta = 1/8$ and its critical temperature is higher than that for SC (cf. Refs. [72, 74]). In the region where CDW appears, just below the optimal doping, the SC dome has a small, but defined plateau (cf. Figs. 1.14 and 1.15). CDW and SC have a similar energy scale and those two phenomena compete with each other, which can be seen when the temperature dependence of the CDW peak intensity is measured by varying the applied magnetic field (cf. Fig. 1.16).[20] The wave vector of the CDW modulation was measured for YBCO to be $\mathbf{Q} \approx (0,\, 0.629(1)\pi)$ or $\mathbf{Q} \approx (0.629(1)\pi,\, 0)$ in the plane of Cu–O layers [72].[21] In

[20] CDW competes not only with SC but also with the SDW phase, cf. Ref. 73.

[21] There are also suggestions that CDW should have a checkerboard like structure [80, 81].

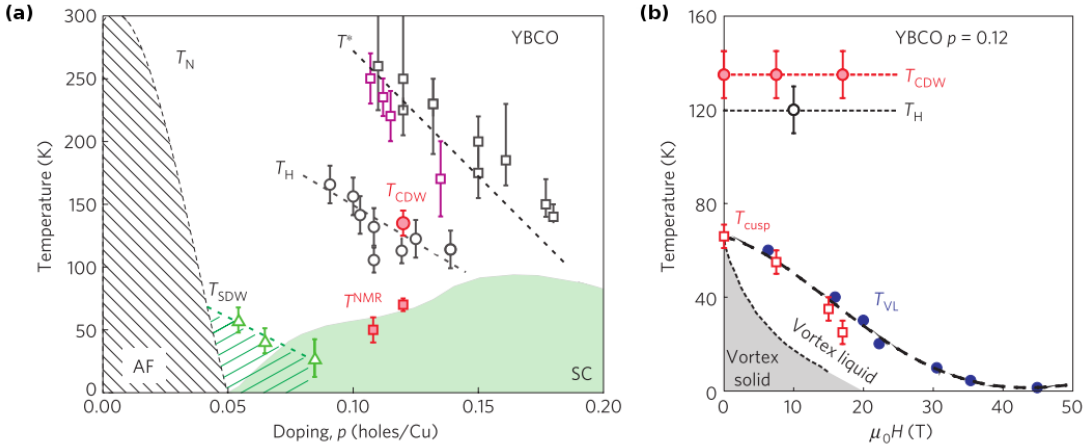

Figure 1.14: **(a)** *Phase diagram of* $YBa_2Cu_3O_{7-x}$ *on temperature–doping plane.* T_N *stands for the Néel Temperature,* T_{SDW} *for the spin density wave,* T_{CDW} *for the charge density wave, T* for the onset of pseudo-gap state (black squares from the Nernst effect, purple from the neutron diffraction).* T_H *and* T_{NMR} *stand for the temperature scales below which a negative Hall coefficient and field-induced charge order are observed, respectively.* **(b)** *Phase diagram of* $YBa_2Cu_3O_{7-x}$ *on a temperature–magnetic–field plane.* T_{cusp} *stands for the temperature below which the CDW is suppressed by SC, while* T_{VL} *for the temperature in which vortex liquid is formed. (Figures taken from Ref. [72]).*

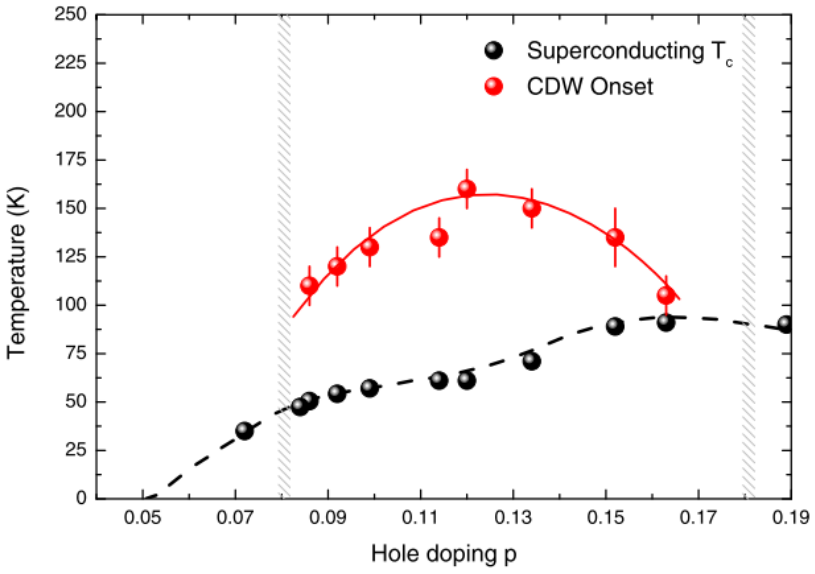

Figure 1.15: *Phase diagram for* $YBa_2Cu_3O_{7-x}$ *on a temperature–doping plane. For the hole doping* $p < 0.09$ *and* $p > 0.18$ *no CDW order was found. The optimal doping for SC is around* $p_o = 0.16$*. Note that the CDW presence coincides with the SC plateau appearance (Figure taken from Ref. [74]).*

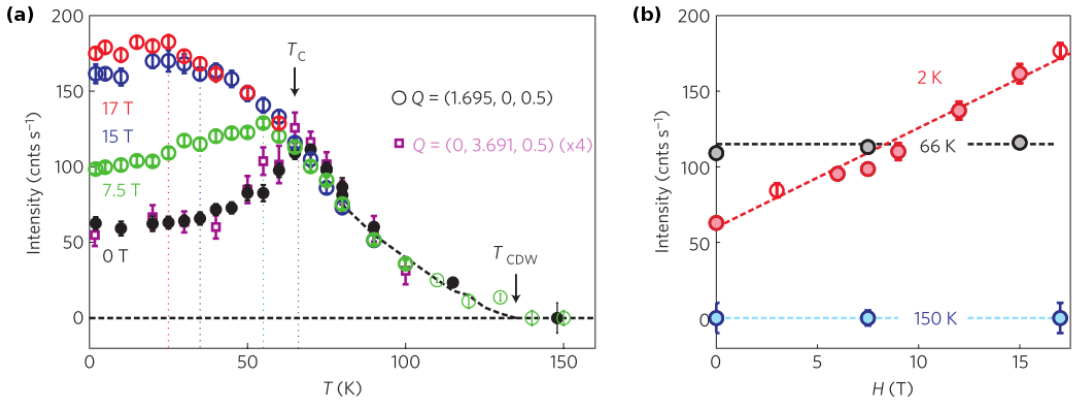

Figure 1.16: **(a)** *Temperature dependence of the CDW peak intensity measured for different magnetic field. Note that when SC is suppressed by magnetic field, CDW intensity increases.* **(b)** *Magnetic field dependence of the CDW peak intensity measured for the different temperatures. For $T = 2$ K there is linear growth of the intensity with the increasing field (at least in the range $H \in (0, 17\ T)$). For $T > T_c$, there is no effect of the magnetic field on the value of the CDW intensity. (Figure taken from Ref. [72]).*

other cuprates, CDW was found to have a similar symmetry, usually in one direction but with a periodicity that is not a simple multiplication of the lattice constant, i.e., the wave vector $\mathbf{Q}$ is close, but not equal to, $(0, 2\pi/3)$ [71, 72]. In the newest work on this subject (cf. for example Ref. [82]), it is suggested that the situation might be even more complicated. Namely, there may appear two distinctive CDW orders: one that appears in each Cu–O layer independently (and is not correlated between layers) and a second that has a three-dimension nature [83] that appears only at low temperature and in higher magnetic fields. Moreover, it was also observed that CDW does not form simple pattern but rather a mosaic of regions with stripes oriented in different directions [84–87], that CDW order parameter may have d-wave symmetry [80, 88], and that the CDW appearance may be connected with the presence of the pseudogap phase [72, 89, 90].

The stability of the CDW phase in the t–J–U–V model regarding different Q vector choices is discussed in our article (cf. Ref. [91]), that is also included in the second part of this Thesis.

Chapter 2

Methods used in the Thesis

2.1 The Gutzwiller Approach

One of the interesting characteristics of any system, is its ground state energy,

$$E = \frac{\langle \Psi \mid \mathcal{H} \mid \Psi \rangle}{\langle \Psi \mid \Psi \rangle}, \tag{2.1}$$

where we assumed that our many-particle ground state is $|\Psi\rangle$. In the original Gutzwiller approach [92, 93], the wave function $|\Psi\rangle$ is approximated by $|\Psi\rangle_G$, derived from an uncorrelated, normalized single-particle state. Namely,

$$|\Psi\rangle \approx |\Psi\rangle_G = \hat{P}\,|\Psi_0\rangle \equiv \prod_i \hat{P}_i\,|\Psi_0\rangle, \tag{2.2}$$

where $\hat{P}_i$ weights the configuration of given occupancies ($\varnothing$, $\uparrow$, $\downarrow$, $\uparrow\downarrow$) of the single lattice site i. In the general form,

$$\hat{P}_i \;=\; \lambda_{i,\varnothing}(1-\hat{n}_{i\uparrow})(1-\hat{n}_{i\downarrow}) + \lambda_{i,\uparrow}\hat{n}_{i\uparrow}(1-\hat{n}_{i\downarrow}) + \lambda_{i,\downarrow}(1-\hat{n}_{i\uparrow})\hat{n}_{i\downarrow} + \lambda_{i,d}\hat{n}_{i\uparrow}\hat{n}_{i\downarrow}. \tag{2.3}$$

Following [94], we assume that $\hat{P}_i^2 = 1 + x_i\,\hat{n}_{i\uparrow}^{HF}\hat{n}_{i\downarrow}^{HF}$, where x_i is a variational parameter, and $\hat{n}_{i\sigma}^{HF} \equiv \hat{n}_{i\sigma} - n_{i\sigma}$. Note that $\hat{P}_i^2$ acting on the local basis, $|\varnothing\rangle_i$, $|\uparrow\rangle_i$, $|\downarrow\rangle_i$, $|\uparrow\downarrow\rangle_i$, yields,

$$\lambda_{i,\varnothing}^2 \;=\; 1 + x_i\,n_{i\sigma}n_{i\bar{\sigma}}, \tag{2.4a}$$
$$\lambda_{i,\sigma}^2 \;=\; 1 - x_i\,(1-n_{i\sigma})n_{i\bar{\sigma}}, \tag{2.4b}$$
$$\lambda_{i,d}^2 \;=\; 1 + x_i\,(1-n_{i\sigma})(1-n_{i\bar{\sigma}}). \tag{2.4c}$$

When $\forall_i\, x_i = 0$, then the operator $\hat{P} = \mathbb{1}$ and $|\Psi\rangle = |\Psi_0\rangle$, but when $x_i < 0$, then the probability that the site i has two electrons is reduced. To keep the average number of electrons for each site in the system constant, $x_i < 0$ requires that the number of the single occupied sites is increased and the number of empty sites is reduced at the same time. Nevertheless, the exact interpretation of parameter x_i is not easy to provide, therefore we introduce d_i^2 as the likelihood of double occupancy at site i, namely,

$$\langle\Psi|\hat{n}_{i\uparrow}\hat{n}_{i\downarrow}|\Psi\rangle \equiv d_i^2. \tag{2.5}$$

We can relate d_i^2 to the x_i parameter, since

$$d_i^2 = \langle\Psi|\hat{n}_{i\uparrow}\hat{n}_{i\downarrow}|\Psi\rangle = \langle\Psi_0|\hat{P}_i\hat{n}_{i\uparrow}\hat{n}_{i\downarrow}\hat{P}_i|\Psi_0\rangle = \lambda_{id}^2\, n_{i\uparrow}n_{i\downarrow}, \tag{2.6}$$

where we assume that $\langle\Psi_0|\hat{n}_{i\uparrow}\hat{n}_{i\downarrow}|\Psi_0\rangle \equiv \langle\hat{n}_{i\uparrow}\hat{n}_{i\downarrow}\rangle_0 = n_{i\uparrow}n_{i\downarrow}$. i.e., that there is no local pairing of electrons, $\langle\hat{c}_{i\uparrow}\hat{c}_{i\downarrow}\rangle_0 = 0$, and that hopping does not change the spin of electron $\langle\hat{c}_{i\uparrow}^\dagger\hat{c}_{i\downarrow}\rangle_0 = 0$. Using Eqs. (2.4c)–(2.6), we can show now, that

$$x_i \equiv \frac{d^2 - n_{i\uparrow}n_{i\downarrow}}{n_{i\uparrow}n_{i\downarrow}(1-n_{i\uparrow})(1-n_{i\downarrow})}, \tag{2.7}$$

and as a result we can rewrite the expressions (2.4a)–(2.4c) in the form:

$$\lambda_{i,\varnothing}^2 = \frac{1+d^2-n_\sigma-n_{\bar\sigma}}{(1-n_\sigma)(1-n_{\bar\sigma})}, \tag{2.8a}$$

$$\lambda_{i,\sigma}^2 = \frac{n_\sigma - d^2}{n_\sigma(1-n_{\bar\sigma})}, \tag{2.8b}$$

$$\lambda_{i,d}^2 = \frac{d^2}{n_\sigma n_{\bar\sigma}}. \tag{2.8c}$$

It allows us to calculate that

$$\hat{P}_i\hat{c}_{i\sigma}^\dagger\hat{P}_i = \Big(\lambda_\sigma\hat{n}_{i\sigma}(1-\hat{n}_{i\bar\sigma}) + \lambda_d\hat{n}_{i\sigma}\hat{n}_{i\bar\sigma}\Big)\hat{c}_{i\sigma}^\dagger\Big(\lambda_{\bar\sigma}\hat{n}_{i\bar\sigma}(1-\hat{n}_{i\sigma}) + \lambda_0(1-\hat{n}_{i\sigma})(1-\hat{n}_{i\bar\sigma})\Big)$$
$$= (\alpha_{i\sigma} + \beta_{i\sigma}\hat{n}_{i\bar\sigma}^{HF})\hat{c}_{i\sigma}^\dagger, \tag{2.9}$$

where

$$\alpha_{i\sigma} = \sqrt{\frac{(n_{i\sigma}-d_i^2)(1-n+d_i^2)}{n_{i\sigma}(1-n_{i\sigma})}} + |d_i|\sqrt{\frac{n_{i\bar\sigma}-d_i^2}{n_{i\sigma}(1-n_{i\sigma})}}, \tag{2.10}$$

$$\beta_{i\sigma} = -\sqrt{\frac{(n_{i\sigma}-d_i^2)(1-n+d_i^2)}{n_{i\sigma}(1-n_{i\sigma})(1-n_{i\bar\sigma})^2}} + |d_i|\sqrt{\frac{n_{i\bar\sigma}-d_i^2}{n_\sigma n_{\bar\sigma}^2(1-n_\sigma)}}. \tag{2.11}$$

Note that for $\hat{P}_i\hat{c}_{i\sigma}\hat{P}_i$ we would obtain the same result as above. Now, using the above expressions, one can calculate the average of any operator. In the next Sections, we present the result for hopping and spin exchange terms. Another example is presented in Appendix B.

2.1.1 Example 1: renormalization factor for hopping term

The average of the hopping term is

$$\langle\hat{c}_{i\sigma}^\dagger\hat{c}_{j\sigma}\rangle = \langle\hat{P}_i\hat{P}_j\hat{c}_{i\sigma}^\dagger\hat{c}_{j\sigma}\hat{P}_i\hat{P}_j\rangle_0 = \langle\hat{P}_i\hat{c}_{i\sigma}^\dagger\hat{P}_i\,\hat{P}_j\hat{c}_{j\sigma}\hat{P}_j\rangle_0 = \alpha_{i\sigma}\alpha_{j\sigma}\langle\hat{c}_{i\sigma}^\dagger\hat{c}_{j\sigma}\rangle_0$$
$$+ \alpha_{i\sigma}\beta_{j\sigma}\langle\hat{n}_{i\bar\sigma}^{HF}\hat{c}_{i\sigma}^\dagger\hat{c}_{j\sigma}\rangle_0 + \alpha_{j\sigma}\beta_{i\sigma}\langle\hat{n}_{j\bar\sigma}^{HF}\hat{c}_{i\sigma}^\dagger\hat{c}_{j\sigma}\rangle_0 + \beta_{i\sigma}\beta_{j\sigma}\langle\hat{n}_{i\bar\sigma}^{HF}\hat{n}_{j\bar\sigma}^{HF}\hat{c}_{i\sigma}^\dagger\hat{c}_{j\sigma}\rangle_0, \tag{2.12}$$

where we denote $\langle\Psi|\ldots|\Psi\rangle \equiv \langle\ldots\rangle$ and $\langle\Psi_0|\ldots|\Psi_0\rangle \equiv \langle\ldots\rangle_0$, in order to make the expressions easier to read. Using the Wick theorem, we can check that

$$\langle\hat{n}_{i\bar\sigma}^{HF}\hat{c}_{i\sigma}^\dagger\hat{c}_{j\sigma}\rangle_0 = 0, \tag{2.13a}$$

$$\alpha_{j\sigma}\beta_{i\sigma}\langle\hat{n}_{j\bar\sigma}^{HF}\hat{c}_{i\sigma}^\dagger\hat{c}_{j\sigma}\rangle_0 = 0, \tag{2.13b}$$

as far as we assume that $\langle \hat{c}^{\dagger}_{i\sigma}\hat{c}^{\dagger}_{i\bar{\sigma}}\rangle_0 = 0$ and $\langle \hat{c}^{\dagger}_{i\sigma}\hat{c}_{j\bar{\sigma}}\rangle_0 = 0$, which is usually a natural expectation (no local pairing of electrons and conservation of spin during hoppings). The last average, $\beta_{i\sigma}\beta_{j\sigma}\langle \hat{n}^{HF}_{i\bar{\sigma}}\hat{n}^{HF}_{j\bar{\sigma}}\hat{c}^{\dagger}_{i\sigma}\hat{c}_{j\sigma}\rangle_0$, is usually non-zero, but small, and therefore it can be neglected here. We are left with,

$$\langle \hat{c}^{\dagger}_{i\sigma}\hat{c}_{j\sigma}\rangle \approx \alpha_{i\sigma}\alpha_{j\sigma}\langle \hat{c}^{\dagger}_{i\sigma}\hat{c}_{j\sigma}\rangle_0, \tag{2.14}$$

where $\alpha_{i\sigma}$ is expressed by Eq. (2.10). In the simpler case, where neither AF nor CDW order is considered, we have $\alpha_{i\sigma} = \alpha_{j\sigma} = \alpha$, and,

$$\alpha_{i\sigma}\alpha_{j\sigma} \equiv \alpha^2 = g_t \equiv \frac{n-2d^2}{n(1-n/2)}\left(\sqrt{1-n+d^2}+|d|\right)^2, \tag{2.15}$$

where g_t is the Gutzwiller factor for the hopping term, well known from the literature [34, 95–97].

2.1.2 Example 2: the renormalization factor for spin exchange term

In a similar manner, the Gutzwiller factors for other averages can be calculated, for example for $\langle \hat{\mathbf{S}}_i \cdot \hat{\mathbf{S}}_j\rangle$. First, we check that

$$\hat{P}_i\hat{S}^{+}_i\hat{P}_i = \hat{P}_i\hat{c}^{\dagger}_{i\sigma}\hat{c}_{i\bar{\sigma}}\hat{P}_i = \lambda_{i,\sigma}\hat{n}_{i\sigma}(1-\hat{n}_{i\bar{\sigma}})\,\hat{c}^{\dagger}_{i\sigma}\hat{c}_{i\bar{\sigma}}\,\lambda_{i,\bar{\sigma}}\hat{n}_{i\bar{\sigma}}(1-\hat{n}_{i\sigma}) = \lambda_{i,\sigma}\lambda_{i,\bar{\sigma}}\,\hat{c}^{\dagger}_{i\sigma}\hat{c}_{i\bar{\sigma}}. \tag{2.16}$$

The same result will be obtained for $\hat{S}^{-}_i$ and $\hat{S}^{\pm}_j$. For simplicity, we consider here only the AF ordering, for which $n_{i\sigma} \equiv n_{j\bar{\sigma}}$, with i and j denoting the nearest neighbors. Thus,

$$\sum_{\langle i,j\rangle}\frac{1}{2}\left(\langle S^{+}_i S^{-}_j\rangle + \langle S^{-}_i S^{+}_j\rangle\right) = g^{\pm}_s \sum_{\langle i,j\rangle}\frac{1}{2}\left(\langle S^{+}_i S^{-}_j\rangle_0 + \langle S^{-}_i S^{+}_j\rangle_0\right), \tag{2.17}$$

where

$$g^{\pm}_s \equiv \lambda^2_{i,\sigma}\lambda^2_{i,\bar{\sigma}} = \frac{(n_{i\sigma}-d^2_i)(n_{i\bar{\sigma}}-d^2_i)}{n_{i\sigma}n_{i\bar{\sigma}}(1-n_{i\sigma})(1-n_{i\bar{\sigma}})} = \frac{n_{i\sigma}n_{i\bar{\sigma}} - n\,d^2_i + d^4_i}{n_{i\sigma}n_{i\bar{\sigma}}(1-n_{i\sigma})(1-n_{i\bar{\sigma}})}. \tag{2.18}$$

Note that because the above expression is invariant under the transformation $\sigma \to \bar{\sigma}$, the $g^{\pm}_s$ does not depend on the index i choice.

For $\hat{S}^{z}_i$ and for $\hat{S}^{z}_j$ we can obtain,

$$\begin{aligned}\Lambda^{-1}\sum_{\langle i,j\rangle}\langle S^{z}_i \cdot S^{z}_j\rangle = \frac{1}{4}\sum_{\langle i,j\rangle}\langle \hat{P}_i S^{z}_i \hat{P}_i\,\hat{P}_j S^{z}_j \hat{P}_j\rangle_0 = \frac{1}{4}\sum_{\langle i,j\rangle,\sigma,\sigma'}\sigma\sigma'\langle \hat{P}_i\hat{c}^{\dagger}_{i\sigma}\hat{c}_{i\sigma}\hat{P}_i\,\hat{P}_j\hat{c}^{\dagger}_{j\sigma'}\hat{c}_{j\sigma'}\hat{P}_j\rangle_0 \\ \approx -g^{z\,\chi}_s\,\chi^2 - g^{z\,\Delta}_s\left(\Delta^2_S + \Delta^2_T\right),\end{aligned} \tag{2.19}$$

with

$$g^{z\,\chi}_s \equiv \Big(1 - n_{i,\sigma}(\lambda^2_{i,d}-\lambda^2_{i,\sigma}) - n_{i,\bar{\sigma}}(\lambda^2_{i,d}-\lambda^2_{i,\bar{\sigma}}) + n_{i,\sigma}(\lambda^2_d-\lambda^2_{i,\sigma})n_{i,\bar{\sigma}}(\lambda^2_{i,d}-\lambda^2_{i,\bar{\sigma}})\Big), \tag{2.20}$$

$$\begin{aligned}g^{z\,\Delta}_s \equiv \Big(1 - n_{i,\sigma}(\lambda^2_{i,d}-\lambda^2_{i,\sigma}) - n_{i,\bar{\sigma}}(\lambda^2_d-\lambda^2_{i,\bar{\sigma}}) \\ + \frac{1}{2}\left(\left[n_{i,\sigma}(\lambda^2_{i,d}-\lambda^2_{i,\sigma})\right]^2 + \left[n_{i,\bar{\sigma}}(\lambda^2_d-\lambda^2_{i,\bar{\sigma}})\right]^2\right)\Big),\end{aligned} \tag{2.21}$$

where we neglected terms proportional to χ^4, Δ_S^4, Δ_T^4, and "mixed" terms like $n_\sigma n_{\bar\sigma}\chi^2$. The average hopping amplitude for the first nearest neighbors is defined by

$$\chi \equiv \langle \hat{c}^\dagger_{i\sigma}\hat{c}_{j\sigma}\rangle_0, \tag{2.22}$$

and the electron pairing amplitude between the nearest neighbors, with spin-singlet and spin-triplet components, Δ_S and Δ_T, are defined by

$$\Delta_{ij\sigma} \equiv \langle \hat{c}_{i\sigma}\hat{c}_{j\bar\sigma}\rangle_0 = -\tau_{ij}\left(\sigma\Delta_S + e^{i\mathbf{Q}\cdot\mathbf{R}_i}\Delta_T\right), \tag{2.23}$$

where $\tau_{ij} \equiv 1$ for $j = i \pm \hat{x}$, and $\tau_{ij} \equiv -1$ for $j = i \pm \hat{y}$ to ensure the d-wave symmetry of $\Delta_{ij\sigma}$ (cf. Ref. [53]).

In the simpler, paramagnetic case, $\forall_i : n_{i\sigma} = n_{i\bar\sigma} = n/2$, and

$$g_s^{\pm} \equiv g_s^{z\,\chi} \equiv g^{z\,\Delta} \equiv \left(\frac{n-2d^2}{n(1-n/2)}\right)^2, \tag{2.24}$$

which is the well known renormalization factor for spin-exchange term in paramagnetic cases (cf. Refs. [34, 95–97]).

For more examples of the Gutzwiller factor's derivation, cf. Appendix B.

2.2 Two ways of defining the Gutzwiller factor in the presence of extra symmetries

In this Section we show that introducing extra ordering, such as AF or CDW, can lead to a specific ambiguity in determining the final form of the Gutzwiller factors. We follow here the material gathered in the Appendix to our paper, Ref. [91], extending the discussion by additional examples.

For simplicity, we assume in this Section that in our model (Hubbard, t–J–U or t–J–U–V) the parameter $U \to \infty$, what results in $d^2 \to 0$. In other words, we consider the case where the correlated state $|\Psi\rangle$ has no double occupancies. Additionally, to make our arguments easy to follow, we consider only the AF order (no CDW) and we focus on the example of the Gutzwiller factor for the hopping term that has been discussed in the previous Section (cf. Eq. (2.15)).

In the Gutzwiller approch, we try to find an operator $\hat{P}$, that makes the following approximation as accurate as possible,

$$\langle\Psi|\hat{c}^\dagger_{i\sigma}\hat{c}_{j\sigma}|\Psi\rangle \approx \langle\Psi_0|\hat{P}_i\hat{c}^\dagger_{i\sigma}\hat{P}_i\,\hat{P}_j\hat{c}_{j\sigma}\hat{P}_j|\Psi_0\rangle \tag{2.25}$$

On the other hand, we can try to find a function $g_t(n_{i\sigma}, n_{i\bar\sigma}, d, \ldots)$ (called the Gutzwiller renormalization factor), that satisfies the following equation:

$$\langle\Psi_0|\hat{P}_i\hat{c}^\dagger_{i\sigma}\hat{P}_i\,\hat{P}_j\hat{c}_{j\sigma}\hat{P}_j|\Psi_0\rangle \equiv g_t\,\langle\Psi_0|\hat{c}^\dagger_{i\sigma}\hat{c}_{j\sigma}|\Psi_0\rangle. \tag{2.26}$$

Therefore, the Gutzwiller renormalization factor can be obtained by comparing the likelihood of a specific process (in this example, hopping) in the correlated $|\Psi\rangle$, and in

Table 2.1: *Likelihood of a site being in the certain state (uncorrelated case $|\Psi_0\rangle$).*

state	for A sublattice	for B sublattice
$\|\uparrow\rangle$ or $\|\uparrow\downarrow\rangle$	$n_{A\uparrow} = \frac{1}{2}(n+m)$	$n_{B\uparrow} = \frac{1}{2}(n-m)$
$\|\downarrow\rangle$ or $\|\uparrow\downarrow\rangle$	$n_{A\downarrow} = \frac{1}{2}(n-m)$	$n_{B\downarrow} = \frac{1}{2}(n+m)$
$\|\uparrow\rangle$	$n_{A\uparrow}(1-n_{A\downarrow})$	$n_{B\uparrow}(1-n_{B\downarrow})$
$\|\downarrow\rangle$	$n_{A\downarrow}(1-n_{A\uparrow})$	$n_{B\downarrow}(1-n_{B\uparrow})$
$\|\varnothing\rangle$	$(1-n_{A\uparrow})(1-n_{A\downarrow})$	$(1-n_{B\uparrow})(1-n_{B\downarrow})$
$\|\uparrow\downarrow\rangle$	$n_{A\uparrow}n_{A\downarrow}$	$n_{B\uparrow}n_{B\downarrow}$

the uncorrelated $|\Psi_0\rangle$ states, namely

$$g_t(n_{i\sigma}, n_{i\bar{\sigma}}, d, \ldots) \approx \frac{\langle\Psi|\hat{c}^\dagger_{i\sigma}\hat{c}_{j\sigma}|\Psi\rangle}{\langle\Psi_0|\hat{c}^\dagger_{i\sigma}\hat{c}_{j\sigma}|\Psi_0\rangle}. \tag{2.27}$$

Let us assume that there are on average n electrons per site and the staggered magnetization is equal to m. We can divide our lattice into two sublattices, A and B, where the average spin σ for the A sublattice is $n_{A\sigma} = \frac{1}{2}(n + \sigma m)$, and $n_{B\sigma} = n_{A\bar{\sigma}} = \frac{1}{2}(n - \sigma m)$ for the B sublattice. For the non-correlated ($U = 0$) case $|\Psi_0\rangle$, on average $n_{\uparrow\downarrow} = n_{A\uparrow}n_{A\downarrow} = n_{B\uparrow}n_{B\downarrow}$ sites are double occupied and consequently, $n_{\varnothing} = (1-n_{A\uparrow})(1-n_{A\downarrow}) = (1-n_{B\uparrow})(1-n_{B\downarrow})$ sites are empty (cf. Table 2.1).

In the correlated ($U \neq 0$) state $|\Psi\rangle$, the likelihood of the double occupancy should be smaller than that determined for $|\Psi_0\rangle$. The appropriate adjustment is made by choosing the proper form of the $\hat{P}$ operator (cf. Refs. [92, 93]). In the specific case of $U \to \infty$, no double occupancies should be allowed in the correlated state, which results in $\forall_i\ \lambda_{i,d} \equiv 0$ (cf. the general form of $\hat{P}$ operator, Eq. (2.3)). However, by changing the probability of states to be doubly occupied, we also change the average number of the electrons in the system. To avoid this, other lambdas, $\lambda_{i,\varnothing}$, $\lambda_{i,\uparrow}$ and $\lambda_{i,\downarrow}$, need to be modified as well.

There are two intuitive ways to achieve this:

1. We can "split" every double occupancy, separating the electrons (one $\uparrow$ and one $\downarrow$) to different, previously empty sites. Such an operation would not change the global magnetization of the system (the difference between the *up* and *down* electrons, $m \equiv n_\uparrow - n_\downarrow$) but it would modify the proportion of the number of the single occupied states $|\uparrow\rangle$ to the number of $|\downarrow\rangle$ states.

2. We can "erase" the double occupancies. However, such action would change the number of electrons in the system. Therefore, to restore the previous number of electrons, we can *proportionally* add *up* and *down* electrons to previously empty sites. This operation would keep the proportion of the number of single occupied states with spin *up* to those with spin *down*, but it would modify the global magnetization of the system.

Each of the presented schemes leads to a different probability of sites to be in certain states, as it is presented in the Table 2.2. Note, that in the first scheme, the proportion of $|\uparrow\rangle$ states is the same as "$|\uparrow\rangle$ or $|\uparrow\downarrow\rangle$" states in the Table 2.1. In the second scheme, after erasing the doubly occupied states, the number of the electrons has changed from n to $n - n_{A\sigma}n_{A\bar{\sigma}}$ in the A sublattice and to $n - n_{B\sigma}n_{B\bar{\sigma}}$ in the B

Table 2.2: *Likelihood of a site being in a certain state (correlated case $|\Psi\rangle$). In the table, only the results for the A sublattice are shown. For the B sublattice simply $n_{B\sigma} = n_{A\bar{\sigma}}$.*

state	scheme 1. ("splitting")	scheme 2. ("erasing")
$\|\uparrow\rangle$	$n_{A\uparrow} = \frac{1}{2}(n+m)$	$n_{A\uparrow}(1-n_{A\downarrow})\frac{n}{n-2n_{A\uparrow}n_{A\downarrow}}$
$\|\downarrow\rangle$	$n_{A\downarrow} = \frac{1}{2}(n-m)$	$n_{A\downarrow}(1-n_{A\uparrow})\frac{n}{n-2n_{A\uparrow}n_{A\downarrow}}$
$\|\varnothing\rangle$	$1-n_{A\uparrow}-n_{A\downarrow}$	$1-n_{A\uparrow}-n_{A\downarrow}$
$\|\uparrow\downarrow\rangle$	0	0

sublattice. Therefore, to restore the previous number of electrons in the system, the probability that the state will have single electron σ was renormalized by the factor $n/(n-2n_{A\uparrow}n_{A\downarrow}) \equiv n/(n-2n_{B\uparrow}n_{B\downarrow})$.

It is possible to derive the g_t Gutzwiller factor for the hopping term in both schemes. For the hopping to occur in the correlated state in one site (for example, belonging to the A sublattice) there needs to be a single electron with the spin σ while the neighboring site (that belongs the the B sublattice) needs to be empty (or vice versa). Therefore, by comparing the amplitudes of the bra and the ket contributions of $\langle\Psi|\hat{c}^\dagger_{i\sigma}\hat{c}_{j\sigma}|\Psi\rangle$, with the help of Table 2.2, we can write that in the first scheme,

$$\langle\Psi|\hat{c}^\dagger_{i\sigma}\hat{c}_{j\sigma}|\Psi\rangle \overset{(1)}{=} \sqrt{n_{A\sigma}n_{B\sigma}}(1-n). \tag{2.28}$$

while in the second,

$$\langle\Psi|\hat{c}^\dagger_{i\sigma}\hat{c}_{j\sigma}|\Psi\rangle \overset{(2)}{=} \sqrt{\frac{n_{A\sigma}(1-n_{A\bar{\sigma}})n_{B\sigma}(1-n_{B\bar{\sigma}})}{(n-2n_{A\uparrow}n_{A\downarrow})(n-2n_{B\uparrow}n_{B\downarrow})}}n(1-n). \tag{2.29}$$

Analagously, we can calculate the hopping probability in the uncorrelated state. Namely, the hopping can occur when either one site has electron with the spin σ or is double occupied, and when either the neighboring site is empty or has one electron with the spin $\bar{\sigma}$ (cf. also Ref. [98]). Using Table 2.1, we get,

$$\langle\Psi_0|\hat{c}^\dagger_{i\sigma}\hat{c}_{j\sigma}|\Psi_0\rangle = \sqrt{n_{A\sigma}(1-n_{B\sigma})n_{B\sigma}(1-n_{A\sigma})}. \tag{2.30}$$

This leads to (cf. Eq. (2.27)) to either

$$g_t^{(1)} = \frac{1-n}{\sqrt{(1-n_{A\uparrow})(1-n_{B\uparrow})}}, \tag{2.31}$$

or

$$g_t^{(2)} = \frac{1-n}{1-\frac{2n_{A\uparrow}n_{A\downarrow}}{n}} \equiv \frac{1-n}{1-\frac{2n_{B\uparrow}n_{B\downarrow}}{n}}. \tag{2.32}$$

Both $g_t^{(1)}$ and $g_t^{(2)}$ are present in the literature, for example $g_t^{(2)}$ in [34, 95, 97, 99], whereas $g_t^{(1)}$ is identical with the zero-order renormalization factors of the DE-GWF method [94, 100–103].

Note that if no AF order is present,

$$g_t^{(1)} = g_t^{(2)} = \frac{1-n}{1-n/2}, \tag{2.33}$$

and there is no difference between $g_t^{(1)}$ and $g_t^{(2)}$ anymore (cf. also Eq. (2.15) and take $d = 0$).

If instead CDW and no AF order were considered, we would simply take in Eqs. (2.31) and (2.31) that $n_{A\sigma} = n_A$ and $n_{B\sigma} = n_B$ such, that $n_A \neq n_B$. In such case the Gutzwiller factors obtained within the first and the second schemes are different as well.

The above discussion can be easily generalized for other terms than hopping (cf. Appendix C).

We have checked that the two schemes lead to substantially different outputs, especially regarding the stability of the AF phase. In the first scheme the AF phase is stable in a wide range of doping, from 0 to about $\delta_{max} = 0.27$ (cf. Ref. [91], while using the second scheme the AF phase is stable only very close to the half-filled band, with $\delta_{max} < 0.006$ (cf. Ref. [53]).

The stability of the AF phase in the t–J–U model with the Gutzwiller factors derived according to the second schema is discussed in our article, Ref. [91]. The stability of the AF phase in the second schema is presented in our article, Ref. [53]. Both articles are included in the second part of the Thesis.

2.3 Statistically-consistent Gutzwiller approach (SGA)

We show here how to use the statistically-consistent Gutzwiller approach (SGA). Let us consider the Hubbard model in the ferromagnetic (FM) case,

$$\hat{\mathcal{H}} = \sum_{i \neq j,\, \sigma} t_{ij} \hat{c}^{\dagger}_{i\sigma} \hat{c}_{j\sigma} + U \sum_{i} \hat{n}_{i\uparrow} \hat{n}_{i\downarrow} - \sum_{i\sigma} \sigma h \hat{c}^{\dagger}_{i\sigma} \hat{c}_{i\sigma}, \tag{2.34}$$

where $h = \frac{1}{2} g \mu_B H$, with H being the external magnetic field. In the standard Gutzwiller approach (GA),

$$E = \langle \psi | \hat{\mathcal{H}} | \psi \rangle \approx \langle \psi_0 | \hat{\mathcal{H}}_{GA} | \psi_0 \rangle, \tag{2.35}$$

where

$$\hat{\mathcal{H}}_{GA} = \sum_{i \neq j,\, \sigma} g_t \, t_{ij} \hat{c}^{\dagger}_{i\sigma} \hat{c}_{j\sigma} + \Lambda U d^2 - \sum_{i\sigma} \sigma h \hat{c}^{\dagger}_{i\sigma} \hat{c}_{i\sigma}, \tag{2.36}$$

with $g_t = g_t(n, m, d)$ being the Gutzwiller renormalization factor (cf. Eq. (2.14) and the discussion in Section 2.2), where Λ is the number of sites, n is the average number of electrons per site, m is the magnetization and d^2 is the probability of sites being doubly occupied.

The Hamiltonian $\hat{\mathcal{H}}_{GA}$ can be easily diagonalized,

$$\mathcal{H}_{GA} = \sum_{\mathbf{k}\sigma} (q_\sigma(d,\, n,\, m) \varepsilon_{\mathbf{k}} - \sigma h) \hat{c}^{\dagger}_{\mathbf{k}\sigma} \hat{c}_{\mathbf{k}\sigma} + \Lambda U d^2, \tag{2.37}$$

with

$$\varepsilon_{\mathbf{k}} = 2t \left(\cos(k_x a) + \cos(k_y a) \right) + 4t' \cos(k_x a) \cos(k_y a) + \ldots \tag{2.38}$$

for the square lattice. We denote here that $t_{ij} \equiv t$ for i and j indicating the nearest neighbors, $t_{ij} \equiv t'$ for i and j indicating the second nearest neighbors, etc.

The grand potential functional for finite temperature T is

$$\mathcal{F}^{(GA)} = -\frac{1}{\beta}\ln \mathcal{Z}, \tag{2.39}$$

with

$$\mathcal{Z} = \mathrm{Tr}\left(e^{-\beta(\hat{\mathcal{H}}_{GA}-\mu\hat{n}_i)}\right) = \prod_{\mathbf{k}\sigma}\sum_{n_i=0}^{1} e^{-\beta n_i E^{(GA)}_{\mathbf{k}\sigma}} e^{-\beta U d^2} = \prod_{\mathbf{k}\sigma}\left(1+e^{-\beta E^{(GA)}_{\mathbf{k}\sigma}}\right) e^{-\beta U d^2}, \tag{2.40}$$

where $\beta \equiv 1/k_B T$, with k_B being the Boltzmann constant $k_B \approx 8.617\cdot 10^{-5}$ eV/K, and

$$E^{(GA)}_{\mathbf{k}\sigma} = g_\sigma \varepsilon_{\mathbf{k}} - \sigma h - \mu. \tag{2.41}$$

It leads to,

$$\mathcal{F}^{(GA)} = -\frac{1}{\beta}\sum_{\mathbf{k}\sigma}\ln(1+e^{-\beta E^{(GA)}_{\mathbf{k}\sigma}}) + \Lambda U d^2. \tag{2.42}$$

that can be minimized. The necessary conditions for the minimum of $\mathcal{F}^{(GA)}$ are,

$$\sum_{\mathbf{k}\sigma}\frac{\partial q_\sigma(d,n,m)}{\partial d} f(E_{\mathbf{k}\sigma})\varepsilon_{\mathbf{k}} = -2\Lambda U d, \tag{2.43a}$$

$$\sum_{\mathbf{k}\sigma}\frac{\partial q_\sigma(d,n,m)}{\partial n} f(E_{\mathbf{k}\sigma})\varepsilon_{\mathbf{k}} = 0, \tag{2.43b}$$

$$\sum_{\mathbf{k}\sigma}\frac{\partial q_\sigma(d,n,m)}{\partial m} f(E_{\mathbf{k}\sigma})\varepsilon_{\mathbf{k}} = 0, \tag{2.43c}$$

where $f(E_{\mathbf{k}\sigma}) \equiv \left(1+e^{\beta E_{\mathbf{k}\sigma}}\right)^{-1}$ is the Fermi function.

However, on the other hand, the definition of m and n implies the following equations,

$$n = \frac{1}{\Lambda}\sum_{\mathbf{k}\sigma} n_{\mathbf{k}\sigma} = \frac{1}{\Lambda}\sum_{\mathbf{k}\sigma} f(E_{\mathbf{k}\sigma}), \tag{2.44a}$$

$$m = \frac{1}{\Lambda}\sum_{\mathbf{k}\sigma} n_{\mathbf{k}\sigma} = \frac{1}{\Lambda}\sum_{\mathbf{k}\sigma} \sigma f(E_{\mathbf{k}\sigma}). \tag{2.44b}$$

There are in total 5 equations for 3 variables (n, m and d), therefore in the general case, there is no solution (no such n, m and d that fulfill all of the equations).

The situation can be fixed, as first presented in Ref. [104], introducing constraints for each mean-field average that appear in calculated energy (cf. Eq. (2.35)). In our case, the modified Hamiltonian has the form,

$$\hat{\mathcal{H}}_\lambda = \hat{\mathcal{H}}_{GA} - \sum_i \lambda_n\left(\sum_\sigma \hat{c}^\dagger_{i\sigma}\hat{c}_{i\sigma} - n\right) - \sum_i \lambda_m\left(\sum_\sigma \sigma \hat{c}^\dagger_{i\sigma}\hat{c}_{i\sigma} - m\right). \tag{2.45}$$

It leads us to

$$\mathcal{F}^{(SGA)} = -\frac{1}{\beta}\sum_{\mathbf{k}\sigma}\ln(1+e^{-\beta E^{(SGA)}_{\mathbf{k}\sigma}}) + \Lambda\left(\lambda_n n + \lambda_m m + U d^2\right), \tag{2.46}$$

with

$$E^{(SGA)}_{\mathbf{k}\sigma} = g_\sigma \varepsilon_{\mathbf{k}} - \sigma(h + \lambda_m) - \mu - \lambda_n. \tag{2.47}$$

The necessary conditions for the minimum of $\mathcal{F}^{(SGA)}$ are now,

$$\lambda_n = -\frac{1}{\Lambda}\sum_{\mathbf{k}\sigma} \frac{\partial g_\sigma}{\partial n} f(E^{(SGA)}_{\mathbf{k}\sigma})\varepsilon_{\mathbf{k}}, \tag{2.48a}$$

$$\lambda_m = -\frac{1}{\Lambda}\sum_{\mathbf{k}\sigma} \frac{\partial g_\sigma}{\partial m} f(E_{\mathbf{k}\sigma^{(SGA)}})\varepsilon_{\mathbf{k}}, \tag{2.48b}$$

$$n = \frac{1}{\Lambda}\sum_{\mathbf{k}\sigma} f(E^{(SGA)}_{\mathbf{k}\sigma}), \tag{2.48c}$$

$$m = \frac{1}{\Lambda}\sum_{\mathbf{k}\sigma} \sigma f(E^{(SGA)}_{\mathbf{k}\sigma}), \tag{2.48d}$$

$$d = -\frac{1}{2\Lambda U}\sum_{\mathbf{k}\sigma} \frac{\partial g_\sigma}{\partial d} f(E^{(SGA)}_{\mathbf{k}\sigma})\varepsilon_{\mathbf{k}}. \tag{2.48e}$$

There is 5 equations for 5 variables, thus in the general case, the solution may exist and can be obtained by solving the above equations numerically.

The introduction of the extra Lagrange multipliers to the Hamiltonian renormalized first by the Gutzwiller factors is the core idea of the statistically consistent Gutzwiller approach (SGA) (cf. Refs. [104–106]). In SGA we ensure that the averages calculated in a self-consistent manner coincide with those determined from the variational minimization principle. That approach was successfully applied in various cases, cf. Refs. [51, 53, 107–113]).

The comparison of GA and SGA for the t–J–U model is presented in the article Ref. [53], that is also included in the second part of this Thesis.

Chapter 3

Heavy fermions and Anderson lattice model

3.1 Introductory remark: heavy fermion materials

Heavy fermion materials are a type of intermetallic compound, containing elements with partially filled $4f$ or $5f$ valence shells. The effective mass of electrons in heavy fermion materials is enhanced hundreds or thousands times, as compared to the value expected for the free electron gas. The first discovered heavy fermion material was $CeAl_3$ [114], but soon other compounds were found [115]. The common characteristic of these materials is that they exhibit both behavior similar to a simple ideal gas (e.g., the linear scaling of the specific heat coefficient, cf. Ref. [116]), and to systems with partly localized electrons (e.g., the mentioned electron mass enhancement and the Kondo effect). Additionally, in heavy fermions materias, the non-BCS pairing mechanism was observed (spin-triplet superconductivity), as well as the coexistence of the SC phase with weak ferromagnetism (FM) [117–119]. First, the SC and FM phases were believed to always compete with each other. However, as it was observed latter for UG_2 [120], that the FM and SC phases for heavy fermion systems seem to be strongly intertwined [121–125]. Such phenomena were soon found in other materials, e.g., in URhGe [126] and in UCoGe [127].

The discoveries regarding FM and SC coexistence have triggered intensive research. In particular, UGe_2 was intensively studied, both theoretically [111–113, 130–143] and experimentally [121–125]. For this compound, the description of its magnetism is particularly challenging due to the emerging complex phase diagram (cf. Fig. 3.1). It comprises two distinct FM phases: with stronger (FM2) and weaker (FM1) magnetization and SC dome spreading in between them [128]. The phase transitions from FM2 to FM1 and from FM1 to paramagnetism (PM) at low temperature are of the first order. When temperature is increased (to above 7K), a metamagnetic phase transition FM2→FM1 is terminated with the critical ending point (CEP) and instead, crossover behavior can be observed. For higher temperature (about 24 K), the FM1→PM first-order transition changes into the second-order one at the tricritical point (TCP). Two symmetric lines of critical points starting at TCP are observed by applying a magnetic field, and lowering the temperature (cf. Fig. 3.1). Those lines form a characteristic *wing-shape* structure and end with the quantum critical ending points (QCEPs) [129, 144].

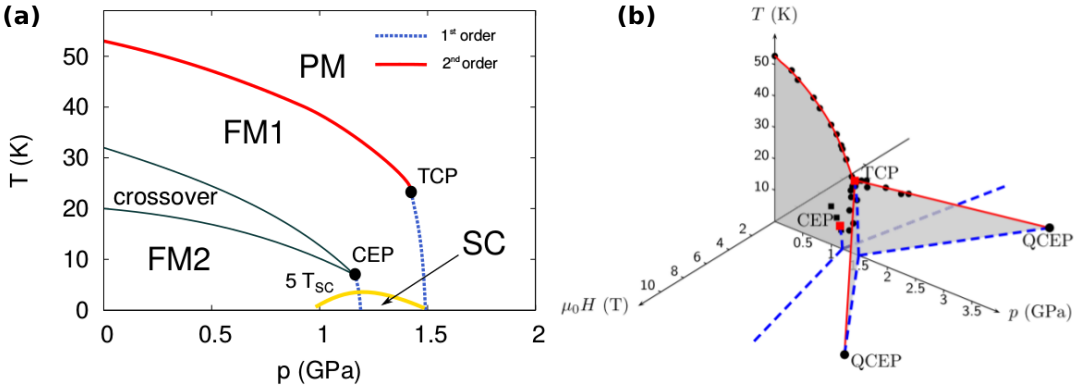

Figure 3.1: **(a)** *Schematic, experimentally determined (cf. Refs. [120, 128, 129]) magnetic phase diagram for UGe_2 on pressure–temperature plane. There are two ferromagnetic phases (FM1 and FM2), as well as paramegnetic (PM) and superconducting (SC) states. The order of the transitions has been marked. For details, see main text.* **(b)** *Phase diagram of UGe_2 on temperature–pressure–magnetic-field. Gray planes are planes of first order transition and the solid (red) lines the second order one (Figure taken from Ref. [129]).*

3.2 Anderson Lattice model (ALM)

We now discuss the second canonical model of correlated electrons, namely the Anderson-lattice model. With this model we account explicitly for the influence of conduction electrons on the correlated, originally atomic f states, and apply the model to the magnetic state of UGe_2. The appropriate Hamiltonian has form,

$$\hat{\mathcal{H}}_{ALM} = \sum_{i\neq j,\,\sigma} t_{ij}\hat{c}^{\dagger}_{i\sigma}\hat{c}_{j\sigma} - \sum_{i,\sigma}\sigma h\hat{n}^{c}_{i\sigma} + \sum_{i,\sigma}(\epsilon_f - \sigma h)\hat{n}^{f}_{i\sigma} + U\sum_{i}\hat{n}^{f}_{i\uparrow}\hat{n}^{f}_{i\downarrow} + V\sum_{i,\sigma}(\hat{f}^{\dagger}_{i\sigma}\hat{c}_{i\sigma} + \hat{c}^{\dagger}_{i\sigma}\hat{f}_{i\sigma}), \quad (3.1)$$

where $h \equiv \frac{1}{2}g\mu_0\mu_B H$ is the reduced magnetic field, H is the external magnetic field, the c-index denotes the conducting electrons (thus, $\hat{n}^{c}_{i\sigma} = \hat{c}^{\dagger}_{i\sigma}\hat{c}_{i\sigma}$) and the f-index denotes the localized (atomic) f-electrons (thus, $\hat{n}^{f}_{i\sigma} = \hat{f}^{\dagger}_{i\sigma}\hat{f}_{i\sigma}$). The first term in Eq. (3.1) represents the hopping of electrons in the conducting band, the second and the third terms describe the effect of the magnetic field (the Zeeman term) and the atomic level (ϵ_f) of f-electrons. Note, that only f-electrons experience the Coulomb onsite repulsion (the fourth term). The last term is the hybridization term, mixing the c- and f-electrons.

Within the statistically consistent approach (SGA), discussed in the previous Chapter, the effective ALM Hamiltonian has form,

$$\hat{\mathcal{H}}_{SGA} \equiv \sum_{\mathbf{k},\sigma}\Psi^{\dagger}\begin{pmatrix}\epsilon^{c}_{\mathbf{k}} - \sigma h - \mu & \sqrt{q_\sigma}\,V \\ \sqrt{q_\sigma}\,V & \epsilon_f - \sigma h - \mu\end{pmatrix}\Psi + \Lambda U d_f^2 - \lambda^{f}_{n}\Big(\sum_{\mathbf{k},\sigma}\hat{n}^{f}_{\mathbf{k},\sigma} - \Lambda n_f\Big) - \lambda^{f}_{m}\Big(\sum_{\mathbf{k},\sigma}\sigma\hat{n}^{f}_{\mathbf{k},\sigma} - \Lambda m_f\Big) \quad (3.2)$$

where $\sqrt{q_\sigma}$ is the Gutzwiller renormalization factor for f-electrons,

$$\sqrt{q_\sigma} = \frac{\sqrt{(n_{f,\sigma} - d_f^2)(1 - n_f + d_f^2)} + d_f\sqrt{n_{f,\bar{\sigma}} - d_f^2}}{\sqrt{n_{f,\sigma}(1 - n_{f,\sigma})}}. \quad (3.3)$$

Furthermore, m_f denotes the magnetization of f-electrons and $\Psi^\dagger \equiv (\hat{c}^\dagger_{\mathbf{k},\sigma}, \hat{f}^\dagger_{\mathbf{k},\sigma})$. We checked [111–113] that the above model is sufficient to describe the magnetic phase diagram and the position of the classical and quantum critical points for UGe_2 compound. Using this model we can also obtain the wing-shape structure described in Fig. 3.1 (b), as well as provide an explanation for the appearance, sequence, character, and evolution in an applied magnetic field the ferromagnetic and paramagnetic phases, as an effect of a competition between the f–f electron Coulomb interaction energy and the f-conduction electron hybridization.

The magnetic phase diagram obtained for ALM Hamiltonian and the qualitative comparison of theoretical results with the experimental findings is presented in Ref. [111]. The phase evolution in the magnetic field and the description of the critical points is provided in Ref. [112]. The quantitative comparison of the second-order transition lines joining the TCP and QCEP points to the experiment is presented in Ref. [113]. All three papers are included as a part of this Thesis in the second part of this manuscript.

Appendix A

Three-site corrections for t–J model

In Section 1.4 the derivation of t–J model was presented, where for simplicity only hoppings that involve two sites were considered. The natural extension of the model is to include the terms that describe processes where three sites are involved. Since hopping between distant sites is less probable than between neighboring sites, we assume that among those three sites, each site is the nearest neighbor of at least one other site from that group. The illustrations of such processes are presented in Figs. A.1 and A.2. Formally, terms describing the three-site hopping can be evaluated from Eqs. (1.15c) and (1.15d), namely

$$
\begin{aligned}
&-\frac{1}{U}\hat{P}_0\hat{H}_1\hat{P}_N\hat{H}_1\hat{P}_0 \overset{(3\text{-site})}{=} \\
&-\sum_{\langle i,j,l\rangle,\sigma}\frac{4t_{ij}t_{jl}}{U}\left(\hat{c}^{\dagger}_{i\sigma}(1-\hat{n}_{i\bar{\sigma}})(1-\hat{n}_{j\sigma})\hat{n}_{j\bar{\sigma}}\hat{c}_{l\sigma}(1-\hat{n}_{l\bar{\sigma}})-\hat{c}^{\dagger}_{i\sigma}(1-\hat{n}_{i\bar{\sigma}})\hat{c}^{\dagger}_{j\bar{\sigma}}\hat{c}_{j\sigma}\hat{c}_{l\bar{\sigma}}(1-\hat{n}_{l\sigma})\right) \\
&\qquad+\sum_{\langle k,i,j\rangle,\sigma}\frac{4t_{ij}t_{ki}}{U}\left(\hat{c}^{\dagger}_{k\sigma}\hat{n}_{k\bar{\sigma}}\hat{n}_{i\sigma}(1-\hat{n}_{i\bar{\sigma}})\hat{c}_{j\sigma}\hat{n}_{j\bar{\sigma}}+\hat{c}^{\dagger}_{k\bar{\sigma}}\hat{n}_{k\sigma}\hat{c}^{\dagger}_{i\sigma}\hat{c}_{i\bar{\sigma}}\hat{c}_{j\sigma}\hat{n}_{j\bar{\sigma}}\right), \quad \text{(A.1)}
\end{aligned}
$$

and

$$
\begin{aligned}
&-\frac{1}{U}\hat{P}_0\hat{H}_1\hat{P}_N\hat{H}_1\hat{P}_0 \overset{(3\text{-site})}{=} \\
&=-\sum_{\langle i,j,l\rangle,\sigma}\frac{4t_{ij}t_{jl}}{U}\left(\hat{c}^{\dagger}_{i\sigma}(1-\hat{n}_{i\bar{\sigma}})(1-\hat{n}_{j\sigma})\hat{n}_{j\bar{\sigma}}\hat{c}_{l\sigma}(1-\hat{n}_{l\bar{\sigma}})-\hat{c}^{\dagger}_{i\sigma}(1-\hat{n}_{i\bar{\sigma}})\hat{c}^{\dagger}_{j\bar{\sigma}}\hat{c}_{j\sigma}\hat{c}_{l\bar{\sigma}}(1-\hat{n}_{l\sigma})\right)+ \\
&\qquad+\sum_{\langle k,i,j\rangle,\sigma}\frac{4t_{ij}t_{ki}}{U}\left(\hat{c}^{\dagger}_{k\sigma}\hat{n}_{k\bar{\sigma}}\hat{n}_{i\sigma}(1-\hat{n}_{i\bar{\sigma}})\hat{c}_{j\sigma}\hat{n}_{j\bar{\sigma}}+\hat{c}^{\dagger}_{k\bar{\sigma}}\hat{n}_{k\sigma}\hat{c}^{\dagger}_{i\sigma}\hat{c}_{i\bar{\sigma}}\hat{c}_{j\sigma}\hat{n}_{j\bar{\sigma}}\right). \quad \text{(A.2)}
\end{aligned}
$$

For the simplicity, we assume $t_{ij} \equiv t$ for i and j denoting the nearest neighbors. With the use of the projected operators notation (cf. Eqs. (1.18a)–(1.18c) and Eqs. (1.20a)–(1.20c)), expanded by,

$$
\begin{aligned}
\hat{B}^{\dagger}_{i\sigma} &= \hat{c}^{\dagger}_{i\sigma}\hat{n}_{i\bar{\sigma}}, && \text{(A.3a)}\\
\hat{B}_{i\sigma} &= \hat{c}_{i\sigma}\hat{n}_{i\bar{\sigma}}, && \text{(A.3b)}\\
\hat{d}_i &= \hat{n}_{i\uparrow}\hat{n}_{i\downarrow}, && \text{(A.3c)}\\
\hat{e}_i &= (1-\hat{n}_{i\uparrow})(1-\hat{n}_{i\downarrow}), && \text{(A.3d)}
\end{aligned}
$$

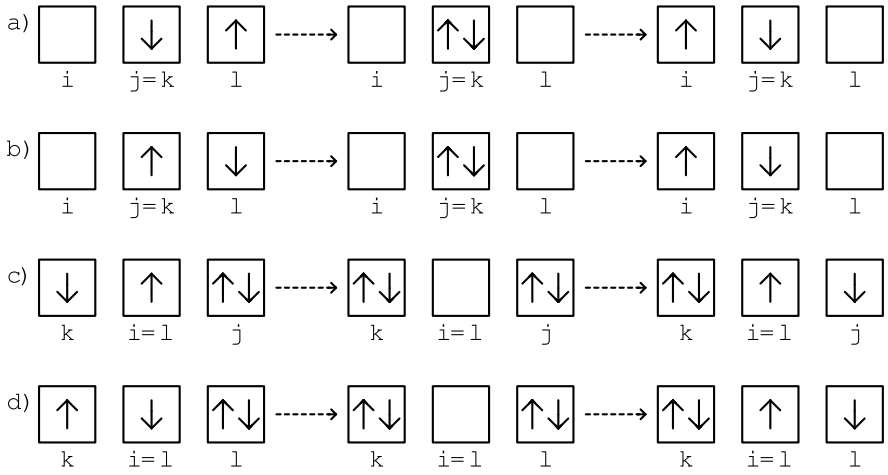

Figure A.1: *Examples of hopping processes involving three sites, described by Eq. (1.15c). The remaining four cases can be obtained by changing the spins to the opposite one,* $\uparrow \leftrightarrow \downarrow$.

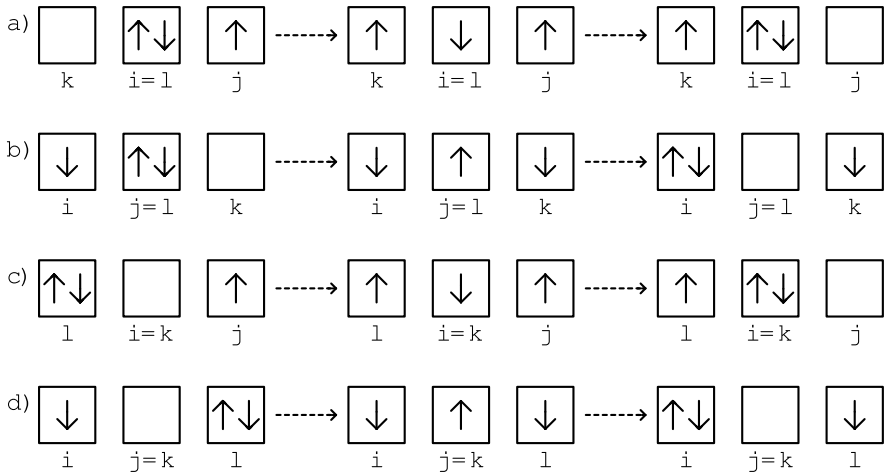

Figure A.2: *Examples of hopping processes involving three sites, described by Eq. (1.15d). The remaining four cases can be obtained by changing the spins to the opposite one,* $\uparrow \leftrightarrow \downarrow$.

we can write the t–J Hamiltonian with the three-site corrections in the following, compact form,

$$\hat{H}^{3\text{-site}} \approx U \sum_i \hat{d}_i + \frac{2t^2}{U} \sum_{\langle i,j\rangle,\sigma} \left(\hat{b}^\dagger_{i\sigma} \hat{b}_{j\sigma} + \hat{B}^\dagger_{i\sigma} \hat{B}_{j\sigma} + \hat{d}_i \hat{e}_j - \hat{c}^\dagger_{i\sigma} \hat{c}^\dagger_{i\bar{\sigma}} \hat{c}_{j\sigma} \hat{c}_{j\bar{\sigma}} - \hat{\nu}_{i\sigma} \hat{\nu}_{j\bar{\sigma}} + \hat{S}^\sigma_i \hat{S}^{\bar{\sigma}}_j \right) +$$
$$+ \frac{4t^2}{U} \sum_{\langle i,j,k\rangle,\sigma} \Big(- \hat{b}^\dagger_{i\sigma} \hat{\nu}_{j\bar{\sigma}} \hat{b}_{k\sigma} + \hat{b}^\dagger_{i\sigma} \hat{S}^{\bar{\sigma}}_j \hat{b}_{k\bar{\sigma}} + \hat{B}^\dagger_{i\sigma} \hat{\nu}_{j\sigma} \hat{B}_{k\sigma} + \hat{B}^\dagger_{i\bar{\sigma}} \hat{S}^\sigma_j \hat{B}_{k\sigma} +$$
$$- \hat{b}^\dagger_{i\sigma} \hat{d}_j \hat{b}_{k\sigma} - \hat{B}^\dagger_{i\sigma} \hat{c}_{j\sigma} \hat{c}_{j\bar{\sigma}} \hat{b}^\dagger_{k\bar{\sigma}} - \hat{B}_{i\bar{\sigma}} \hat{c}^\dagger_{j\sigma} \hat{c}^\dagger_{j\bar{\sigma}} \hat{b}_{k\sigma} + \hat{B}^\dagger_{i\sigma} e_j \hat{B}_{k\sigma} \Big). \quad \text{(A.4)}$$

Appendix B

Another example of Gutzwiller factor derivation

We show here how to derive the Gutzwiller factors for the term $\langle \hat{n}_{i\sigma}\hat{n}_{j\sigma'}\rangle$, in the presence of the AF order, motivated by fact, that this topic is rarely (if even) discussed in the literature. The AF order implies, that $n_{i\sigma} \equiv n_{j\bar{\sigma}} \equiv n_\sigma$ for i and j denoting the neighboring sites. In such case, using the notation presented in Section 2.1, we can calculate,

$$\begin{aligned}
\Lambda^{-1} \sum_{\langle i,j\rangle,\,\sigma,\,\sigma'} \langle \hat{n}_{i\sigma}\hat{n}_{j\sigma'}\rangle &= \Lambda^{-1} \sum_{\langle i,j\rangle,\,\sigma,\,\sigma'} \langle \hat{P}_i\hat{n}_{i\sigma}\hat{P}_i\hat{P}_j\hat{n}_{j\sigma'}\hat{P}_j\rangle_0 = \\
&= \Lambda^{-1} \sum_{\langle i,j\rangle,\,\sigma,\,\sigma'} \left\langle \left(\hat{n}_{i\sigma} + (\lambda_d^2-\lambda_\sigma^2)\hat{n}_{i\sigma}\hat{n}_{i\bar{\sigma}}^{HF}\right)\left(\hat{n}_{j\sigma'} + (\lambda_d^2-\lambda_{\bar{\sigma}'}^2)\hat{n}_{j\sigma'}\hat{n}_{j\bar{\sigma}'}^{HF}\right)\right\rangle_0 \\
&\approx \Lambda^{-1} \sum_{\langle i,j\rangle,\,\sigma} \langle n_{i\sigma}n_{j\sigma}\rangle_0 + \langle n_{i\sigma}n_{j\bar{\sigma}}\rangle_0 \\
&\quad + \Big(\langle \hat{n}_{j\bar{\sigma}}\rangle_0\langle \hat{n}_{i\bar{\sigma}}\hat{n}_{j\sigma}^{HF}\rangle_0 + \langle \hat{n}_{j\bar{\sigma}}\rangle_0\langle \hat{n}_{i\sigma}\hat{n}_{j\sigma}^{HF}\rangle_0 + \langle \hat{n}_{i\sigma}\rangle_0\langle \hat{n}_{j\sigma}\hat{n}_{i\bar{\sigma}}^{HF}\rangle_0 + \langle \hat{n}_{i\sigma}\rangle_0\langle \hat{n}_{j\bar{\sigma}}\hat{n}_{i\bar{\sigma}}^{HF}\rangle_0\Big)(\lambda_d^2-\lambda_\sigma^2) \\
&\quad + (\lambda_d^2-\lambda_\sigma^2)(\lambda_d^2-\lambda_{\bar{\sigma}}^2)\langle \hat{n}_{i\sigma}\rangle_0\langle \hat{n}_{j\sigma}\rangle_0\langle \hat{n}_{i\bar{\sigma}}^{HF}\hat{n}_{j\bar{\sigma}}^{HF}\rangle_0 + (\lambda_d^2-\lambda_\sigma^2)(\lambda_d^2-\lambda_\sigma^2)\langle \hat{n}_{i\sigma}\rangle_0\langle \hat{n}_{j\bar{\sigma}}\rangle_0\langle \hat{n}_{i\bar{\sigma}}^{HF}\hat{n}_{j\sigma}^{HF}\rangle_0 \\
&= 2n^2 + (-4\chi^2 + 4\Delta_S^2 + 4\Delta_T^2)\left(1 + n_\sigma(\lambda_d^2-\lambda_\sigma^2) + n_{\bar{\sigma}}(\lambda_d^2-\lambda_{\bar{\sigma}}^2)\right) \\
&\quad + 4n_\sigma(\lambda_d^2-\lambda_\sigma^2)n_{\bar{\sigma}}(\lambda_d^2-\lambda_{\bar{\sigma}}^2)(-\chi^2) + 2\left(\left[n_\sigma(\lambda_d^2-\lambda_\sigma^2)\right]^2 + \left[n_{\bar{\sigma}}(\lambda_d^2-\lambda_{\bar{\sigma}}^2)\right]^2\right)(\Delta_S^2+\Delta_T^2) \\
&= 2n^2 + 4g_v^\chi(-\chi^2) + 4g_v^\Delta(\Delta_S^2+\Delta_T^2),
\end{aligned} \tag{B.1}$$

where for the definition of χ, Δ_S and Δ_T cf. Eqs. (2.22)–(2.23), while the Gutzwiller factors g_v^χ and g_v have form,

$$g_v^\chi \equiv \left(1 + n_\sigma(\lambda_d^2-\lambda_\sigma^2) + n_{\bar{\sigma}}(\lambda_d^2-\lambda_{\bar{\sigma}}^2) + n_\sigma(\lambda_d^2-\lambda_\sigma^2)n_{\bar{\sigma}}(\lambda_d^2-\lambda_{\bar{\sigma}}^2)\right), \tag{B.2}$$

$$g_v^\Delta \equiv \left(1 + n_\sigma(\lambda_d^2-\lambda_\sigma^2) + n_{\bar{\sigma}}(\lambda_d^2-\lambda_{\bar{\sigma}}^2) + \frac{1}{2}\left(\left[n_\sigma(\lambda_d^2-\lambda_\sigma^2)\right]^2 + \left[n_{\bar{\sigma}}(\lambda_d^2-\lambda_{\bar{\sigma}}^2)\right]^2\right)\right). \tag{B.3}$$

Note, that the approximate sign in Eq. (B.1) results from the fact, that we neglected terms proportional to χ^4, Δ_S^4, Δ_T^4 or $n_\sigma n_{\bar{\sigma}}\chi^2$.

If AF order is not present, then $n_\sigma = n_{\bar{\sigma}} = n/2$ and the Eqs. (B.2)–(B.3) are simplified to the form,

$$g_v^\chi = g_v^\Delta = \left(\frac{2d^2 + n(1-n)}{n(1-n/2)}\right)^2. \tag{B.4}$$

Appendix C

Another example of Gutzwiller factors derivation ambiguity

We show here the Gutzwiller factors for $S_i^+ S_j^-$ term derived in the two schemes discussed in Section 2.2. For simplicity, we assume that only AF ordering is present (no CDW) and we assume that in the correlated state no doubly occupied states are allowed ($U \to \infty$).

The first scheme leads to

$$\langle S_i^+ S_j^- \rangle = g_s \sum_{\langle i,j \rangle} \langle S_i^+ S_j^- \rangle_0, \tag{C.1}$$

where (cf. Eqs. (2.18) or use tables 2.1 and 2.2 as it was presented in the Section 2.2),

$$g_s^{(1)} = \frac{1}{(1-n_{i\sigma})(1-n_{j\sigma})}, \tag{C.2}$$

while the second scheme leads to (use tables 2.1 and 2.2),

$$g_s^{(1)} = \left(\frac{n}{n - 2n_{i\sigma} n_{j\sigma}} \right). \tag{C.3}$$

When no AF order is considered, then $n_{i\sigma} \equiv n_{i\bar{\sigma}} \equiv n/2$, and

$$g_s^{(1)} \equiv g_s^{(2)} \equiv g_s = \frac{1}{\left(1 - \frac{n}{2}\right)^2}, \tag{C.4}$$

what is well know Gutzwiller factor for the spin exchange term (cf. Refs. [34,95,97,99]). However, when AF ordering is considered, then $g_s^{(1)} \neq g_s^{(2)}$, and the results differ in regard to the choice of $g_s^{(1)}$ or $g_s^{(2)}$.

Bibliography

[1] D. B. McWhan, T. M. Rice, and J. P. Remeika, Phys. Rev. Lett. **23**, 1384 (1969).

[2] D. B. McWhan and J. P. Remeika, Phys. Rev. B **2**, 3734 (1970).

[3] D. B. McWhan, A. Menth, J. P. Remeika, W. F. Brinkman, and T. M. Rice, Phys. Rev. B **7**, 1920 (1973).

[4] F. Rodolakis *et al.*, Phys. Rev. Lett. **104**, 047401 (2010).

[5] S. Lupi and et al., Nat. Commun. **1**, 105 (2010).

[6] J. Hubbard, Proc. R. Soc. A **276**, 238 (1963).

[7] J. Hubbard, Proc. R. Soc. A **281**, 401 (1964).

[8] P. W. Anderson, Phys. Rev. **115**, 2 (1959).

[9] J. Spałek, Acta. Phys. Pol. A **111**, 409 (2007).

[10] N. F. Mott, Rev. Mod. Phys. **40**, 677 (1968).

[11] N. F. Mott, *Metal-Insulator Transitions 2nd edn* (London: Taylor and Francis, 1990).

[12] M. Imada, A. Fujimori, and Y. Tokura, Rev. Mod. Phys. **70**, 1039 (1998).

[13] J. Bardeen, L. N. Cooper, and J. R. Schrieffer, Phys. Rev. **106**, 162 (1957).

[14] D. C. Johnston, Supercond. Sci. Technol **26**, 115011 (2013).

[15] J. Spałek, *Wstęp do fizyki fazy skondensowanej* (Warszawa, PWN, 2015), (in Polish).

[16] N. E. Phillips, Phys. Rev. **114**, 676 (1959).

[17] P. J. Ray, *Structural investigation of La(2-x)Sr(x)CuO(4+y) – Following staging as a function of temperature*, Master's thesis, Niels Bohr Institute, Faculty of Science, University of Copenhagen, 2011.

[18] R. B. van Dover, R. J. Cava, B. Batlogg, and E. A. Rietman, Phys. Rev. B **35**, 5337 (1987).

[19] M. K. Wu *et al.*, Phys. Rev. Lett. **58**, 908 (1987).

[20] Z. Z. Sheng *et al.*, Phys. Rev. Lett. **60**, 937 (1988).

[21] S. N. Putilin, E. V. Antipov, O. Chmaissem, and M. Mareziow, Nature **362**, 226 (1993).

[22] A. Schilling, M. Cantoni, J. D. Guo, and H. R. Ott, Mature **363**, 56 (1993).

[23] Z. J. Huang *et al.*, Physica C: Supercond. **217**, 1 (1993).

[24] A. Yamamoto, N. Takeshita, C. Terakura, and Y. Tokura, Nat. Commun. **6**, 8990 (2015).

[25] J. G. Bednorz and K. A. Müller, Physik B Condensed Matter **64**, 189 (1986).

[26] H. Takagi, S. ichi Uchida, K. Kitazawa, and S. Tanaka, Japanese Journal of Applied Physics **26**, L123 (1987).

[27] L. Gao *et al.*, Phys. Rev. B **50**, 4260 (1994).

[28] M. Monteverde *et al.*, Europhys. Lett. **72**, 458 (2005).

[29] N. C. S. of Science and Mathematic, Teachers' Instructional Graphic Educational Resource, 2003, online access: `http://www.dlt.ncssm.edu/tiger/chem8.htm` (6th April 2016).

[30] Wikibooks, High School Chemistry/Shapes of Atomic Orbitals, 2015, online access: `https://en.wikibooks.org/w/index.php?title=High_School_Chemistry/Shapes_of_Atomic_Orbitals&oldid=2991510` (6th April 2016).

[31] N. Plakida, *High-Temperature Cuprate Superconductors* (Springer, 2010), Chapters 5, 7.

[32] E. Pavarini, E. Koch, F. Anders, and M. E. . Jarrell, *Correlated electrons: from models to materials*, Schriften des Forschungszentrums Jülich. Reihe Modeling and simulation Vol. 2 (Forschungszentrum Jülich GmbH, Jülich, 2012), Chapter 6, Crystal-Field Theory, Tight-Binding Method and Jahn-Teller Effect.

[33] P. W. Anderson, Science **235**, 1196 (1987).

[34] F. C. Zhang and T. M. Rice, Phys. Rev. B **37**, 3759 (1988).

[35] W. E. Pickett, Rev. Mod. Phys. **61**, 433 (1989).

[36] L. F. Mattheiss, Phys. Rev. Lett. **58**, 1028 (1987).

[37] A. Damascelli, Z. Hussain, and Z.-X. Shen, Rev. Mod. Phys. **75**, 473 (2003).

[38] D. N. Basov and a. V. Chubukov, Nature Publishing Group **7**, 272 (2011).

[39] J. Spatek and A. M. Oleś, Physica B+C **86-88**, 375 (1977), (the jurnal made a a mistake in the authors names; it should be "Spałek" and "Oleś").

[40] K. A. Chao, J. Spalek, and A. M. Oles, Journal of Physics C: Solid State Physics **10**, L271 (1977).

[41] K. A. Chao, J. Spałek, and A. M. Oleś, Phys. Rev. B **18**, 3453 (1978).

[42] J. Spalek, A. M. Oleś, and K. A. Chao, Phys. Status Solidi B **108**, 329 (1981).

[43] J. Spałek, Phys. Rev. B **37**, 533 (1988).

[44] J. Spałek and J. M. Honig, *Metal-Insulator Transitions, Exchange Interactions, and Real Space Pairing* (Vol. 8, Nova Science Publishers, editor A. Narlikar, 1991), pp. 1–67.

[45] L. F. Feiner, J. H. Jefferson, and R. Raimondi, Phys. Rev. B **53**, 8751 (1996).

[46] M. Abram, Selected methods of correlated particles applied to atomic systems in optical lattices, Master's thesis, MSc Thesis, Jagiellonian University, 2011, (in Polish).

[47] H. Eskes and A. M. Oleś, Phys. Rev. Lett. **73**, 1279 (1994).

[48] H. Eskes, A. M. Oleś, M. B. J. Meinders, and W. Stephan, Phys. Rev. B **50**, 17980 (1994).

[49] J. Jędrak, *Real-space pairing in an extended t-J model*, PhD thesis, Jagiellonian University, Kraków, Poland, 2011, online access: `http://th-www.if.uj.edu.pl/ztms/eng/phdTheses.php`.

[50] M. Ogata, J. Phys. Soc. Jpn. **72**, 1839 (2003).

[51] M. Abram, Acta Phys. Pol. A **126**, A (2014).

[52] S. Uchida, *High-Temperature Cuprate Superconductivity: The Road to Higher Critical Temperature* (Springer, 2015).

[53] M. Abram, J. Kaczmarczyk, J. Jędrak, and J. Spałek, Phys. Rev. B **88**, 094502 (2013).

[54] R. Eder, Y. Ohta, and G. A. Sawatzky, Phys. Rev. B **55**, R3414 (1997).

[55] A. Nazarenko, K. J. E. Vos, S. Haas, E. Dagotto, and R. J. Gooding, Phys. Rev. B **51**, 8676 (1995).

[56] V. I. Belinicher, A. L. Chernyshev, and V. A. Shubin, Phys. Rev. B **54**, 14914 (1996).

[57] B. Kyung and R. A. Ferrell, Phys. Rev. B **54**, 10125 (1996).

[58] T. Xiang and J. M. Wheatley, Phys. Rev. B **54**, R12653 (1996).

[59] T. K. Lee and C. T. Shih, Phys. Rev. B **55**, 5983 (1997).

[60] T. Tohyama, S. Nagai, Y. Shibata, and S. Maekawa, Phys. Rev. Lett. **82**, 4910 (1999).

[61] J. Y. Gan, Y. Chen, Z. B. Su, and F. C. Zhang, Phys. Rev. Lett. **94**, 067005 (2005).

[62] V. J. Emery, Phys. Rev. Lett. **58**, 2794 (1987).

[63] J. Spałek and M. Zegrodnik, (unpublished).

[64] E. J. W. Verwey, Nature **144**, 327 (1939).

[65] E. J. W. Verwey and P. W. Haayman, Physica **8**, 979 (1941).

[66] J. P. Attfield, Solid State Sciences **8**, 861 (2006).

[67] J. M. Tranquada, B. J. Sternlieb, J. D. Axe, Y. Nakamura, and S. Uchida, Nature **375**, 561 (1995).

[68] J. M. Tranquada, Physica C: Supercond. **282–287, Part 1**, 166 (1997).

[69] G. Ghiringhelli *et al.*, Science **337**, 821 (2012).

[70] R. Comin *et al.*, Science **343**, 390 (2014).

[71] E. H. da Silva Neto *et al.*, Science **343**, 393 (2014).

[72] J. Chang *et al.*, Nature Physics **8**, 871 (2012).

[73] M. Hücker *et al.*, Phys. Rev. B **90**, 054514 (2014).

[74] S. Blanco-Canosa *et al.*, Phys. Rev. B **90**, 054513 (2014).

[75] A. Amaricci, A. Camjayi, K. Haule, and G. Kotliar, Phys. Rev. B **82**, 155102 (2010).

[76] S. Sachdev and R. La Placa, Phys. Rev. Lett. **111**, 027202 (2013).

[77] A. Allais, J. Bauer, and S. Sachdev, Phys. Rev. B **90**, 155114 (2014).

[78] P. Corboz, T. M. Rice, and M. Troyer, Phys. Rev. Lett. **113**, 046402 (2014).

[79] W.-L. Tu and T.-K. Lee, Scientific Reports **6** (2016).

[80] K. Fujita *et al.*, Proceedings of the National Academy of Sciences **111**, E3026 (2014).

[81] J.-X. Li, C.-Q. Wu, and D.-H. Lee, Physical Review B **74**, 1 (2006).

[82] M.-H. Julien, Science **350**, 914 (2015).

[83] S. Gerber *et al.*, Science **350**, 949 (2015).

[84] T. Hanaguri *et al.*, Nature **430**, 1001 (2004).

[85] W. D. Wise *et al.*, Nature Physics **4**, 5 (2008).

[86] G. Campi *et al.*, Nature **525**, 359 (2015).

[87] E. W. Carlson, Nature **525**, 329 (2015).

[88] E. Fradkin, S. A. Kivelson, and J. M. Tranquada, Rev. Mod. Phys. **87**, 457 (2015).

[89] W. D. Wise *et al.*, Nature Physics **4**, 696 (2008).

[90] K. M. Shen *et al.*, Science **307**, 901 (2005).

[91] M. Abram, M. Zegrodnik, and J. Spałek, arXiv: , 1607.05399 (2016).

[92] M. C. Gutzwiller, Phys. Rev. Lett. **10**, 159 (1963).

[93] M. C. Gutzwiller, Phys. Rev. **137**, A1726 (1965).

[94] J. Bünemann, T. Schickling, and F. Gebhard, EPL (Europhysics Letters) **98**, 27006 (2012).

[95] T. Ogawa, K. Kanda, and T. Matsubara, Prog. Theor. Phys. **53**, 614 (1975).

[96] D. Vollhardt, Rev. Mod. Phys. **56**, 99 (1984).

[97] M. Ogata and H. Fukuyama, Reports on Progress in Physics **71**, 036501 (2008).

[98] B. Edegger, V. N. Muthukumar, and C. Gros, Adv. Phys. **56**, 927 (2007).

[99] R. Eder, J. van den Brink, and G. A. Sawatzky, Phys. Rev. B **54**, R732 (1996).

[100] J. Kaczmarczyk, J. Spałek, T. Schickling, and J. Bünemann, Phys. Rev. B **88**, 115127 (2013).

[101] J. Kaczmarczyk, J. Bünemann, and J. Spałek, New J. Phys. **16**, 073018 (2014).

[102] J. Kaczmarczyk, T. Schickling, and J. Bünemann, Phys. Status Solidi B **252**, 2059 (2015).

[103] M. M. Wysokiński, J. Kaczmarczyk, and J. Spałek, Phys. Rev. B **92**, 125135 (2015).

[104] J. Jędrak, J. Kaczmarczyk, and J. Spałek, 1008.0021.

[105] J. Jędrak and J. Spałek, Phys. Rev. B **81**, 073108 (2010).

[106] J. Jędrak and J. Spałek, Phys. Rev. B **83**, 104512 (2011).

[107] J. Kaczmarczyk and J. Spałek, Phys. Rev. B **84**, 125140 (2011).

[108] O. Howczak, J. Kaczmarczyk, and J. Spałek, Phys. Stat. Solidi (b) **250**, 609 (2013).

[109] A. P. Kądzielawa, J. Spałek, J. Kurzyk, and W. Wójcik, Eur. Phys. J. B **86**, 252 (2013).

[110] M. M. Wysokiński and J. Spałek, J. Phys.: Condens. Matter **26**, 055601 (2014).

[111] M. M. Wysokiński, M. Abram, and J. Spałek, Phys. Rev. B **90**, 081114(R) (2014).

[112] M. M. Wysokiński, M. Abram, and J. Spałek, Phys. Rev. B **91**, 081108 (2015).

[113] M. Abram, M. M. Wysokiński, and J. Spałek, J. Magn. Magn. Mater. **400**, 27 (2016).

[114] K. Andres, J. E. Graebner, and H. R. Ott, Phys. Rev. Lett. **35**, 1779 (1975).

[115] G. R. Stewart, Rev. Mod. Phys. **56**, 755 (1984).

[116] A. Auerbach and K. Levin, J. Appl. Phys. **61**, 3162 (1987).

[117] A. Kołodziejczyk, B. V. Sarkissian, and B. R. Coles, J. Phys. F **10**, L333 (1980).

[118] A. Kołodziejczyk, Physica B **130**, 189 (1985).

[119] K. Rogacki, A. Kołodziejczyk, L. Bochenek, and T. Cichorek, Phil. Mag. **95**, 503 (2015).

[120] S. S. Saxena *et al.*, Nature **406**, 587 (2000).

[121] C. Pfleiderer, Rev. Mod. Phys. **81**, 1551 (2009), (chapter III. A).

[122] D. Aoki and J. Flouquet, J. Phys. Soc. Jpn. **81**, 011003 (2012).

[123] D. Aoki *et al.*, C. R. Physique **15**, 630 (2014).

[124] D. Aoki and J. Flouquet, J. Phys. Soc. Jpn. **83** (2014).

[125] A. D. Huxley, Physica C **514**, 368 (2015).

[126] D. Aoki *et al.*, Nature **413**, 613 (2001).

[127] N. T. Huy *et al.*, Phys. Rev. Lett. **99**, 067006 (2007).

[128] C. Pfleiderer and A. D. Huxley, Phys. Rev. Lett. **89**, 147005 (2002).

[129] V. Taufour, D. Aoki, G. Knebel, and J. Flouquet, Phys. Rev. Lett. **105**, 217201 (2010).

[130] R. Roussev and A. J. Millis, Phys. Rev. B **63**, 140504 (2001).

[131] T. R. Kirkpatrick, D. Belitz, T. Vojta, and R. Narayanan, Phys. Rev. Lett. **87**, 127003 (2001).

[132] H. Suhl, Phys. Rev. Lett. **87**, 167007 (2001).

[133] A. A. Abrikosov, J. Phys: Condens. Matter **13**, L943 (2001).

[134] K. Machida and T. Ohmi, Phys. Rev. Lett. **86**, 850 (2001).

[135] D. Sa, Phys. Rev. B **66**, 140505 (2002).

[136] S. Watanabe and K. Miyake, J. Phys. Soc. Jpn. **71**, 2489 (2002).

[137] K. G. Sandeman, G. G. Lonzarich, and A. J. Schofield, Phys. Rev. Lett. **90**, 167005 (2003).

[138] K. Hirohashi and K. Ueda, J. Phys. Soc. Jpn. **73**, 1576 (2004).

[139] K. Kubo, Phys. Rev. B **87**, 195127 (2013).

[140] M. Zegrodnik and J. Spałek, Phys. Rev. B **86**, 014505 (2012).

[141] J. Spałek and M. Zegrodnik, J. Phys.: Condens. Matter **25**, 435601 (2013).

[142] M. Zegrodnik, J. Spałek, and J. Bünemann, New J. Phys. **15**, 073050 (2013).

[143] M. Zegrodnik, J. Bünemann, and J. Spałek, New J. Phys. **16**, 033001 (2014).

[144] H. Kotegawa, V. Taufour, D. Aoki, G. Knebel, and J. Flouquet, J. Phys. Soc. Jpn. **80**, 083703 (2011).

Part II

Research Papers

List of published articles related to the Thesis

1. Marcin Abram, Jan Kaczmarczyk, Jakub Jędrak, and Józef Spałek, *d-wave superconductivity and its coexistence with antiferromagnetism in t–J–U model: Statistically consistent Gutzwiller approach*, Physical Review B **88**, 094502 (2013), 10 pages, 7 figures.

2. Marcin Abram, *t–t′–J–U Model in Mean-Field Approximation: Coexistence of Superconductivity and Antiferromagnetism*, Acta Physica Polonica A **126** (2014), 5 pages, 6 figures.

3. Marcin M. Wysokiński, Marcin Abram, and Józef Spałek, *Ferromagnetism in UGe_2: A microscopic model*, Physical Review B **90**, 081114(R) (2014), 5 pages, 3 figures.

4. Marcin M. Wysokiński, Marcin Abram, and Józef Spałek, *Criticalities in the itinerant ferromagnet UGe_2*, Physical Review B **91**, 081108(R) (2015), 5 pages, 3 figures.

5. Marcin Abram, Marcin M. Wysokiński, and Józef Spałek, *Tricritical wings in UGe_2: A microscopic interpretation*, Journal of Magnetism and Magnetic Materials **400**, 27 (2016), 4 pages, 4 figures.

Preprints

6. Marcin Abram, Michał Zegrodnik, and Józef Spałek, *Antiferromagnetism, charge density wave and d-wave superconductivity in the t–J–U–V model of correlated electrons*, arXiv:1607.05399 (2016), 13 pages, 6 figures.

Additional article

7. Andrzej Kapanowski and Marcin Abram, *Model of hard spheroplatelets near a hard wall*, Physical Review E **89**, 062503 (2014), 9 pages, 9 figures.

Article 1

In this article we introduce the t–J–U model and apply it to the discussion of the coexistence of hight temperature superconductivity (HTS) with the two-sublattice antiferromagnetism (AF). We use the statistically consistent Gutzwiller approximation (SGA) and discuss two alternative ways of implementing it. The AF phase appears only in a very narrow range of doping $\delta \lesssim 0.006$, i.e., in the close vicinity to the Mott insulating state appearing for $\delta = 0$ ($n = 1$). The upper hole doping $\delta \approx 0.3$ for the disappearance of the HTS state has also been discussed as a function of U. We also stress that in the AF-SC coexistent phase, a small spin-triplet component of the pairing appears. Self-consistent calculations of order parameters and remaining renormalized characteristics such as the hopping amplitudes and the chemical potential require solving system of 6 integral equations. All the calculated characteristics are listed for exemplary values of the microscopic parameters in Table I.

d-wave superconductivity and its coexistence with antiferromagnetism in the *t*–*J*–*U* model: Statistically consistent Gutzwiller approach

M. Abram,[1,*] J. Kaczmarczyk,[1] J. Jędrak,[2] and J. Spałek[1,3,†]

[1]*Marian Smoluchowski Institute of Physics, Jagiellonian University, Reymonta 4, 30-059 Kraków, Poland*

[2]*Faculty of Non-Ferrous Metals, AGH University of Science and Technology, Al. Mickiewicza 30, 30-059 Kraków, Poland*

[3]*Academic Centre for Materials and Nanotechnology, Faculty of Physics and Applied Computer Science, AGH University of Science and Technology, Reymonta 19, 30-059 Kraków, Poland*

(Received 8 May 2013; revised manuscript received 16 July 2013; published 3 September 2013)

We discuss the coexistence of antiferromagnetism and *d*-wave superconductivity within the so-called statistically consistent Gutzwiller approximation (SGA) applied to the *t*–*J*–*U* model. In this approach, the averages calculated in a self-consistent manner coincide with those determined variationally. Such consistency is not guaranteed within the standard renormalized mean-field theory. With the help of SGA, we show that for the typical value $J/|t| = \frac{1}{3}$, coexistence of antiferromagnetism (AF) and superconductivity (SC) appears only for $U/|t| > 10.6$ and in a very narrow range of doping ($\delta \lesssim 0.006$) in the vicinity of the Mott insulating state, in contrast to some previous reports. In the coexistent AF + SC phase, a staggered spin-triplet component of the superconducting gap appears also naturally; its value is very small.

DOI: 10.1103/PhysRevB.88.094502 PACS number(s): 71.27.+a, 74.25.Dw, 74.72.Gh

I. INTRODUCTION: RATIONALE FOR *t*–*J*–*U* MODEL

High-temperature superconductivity in cuprates is often described within the effective *t*–*J* model[1,2] (for a preliminary treatment of the topic cf. also Ref. 3). The model justifies a number of experimental results, such as superconductivity's domelike shape on doping-temperature phase diagram,[4] non-Fermi-liquid behavior of the normal state for underdoped and optimally doped systems,[5–7] the disappearance of the pairing gap magnitude in the antiferromagnetic state (albeit only at the doping $\delta = 0$),[7,8] and the doping dependence of the photoemission spectrum in the antinodal direction.[9,10] All of these features represent an attractive starting point for further analysis (cf. Ref. 11).

In the effective *t*–*J* model, the value of the kinetic exchange integral J_{ij} does not necessarily coincide with the value $J_{ij} = 4t_{ij}^2/U$ obtained perturbationally from the Hubbard model.[2] Instead, it expresses an effective coupling between the copper spins in mixed copper-oxygen $3d$-$2p$ holes.[12] Therefore, one may say that the values of the hopping integral t_{ij} and that of antiferromagnetic exchange J_{ij} in that model are practically independent. Typically, the ratio $|t|/J \approx 3$ is taken and corresponds to the value $U/(8|t|) = 1.5$ in the context of the two-dimensional Hubbard model. However, after introducing the bare bandwidth $W = 8|t|$ in the tight-binding approximation for a square lattice, we obtain the ratio $U/W = 1.5$, which is not sufficiently large for the transformation of the original Hubbard model into the *t*–*J* model to be valid in the low order. In that situation, we are, strictly speaking, not within the strong correlation limit $U/W \gg 1$, in which the *t*–*J* model was originally derived.[1,2]

In order to account properly for the strong electronic correlations (the bare Hubbard parameter U for Cu^{2+} ion is 8–10 eV $\gg W \approx$ 2–3 eV), we can add the Hubbard term $U\sum_i \hat{n}_{i\uparrow}\hat{n}_{i\downarrow}$ to the *t*–*J* model. In this manner, we consider the exchange integral J_{ij} in this still-effective single-band model as coming from the full superexchange involving the oxygen ions rather than from the effective kinetic exchange only (for critical overview, cf. Ref. 13). This argument may be regarded as one of the justifications for introducing the *t*–*J*–*U* model, first used by Daul,[14] Basu,[15] and Zhang[16] (cf. Ref. 17, where comprehensive justification of the *t*–*J*–*U* is provided).

There is an additional reason for the *t*–*J*–*U* model applicability to the cuprates. Namely, in the starting, bare configuration of CuO_2^{2-} structural unit, the hybridization between the antibonding $2p_\sigma$ states due to oxygen and one-hole ($3d^9$) states due to Cu is strong, with the hybridization matrix element $|V_{\langle im\rangle}| \sim 1.5$ eV. Therefore, the hybridization contribution to the hole state itinerancy, at least on the single-particle level, is essential and hence the effective *d*–*d* (Hubbard) interaction is substantially reduced. In effect, we may safely assume that $U \gtrsim W$ instead $U \gg W$. In this manner, the basic simplicity of the single-band model is preserved, as it provides not only the description of the strongly correlated metallic state close to the Mott insulating limit, but also reduces to the correct limit of the Heisenberg magnet of spin $\frac{1}{2}$ with strong antiferromagnetic exchange integral $J \approx 0.1$ eV in the absence of holes (the Mott-Hubbard insulating state). Last but not least, within the present model we can study the limit $U \to \infty$ and compare explicitly the results with those of canonical *t*–*J* model.

Antiferromagnetism (AF) and superconductivity (SC) can coexist in the *electron-doped* cuprates,[18,19] but in the *hole-doped* cuprates the two phases are usually separated (cf., e.g., the review of Dagotto[4]). However, in the late 1990s, reports of a possible coexistence in the cuprates appeared, first vague [cf. Ref. 20 ($La_{2-x}Sr_xCu_{1-y}Zn_yO_4$)], then more convincing [cf., e.g., Ref. 21 (La_2CuO_{4+y}), Ref. 22 ($YBa_2Cu_3O_{6.5}$), or Ref. 23 ($YBa_2(Cu_{0.987}Co_{0.013})_3O_{y+\delta}$)]. Other systems, where the coexistence has been reported, are organic superconductors,[24] heavy-fermion systems,[25] iron-based superconductors such as $Ba(Fe_{1-x}Ru_x)_2As_2$ (Ref. 26), $Ba_{0.77}K_{0.23}Fe_2As_2$ (Ref. 27), $Ba(Fe_{1-x}Co_x)_2As_2$ (Refs. 28 and 29), as well as graphene bilayer systems (cf. Ref. 30).

Our purpose is to undertake a detailed analysis of the paired (SC) state within the *t*–*J*–*U* model and its coexistence with the two-sublattice antiferromagnetism in two dimensions. Detailed studies of the *t*–*J*–*U* model have been carried out by

Zhang,[16] Gan,[31,32] and Bernevig[33] who described a transition from gossamer[34] and d-wave[35,36] superconductivity to the Mott insulator. However, the existence of AF order was not considered in those studies. Some attempts to include AF order were made by Yuan[37] and Heiselberg,[38] and very recently by Voo[39] and Liu,[40] but in all those works one can question the authors' approach. Specifically, the equations used do not guarantee self-consistency, i.e., the mean-field averages introduced in a self-consistent manner do not match those determined variationally.[41] We show that the above problem that appears in the renormalized mean-field theory (RMFT) formulation can be overcome by introducing constraints that ensure the statistical consistency between the two above ways of determining mean-field values. This is the principal concept of our *statistically consistent Gutzwiller approach* (SGA).[42,43]

Using SGA we obtain that the AF phase is stable only in the presence of SC in a very narrow region close to the Mott-Hubbard insulating state, corresponding to the half-filled (undoped) situation. Additionally, in this AF-SC coexisting phase, a small staggered spin-triplet component of the superconducting gap appears naturally, in addition to the predominant spin-singlet component.

The structure of the paper is as follows. In Sec. II, we define the model and provide definitions of the mean-field parameters. In Sec. III, we introduce the constraints with the corresponding Lagrange multipliers to guarantee the consistency of the self-consistent and the variational procedures of determining the mean-field parameters. The full minimization procedure is also outlined there. In Sec. IV, we discuss the numerical results, as well as provide the values of the introduced Lagrange multipliers. In Sec. V, we summarize our results and compare them with those of other studies. In Appendix A, we discuss the general form of the hopping amplitude and the superconducting gap, as well as some details of the analytic calculations required to determine the ground-state energy. In Appendixes B and C, we show some details of our calculations. In Appendix D, we present an alternative and equivalent procedure of introducing the Lagrange multipliers to that presented in the main text. In Appendix E, we list representative values of the parameters calculated for different phases.

II. t–J–U MODEL AND EFFECTIVE SINGLE-PARTICLE HAMILTONIAN

We start from the t–J–U model as represented by the Hamiltonian[16,31,32]

$$\hat{\mathcal{H}} = t \sum_{\langle i\,j\rangle,\,\sigma} (\hat{c}^{\dagger}_{i\sigma}\hat{c}_{j\sigma} + \text{H.c.}) + J \sum_{\langle i\,j\rangle} \hat{\mathbf{S}}_i \cdot \hat{\mathbf{S}}_j + U \sum_i \hat{n}_{i\uparrow}\hat{n}_{i\downarrow}, \tag{1}$$

where $\sum_{\langle i\,j\rangle}$ denotes the summation over the nearest-neighboring sites, t is the nearest-neighbor hopping integral, J is the effective antiferromagnetic exchange integral, $\hat{\mathbf{S}}_i$ is the spin operator in the fermion representation, and U is the onsite Coulomb repulsion magnitude.

One methodological remark is in place here. Usually, when starting from the Hubbard or t–J models and discussing subsequently the correlated states and phases, one neglects the intersite repulsive Coulomb interaction $\sim K \sum_{\langle ij\rangle} \hat{n}_i\hat{n}_j$, where $\hat{n}_i = \sum_\sigma \hat{n}_{i\sigma}$ is the number of particles on site i. In the strong-correlation limit $U \gg W$, the corresponding transformation to the effective t–J model provides[2] the effective exchange integral $J_{ij} = 4t_{ij}^2/(U-K)$, and since $K \sim U/3$, we have a strong enhancement ($\sim$30%) of the kinetic exchange integral. Strictly speaking, the contribution $\sim K$ should be then also added to the effective Hamiltonian (1). However, this term has been neglected, as well as the similar contribution $\sim (J/4)\sum_{\langle ij\rangle} \hat{n}_i\hat{n}_j$ appearing in the full Dirac exchange operator[2] since we assume that the physically meaningful regime is that with $U \gtrsim W \gg K$ so that any charge-density-wave instability is irrelevant in this limit.

We study properties of the above Hamiltonian using the Gutzwiller variational approach,[44] in which the trial wave function has the form[34,37,38] $|\Psi\rangle = \hat{P}_G|\Psi_0\rangle$, where $\hat{P}_G$ is an operator specifying explicitly the configurations with double onsite occupancies, and $|\Psi_0\rangle$ is an eigenstate of a single-particle Hamiltonian (to be defined later). Since the correlated state $|\Psi\rangle$ is related to $|\Psi_0\rangle$, the average value of the Hamiltonian $\hat{\mathcal{H}}$ can be expressed as

$$\frac{\langle\Psi|\hat{\mathcal{H}}|\Psi\rangle}{\langle\Psi|\Psi\rangle} = \frac{\langle\Psi_0|\hat{P}_G\hat{\mathcal{H}}\hat{P}_G|\Psi_0\rangle}{\langle\Psi_0|\hat{P}_G^2|\Psi_0\rangle} \approx \langle\Psi_0|\hat{\mathcal{H}}_{\text{eff}}|\Psi_0\rangle \equiv \langle\hat{\mathcal{H}}_{\text{eff}}\rangle_0, \tag{2}$$

where $\langle\ldots\rangle_0$ means the average evaluated with respect to $|\Psi_0\rangle$, and[16,31,32,37,38]

$$\hat{\mathcal{H}}_{\text{eff}} = g_t t \sum_{\langle i\,j\rangle,\,\sigma} (\hat{c}^{\dagger}_{i\sigma}\hat{c}_{j\sigma} + \text{H.c.}) + g_s J \sum_{\langle i\,j\rangle} \hat{\mathbf{S}}_i \cdot \hat{\mathbf{S}}_j + U d^2 \tag{3}$$

is the effective Hamiltonian resulting from the Gutzwiller approximation[44] (GA). In the above formula, $d^2 \equiv \langle\hat{n}_{i\uparrow}\hat{n}_{i\downarrow}\rangle_0$ is the double-occupancy probability, g_t and g_s are the so-called Gutzwiller renormalization factors determined by the statistical counting of configuration with given Nd^2, Nw, and Nr (cf. Refs. 45 and 46):

$$g_t = \frac{n-2d^2}{n-2rw}\left(\sqrt{\frac{(1-w)(1-n+d^2)}{1-r}} + \sqrt{\frac{wd^2}{r}}\right) \times \left(\sqrt{\frac{(1-r)(1-n+d^2)}{1-w}} + \sqrt{\frac{rd^2}{w}}\right), \tag{4a}$$

$$g_s = \left(\frac{n-2d^2}{n-2rw}\right)^2, \tag{4b}$$

where n is the average number of electrons (occupancy) per site. To discuss AF order, the lattice is divided into two interpenetrating sublattices: A, where the majority of spins are oriented $\uparrow$, and B, where the majority of spins are oriented $\downarrow$. For sublattice A, $r \equiv \langle\hat{n}_{i\uparrow}\rangle = \frac{1}{2}(n + m_{\text{AF}})$ and $w \equiv \langle\hat{n}_{i\downarrow}\rangle = \frac{1}{2}(n - m_{\text{AF}})$, where m_{AF} is the antiferromagnetic (staggered) spin polarization per site. For sublattice B, the definitions of w and r are interchanged. Note that the Gutzwiller factor (4b) has the same form for both $\frac{1}{2}(\hat{S}_i^x\hat{S}_j^y + \hat{S}_i^y\hat{S}_j^x)$ and $\hat{S}_i^z\hat{S}_j^z$ parts of $\hat{\mathbf{S}}_i \cdot \hat{\mathbf{S}}_j$. In a refined approach, two distinct Gutzwiller factors g_s^{xy} and g_x^z may be considered (cf. Ref. 47). However, in this paper it is assumed that $g_s^{xy} = g_x^z \equiv g_s$, which is broadly

accepted (see, e.g., Refs. 16,31,32,37, and 38). The reason is that the spin-singlet paired state is spin-rotationally invariant and in the case of coexistent antiferromagnetic state we limit ourselves to the mean-field-approach paradigm with the resulting Néel state.

In order to evaluate $\langle\hat{\mathcal{H}}_{\rm eff}\rangle_0$, we define the average number of electrons per site with spin σ as

$$n_{i\sigma} \equiv \langle \hat{c}^{\dagger}_{i\sigma}\hat{c}_{i\sigma}\rangle_0 = \tfrac{1}{2}(n + \sigma\, e^{i\mathbf{Q}\cdot\mathbf{R}_i}\, m_{\rm AF}), \tag{5}$$

with $\mathbf{Q} \equiv (\pi,\pi)$, and with $\mathbf{R}_i$ denoting position vector of site i and the following bare (nonrenormalized) quantities: the hopping amplitude for the nearest neighbors $\langle i,j\rangle$ as

$$\chi_{ij\sigma} \equiv \langle \hat{c}^{\dagger}_{i\sigma}\hat{c}_{j\sigma}\rangle_0 = \chi_{AB}, \tag{6}$$

and the pairing order parameter in real space in the form

$$\Delta_{ij\sigma} \equiv \langle \hat{c}_{i\sigma}\hat{c}_{j\bar{\sigma}}\rangle_0 \equiv -\tau_{ij}(\sigma\Delta_S + e^{i\mathbf{Q}\cdot\mathbf{R}_i}\Delta_T), \tag{7}$$

where $\tau_{ij} \equiv 1$ for $j = i \pm \hat{x}$ and $\tau_{ij} \equiv -1$ for $j = i \pm \hat{y}$ (in order to ensure the d-wave symmetry). In consequence, the spin-singlet (Δ_S) and the spin-triplet (Δ_T) components of the gap are defined as

$$\begin{aligned}\tau_{ij}\Delta_S &= \tfrac{1}{4}(\langle \hat{c}_{j\in B\downarrow}\hat{c}_{i\in A\uparrow}\rangle_0 + \langle \hat{c}_{i\in A\downarrow}\hat{c}_{j\in B\uparrow}\rangle_0 + \text{H.c.}) \\ &= \tfrac{1}{4}\tau_{ij}(\Delta_A + \Delta_B + \text{H.c.}), \qquad (8a)\\ \tau_{ij}\Delta_T &= \tfrac{1}{4}(\langle \hat{c}_{j\in B\downarrow}\hat{c}_{i\in A\uparrow}\rangle_0 - \langle \hat{c}_{i\in A\downarrow}\hat{c}_{j\in B\uparrow}\rangle_0 + \text{H.c.}) \\ &= \tfrac{1}{4}\tau_{ij}(\Delta_A - \Delta_B + \text{H.c.}). \qquad (8b)\end{aligned}$$

In some works (e.g., in Refs. 37 and 38), the triplet component is disregarded. However, since Δ_A represents an average pairing for *majority spins* on nearest-neighboring sites and Δ_B an average pairing of *minority spins* (when AF order is present, cf. Fig. 1), the real part of Δ_A and Δ_B might be different (cf. also the work of Tsonis[48] and Aperis[49] regarding the inadequacy of a single-component order parameter to describe the SC phase). Therefore, in this paper, this more comprehensive structure is introduced. Nonetheless, in order to evaluate the significance of introducing the triplet term for the SC gap, the results are compared also with those obtained for the case when Δ_T is set to zero.

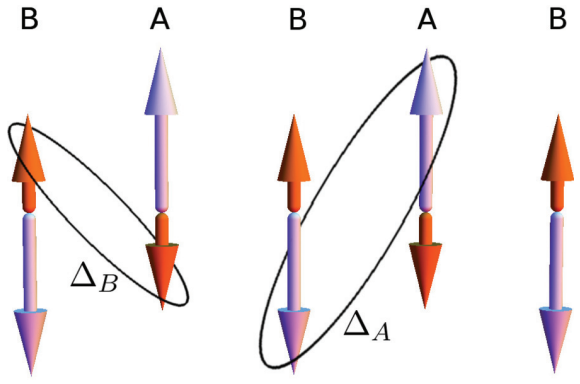

FIG. 1. (Color online) Schematic representation of the difference between the pairing parameters for the majority-spin electrons (large arrows) and the minority-spin electrons (small arrows) in the two-sublattice system with AF order. Since for $m_{\rm AF} \neq 0$ there may be that the real part of Δ_A and Δ_B might be different, and a spin-triplet component of the superconducting order has to be considered [cf. Eq. (8b)].

Applying the Wick's theorem to the Eq. (2), the expectation value $\langle\hat{\mathcal{H}}_{\rm eff}\rangle_0 \equiv W$ can be obtained in the form (see Appendix A for details)

$$\begin{aligned}\frac{W}{\Lambda} &= 8g_t t\chi_{AB} + Ud^2 \\ &\quad - g_s J\left(\frac{1}{2}m^2_{\rm AF} + 3\chi^2_{AB} + 3\Delta^2_S - \Delta^2_T\right),\end{aligned} \tag{9}$$

where Λ is the number of atomic sites in the system. Note that the total energy of this correlated system is composed of three interdependent parts: (i) the renormalized hopping energy $\sim t g_t \chi_{AB} < 0$, (ii) the correlation energy $Ud^2 > 0$, and (iii) the exchange contribution $\sim g_s J$ lowering both the energies of AF and SC states. This balance of physical energies will be amended next by the constraints introducing the statistical consistency into this mean-field system to guarantee that the self-consistent and the variational procedures will lead to the same single-particle states (this is the so-called Bogoliubov principle for the optimal single-particle states).

To summarize, the process of derivation of the effective single-particle Hamiltonian (3) is fully justified by its definition (2) which involves an averaging procedure over an uncorrelated state $|\Psi_0\rangle$. This state is selected implicitly. In general, it is the state with broken symmetry, i.e., with nonzero values of $m_{\rm AF}$, Δ_S, and Δ_T. In other words, $|\Psi_0\rangle$ is defined through the values of order parameters to be determined either self-consistently or variationally. This is the usual procedure proposed originally by Bogoliubov[50] in his version of BCS theory and by Slater[51] in the theory of itinerant antiferromagnetism. Here, their simple version of mean theory becomes more sophisticated since the renormalization factors contain also the order parameters and in a singular formal form. This last feature leads to basic formal changes in formulation of the renormalized mean-field theory, as discussed next.

III. QUASIPARTICLE STATES AND MINIMIZATION PROCEDURE FOR THE GROUND STATE

Following Refs. 41–43,52, and 53, we write the mean-field grand Hamiltonian in the form

$$\begin{aligned}\hat{K} \equiv W &- \sum_{\langle i\,j\rangle,\,\sigma}\left[\lambda^{\chi}_{ij\sigma}(\hat{c}^{\dagger}_{i\sigma}\hat{c}_{j\sigma} - \chi_{ij\sigma}) + \text{H.c.}\right] \\ &- \sum_{\langle i\,j\rangle,\,\sigma}\left[\lambda^{\Delta}_{ij\sigma}(\hat{c}_{i\sigma}\hat{c}_{j\bar{\sigma}} - \Delta_{ij\sigma}) + \text{H.c.}\right] \\ &- \sum_{i\sigma}\left[\lambda^{n}_{i\sigma}(\hat{n}_{i\sigma} - n_{i\sigma})\right] - \mu\sum_{i\sigma}\hat{n}_{i\sigma},\end{aligned} \tag{10}$$

where μ is the chemical potential, and the Lagrange multipliers $\{\lambda\}$ are introduced for each operator whose average appears in W [Eq. (9)]. The Lagrange multipliers can be interpreted as the correlation-induced effective fields. We should underline that the additional terms guarantee that the averages calculated in a self-consistent manner coincide with those determined from variational minimization principle of the appropriate free- or ground-state energy functional. Due to the dependence of the renormalization factors on the mean-field values, the two ways

of their calculation do differ, but the introduced constraints ensure their equality. In this manner, as said above, the approach is explicitly in agreement with the Bogoliubov theorem that the single-particle approach represents the optimal formulation from the principle of maximal-entropy point of view.[42,43] Also, the fields $\{\lambda\}$ are assumed to have the same symmetry as the broken-symmetry states, to which they are applied [cf. Eqs. (5), (6), and (7)]. Namely,

$$\lambda^{n}_{i\sigma} = \tfrac{1}{2}(\lambda_n + \sigma e^{i\mathbf{Q}\cdot\mathbf{r}_i}\lambda_m), \tag{11a}$$

$$\lambda^{\chi}_{ij\sigma} = \lambda_\chi, \tag{11b}$$

$$\lambda^{\Delta}_{ij\sigma} = -\tau_{ij}(\sigma\lambda_{\Delta_S} + e^{i\mathbf{Q}\cdot\mathbf{r}_i}\lambda_{\Delta_T}). \tag{11c}$$

To solve Hamiltonian (10), space Fourier transformation is performed first. Then, the Hamiltonian is diagonalized and yields four branches of eigenvalues (details of the calculations are presented in Appendix B). Next, we define the generalized grand potential functional at temperature $T > 0$ as given by

$$\mathcal{F} = -\frac{1}{\beta}\ln\mathcal{Z}, \quad \text{with} \quad \mathcal{Z} = \mathrm{Tr}(e^{-\beta\hat{K}}), \tag{12}$$

with $\beta \equiv 1/k_BT$. Explicitly, $\mathcal{F}$ then has the following form [cf. Eq. (B7)]:

$$\begin{aligned}\mathcal{F}/\Lambda = {} & 8g_t t\chi_{AB} - g_s J\left(\frac{1}{2}m^2_{\mathrm{AF}} + 3\chi^2_{AB} + 3\Delta^2_S - \Delta^2_T\right)\\ & + \frac{1}{2}\lambda_n(n-1) + \frac{1}{2}\lambda_m m_{\mathrm{AF}}\\ & + 8(\lambda_\chi\chi_{AB} + \lambda_{\Delta_S}\Delta_S + \lambda_{\Delta_T}\Delta_T)\\ & - \frac{1}{\Lambda\beta}\sum_{l,\mathbf{k}}\ln(1+e^{-\beta E_{l\mathbf{k}}}) + Ud^2 - \mu.\end{aligned} \tag{13}$$

The necessary conditions for the minimum of $\mathcal{F}$ subject to all constraints are

$$\frac{\partial\mathcal{F}}{\partial\vec{A}} = 0, \quad \frac{\partial\mathcal{F}}{\partial\vec{\lambda}} = 0, \quad \text{and} \quad \frac{\partial\mathcal{F}}{\partial d} = 0, \tag{14}$$

where the five mean-field parameters are labeled collectively as $\vec{A}$, and the Lagrange multipliers as $\vec{\lambda}$ [the full form of Eqs. (14) is presented in Appendix C]. Note that five above equations ($\partial\mathcal{F}/\partial\vec{A} = 0$) can be easily eliminated, reducing the system of algebraic equations to be solved (cf. Appendix C and discussion in Appendix D).

One should note one nontrivial methodological feature of the approach contained in the grand Hamiltonian (10). namely, the effective Hamiltonian (3) appears in it in the form of expectation value W [cf. Eq. (9)], whereas the constraints appear in Eq. (10) in the explicit operator form. This is a nonstandard mean-field version of approach. The correspondence to and main difference with the standard renormalized mean-field approach is discussed in Appendix D.

As we are interested in the ground-state properties ($T = 0$), we take the $T \to 0$ limit. We have checked that taking $\beta^{-1} = k_BT = 0.002\,|t|$ is sufficient for practical purposes.[54]

IV. RESULTS: PHASE DIAGRAM AND MICROSCOPIC CHARACTERISTICS

The stable phase is determined by the solution which has the lowest physical free energy defined as minimal value of

$$F = \mathcal{F}_0 + \mu\Lambda n, \tag{15}$$

where $\mathcal{F}_0$ denotes the value of $\mathcal{F}$ obtained at the minimum [cf. conditions (14)].

The minimum of $\mathcal{F}$ was obtained numerically using GNU Scientific Library (GSL),[55] and unless stated otherwise, all calculations were made for $t = -1$, $J = |t|/3$, $\beta|t| = 500$ on a two-dimensional square lattice of size $\Lambda = 512 \times 512$ with periodic boundary conditions.

A representative phase diagram on the Coulomb repulsion U–hole doping δ plane is exhibited in Fig. 2. We find three stable phases: SC, AF, and phase with coexisting SC and AF order (labeled collectively as AF + SC). The pure AF stable phase is found only for $\delta \equiv 1 - n = 0$ and $U/|t| > 10.6$. The region where the AF + SC appears is limited to a very close proximity to the Mott insulating state [hole-doping range $\delta \in (0, 0.006)$]. Our results differ significantly from previous studies (cf., e.g., Refs. 37,38, and 40), where a much wider coexistence region was reported (dashed line in Fig. 2). The previous results were an effect of the nonstatistically consisted RMFT approach used, as also is explained below. Using our method, such a consistency is achieved, and as a result a much narrower coexistence regime appears. It squares with recent experimental studies, where the region of AF + SC was reported to be narrow {cf., e.g., Bernhard[29] [study of $Ba(Fe_{1-x}Co_x)_2As_2$], where the coexistence region is not wider than 0.02 (of the hole doping range)}.

For further analysis, we restrict ourselves to $U/|t| = 12$, as marked by the dashed vertical line in Fig. 2. In Figs. 3 and 4, we plot the doping dependence of the mean fields and the correlation fields. The magnitude of Δ_T is nonzero only in the region with AF order (i.e., when $m_{\mathrm{AF}} \neq 0$).

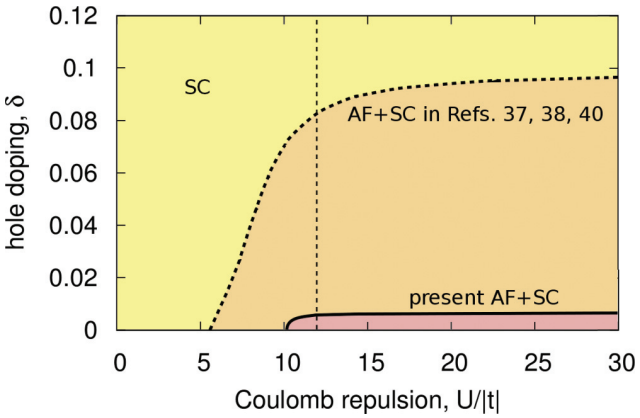

FIG. 2. (Color online) Representative phase diagram for the t–J–U model on the Coulomb repulsion–hole-doping plane. The phases are labeled as follows: SC: superconducting phase, AF + SC: phase with coexisting superconducting and antiferromagnetic orders. The pure stable AF phase is found only for $\delta = 0$ and for $U > 10.6|t|$. The value $U/|t| = 12$ marked by the dashed vertical line is taken in the subsequent analysis. The solid line is a our result. The dashed line is the result of previous studies (Refs. 37,38, and 40).

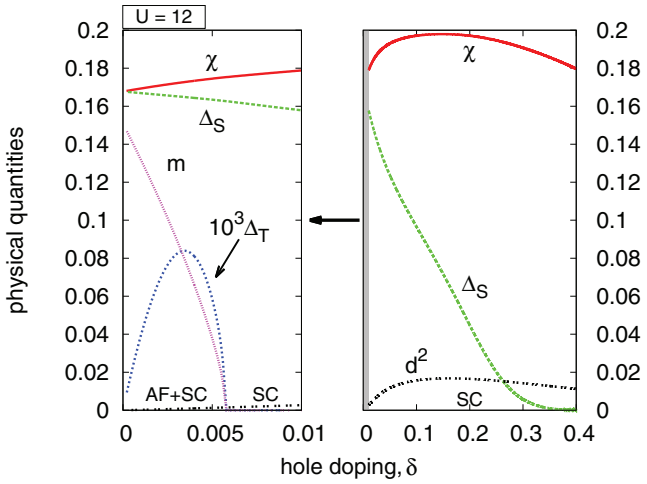

FIG. 3. (Color online) Selected bare physical quantities χ_{AB}, Δ_S, Δ_T, $m_{\rm AF}$, and d^2, all as a function of doping δ and for $U/|t| = 12$. In the coexistent AF + SC phase we have $\Delta_S \neq 0$, $\Delta_T \neq 0$, and $m_{\rm AF} \neq 0$. Such phase is stable only in the vicinity of the half-filling, as detailed in the left panel where $\delta \in [0, 0.01]$. On the right panel, we present overall behavior in the wider range of the doping.

The correlated spin-singlet gap parameter in real space is defined as

$$\tau_{ij}\Delta_S^c = \tfrac{1}{4}(\langle \hat{c}_{i\in A\downarrow}\hat{c}_{j\in B\uparrow}\rangle - \langle \hat{c}_{i\in A\uparrow}\hat{c}_{j\in B\downarrow}\rangle + \text{H.c.}), \quad (16)$$

where the average is calculated using the Gutzwiller wave function $|\Psi\rangle$, instead of $|\Psi_0\rangle$. Approximately (within GA), the correlated (physical) SC order parameters can be expressed as[37,38]

$$\Delta_S^c = g_\Delta \Delta_S, \quad \text{and} \quad \Delta_T^c = g_\Delta \Delta_T, \quad (17)$$

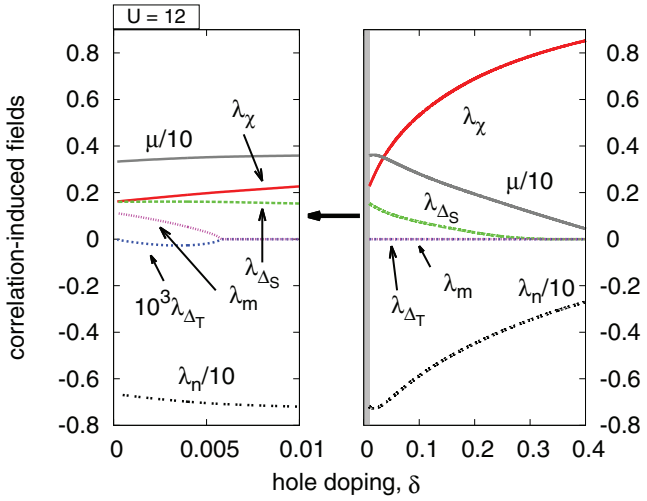

FIG. 4. (Color online) Correlation-induced fields $\lambda\chi_{AB}, \lambda_{\Delta_S}, \lambda_{\Delta_T}$, λ_m, and the chemical potential μ, all as a function of doping δ for $U/|t| = 12$. The fields $\{\lambda\}$ have nonzero values only when the corresponding mean fields are also nonzero. Note that on the left panel $\mu \sim W/2 \sim 4|t|$, corresponding to the almost-filled lower Hubbard subband.

where

$$g_\Delta = \frac{n-2d^2}{2(n-2rw)}\left[\left(\sqrt{\frac{(1-w)(1-n+d^2)}{1-r}}+\sqrt{\frac{wd^2}{r}}\right)^2 + \left(\sqrt{\frac{(1-r)(1-n+d^2)}{1-w}}+\sqrt{\frac{rd^2}{w}}\right)^2\right]. \quad (18)$$

The AF order parameter and the renormalized hopping parameter are defined in a similar manner, specifically

$$m_{\rm AF}^c = g_m\, m_{\rm AF}, \quad (19)$$

$$\chi_{AB}^c = g_t\, \chi_{AB}, \quad (20)$$

where g_t is presented in Eq. (4a) and

$$g_m = \frac{n-2d^2}{n-2wr}. \quad (21)$$

The magnitude of Δ_T^c is about 10^4 times smaller than the magnitude of Δ_S^c, so most probably, it may not be observable. For $\delta \gtrsim \frac{1}{3}$ the order parameter Δ_S^c decreases exponentially. Note a spectacular increase of the hopping probability χ_{AB}^c with increased doping in Fig. 5, leading to an effective Fermi liquid state for $\delta \gtrsim \frac{1}{3}$.

The nonzero correlated gap at $n = 1$ for low-U values provides an evidence for a gossamer superconductivity. The concept of gossamer superconductivity was introduced by Laughlin[34] and it describes the situation when the pure SC phase is stable at the half-filling. For $U/|t| \approx 10.6$ and $n = 1$, where AF + SC phase sets in, the correlated gap Δ_S^c vanishes. Details of the transition are presented in Fig. 6 (cf. the bottom

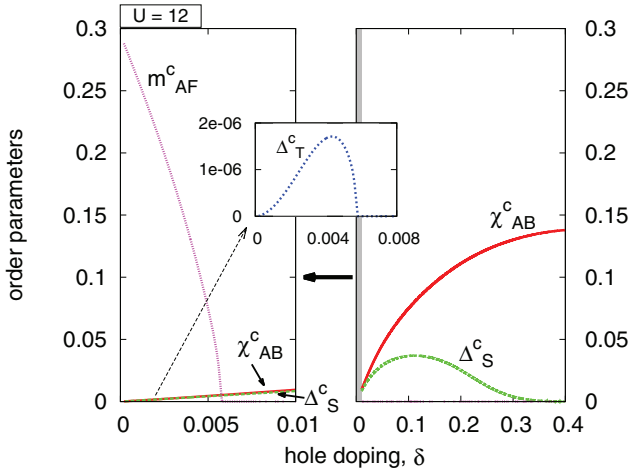

FIG. 5. (Color online) Order parameters of SC and AF states in the correlated state versus doping δ and for $U/|t| = 12$. AF disappears for $\delta \approx 6 \times 10^{-3}$. In the limit $\delta = 0$ the state transforms into an AF insulator. For $\delta \gtrsim 0.1$, the hopping amplitude χ_{AB}^c increases substantially. Inset: dependence of Δ_T^c in the vicinity of the half-filling. Note that the value of Δ_T^c is about 10^4 times smaller than the value of Δ_S^c.

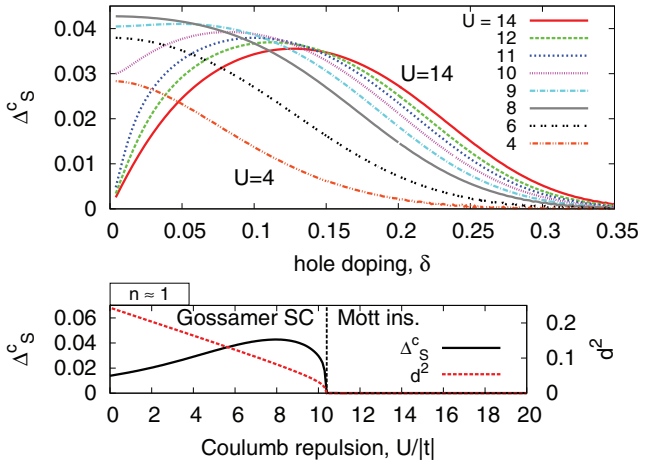

FIG. 6. (Color online) Profile of the correlated singlet gap Δ_S^c for selected values of $U/|t|$ versus hole doping (top). The limiting values of Δ_S^c and d^2 for $n \approx 1$ are presented in the bottom panel.

panel). The critical $U/|t|$ value for the disappearance of Δ_S is marked by the dotted vertical line.

In the sake of completeness, we have drawn for $U = 12|t|$ in Fig. 7 the components of the total energy [Eq. (13)] to show that in the underdoped regime the effective hopping energy $E_\chi \equiv 8g_t|t|\chi_{AB}$, the total exchange contribution $E_S \equiv g_s J(m_{\rm AF}^2/2 + 3\chi_{AB}^2 + 3\Delta_S^2 - \Delta_T^2)$, and the Coulomb energy $E_U = Ud^2$ are all of comparable magnitude. This is the regime of strong correlations.

The overall behavior of the obtained characteristics can be summarized as follows. First, the coexistent AF + SC phase appears only for the doping $\delta < 0.006$ and transforms into the pure Mott insulating state (AF) only at the half-filling $\delta = 0$ and large U. The spin-triplet gap component is practically negligible in the AF + SC phase. Introducing the molecular fields λ_χ, λ_{Δ_S}, and λ_m (where nonzero), and λ_n change the phase diagram in a significant manner which means that the influence of the consistency constraints on the single-particle states is important. The spin-singlet d-wave superconductivity vanishes exponentially for large δ. The optimal doping appears in the interval $\delta \sim 0.1$–0.15 and is weakly dependent on U for $U \gtrsim 12|t|$.

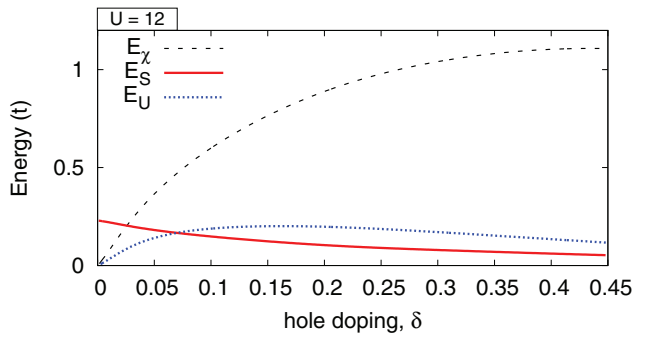

FIG. 7. (Color online) The optimized component energies composing the total energy [Eq. (9), which represents $T \to 0$ limit of Eq. (13)]. For discussion, see main text.

V. CONCLUSIONS AND COMMENTS

Using the statistically consistent Gutzwiller approximation (SGA), we have analyzed in detail the effective Hamiltonian considered previously in Refs. 37,38, and 40. However, in contrast to those papers, we have considered a more complete structure of the SC gap (the components Δ_S and Δ_T). Also, a significantly narrower region of the coexistence of AF and SC is obtained. Furthermore, the critical value of U for AF + SC appearance is higher, and for $J/|t| = \frac{1}{3}$ the value is about $10.6|t|$. We have checked that the bare amplitude Δ_T is about 10^3 times smaller than that of Δ_S (similarly, the order parameters ratio $\Delta_T^c/\Delta_S^c \approx 10^{-4}$). We have checked that when the Δ_T is omitted, the results do not change in any significant manner. Therefore, the spin-triplet component of the superconducting order is most probably not detectable experimentally.

In previous studies (cf. Refs. 37,38, and 40), a much wider coexistence region was reported. In this paper, we correct those predictions (cf. Fig. 2). Namely, we show, that the previous results were an effect of the nonstatistically consistent RMFT approach used. Illustratively, in Ref. 37, a minimization procedure is formulated by setting $\partial E_{\rm var}/\partial m = 0$, yielding Eq. (21) in Ref. 37 for m which is different than that defining m [cf. Eq. (16) in Ref. 37]. We claim that a more correct approach is provided by SGA, where the Lagrange multipliers are introduced for each operator for which the average appears in the effective mean-field Hamiltonian. In other words, without incorporating the multipliers, the free-energy functional $\mathcal{F}$ is minimized in an overextended Fock space containing, along with physical configurations, also those that lead to the statistical inconsistency. Using the constraints introduced by SGA, this space is limited to a subspace, in which such an inconsistency does not appear. Hence, the energy obtained in SGA can either be equal to or even *higher* than the energy obtained using nonconsistent approaches. Obviously, this circumstance should not be used as an argument against SGA. Different formulations, where the model is solved in a self-consistent manner, are also presented in Refs. 56 and 57.

As said above, in the SGA method, an effective single-particle approach with conditions (14) is developed. In such an approach the question of a pseudogap is not addressed. This is because (i) the order parameter Δ_S is assumed as real (i.e., no phase fluctuation appears), and (ii) the collective spin degrees of freedom are not separated from single-particle fermionic correlations. In order to address that issue, one would have to generalize the approach to include, e.g., the spin sector of the excitations,[58] even in the absence of AF order. As the antiferromagnetism is built into the SGA approach automatically, work on extension of this approach to include magnetic fluctuations in the paramagnetic phase is in progress.

One should note that the definition of the Mott (or Mott-Hubbard) insulator here complements that for the Hubbard model within the standard Gutzwiller approximation (GA) which represents the infinite-dimension variant of the approach.[59] Namely, with an assumption that $J \neq 0$, we have a gradual evolution of the antiferromagnetic order parameter $m_{\rm AF} \to 1$ with the increasing U, i.e., the system evolves from the Slater to the Mott antiferromagnet. This is what is also obtained in the saddle-point approximation within the

slave-boson approach,[60] which differs from the standard GA by incorporating constraints, some of them of similar character as those introduced here in SGA. In this respect, both SGA and the saddle-point approximation to slave-boson approach go beyond GA, albeit not in an explicitly systematic formal manner.

ACKNOWLEDGMENT

This research was supported in part by the Foundation for Polish Science (FNP) under the Grant TEAM and in part by the National Science Center (NCN) through the Grant MAESTRO, No. DEC-2012/04/A/ST3/00342.

APPENDIX A: DEFINITIONS OF THE MEAN FIELDS AND EVALUATION OF $\langle\hat{\mathcal{H}}_{\rm eff}\rangle_0 \equiv W$

In the main text, the uniform bond order parameter for i and j sites indicating the nearest-neighboring sites is defined as $\langle\hat{c}^\dagger_{i\sigma}\hat{c}_{j\sigma}\rangle_0 \equiv \chi_{AB}$. It was assumed that $\langle\hat{c}^\dagger_{i\sigma}\hat{c}_{j\sigma}\rangle_0$ is real. Let us consider in this appendix a more general form. Since the sublattice A contains the sites where the majority spin is $\uparrow$ and the sublattice B the sites where majority spin is $\downarrow$, the general form can be written as

$$\langle\hat{c}^\dagger_{i\in A\uparrow}\hat{c}_{j\in B\uparrow}\rangle_0 = \langle\hat{c}^\dagger_{j\in B\downarrow}\hat{c}_{i\in A\downarrow}\rangle_0 = \langle\hat{c}^\dagger_{i\in A\downarrow}\hat{c}_{j\in B\downarrow}\rangle^*_0 = \chi_{o-c}, \tag{A1}$$

$$\langle\hat{c}^\dagger_{i\in A\downarrow}\hat{c}_{j\in B\downarrow}\rangle_0 = \langle\hat{c}^\dagger_{j\in B\uparrow}\hat{c}_{i\in A\uparrow}\rangle_0 = \langle\hat{c}^\dagger_{i\in A\uparrow}\hat{c}_{j\in B\uparrow}\rangle^*_0 = \chi_{c-o}, \tag{A2}$$

for i and j being the nearest neighbors, where χ_{o-c} is an average of the operator describing the hopping of an electron from a site, where the average spin is *opposite* to the spin of the electron to the site where the average spin is *congruent* to the spin of the electron. χ_{o-c} describes the opposite situation. This results in the general expression that

$$\chi_{ij\sigma} \equiv \langle\hat{c}^\dagger_{i\sigma}\hat{c}_{j\sigma}\rangle_0 = \chi_{AB} + i\sigma e^{i\mathbf{Q}\cdot\mathbf{R}_i}\delta\chi_{AB}, \tag{A3}$$

where $\chi_{AB} \equiv \frac{1}{2}(\chi_{o-c} + \chi_{c-o})$ and $\delta\chi_{AB} \equiv \frac{1}{2i}(\chi_{o-c} - \chi_{c-o})$.

The electron-pairing order parameter for the nearest neighbors is defined as

$$\Delta_{ij\downarrow} \equiv \langle\hat{c}_{j\downarrow}\hat{c}_{i\uparrow}\rangle_0 \equiv \begin{cases} \tau_{ij}\tilde{\Delta}_A & \text{for} \quad i \in \mathrm{A}, \\ \tau_{ij}\tilde{\Delta}_B & \text{for} \quad i \in B, \end{cases} \tag{A4}$$

where $\tau_{ij} \equiv 1$ for $j = i \pm \hat{x}$ and $\tau_{ij} \equiv -1$ for $j = i \pm \hat{y}$ ($\Delta_{ij\uparrow}$ is defined in similar manner). For the staggered magnetic moment $m_{\rm AF} = 0$, one can assume that $\tilde{\Delta}_A = \tilde{\Delta}_B$. However, when $m_{\rm AF} \neq 0$, the order parameter $\tilde{\Delta}_A$ is a product of two operators, both of which annihilate electrons whose spin is *congruent* to the average spin of individual sites. On the contrary, $\tilde{\Delta}_B$ is a product of two operators that annihilate electrons whose spin is *opposite* to the average spin of individual sites. Hence, it may be that $\tilde{\Delta}_A \neq \tilde{\Delta}_B$. Also, similar as with the hopping amplitude, $\tilde{\Delta}_A$ and $\tilde{\Delta}_B$ might be complex numbers. Let us denote $\tilde{\Delta}_A \equiv (\Delta_A,\ \delta\Delta_A)$ and $\tilde{\Delta}_B \equiv (\Delta_B,\ \delta\Delta_B)$, where the parameters in brackets are the real and imaginary parts of the corresponding gaps, respectively.

The only nontrivial part of $\langle\hat{\mathcal{H}}_{\rm eff}\rangle_0$ [cf. Eq. (3)] can be evaluated in the form

$$\begin{aligned} 4\langle\hat{\mathbf{S}}_i\cdot\hat{\mathbf{S}}_j\rangle_0 \approx & -(\langle\hat{c}^\dagger_{i\downarrow}\hat{c}_{i\downarrow}\rangle_0 - \langle\hat{c}^\dagger_{i\uparrow}\hat{c}_{i\uparrow}\rangle_0)^2 \\ & -(\langle\hat{c}^\dagger_{i\downarrow}\hat{c}_{j\downarrow}\rangle_0 + 2\langle\hat{c}^\dagger_{i\uparrow}\hat{c}_{j\uparrow}\rangle_0)\langle\hat{c}^\dagger_{j\downarrow}\hat{c}_{i\downarrow}\rangle_0 \\ & -(2\langle\hat{c}^\dagger_{i\downarrow}\hat{c}_{j\downarrow}\rangle_0 + \langle\hat{c}^\dagger_{i\uparrow}\hat{c}_{j\uparrow}\rangle_0)\langle\hat{c}^\dagger_{j\uparrow}\hat{c}_{i\uparrow}\rangle_0 \\ & -(-\langle\hat{c}_{i\uparrow}\hat{c}_{j\downarrow}\rangle_0 + 2\langle\hat{c}_{i\downarrow}\hat{c}_{j\uparrow}\rangle_0)\langle\hat{c}^\dagger_{i\uparrow}\hat{c}^\dagger_{j\downarrow}\rangle_0 \\ & -(2\langle\hat{c}_{i\uparrow}\hat{c}_{j\downarrow}\rangle_0 - \langle\hat{c}_{i\downarrow}\hat{c}_{j\uparrow}\rangle_0)\langle\hat{c}^\dagger_{i\downarrow}\hat{c}^\dagger_{j\uparrow}\rangle_0, \end{aligned} \tag{A5}$$

where we have applied the Wick's theorem and we have assumed that $\langle\hat{c}^\dagger_{i\uparrow}\hat{c}_{i\downarrow}\rangle_0 \equiv 0$, $\langle\hat{c}_{i\uparrow}\hat{c}_{i\downarrow}\rangle_0 \equiv 0$, and $\langle\hat{c}_{i\downarrow}\hat{c}_{j\downarrow}\rangle_0 = \langle\hat{c}_{i\uparrow}\hat{c}_{j\uparrow}\rangle_0 \equiv 0$. Using the notation introduced above and Eq. (5), we have

$$\begin{aligned} 4\langle\hat{\mathbf{S}}_i\cdot\hat{\mathbf{S}}_j\rangle_0 = & -m^2_{\rm AF} - 6\chi^2_{AB} + 2(\delta\chi_{AB})^2 \\ & -|\tilde{\Delta}_A|^2 - |\tilde{\Delta}_B|^2 - 4\tilde{\Delta}_A\tilde{\Delta}_B. \end{aligned} \tag{A6}$$

Since the above expression is invariant with respect to the same rotations of both vectors $\tilde{\Delta}_A$ and $\tilde{\Delta}_B$, one component of the vectors can be assumed to be eliminated. With the choice $\delta\Delta_A = 0$, we have

$$\begin{aligned} \Delta_{ij\sigma} \equiv & \langle\hat{c}_{i\sigma}\hat{c}_{j\bar{\sigma}}\rangle_0 \equiv -\tau_{ij}(\sigma\Delta_S + e^{i\mathbf{Q}\cdot\mathbf{r}_i}\Delta_T) \\ & -\tau_{ij}\tfrac{1}{2}i(\sigma - e^{i\mathbf{Q}\cdot\mathbf{r}_i})\delta\Delta_B, \end{aligned} \tag{A7}$$

where $\Delta_S \equiv \Delta_A + \Delta_B$ and $\Delta_T \equiv \Delta_A - \Delta_B$.

Therefore, the $\langle\hat{\mathcal{H}}_{\rm eff}\rangle_0 \equiv W$ can be presented in the full form

$$\begin{aligned} \frac{W}{\Lambda} = & 8g_t t\chi_{AB} + Ud^2 - g_s J\left(\frac{1}{2}m^2_{\rm AF} + 3\chi^2_{AB} - (\delta\chi_{AB})^2\right. \\ & \left. + 3\Delta^2_S - \Delta^2_T + \frac{1}{2}(\delta\Delta_B)^2\right). \end{aligned} \tag{A8}$$

Introduction of $\delta\chi_{AB}$ and $\delta\Delta_B$ affects the form of selecting the correlated fields $\lambda^\chi_{ij\sigma}$ and $\lambda^\Delta_{ij\sigma}$, and the final set of necessary conditions for a local minimum of the free energy [cf. Eqs. (11b), (11c), and (14)]. However, it was found that the state with the lowest energy (for the considered model) has always been that with $\delta\chi_{AB} \equiv 0$ and $\delta\Delta_B \equiv 0$. Hence, it is acceptable to neglect both terms and claim that $\Delta_{ij\sigma}$ and $\chi_{ij\sigma}$ are both real. For simplicity and clarity it is how the averages are presented in the main text. Finally, Eq. (A8) is reduced to Eq. (9).

APPENDIX B: DETERMINATION OF THE GRAND POTENTIAL FUNCTIONAL [EQ. (13)]

To diagonalize $\hat{K}$ [Eq. (10)], we first perform the space Fourier transform. The result can be rewritten in the following 4×4 matrix form:

$$\begin{aligned} \hat{K} = & W + {\sum_{\mathbf{k}}}' \hat{\Psi}^\dagger_{\mathbf{k}}\tilde{\mathbb{M}}_{\mathbf{k}}\hat{\Psi}_{\mathbf{k}} + \frac{1}{2}\Lambda[\lambda_n(n-1) + \lambda_m m_{\rm AF}] \\ & -\Lambda\mu + 8\Lambda\lambda_\chi\chi_{AB} + 8\Lambda(\lambda_{\Delta_S}\Delta_S + \lambda_{\Delta_T}\Delta_T), \end{aligned} \tag{B1}$$

where $\hat{\Psi}^\dagger_{\mathbf{k}} = (\hat{c}^\dagger_{\mathbf{k}\uparrow}, \hat{c}_{-\mathbf{k}\downarrow}, \hat{c}^\dagger_{\mathbf{k}+\mathbf{Q}\uparrow}, \hat{c}_{-\mathbf{k}+\mathbf{Q}\downarrow})$, the sum is evaluated over the reduced (magnetic) Brillouin zone ($|k_x| + |k_y| \leqslant \pi$),

and

$$\tilde{\mathbb{M}}_{\mathbf{k}} = \begin{pmatrix} -\lambda_\chi \epsilon_{\mathbf{k}} - \frac{1}{2}\lambda_n - \mu & -\lambda_{\Delta_S}\eta_{\mathbf{k}} & -\frac{1}{2}\lambda_m & \lambda_{\Delta_T}\eta_{\mathbf{k}} \\ -\lambda_{\Delta_S}\eta_{\mathbf{k}} & \lambda_\chi \epsilon_{\mathbf{k}} + \frac{1}{2}\lambda_n + \mu & -\lambda_{\Delta_T}\eta_{\mathbf{k}} & -\frac{1}{2}\lambda_m \\ -\frac{1}{2}\lambda_m & -\lambda_{\Delta_T}\eta_{\mathbf{k}} & \lambda_\chi \epsilon_{\mathbf{k}} - \frac{1}{2}\lambda_n - \mu & \lambda_{\Delta_S}\eta_{\mathbf{k}} \\ \lambda_{\Delta_T}\eta_{\mathbf{k}} & -\frac{1}{2}\lambda_m & \lambda_{\Delta_S}\eta_{\mathbf{k}} & -\lambda_\chi \epsilon_{\mathbf{k}} + \frac{1}{2}\lambda_n + \mu \end{pmatrix}, \tag{B2}$$

where for the square lattice

$$\epsilon_{\mathbf{k}} \equiv 2(\cos k_x + \cos k_y), \tag{B3a}$$

$$\eta_{\mathbf{k}} \equiv 2(\cos k_x - \cos k_y). \tag{B3b}$$

Diagonalization of $\tilde{\mathbb{M}}_{\mathbf{k}}$ yields four branches of eigenvalues with their explicit form

$$E_{l\mathbf{k}} \equiv E_{\pm\pm\mathbf{k}} = \pm\tfrac{1}{2}\sqrt{K_{1\mathbf{k}} \pm 2\sqrt{K_{2\mathbf{k}}}}, \tag{B4}$$

where $l = 1, \ldots, 4$, and

$$K_{1\mathbf{k}} \equiv 4\epsilon_{\mathbf{k}}^2\lambda_\chi^2 + (\lambda_n + 2\mu)^2 + 4\eta_{\mathbf{k}}^2\left(\lambda_{\Delta_S}^2 + \lambda_{\Delta_T}^2\right) + \lambda_m^2, \tag{B5a}$$

$$K_{2\mathbf{k}} \equiv \left[4\eta_{\mathbf{k}}^2\lambda_{\Delta_S}\lambda_{\Delta_T} + \lambda_m(\lambda_n + 2\mu)\right]^2 + 4\epsilon_{\mathbf{k}}^2\lambda_\chi^2\left[4\eta_{\mathbf{k}}^2\lambda_{\Delta_T}^2 + (\lambda_n + 2\mu)^2\right]. \tag{B5b}$$

The energies $\{E_{l\mathbf{k}}\}_{l=1,\ldots,4}$ represent quasiparticle bands after all parameters (mean-field parameters, the Lagrange multipliers, and d) are determined variationally.

The generalized grand potential functional at temperature $T > 0$ is given by

$$\mathcal{F} = -\frac{1}{\beta}\ln\mathcal{Z}, \quad \text{with} \quad \mathcal{Z} = \mathrm{Tr}(e^{-\beta\hat{K}}), \tag{B6}$$

and $\beta \equiv 1/k_B T$, thus,

$$\mathcal{F}/\Lambda = 8g_t t\chi_{AB} - g_s J\left(\frac{1}{2}m_{\mathrm{AF}}^2 + 3\chi_{AB}^2 + 3\Delta_S^2 - \Delta_T^2\right) + \frac{1}{2}\lambda_n(n-1) + \frac{1}{2}\lambda_m m_{\mathrm{AF}} + 8(\lambda_\chi\chi_{AB} + \lambda_{\Delta_S}\Delta_S + \lambda_{\Delta_T}\Delta_T) - \frac{1}{\Lambda\beta}\sum_{l,\mathbf{k}}\ln(1 + e^{-\beta E_{l\mathbf{k}}}) + Ud^2 - \mu. \tag{B7}$$

APPENDIX C: EXPLICIT FORM OF THE CONDITIONS FOR THE MINIMUM OF $\mathcal{F}$

The necessary conditions for the minimum of $\mathcal{F}$, subject to all constraints [introduced in Eq. (10)] are

$$\frac{\partial\mathcal{F}}{\partial\vec{A}} = 0, \quad \frac{\partial\mathcal{F}}{\partial\vec{\lambda}} = 0, \quad \text{and} \quad \frac{\partial\mathcal{F}}{\partial d} = 0, \tag{C1}$$

where the five mean-field parameters are labeled collectively as $\vec{A}$, the five Lagrange multipliers as $\vec{\lambda}$, and d^2 is double-occupancy probability. In explicit form, $\partial\mathcal{F}/\partial\vec{A} = 0$ stands for

$$\lambda_\chi = -g_t t + \frac{3}{4}g_s J\chi_{AB}, \tag{C2a}$$

$$\lambda_{\Delta_S} = \frac{3}{4}g_s J\Delta_S, \tag{C2b}$$

$$\lambda_{\Delta_T} = -\frac{1}{4}g_s J\Delta_T, \tag{C2c}$$

$$\lambda_n = -16t\chi_{AB}\frac{\partial g_t}{\partial n} - 2J\left(-\frac{1}{2}m_{\mathrm{AF}}^2 - 3\chi_{AB}^2 - 3\Delta_S^2 + \Delta_T^2\right)\frac{\partial g_s}{\partial n}, \tag{C2d}$$

$$\lambda_m = 2g_s J m_{\mathrm{AF}} - 16t\chi_{AB}\frac{\partial g_t}{\partial m_{\mathrm{AF}}} - 2J\left(-\frac{1}{2}m_{\mathrm{AF}}^2 - 3\chi_{AB}^2 - 3\Delta_S^2 + \Delta_T^2\right)\frac{\partial g_s}{\partial m_{\mathrm{AF}}}, \tag{C2e}$$

$\partial\mathcal{F}/\partial\vec{\lambda} = 0$ can be evaluated as

$$\frac{1}{\Lambda}\sum_{\mathbf{k},l} f(E_{l\mathbf{k}})\,\partial_{\lambda_\chi}E_{l\mathbf{k}} + 8\chi_{AB} = 0, \tag{C3a}$$

$$\frac{1}{\Lambda}\sum_{\mathbf{k},l} f(E_{l\mathbf{k}})\,\partial_{\lambda_{\Delta_S}}E_{l\mathbf{k}} + 8\Delta_S = 0, \tag{C3b}$$

$$\frac{1}{\Lambda}\sum_{\mathbf{k},l} f(E_{l\mathbf{k}})\,\partial_{\lambda_{\Delta_T}}E_{l\mathbf{k}} + 8\Delta_T = 0, \tag{C3c}$$

$$\frac{1}{\Lambda}\sum_{\mathbf{k},l} f(E_{l\mathbf{k}})\,\partial_{\lambda_n}E_{l\mathbf{k}} - \frac{1}{2}(1-n) = 0, \tag{C3d}$$

$$\frac{1}{\Lambda}\sum_{\mathbf{k},l} f(E_{l\mathbf{k}})\,\partial_{\lambda_m}E_{l\mathbf{k}} + \frac{1}{2}m_{\mathrm{AF}} = 0, \tag{C3e}$$

and $\partial\mathcal{F}/\partial d = 0$ denotes

$$2Ud + 8t\chi_{AB}\frac{\partial g_t}{\partial d} + J\left(-\frac{1}{2}m_{\mathrm{AF}}^2 - 3\chi_{AB}^2 - 3\Delta_S^2 + \Delta_T^2\right)\frac{\partial g_s}{\partial d} = 0, \tag{C4a}$$

where $f(E_{l\mathbf{k}}) \equiv 1/(1 + e^{\beta E_{l\mathbf{k}}})$. Equations (C2a)–(C2e) can be used to eliminate the parameters $\{\lambda\}$ from the numerical solution procedure, reducing the number of algebraic equations to six. Consequently, we are left with Eqs. (C3a)–(C3e) (the conditions $\partial\mathcal{F}/\partial\vec{\lambda} = 0$) and Eq. (C4a) ($\partial\mathcal{F}/\partial d = 0$).

APPENDIX D: AN ALTERNATIVE PROCEDURE OF INTRODUCING THE CONSTRAINTS VIA LAGRANGE MULTIPLIERS

In the main text, we work with the mean-field grand Hamiltonian $\hat{K}$, defined as $\hat{K} \equiv W - \sum_\iota [\lambda_\iota (\hat{O}_\iota - O_\iota) + \text{H.c.}] - \mu \hat{N}$, where $W \equiv \langle \hat{\mathcal{H}}_{\text{eff}} \rangle_0$ [cf. Eqs. (3) and (9)], and $\{\hat{O}_\iota\}$ are those operators whose averages are used to construct W. Lagrange multipliers λ_ι are introduced to ensure self-consistency of the solution, i.e., $O_\iota \equiv \langle \hat{O}_\iota \rangle_0$ [cf. Eq. (10)].

Next, in order to find optimal (equilibrium) values of mean fields, the grand potential functional $\mathcal{F} = -\beta^{-1} \ln \mathcal{Z}$, where $\mathcal{Z} = \text{Tr}(e^{-\beta \hat{K}})$ [cf. Eq. (12)] is subsequently minimized with respect to mean fields subject to constraints included in $\hat{K}$.

An alternative procedure to the one sketched above is to add the self-consistency preserving constraints directly to $\hat{\mathcal{H}}_{\text{eff}}^{MF}$, i.e., to the mean-field approximated $\hat{\mathcal{H}}_{\text{eff}}$. In this formulation, we have again a separate Lagrange multiplier λ'_ι for each mean-field average $O'_\iota \equiv \langle \hat{O}'_\iota \rangle_0$ present in $\hat{\mathcal{H}}_{\text{eff}}^{MF}$. In effect, we construct the effective mean-field Hamiltonian of the form $\hat{\mathcal{H}}_\lambda \equiv \hat{\mathcal{H}}_{\text{eff}}^{\text{MF}} - \sum_\iota [\lambda'_\iota (\hat{O}'_\iota - O'_\iota) + \text{H.c.}]$ and the corresponding mean-field grand Hamiltonian $\hat{K}' \equiv \hat{\mathcal{H}}_\lambda - \mu \hat{N}$. As a next step, the functional $\mathcal{F}'$ is constructed (exactly as discussed above). It should be noted that minimization of $\mathcal{F}'$ subject to constraints included in $\hat{\mathcal{H}}_\lambda$ leads to a set of equations *different* than Eqs. (C2a)–(C4a). However, *those two procedures are equivalent*, i.e., the optimal (equilibrium) values of the mean fields, corresponding to the minimum of $\mathcal{F}$ and $\mathcal{F}'$ (subject to the same constraints), coincide. A difference in the results may occur only for the values of the Lagrange multipliers, but this does not affect the equilibrium values of the calculated physical quantities. Hence, the two approaches are formally equivalent, which can be shown analytically and has also been verified numerically.

Those two approaches differ also with respect to numerical execution. Namely, within the first procedure, we can easily find the functional dependence of Lagrange multipliers $\vec{\lambda}_\iota$ on mean fields O_ι (as shown in Appendix C). As a result, the number of equations to be solved numerically is reduced by a factor of 2. In the second approach discussed here, the corresponding equations for $\vec{\lambda}'_\iota$ are much more complicated and it is not possible to solve them analytically. Therefore, one can not reduce the effort and numerical cost of solving the model at the same time. So, even though the latter method appears more intuitively appealing, as being more similar to the standard mean-field approach, we have used the former method in the discussion in the main text.

TABLE I. Values of the parameters obtained for the SC phase ($U/|t| = 5$ and $\delta = 0.3$) (example 1), for SC phase ($U/|t| = 12$ and $\delta = 0.03$) (example 2), and for the AF + SC phase ($U/|t| = 12$ and $\delta = 0.001$). The calculations were made for the lattice with $\Lambda = 1024 \times 1024$ sites. The numerical accuracy is at the last digit specified.

Variable	SC (1)	SC (2)	AF + SC
χ_{AB}	0.1907587	0.1887189	0.1693210
Δ_S	0.00027	0.138176	0.166906
Δ_T	0	0	3.92×10^{-5}
μ	0.5664	3.5570	3.37154
m_{AF}	0	0	0.13194
d^2	5.22266×10^{-2}	8.16196×10^{-3}	2.2406×10^{-4}
λ_χ	0.9661403	0.327769	0.168074
λ_{Δ_S}	0	0.1258974	0.160777
λ_{Δ_T}	0	0	1.2595×10^{-5}
λ_n	−2.526087	−7.176836	−6.744724
λ_m	0	0	0.100911
W	−1.150925	−0.33669191	−0.233031
g_t	0.884438	0.1558210	4.97139×10^{-3}
g_s	1.713202	3.644549	3.85310
g_Δ	0.884438	0.1558210	4.99912×10^{-3}
g_m	1.3088937	1.9090702	1.96293
χ^c_{AB}	0.1687143	2.94064×10^{-2}	8.41761×10^{-4}
Δ^c_S	0.00024	2.15306×10^{-2}	8.343884×10^{-4}
Δ^c_T	0	0	1.960×10^{-8}
m^c_{AF}	0	0	0.25900

APPENDIX E: SUPPLEMENTARY INFORMATION

For the sake of completeness, in Table I we provide the representative values of the parameters calculated for the following phases: SC for ($U/|t| = 5$, $\delta = 0.1$, and $U/|t| = 12$, $\delta = 0.03$), and AF + SC ($U/|t| = 12$, $\delta = 0.001$). The energies in the columns should not be compared directly, as they correspond to different sets of microscopic parameters. Numerical accuracy is at the level of the last digit specified.

*marcin.abram@uj.edu.pl
†ufspalek@if.uj.edu.pl

[1] J. Spałek and A. Oleś, Phys. B + C (Amsterdam) **86–88**, 375 (1977); K. A. Chao, J. Spałek, and A. M. Oleś, J. Phys. C: Solid State Phys. **10**, L271 (1977).
[2] J. Spałek, Acta Phys. Pol., A **111**, 409 (2007).
[3] P. W. Anderson, in *Frontiers and Borderlines in Many-Particle Physics*, edited by R. A. Broglia and J. R. Schrieffer (North-Holland, Amsterdam, 1988), pp. 1–40.
[4] E. Dagotto, Rev. Mod. Phys. **66**, 763 (1994).
[5] S. K. Sarker, C. Jayaprakash, and H. R. Krishnamurthy, Phys. C. (Amsterdam) **228**, 309 (1994); S. K. Sarker and T. Lovorn, Phys. Rev. B **82**, 014504 (2010).
[6] P. Johnson, A. Fedorov, and T. Valla, J. Electron. Spectrosc. Relat. Phenom. **117**, 153 (2001).
[7] P. A. Lee, N. Nagaosa, and X.-G. Wen, Rev. Mod. Phys. **78**, 17 (2006).
[8] M. Imada, A. Fujimori, and Y. Tokura, Rev. Mod. Phys. **70**, 1039 (1998).
[9] A. Damascelli, Z. Hussain, and Z.-X. Shen, Rev. Mod. Phys. **75**, 473 (2003).
[10] K. Tanaka, W. S. Lee, D. H. Lu, A. Fujimori, T. Fujii, Risdiana, I. Terasaki, D. J. Scalapino, T. P. Devereaux, Z. Hussain *et al.*, Science **314**, 1910 (2006).
[11] D. J. Scalapino, Rev. Mod. Phys. **84**, 1383 (2012).
[12] F. C. Zhang and T. M. Rice, Phys. Rev. B **37**, 3759 (1988).

[13]J. Zaanen and G. Sawatzky, J. Solid State Chem. **88**, 8 (1990).
[14]S. Daul, D. J. Scalapino, and S. R. White, Phys. Rev. Lett. **84**, 4188 (2000).
[15]S. Basu, R. J. Gooding, and P. W. Leung, Phys. Rev. B **63**, 100506 (2001).
[16]F. C. Zhang, Phys. Rev. Lett. **90**, 207002 (2003).
[17]T. Xiang, H. G. Luo, D. H. Lu, K. M. Shen, and Z. X. Shen, Phys. Rev. B **79**, 014524 (2009).
[18]W. Yu, J. S. Higgins, P. Bach, and R. L. Greene, Phys. Rev. B **76**, 020503 (2007).
[19]N. P. Armitage, P. Fournier, and R. L. Greene, Rev. Mod. Phys. **82**, 2421 (2010).
[20]H. Kimura, K. Hirota, H. Matsushita, K. Yamada, Y. Endoh, S.-H. Lee, C. F. Majkrzak, R. Erwin, G. Shirane, M. Greven *et al.*, Phys. Rev. B **59**, 6517 (1999).
[21]Y. S. Lee, R. J. Birgeneau, M. A. Kastner, Y. Endoh, S. Wakimoto, K. Yamada, R. W. Erwin, S.-H. Lee, and G. Shirane, Phys. Rev. B **60**, 3643 (1999).
[22]Y. Sidis, C. Ulrich, P. Bourges, C. Bernhard, C. Niedermayer, L. P. Regnault, N. H. Andersen, and B. Keimer, Phys. Rev. Lett. **86**, 4100 (2001).
[23]J. A. Hodges, Y. Sidis, P. Bourges, I. Mirebeau, M. Hennion, and X. Chaud, Phys. Rev. B **66**, 020501 (2002).
[24]T. Kawamoto, Y. Bando, T. Mori, T. Konoike, Y. Takahide, T. Terashima, S. Uji, K. Takimiya, and T. Otsubo, Phys. Rev. B **77**, 224506 (2008).
[25]N. D. Mathur, F. M. Grosche, S. R. Julian, I. R. Walker, D. M. Freye, R. K. W. Haselwimmer, and G. G. Lonzarich, Nature (London) **394**, 39 (1998).
[26]L. Ma, G. F. Ji, J. Dai, X. R. Lu, M. J. Eom, J. S. Kim, B. Normand, and W. Yu, Phys. Rev. Lett. **109**, 197002 (2012).
[27]Z. Li, R. Zhou, Y. Liu, D. L. Sun, J. Yang, C. T. Lin, and G.-q. Zheng, Phys. Rev. B **86**, 180501 (2012).
[28]P. Marsik, K. W. Kim, A. Dubroka, M. Rössle, V. K. Malik, L. Schulz, C. N. Wang, C. Niedermayer, A. J. Drew, M. Willis *et al.*, Phys. Rev. Lett. **105**, 057001 (2010).
[29]C. Bernhard, C. N. Wang, L. Nuccio, L. Schulz, O. Zaharko, J. Larsen, C. Aristizabal, M. Willis, A. J. Drew, G. D. Varma *et al.*, Phys. Rev. B **86**, 184509 (2012).
[30]M. V. Milovanović and S. Predin, Phys. Rev. B **86**, 195113 (2012).
[31]J. Y. Gan, F. C. Zhang, and Z. B. Su, Phys. Rev. B **71**, 014508 (2005).
[32]J. Y. Gan, Y. Chen, Z. B. Su, and F. C. Zhang, Phys. Rev. Lett. **94**, 067005 (2005).
[33]B. A. Bernevig, R. B. Laughlin, and D. I. Santiago, Phys. Rev. Lett. **91**, 147003 (2003).
[34]R. B. Laughlin, Philos. Mag. **86**, 1165 (2006).
[35]D. J. Van Harlingen, Rev. Mod. Phys. **67**, 515 (1995).
[36]C. C. Tsuei and J. R. Kirtley, Rev. Mod. Phys. **72**, 969 (2000).
[37]F. Yuan, Q. Yuan, and C. S. Ting, Phys. Rev. B **71**, 104505 (2005).
[38]H. Heiselberg, Phys. Rev. A **79**, 063611 (2009).
[39]K.-K. Voo, J. Phys.: Condens. Matter **23**, 495602 (2011).
[40]F.-F. Liu, Y. Zhang, F. Yuan, and L.-H. Xia, Commun. Theor. Phys. **57**, 727 (2012).
[41]J. Jędrak, J. Kaczmarczyk, and J. Spałek, arXiv:1008.0021.
[42]J. Jędrak and J. Spałek, Phys. Rev. B **81**, 073108 (2010).
[43]J. Jędrak, Ph.D. thesis, Jagiellonian University, Kraków, 2011, http://th-www.if.uj.edu.pl/ztms/download/phdTheses/Jakub_Jedrak_doktorat.pdf.
[44]M. C. Gutzwiller, Phys. Rev. Lett. **10**, 159 (1963); Phys. Rev. **137**, A1726 (1965).
[45]T. Ogawa, K. Kanda, and T. Matsubara, Prog. Theor. Phys. **53**, 614 (1975).
[46]F. C. Zhang, C. Gros, T. M. Rice, and H. Shiba, Supercond. Sci. Technol. **1**, 36 (1988).
[47]A. Himeda and M. Ogata, Phys. Rev. B **60**, R9935 (1999).
[48]S. Tsonis, P. Kotetes, G. Varelogiannis, and P. B. Littlewood, J. Phys.: Condens. Matter **20**, 434234 (2008).
[49]A. Aperis, G. Varelogiannis, and P. B. Littlewood, Phys. Rev. Lett. **104**, 216403 (2010).
[50]N. N. Bogoliubov, Zh. Exp. Teor. Fiz. **34**, 58 (1958) [Sov. Phys.–JETP **34**, 41 (1958)]; N. N. Bogolyubov, V. V. Tolmachev, and D. V. Shirkov, Fortschr. Phys. **6**, 605 (1958).
[51]J. C. Slater, Phys. Rev. **82**, 538 (1951).
[52]J. Kaczmarczyk and J. Spałek, Phys. Rev. B **84**, 125140 (2011).
[53]J. Kaczmarczyk, Ph.D. thesis, Jagiellonian University, Kraków, 2011, http://th-www.if.uj.edu.pl/ztms/download/phdTheses/Jan_Kaczmarczyk_doktorat.pdf.
[54]With an increase of hole doping, the approximation of zero temperature described in the main text became weaker. For bigger δ (e.g., for $U/|t| = 12$ bigger than 0.3) it starts to be insufficient. Taking bigger β moves the limiting value of δ just a little. Thus, for a limit of strong hole doping other computational techniques have to be used (since the correlations are weak in such a limit, it can be a basic RMFT methods as described in Ref. 37).
[55]M. Galassi, J. Davies, J. Theiler, B. Gough, P. Jungman, G. abd Alken, M. Booth, and F. Rossi, *GNU Scientific Library Reference Manual*, 3rd ed. (Network Theory, Ltd., London, 2009).
[56]J. Bünemann, J. Phys.: Condens. Matter **17**, 3807 (2005).
[57]K.-Y. Yang, New J. Phys. **11**, 055053 (2009).
[58]S. Feng, H. Zhao, and Z. Huang, Phys. Rev. B **85**, 054509 (2012).
[59]K. Kubo and M. Uchinami, Prog. Theor. Phys **54**, 1289 (1975).
[60]P. Korbel, W. Wójcik, A. Klejnberg, J. Spałek, M. Acquarone, and M. Lavagna, Eur. Phys. J. B **32**, 315 (2003).

Article 2

This article is a continuation and extension of the previous paper (cf. Ref. [53]), where t–J–U model was studied. Namely, we consider the additional hopping between the second nearest neighbors (t–t'–J–U model). The role of the spin-exchange coupling J and the t' term is analyzed, as well as the stability of the superconducting (SC) and antiferromagnetic (AF) phases with respect to the temperature. The critical value of Coulomb repulsion U_{cr} for AF+SC region was found proportional to the value of J in the whole studied range, except the limit of small J, where U_{cr} grows rapidly with decreasing value of J. The t' term appears to have very limited effect on the stability of phases. For non-zero temperature, additionally to AF, SC and AF+SC phases, paramagnetic (PM) phase can be found. The increasing temperature reduces the range of SC and AF phases in favor of PM phase, what is in qualitative agreement with the experiment. However, even in relatively hight temperature, pockets of SC and AF region remain stable, what is non-physical result, showing perhaps the limit of single-band models in description of high-temperature superconductors.

Proceedings of the XVI National Conference on Superconductivity and Strongly Correlated Systems, Zakopane 2013

$t-t'-J-U$ Model in Mean-Field Approximation: Coexistence of Superconductivity and Antiferromagnetism

M. Abram*

Marian Smoluchowski Institute of Physics, Jagiellonian University, W.S. Reymonta 4, 30-059 Kraków, Poland

We discuss the $t-J-U$ model in the mean-field approximation. The role of spin-exchange coupling J and the second nearest hopping t' are examined in the context of the coexistence of superconductivity and antiferromagnetism. Stability of the phases is studied with respect to temperature. The coexistence region exists for the sufficiently large Coulomb repulsion ($U > U_{\rm cr}$), and in the vicinity of the half-filled band (hole doping $\delta < \delta_{\rm cr}$). The critical hole doping is relatively small ($\delta_{\rm cr} \approx 0.006$ for $J/|t| = 1/3$) and linear with respect to J. The decrease of $U_{\rm cr}$ is proportional to J, except the limit of small J ($J/|t| < 0.03$), where $U_{\rm cr}$ grows rapidly with decreasing J. The effect of the second nearest hopping is limited — the phase diagram does not change in a qualitative manner when the t' value is changed. In the limit of $T \to 0$, SC phase is stable even for large hole-doping (such as $\delta = 0.5$). Additional paramagnetic phase appears for large δ or small U at non-zero temperature. When temperature increases, both SC and AF+SC phase regions are reduced.

DOI: 10.12693/APhysPolA.126.A-25

PACS: 71.27.+a, 74.25.Dw, 74.72.Gh

1. Introduction

One of the basic models for high-temperature superconductors and correlated systems is $t-J$ model, which can be derived from the Hubbard model in the limit of large Coulomb repulsion U [1, 2]. In the simplest version the $t-J$ model has the form [1–4]:

$$\hat{\mathcal{H}}_{t-J} = \sum_{i\neq j,\,\sigma} \hat{\mathcal{P}}_0\, t_{ij} \hat{c}^{\dagger}_{i\sigma} \hat{c}_{j\sigma}\, \hat{\mathcal{P}}_0 + \sum_{i\neq j} J_{ij}\, \hat{\mathcal{P}}_0 \left(\boldsymbol{S}_i \cdot \boldsymbol{S}_j - \frac{1}{4} \hat{n}_i \hat{n}_j \right) \hat{\mathcal{P}}_0, \tag{1}$$

where t_{ij} is the hopping integral, $J_{ij} \equiv 4t_{ij}^2/U$ is the kinetic-exchange integral, and $\hat{\mathcal{P}}_0 = \prod_i (1 - \hat{n}_{i\uparrow}\hat{n}_{i\downarrow})$ is the Gutzwiller projector operator eliminating the double site occupancies. Sometimes, for simplicity, the term $\frac{1}{4}\hat{n}_i\hat{n}_j$ is neglected (cf. discussion of the term's relevance in Ref. [5, Ch. 9]).

For the Hubbard model, the energy cost for two electrons residing on the same site is equal to U, hence in the limit of $U \to +\infty$ (which was assumed when deriving the $t-J$ model [1]), the double occupancies are prohibited. It is realized through the projector $\hat{\mathcal{P}}_0$ which eliminates them. Alternatively, interaction term of the Hubbard type, $U \sum_i \hat{n}_{i\uparrow}\hat{n}_{i\downarrow}$, can be added to the Hamiltonian (1) explicitly. In such situation and for sufficiently large U, the energy of the double occupancies is high so that they effectively are not present in the system. In effect, the projector $\hat{\mathcal{P}}_0$ can be omitted (cf. e.g. Ref. [6], where such approach was formulated).

However, one could argue that e.g. for the cuprates, the term proportional to J_{ij} does not only reflect the kinetic exchange interactions of d-holes in the Cu plane, but also incorporates effects of the Cu–O hybridization, hence the $J_{ij} \equiv 4t_{ij}^2/U$ identity is no longer valid [7]. Furthermore, the Cu-O hybridization can reduce the cost of double occupancy, and the requirement of large U may no longer be necessary. Thus, the enlarged Hamiltonian becomes effective and all three parameters, t_{ij}, J_{ij}, and U, can now be treated as independent parameters. This can be regarded as rationale for introducing the $t-J-U$ model.

The $t-J-U$ model was extensively studied by Zhang [8], Gan et al. [9, 10], and Bernevig et al. [11]. However, no antiferromagnetic order was considered in those works†.

Recently, we have covered the topic (cf. Ref. [13]) and we have found that in the $t-J-U$ model for sufficiently large U, a coexistence of antiferromagnetism and superconductivity (AF+SC) appears, but only in a very limited hole-doping (close range to the half-filled band). The present article is an extension of the previous work [13]. The model is refined to consider also the second nearest-neighbor hopping.

The structure of this paper is as follows: in Sect. 2 the model is defined, as well as the approximations leading to the effective single-particle Hamiltonian. In Sect. 3 the details of the solving procedure are provided. Results and discussions are presented in Sects. 4 and 5, respectively.

*e-mail: marcin.abram@uj.edu.pl

†Some attempts was made by some authors, cf. Ref. [12], but their method suffered of some inconsistencies (cf. discussion in Ref. [13]).

2. The model and the effective single-particle Hamiltonian

The starting Hamiltonian for t–J–U model has the form [8–10]:

$$\hat{\mathcal{H}} = \sum_{i\neq j,\,\sigma} t_{ij}\hat{c}^{\dagger}_{i\sigma}\hat{c}_{j\sigma} + \sum_{i\neq j} J_{ij}\,\boldsymbol{S}_i\cdot\boldsymbol{S}_j + U\sum_i \hat{n}_{i\uparrow}\hat{n}_{i\downarrow}, \quad (2)$$

where t_{ij} denotes the hopping term, J_{ij} the spin-exchange coupling, U the on-site Coulomb repulsion, $\hat{c}^{\dagger}_{i\sigma}$ ($\hat{c}_{i\sigma}$) are creation (annihilation) operators of an electron on site i and with spin σ; $\hat{n}_{i\sigma}\equiv\hat{c}^{\dagger}_{i\sigma}\hat{c}_{i\sigma}$ denotes electron number operator, $\boldsymbol{S}_i\equiv(\hat{S}^x_i,\,\hat{S}^y_i,\,\hat{S}^z_i)$ spin operator. In the fermion representation $\hat{S}^{\sigma}_i\equiv\frac{1}{2}(\hat{S}^x_i+\sigma\hat{S}^y_i)=\hat{c}^{\dagger}_{i\sigma}\hat{c}_{i\sigma}$, while $\hat{S}^z_i=\frac{1}{2}(\hat{n}_{i\uparrow}-\hat{n}_{i\downarrow})$.

Here, we consider a two-dimensional, square lattice. This is justified since cuprates have a quasi two--dimensional structure. We assume that $J_{ij}\equiv J/2$ if i, j indicate the nearest neighbors, and $J_{ij}=0$ otherwise. We restrict hopping to the first (t) and the second nearest neighbors (t'). We use the Gutzwiller approach (GA) [14, 15] to obtain an effective single-particle Hamiltonian. Specifically, to calculate the average $\langle\hat{\mathcal{H}}\rangle\equiv\langle\Psi\mid\hat{\mathcal{H}}\mid\Psi\rangle$, the form of $|\Psi\rangle$ has to be known. We are assuming that $|\Psi\rangle\approx|\Psi_G\rangle\equiv\hat{P}_G|\Psi_0\rangle=\prod_i\left(1-(1-g)\hat{n}_{i\uparrow}\hat{n}_{i\downarrow}\right)|\Psi_0\rangle$, where g is a variational parameter and $|\Psi_0\rangle$ is a single-particle wave function. Let us note that for $g=0$ the projector cuts off all states with double occupation (two electrons on one site), while for $g=1$ we have simple $|\Psi_G\rangle=|\Psi_0\rangle$. In GA, we assume that

$$\frac{\langle\Psi_G\mid\mathcal{H}\mid\Psi_G\rangle}{\langle\Psi_G\mid\Psi_G\rangle}=\langle\Psi_0\mid\hat{\mathcal{H}}_{\rm eff}\mid\Psi_0\rangle\equiv\langle\hat{\mathcal{H}}_{\rm eff}\rangle_0, \quad (3)$$

where

$$\begin{aligned}\hat{\mathcal{H}}_{\rm eff} &= t\sum_{\langle i,j\rangle,\sigma} g_{i\sigma}g_{j\sigma}\left(\hat{c}^{\dagger}_{i\sigma}\hat{c}_{j\sigma}+{\rm H.c.}\right)\\ &+t'\sum_{\langle\langle i,j\rangle\rangle,\sigma} g_{i\sigma}g_{j\sigma}\left(\hat{c}^{\dagger}_{i\sigma}\hat{c}_{j\sigma}+{\rm H.c.}\right)\\ &+J\sum_{\langle i,\,j\rangle,\,\sigma} g^s_i g^s_j\,\boldsymbol{S}_i\cdot\boldsymbol{S}_j+U\sum_i\hat{n}_{i\uparrow}\hat{n}_{i\downarrow}, \end{aligned} \quad (4)$$

where $\sum_{\langle i,j\rangle}$ and $\sum_{\langle\langle i,j\rangle\rangle}$ denotes summation over all unique pairs of first and second nearest neighbors, H.c. is the Hermitian conjugation, and $g_{i\sigma}$, g^s_i are renormalization factors [16, 17]

$$g_{i\sigma}=\sqrt{g^s_i}\left(\sqrt{\frac{(1-n_{i\bar{\sigma}})(1-n+d^2)}{1-n_{i\sigma}}}+\sqrt{\frac{n_{i\bar{\sigma}}\,d^2}{n_{i\sigma}}}\right), \quad (5)$$

$$g^s_i=\frac{n-2d^2}{n-2n_{i\sigma}n_{i\bar{\sigma}}}, \quad (6)$$

with $n\equiv\langle\hat{n}_{i\uparrow}+\hat{n}_{i\downarrow}\rangle_0$, $d^2\equiv\langle\hat{n}_{i\uparrow}\hat{n}_{i\downarrow}\rangle_0$, and

$$n_{i\sigma}\equiv\langle\hat{c}^{\dagger}_{i\sigma}\hat{c}_{i\sigma}\rangle_0\equiv\frac{1}{2}\left(n+\sigma\,{\rm e}^{{\rm i}\boldsymbol{Q}\cdot\boldsymbol{R}_i}\,m\right), \quad (7)$$

where m is (bare) sublattice magnetization per site, $\boldsymbol{Q}\equiv(\pi,\,\pi)$, and $\boldsymbol{R}_i$ is the position vector of site i. We divide the lattice into two sublattices, A where on average the spin is *up*, and B where on average is *down* (cf. Fig. 1). Thus $n_{i\in A,\sigma}\equiv\frac{1}{2}\,(n+\sigma m)$, and $n_{i\in B,\sigma}\equiv\frac{1}{2}\,(n-\sigma m)$.

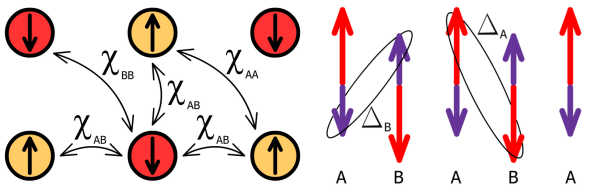

Fig. 1. Schematic interpretation of χ, $\chi_{\rm AA}$ and $\chi_{\rm BB}$ (left part) and $\Delta_{\rm A}$ and $\Delta_{\rm B}$ (right part). To consider antiferromagnetism in the system, we can divide the lattice into two sublattices, A where in average the spin is *up*, and B where in average is *down*. Thus χ denotes hopping between sites belonging to sublattices A and B, while $\chi_{\rm AA}$ and $\chi_{\rm BB}$ hopping within one sublattice (A or B, respectively); $\Delta_{\rm A}$ denotes pairing of majority spins (*up* from sublattice A and *down* from B), and $\Delta_{\rm B}$ pairing of minority spins (*up* from B and *down* from A).

We define average hopping amplitude for the first and the second nearest neighbors (n.n.) as:

$$\chi_{ij\sigma}\equiv\langle\hat{c}^{\dagger}_{i\sigma}\hat{c}_{j\sigma}\rangle_0\equiv \begin{cases}\chi & \text{for 1st nearest neighbor,}\\ \chi_S+\sigma\,{\rm e}^{{\rm i}\boldsymbol{Q}\cdot\boldsymbol{R}_i}\chi_T & \text{for 2nd nearest neighbor,}\end{cases} \quad (8)$$

where $\chi\equiv\chi_{\rm AB}$ denotes hopping between sublattices A and B (or vice versa, cf. left part in Fig. 1); $\chi_S\equiv\frac{1}{2}(\chi_{\rm AA}+\chi_{\rm BB})$ and $\chi_T\equiv\frac{1}{2}(\chi_{\rm AA}-\chi_{\rm BB})$, where $\chi_{\rm AA}$ and $\chi_{\rm BB}$ denotes hopping within one sublattice. We define also the electron pairing between nearest neighbors as

$$\Delta_{ij\sigma}\equiv\langle\hat{c}_{i\sigma}\hat{c}_{j\bar{\sigma}}\rangle_0=-\tau_{ij}\left(\sigma\Delta_S+{\rm e}^{{\rm i}\boldsymbol{Q}\cdot\boldsymbol{R}_i}\Delta_T\right), \quad (9)$$

where $\tau_{ij}\equiv1$ for $j=i\pm\hat{x}$, and $\tau_{ij}\equiv-1$ for $j=i\pm\hat{y}$ to ensure d-wave symmetry. $\Delta_S\equiv\frac{1}{4}\,(\Delta_{\rm A}+\Delta_{\rm B}+{\rm H.c.})$ and $\Delta_T\equiv\frac{1}{4}\,(\Delta_{\rm A}-\Delta_{\rm B}+{\rm H.c.})$, cf. right part in Fig. 1. We assume that all the above averages: χ, χ_S, χ_T, Δ_S, and Δ_T, are real. Finally, we are able to calculate the average $W\equiv\langle\hat{\mathcal{H}}\rangle_0$, which has the form

$$\begin{aligned}\frac{W}{\Lambda} &= 8g_t t\chi+4g^{\rm max}_{t'}t'\chi_S+4g^{\rm min}_{t'}t'\chi_S)\\ &+g_sJ\left(-\frac{1}{2}m^2-3\chi^2-3\Delta_S^2+\Delta_T^2\right)+Ud^2, \end{aligned} \quad (10)$$

where the renormalization factors $g_t\equiv g_{i\in{\rm A}\sigma}g_{j\in{\rm B}\sigma}$, $g^{\rm max}_{t'}\equiv g_{i\in{\rm A}\uparrow}g_{j\in{\rm A}\uparrow}$, $g^{\rm min}_{t'}\equiv g_{i\in{\rm A}\downarrow}g_{j\in{\rm A}\downarrow}$, and $g_s\equiv g^s_{i\in{\rm A}}g^s_{j\in{\rm B}}$.

3. Statistically-consistent Gutzwiller approximation

To determine the stable phases and their characteristics (sublattice magnetization, SC gap, etc.) we construct the grand potential functional, which we next minimize with respect to all parameters. However, to ensure that the averages calculated in a self-consistent manner are equal to those obtained variationally, we first use the so-called statistically-consistent Gutzwiller

approximation (SGA) (cf. introduction to SGA [18], and examples of its use in the context of the t–J model [19, 20], the t–J–U model [13], the Anderson–Kondo lattice model [21, 22], the extended Hubbard models [23–25], or the liquid ^{3}He [26]). Here, we impose constraints on each average, which is present in Eq. (10). Hence, our effective Hamiltonian takes the form

$$\begin{aligned}\hat{K} = W &- \sum_{\langle i,j\rangle,\sigma} \left(\lambda^{\chi}_{ij\sigma}\left(\hat{c}^{\dagger}_{i\sigma}\hat{c}_{j\sigma} - \chi_{ij\sigma}\right) + \text{H.c.}\right) \\ &- \sum_{\langle\langle i,j\rangle\rangle,\sigma} \left(\lambda^{\chi}_{ij\sigma}\left(\hat{c}^{\dagger}_{i\sigma}\hat{c}_{j\sigma} - \chi_{ij\sigma}\right) + \text{H.c.}\right) \\ &- \sum_{\langle i,j\rangle} \left(\lambda^{\Delta}_{ij\sigma}\left(\hat{c}_{i\sigma}\hat{c}_{j\bar{\sigma}} - \Delta_{ij\sigma}\right) + \text{H.c.}\right) \\ &- \sum_{i\sigma} \left(\lambda^{n}_{i\sigma}\left(\hat{n}_{i\sigma} - n_{i\sigma}\right)\right) - \mu\sum_{i\sigma}\hat{n}_{i\sigma}, \end{aligned} \tag{11}$$

where we have also introduced the chemical potential term $-\mu\sum_{i\sigma}\hat{n}_{i\sigma}$. Symbols $\{\lambda_i\}$ stand for Lagrange multipliers, having the same form as the corresponding to them averages, namely

$$\lambda^{n}_{i\sigma} = \frac{1}{2}\left(\lambda_n + \sigma\,\mathrm{e}^{\mathrm{i}\boldsymbol{Q}\cdot\boldsymbol{R}_i}\lambda_m\right), \tag{12a}$$

$$\lambda^{\chi}_{ij\sigma} \equiv \begin{cases} \lambda_{\chi} & \text{for 1st n.n.,} \\ \lambda_{\chi_S} + \sigma\,\mathrm{e}^{\mathrm{i}\boldsymbol{Q}\cdot\boldsymbol{R}_i}\lambda_{\chi_T} & \text{for 2nd n.n.,} \end{cases} \tag{12b}$$

$$\lambda^{\Delta}_{ij\sigma} = -\tau_{ij}\left(\sigma\lambda_{\Delta_S} + \mathrm{i}\,\mathrm{e}^{\mathrm{i}\boldsymbol{Q}\cdot\boldsymbol{R}_i}\lambda_{\Delta_T}\right). \tag{12c}$$

In the next step we diagonalize the grand Hamiltonian $\hat{K}$ and construct the grand potential functional $\mathcal{F} = -\frac{1}{\beta}\ln\mathcal{Z}$, where $\beta = 1/k_{\mathrm{B}}T$, and $\mathcal{Z} = \mathrm{Tr}\left(\mathrm{e}^{-\beta\hat{K}}\right)$. The minimization conditions for determining all quantities and Lagrange multiplies are

$$\frac{\partial\mathcal{F}}{\partial A_i} = 0, \quad \frac{\partial\mathcal{F}}{\partial\lambda_i} = 0, \quad \frac{\partial\mathcal{F}}{\partial d} = 0, \tag{13}$$

where $\{A_i\}$ denote here all 7 averages: χ, χ_S, χ_T, Δ_S, Δ_T, n, and m, while $\{\lambda_i\}$ denote all Lagrange multipliers λ_{χ}, λ_{χ_S}, λ_{χ_T}, λ_{Δ_S}, λ_{Δ_T}, λ_n, and λ_m. The system of equations is solved self-consistently. To determine the stability of physical phases, free energy has to be calculated according to the prescription

$$F = \mathcal{F}_0 + \Lambda\mu n, \tag{14}$$

where $\mathcal{F}_0$ is the value of the grand potential functional $\mathcal{F}$ at minimum, and Λ is the number of lattice sites.

4. Results

The numerical calculations were carried out using GNU Scientific Library (GSL) [27] for a two-dimensional, square lattice of $\Lambda = 512\times512$ size, and unless stated otherwise, $t = -1$, $J = |t|/3$, and $\beta|t| = 1500$ (it was checked that for such large $\beta \equiv 1/k_{\mathrm{B}}T$ we have effectively $T = 0$).

Here, χ, χ_S, χ_T, Δ_S, Δ_T, and m are bare averages. Renormalized by a proper Gutzwiller factors, they become order parameters of the corresponding phases. Thus: $\chi^c \equiv g_t\chi$, $\chi^c_S \equiv g_{t'}\chi_S$, $\chi^c_T \equiv g_{t'}\chi_T$, $\Delta^c_S \equiv g_{\Delta}\Delta_S$, $\Delta^c_T \equiv g_{\Delta}\Delta_T$, and $m^c = g_m m$, where (cf. Eqs. (5) and (6)), $g_t \equiv g_{i\in\mathrm{A}\sigma}g_{j\in\mathrm{B}\sigma}$, $g_{t'} \equiv \frac{1}{2}(g_{i\in\mathrm{A}\uparrow}g_{j\in\mathrm{A}\uparrow} + g_{i\in\mathrm{A}\downarrow}g_{j\in\mathrm{A}\downarrow})$, $g_{\Delta} \equiv \frac{1}{2}(g_{i\in\mathrm{A}\uparrow}g_{i\in\mathrm{B}\downarrow} + g_{i\in\mathrm{A}\downarrow}g_{i\in\mathrm{B}\uparrow})$, and $g_m \equiv g^s_{i\in\mathrm{A}}g^s_{j\in\mathrm{B}}$.

4.1. Results for t–J–U model, for $t' = 0$

In the limit of the low temperature ($T \to 0$, i.e. $\beta \to +\infty$) the SC phase is stable for any value of $\delta > 0$, $U > 0$, or $J > 0$. For sufficiently large Coulomb repulsion ($U > U_{\mathrm{cr}}$) and for small hole doping ($\delta < \delta_{\mathrm{cr}}$), a coexistent AF+SC phase can be found (cf. Fig. 2). For $\delta = 0$ and for $U > U_{\mathrm{cr}}$ we obtain the Mott insulating state. For $\delta = 0$ and $U < U_{\mathrm{cr}}$ electrons can have double occupancies ($d^2 \neq 0$) and the superconducting pairing is maintained (such a feature in literature is called the gossamer superconductivity [28]).

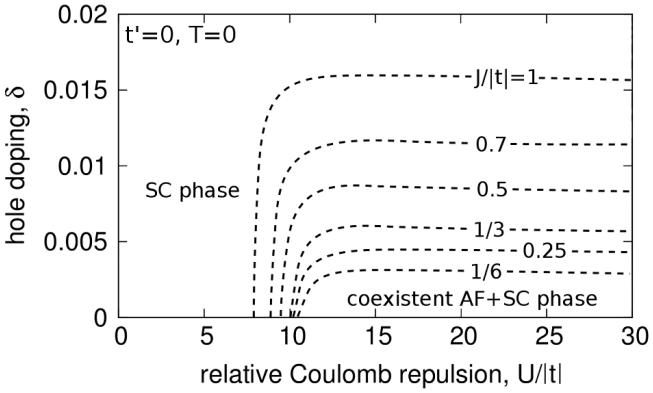

Fig. 2. The AF+SC coexistence region for $t' = 0$, $T = 0$, and different values of the the exchange coupling J (in units of t).

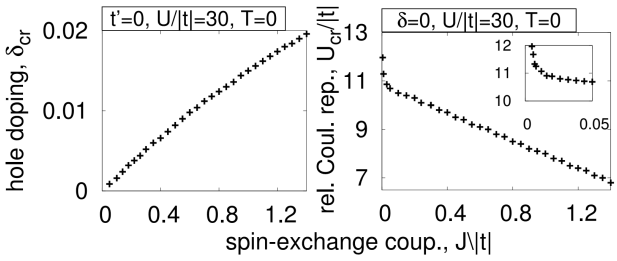

Fig. 3. In the left part, the effect of the spin-exchange coupling J on the critical hole doping (δ_{cr}). In the right part, the effect of J on the critical relative Coulomb repulsion (U_{cr}). Let us note that $\delta_{\mathrm{cr}}(J)$ is quasi-linear in the whole range of the tested parameter, while for $U_{\mathrm{cr}}(J)$ we observe non-linear behavior for $J/|t| < 0.03$ (cf. the inset in the right part).

The influence of the spin-exchange coupling J on the range of the coexistence region AF+SC was examined. δ_{cr} is a linear function of J (cf. the left part in Fig. 3), while the critical Coulomb repulsion U_{cr} has non-linear behavior for $J/|t| < 0.03$ (the value of U_{cr} grows rapidly when J decrease, cf. the right part in Fig. 3).

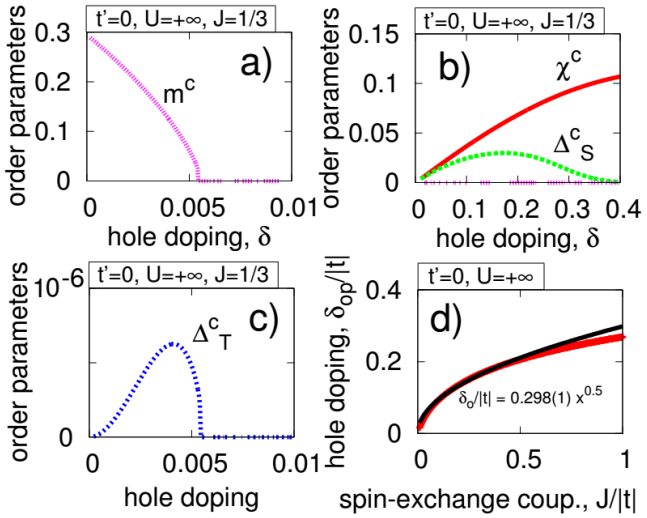

Fig. 4. In the parts (a)–(c), selected order parameters as a function of doping δ are presented. Let us note that $\Delta_T \neq 0$ only if $m^c \neq 0$. In the part (d), the optimal doping for a singled SC gap (Δ_S^c) is shown, as a function of the exchange coupling J, in $U \to +\infty$ limit (red line). The black line is a numerical fit, $f(x) = 0.298(1)\, x^{0.5}$.

For $U \to +\infty$ we reproduce the results of the t–J model. As was checked, even for not too large U the convergence to t–J model results is sufficient. For instance, for $U = 30$ our results match those for the t–J model (so the limit $U = +\infty$) within less than 1% error, and for $U = 100$ within an error of less than 0.1%. In Fig. 4 in parts (a)–(c), the correlated states χ^c, Δ_S^c, Δ_T^c, m^c, and d^2 are presented for $U = 100$ and $\beta|t| = 1500$ (effectively $U = +\infty$ and $T = 0$). Let us note that the staggered component of the superconducting gap (Δ_T) is very small and appears only when $m^c \neq 0$, i.e., in the AF+SC phase. However, Δ_T value is very small when compared to value of Δ_S (there is $\Delta_T^c/\Delta_S^c < 10^{-4}$), thus its effect can be practically neglected[‡].

In the last part (d) in Fig. 4 we show (red line) the optimal doping δ_{op} for singled SC gap (Δ_S^c) as a function of J. The black line in this part is a function $f \sim \sqrt{J/|t|}$, numerically fitted to the data.

4.2. A significance of the second nearest neighbors hopping t'

The influence of the second nearest neighbors hopping term t' is exhibited in Fig. 5. Let us note that the critical Coulomb repulsion for AF+SC phase ($U_{\rm cr}$) is practically independent of the value of t' (it was checked, $U_{\rm cr}(t'=0)$ and $U_{\rm cr}(t'=1)$ differ about 1%). The critical doping

[‡]The free energy F_0 in minimum (for $T = 0$) is equal to W (cf. Eq. (10)). If $\Delta_T^c/\Delta_S^c \equiv \Delta_T/\Delta_S < 10^{-4}$ then the impact of Δ_T^c for the final energy of the solution is about 10^{-8} smaller than the impact of Δ_S^c. Thus Δ_T in practical calculations can be neglected.

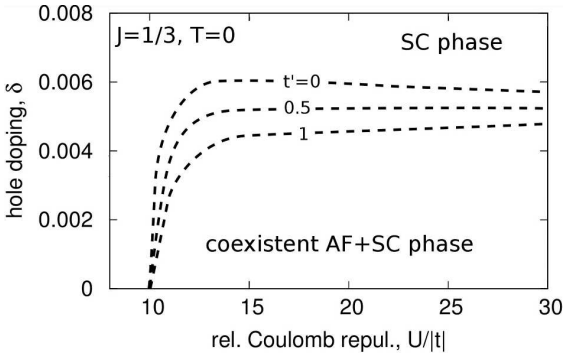

Fig. 5. Significance of the second nearest neighbors hopping. Values of t' are given in units of t. The presence of t' does not change the AF+SC range in qualitative manner.

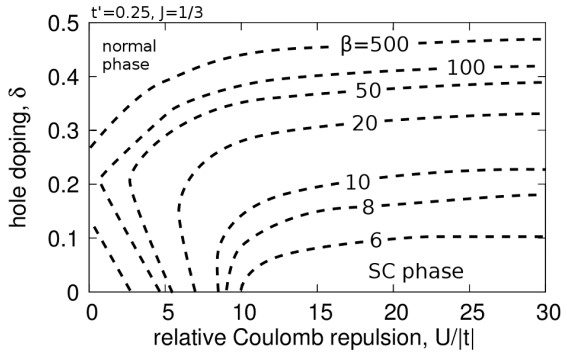

Fig. 6. The effect of the temperature (meassured in units of $|t|$) on the stability of SC phase in t–t'–J–U model ($t = -1$, $t' = 0.25$). The dashed lines correspond to the range of SC phase for $\beta = 500$ ($T \sim 5$–12 K), $\beta = 100$ (25–60 K), $\beta = 50$ (50–120 K), $\beta = 20$ (130–290 K), $\beta = 10$ (250–580 K), $\beta = 8$ (320–720 K), $\beta = 6$ (420–1000 K).

($\delta_{\rm cr}$) is more susceptible to the value of t', but note that the typical value of the t' ranges from $-0.1t$ to $-0.5t$ (cf. Ref. [29, Ch. 7.1.2]), and in such a range $\delta_{\rm cr}$ changes only about 10%.

4.3. Nonzero temperature

In the limit of the zero temperature, for small U or/and large δ, the value of the SC order parameter Δ_S^c is small, but still nonzero. Increasing the temperature (decreasing the parameter β), the paramagnetic (PM) phase appears in region where the order parameter of SC phase was weak (cf. Fig. 6). For large T (small β), the range of the SC phase is reduced to the vicinity of the Mott-insulator phase ($\delta \gtrsim 0$, and $U > U_{\rm cr}$).

The measured value of the hopping term t for the cuprates ranges from 0.22 eV to 0.5 eV (cf. Ref. [30, Ch. 7.1.2]). Hence the $\beta|t| = 1500$ corresponds to the temperature 2–4 K, $\beta|t| = 500$ to 5–12 K, $\beta|t| = 100$ to 25–60 K, $\beta|t| = 50$ to 50–120 K, $\beta|t| = 20$ to 130–290 K, $\beta|t| = 10$ to 250–580 K, $\beta|t| = 8$ to 320–720 K, $\beta|t| = 6$ to 420–1000 K.

5. Conclusions

In this work, the t–t'–J–U model was studied in the SGA scheme which plays the role of the mean-field approximation. In the limit of the zero temperature, three phases were found: superconductivity (SC), coexistent antiferromagnetic-superconducting state (AF+SC), and the Mott-insulating phase (for the half filling). The AF+SC phase exists only for sufficiently large Coulomb repulsion ($U > U_{\rm cr}$) and for small hole doping ($\delta < \delta_{\rm cr}$). We have shown how the range of AF+SC coexistence varies with J and t'. The impact of J was significant, both for $U_{\rm cr}$ and for $\delta_{\rm cr}$. However, the impact of t' was much smaller and in the range of physical values (for cuprates $t' \sim 0.1$–$0.5|t|$), it can be marginal.

The impact of the non-zero temperatures was tested. For $T > 0$, additionally to SC and AF+SC phases, a paramagnetic phase (normal phase) appears. The ranges of SC and AF+SC phases decrease with the temperature, but they remain stable even for relatively high temperature (≈ 1000 K). Such results, contradictory to the experiments, can be explained by the used method (the saddle-point method) and approximations used (the mean-field and the Gutzwiller approximation). To study more accurately the stability of the phases, more sophisticated method should be used (cf. e.g. the diagrammatic expansion for Gutzwiller-wave functions (DE-GWF) [29]).

Acknowledgments

I would like to express my gratitude to Prof. J. Spałek for his support and helpful detailed comments. I would also like to thank M. Wysokiński for discussions, and A. Hartnett for her critical reading of the manuscript. This research was supported by the Foundation for Polish Science (FNP) under the grant TEAM. Parts of the calculations were performed on the TERAACMIN supercomputer in the Academic Centre for Materials and Nanotechnology (ACMIN) of AGH University of Science and Technology in Kraków.

References

[1] J. Spałek, A.M. Oleś, *Physica B+C* **86-88**, 375 (1977); K.A. Chao, J. Spałek, A.M. Oleś, *J. Phys. C* **10**, L271 (1977).

[2] J. Spałek, *Acta Phys. Pol. A* **111**, 409 (2007).

[3] E. Dagotto, *Rev. Mod. Phys.* **66**, 763 (1994).

[4] P.A. Lee, N. Nagaosa, X.-G. Wen, *Rev. Mod. Phys.* **78**, 17 (2006).

[5] J. Jędrak, Ph.D. thesis, Jagiellonian University, Kraków 2011.

[6] H.Q. Lin, *Phys. Rev. B* **44**, 4674 (1991).

[7] F.C. Zhang, T.M. Rice, *Phys. Rev. B* **37**, 3759 (1988).

[8] F.C. Zhang, *Phys. Rev. Lett.* **90**, 207002 (2003).

[9] J.Y. Gan, F.C. Zhang, Z.B. Su, *Phys. Rev. B* **71**, 014508 (2005).

[10] J.Y. Gan, Y. Chen, Z.B. Su, F.C. Zhang, *Phys. Rev. Lett.* **94**, 067005 (2005).

[11] B.A. Bernevig, R.B. Laughlin, D.I. Santiago, *Phys. Rev. Lett.* **91**, 147003 (2003).

[12] F. Yuan, Q. Yuan, C.S. Ting, *Phys. Rev. B* **71**, 104505 (2005); H. Heiselberg, *Phys. Rev. A* **79**, 063611 (2009); K.-K. Voo, *J. Phys., Condens. Matter* **23**, 495602 (2011).

[13] M. Abram, J. Kaczmarczyk, J. Jędrak, J. Spałek, *Phys. Rev. B* **88**, 094502 (2013).

[14] M.C. Gutzwiller, *Phys. Rev. Lett.* **10**, 159 (1963).

[15] M.C. Gutzwiller, *Phys. Rev.* **137**, A1726 (1965).

[16] T. Ogawa, K. Kanda, T. Matsubara, *Prog. Theor. Phys.* **53**, 614 (1975).

[17] F.C. Zhang, C. Gros, T.M. Rice, H. Shiba, *Supercond. Sci. Technol.* **1**, 36 (1988).

[18] J. Jędrak, J. Kaczmarczyk, J. Spałek, arXiv:1008.0021, 2010, unpublished.

[19] J. Jędrak, J. Spałek, *Phys. Rev. B* **81**, 073108 (2010); J. Jędrak, J. Spałek, *Phys. Rev. B* **83**, 104512 (2011).

[20] J. Kaczmarczyk, J. Spałek, *Phys. Rev. B* **84**, 125140 (2011).

[21] O. Howczak, J. Spałek, *J. Phys., Condens. Matter* **24**, 205602 (2012).

[22] O. Howczak, J. Kaczmarczyk, J. Spałek, *Phys. Status Solidi B* **250**, 609 (2013).

[23] M. Zegrodnik, J. Spałek, J. Bünemann, *New J. Phys.* **15**, 073050 (2013).

[24] J. Spałek, M. Zegrodnik, *J. Phys. Condens. Matter* **25**, 435601 (2013).

[25] A.P. Kądzielawa, J. Spałek, J. Kurzyk, W. Wójcik, *Eur. Phys. J. B* **86**, 252 (2013).

[26] M.M. Wysokiński, J. Spałek, *J. Phys. Condens. Matter* **26**, 055601 (2014).

[27] M. Galassi, J. Davies, J. Theiler, B. Gough, P. Jungman, G. abd Alken, M. Booth, F. Rossi, *GNU Scientific Library Reference Manual*, 3rd ed., Network Theory, Ltd., London 2009.

[28] R.B. Laughlin, *Philos. Mag.* **86**, 1165 (2006).

[29] J. Kaczmarczyk, J. Spałek, T. Schickling, J. Bünemann, *Phys. Rev. B* **88**, 115127 (2013).

[30] N. Plakida, *High-Temperature Cuprate Superconductors: Experiment, Theory and Applications*, Springer, New York 2010.

Article 3:

It is the first out of three papers, where we study the Anderson lattice model (ALM) by means of the statistically consistent Gutzwiller approximation (SGA). We compare our results with the experimental findings for UGe_2 compound, namely the magnetic phase sequence, order of phase transitions and the appearance of critical points, finding qualitative agreement. We address the problem of the origin of observed ferromagnetic states in UGe_2. Namely, we show that using ALM the phase sequence can be explained as an effect of competition between the f–f electron Coulomb interaction energy and the hybridization between the f-electron and the conduction band.

PHYSICAL REVIEW B **90**, 081114(R) (2014)

Ferromagnetism in UGe_2: A microscopic model

Marcin M. Wysokiński,* Marcin Abram,† and Józef Spałek‡
Marian Smoluchowski Institute of Physics, Jagiellonian University, Reymonta 4, PL-30-059 Kraków, Poland
(Received 25 July 2014; revised manuscript received 18 August 2014; published 26 August 2014)

The Anderson lattice model is used to explain the principal features of the heavy fermion compound UGe_2 by means of the *generalized Gutzwiller approach* (the statistically consistent Gutzwiller approximation method). This microscopic approach successfully reproduces the magnetic and electronic properties of this material, in qualitative agreement with experimental findings from magnetization measurements, neutron scattering, and de Haas–van Alphen oscillations. Most importantly, it explains the appearance, sequence, character, and evolution in an applied magnetic field of the observed in UGe_2 ferromagnetic and paramagnetic phases as an effect of a competition between the f-f electron Coulomb interaction energy and f-conduction electron hybridization.

DOI: 10.1103/PhysRevB.90.081114 PACS number(s): 71.27.+a, 75.30.Kz, 71.10.−w

Introduction. The discovery of spin-triplet superconductivity (SC) inside the ferromagnetic (FM) phase of the heavy fermion compound UGe_2 [1] sparked an intense discussion about the cause of such a coexistence. Although the spin-triplet paired phase has been known to appear in condensed ^{3}He [2] and most likely in Sr_2RuO_4 [3], until its discovery in UGe_2 there was no convincing example for a strongly FM material hosting SC.

Specifically, the phase diagram for UGe_2 on the temperature-pressure (T-p) plane contains both SC and two FM phases, with stronger and weaker magnetization [4], usually referred to as FM2 and FM1, respectively, as well as a paramagnetic phase (PM), with first-order phase transitions between them at low temperature, $T \lesssim 7$ K [5]. The FM-SC coexistence is strongly suggestive of a single mechanism based on magnetic correlations which is responsible for the appearance of both FM and SC and thus should be treated on equal footing, as, e.g., in UGe_2 both phases disappear at the same pressure [1,4]. Another indication of the coupled nature of both phases is that the SC dome on the T-p plane coincides with the phase transition between FM2 and FM1 [4]. Thus, we address here in detail the question of the microscopic origin of the observed ferromagnetism, as it should bring us closer to determining the mechanism of superconductivity. The question related to the inclusion of SC requires a separate study [6,7] (see the discussion at the end).

Experimental observations suggest that the ferromagnetism in UGe_2 has an itinerant nature [1,8,9] and is mediated by the uranium $5f$ electrons [1,10,11]. Delocalization of the $5f$ electrons can be interpreted as resulting from the hybridization of the original $5f$ atomic states with those from the conduction band [8] derived from p states due to Ge and d-s states due to U. This is supported by a noticeable difference in the effective paramagnetic moment per uranium atom in this compound with respect to the corresponding atomic value for either the f^3 or f^2 configurations [1], as well as from a fractional value of the magnetization relative to the atomic-moment saturation. This means that the Hund's rule coupling in the atomic sense is broken, and the itineracy of the $5f$ electrons is the source of the band ferromagnetism in which Hund's ferromagnetic interaction plays a role, in combination with a stronger intra-atomic Coulomb interaction. Thus, f-electron orbital degeneracy is not essential, but the role of hybridization is.

Apart from other theories concerning the origin of FM in the considered class of materials [12,13], there exists [14] a phenomenological explanation of the magnetic properties within a rigid-band Stoner approach, which requires introduction of an *ad hoc* two-peaked structure of the density of states (DOS) near the Fermi surface (FS). Our purpose is to invoke a microscopic description starting from the Anderson-lattice model (ALM) which is appropriately adapted to the heavy fermion compound UGe_2. This comprises a relatively simple quasi-two-dimensional electronic structure [15–17]. From such a starting point an effective nonrigid two-band description arises naturally and allows for a detailed explanation of the magnetic and electronic properties, at least on a semiquantitative level. Additionally, as the correlations among $5f$ electrons are sizable, an emergence of the Stoner-like picture of FM can be accounted for only with the inclusion of specific features coming from the electronic correlations. Although the resulting explanation of the physical properties is semiquantitative in nature, it provides, in our view, a coherent picture of a number of properties [4,10,11,18,19].

Model. We base our predictions for the ALM on a variational treatment with the Gutzwiller wave function $|\psi_G\rangle = \prod_{\mathbf{i}} \hat{P}_{\mathbf{i}} |\psi_0\rangle$, where $\hat{P}_{\mathbf{i}}$ is the operator projecting out part of the double occupancies from the uncorrelated ground state $|\psi_0\rangle$ at site $\mathbf{i}$. We have extended the standard approach [20–22] to the *statistically consistent form* [23] [statistically consistent Gutzwiller approximation (SGA) method]. Explicitly, we start with the ALM Hamiltonian, with an applied magnetic field introduced via the Zeeman term ($h \equiv \frac{1}{2} g \mu_B H$), i.e.,

$$\begin{aligned}\hat{\mathcal{H}} - \mu\hat{N} = {} & {\sum_{\mathbf{i},\mathbf{j},\sigma}}' t_{\mathbf{ij}} \hat{c}^{\dagger}_{\mathbf{i},\sigma} \hat{c}_{\mathbf{j},\sigma} - \sum_{\mathbf{i},\sigma} (\mu + \sigma h) \hat{n}^{c}_{\mathbf{i},\sigma} \\ & + \sum_{\mathbf{i},\sigma} (\epsilon_f - \mu - \sigma h) \hat{n}^{f}_{\mathbf{i},\sigma} + U \sum_{\mathbf{i}} \hat{n}^{f}_{\mathbf{i},\uparrow} \hat{n}^{f}_{\mathbf{i},\downarrow} \\ & + V \sum_{\mathbf{i},\sigma} (\hat{f}^{\dagger}_{\mathbf{i},\sigma} \hat{c}_{\mathbf{i},\sigma} + \hat{c}^{\dagger}_{\mathbf{i},\sigma} \hat{f}_{\mathbf{i},\sigma}), \end{aligned} \tag{1}$$

*marcin.wysokinski@uj.edu.pl
†marcin.abram@uj.edu.pl
‡ufspalek@if.uj.edu.pl

where the primed sum denotes summation over all lattice sites $\mathbf{i} \neq \mathbf{j}$, and $\hat{f}$ and $\hat{c}$ are operators related to f and c orbitals, respectively, with spin $\sigma = \uparrow, \downarrow$. We have also defined the total number of electrons operator as $\hat{N}$, and for the respective orbitals and spins as $\hat{n}^f_{\mathbf{i},\sigma} \equiv \hat{f}^\dagger_{\mathbf{i},\sigma}\hat{f}_{\mathbf{i},\sigma}$, $\hat{n}^c_{\mathbf{i},\sigma} \equiv \hat{c}^\dagger_{\mathbf{i},\sigma}\hat{c}_{\mathbf{i},\sigma}$. In our model, we consider the finite intra-f-orbital Coulomb interaction U, the on-site interorbital hybridization $V < 0$, the hopping amplitude between the first (t) and the second ($t' = 0.25\,|t|$) nearest neighboring sites, and the atomic level for f states placed at $\epsilon_f = -3|t|$. In the following $|t|$ is used as the energy unit.

First, we would like to evaluate the ground-state energy, $E_G \equiv \langle\psi_G \mid \hat{\mathcal{H}} \mid \psi_G\rangle / \langle\psi_G \mid \psi_G\rangle$. Applying the usual procedure [21,22], called the Gutzwiller approximation (GA), we simplify the projection to the local sites on which the operators from (1) act. In that manner one obtains the effective single-particle Hamiltonian in a momentum space with renormalized hybridization by the Gutzwiller narrowing factor q_σ [24–26], namely,

$$\hat{\mathcal{H}}_{\mathrm{GA}} \equiv \sum_{\mathbf{k},\sigma} \Psi^\dagger \begin{pmatrix} \epsilon^c_{\mathbf{k}} - \sigma h - \mu & \sqrt{q_\sigma}\, V \\ \sqrt{q_\sigma}\, V & \epsilon_f - \sigma h - \mu \end{pmatrix} \Psi + \Lambda U d^2, \tag{2}$$

where we have defined $\Psi^\dagger \equiv (\hat{c}^\dagger_{\mathbf{k},\sigma}, \hat{f}^\dagger_{\mathbf{k},\sigma})$, and $\epsilon^c_{\mathbf{k}}$ is the starting conduction band energy, Λ denotes the number of lattice sites, and d^2 is the probability of a having doubly occupied f orbital that we optimize variationally. In order to ensure that variationally calculated polarization and the f-level occupancy would coincide with those coming from the self-consistent procedure [23], we modify our effective Hamiltonian (2) by introducing additional constraints on the polarization (m_f) and the number (n_f) of f electrons via the Lagrange-multiplier method. The effective Hamiltonian with the constraints now takes the form

$$\begin{aligned} &\hat{\mathcal{H}}_{\mathrm{SGA}} \\ &\equiv \hat{\mathcal{H}}_{\mathrm{GA}} - \lambda^f_n \left(\sum_{\mathbf{k},\sigma} \hat{n}^f_{\mathbf{k},\sigma} - \Lambda n_f \right) - \lambda^f_m \left(\sum_{\mathbf{k},\sigma} \sigma \hat{n}^f_{\mathbf{k},\sigma} - \Lambda m_f \right) \\ &= \sum_{\mathbf{k},\sigma} \Psi^\dagger \begin{pmatrix} \epsilon^c_{\mathbf{k}} - \sigma h - \mu & \sqrt{q_\sigma} V \\ \sqrt{q_\sigma} V & \epsilon_f - \sigma\left(h + \lambda^f_m\right) - \lambda^f_n - \mu \end{pmatrix} \Psi \\ &\quad + \Lambda\left(U d^2 + \lambda^f_n n_f + \lambda^f_m m_f\right). \end{aligned} \tag{3}$$

Those constraint parameters λ^f_n and λ^f_m are also determined variationally. They play the role of nonlinear self-consistent fields acting on the charge and the spin degrees of freedom, respectively. Diagonalization of (3) in this spatially homogeneous case leads to four branches of eigenenergies, $E^\pm_{\mathbf{k}\sigma}$ representing two spin-split hybridized bands $E^\pm$. In order to determine the equilibrium properties of the system, we need to find the minimum of the generalized Landau grand-potential functional $\mathcal{F}$,

$$\frac{\mathcal{F}}{\Lambda} = -\frac{1}{\Lambda\beta} \sum_{\mathbf{k}\sigma b} \ln\left[1 + e^{-\beta E^b_{\mathbf{k}\sigma}}\right] + \left(\lambda^f_n n_f + \lambda^f_m m_f + U d^2\right), \tag{4}$$

where $b = \pm$. Effectively, it leads to the set of five nonlinear equations, $\partial\mathcal{F}/\partial\vec{\lambda} = 0$ for $\vec{\lambda} \equiv \{d, n_f, m_f, \lambda^f_n, \lambda^f_m\}$. However, due to the fact that the total number of electrons remains constant when pressure or the magnetic field is applied, we need also to satisfy the equation for the chemical potential μ via the condition

$$n = \frac{1}{\Lambda} \sum_{\mathbf{k}b\sigma} f\left(E^b_{\mathbf{k}\sigma}\right), \tag{5}$$

with f being the Fermi distribution. The equilibrium thermodynamic potential functional defines also the ground-state energy $E_G = \mathcal{F}|_0 + \Lambda\mu_0 n$, where the subscript 0 denotes the optimal values. After carrying out the minimization, we can also calculate the total spin polarization from

$$m \equiv m_c + m_f = \frac{1}{\Lambda} \sum_{\mathbf{k}b\sigma} \sigma f\left(E^b_{\mathbf{k}\sigma}\right). \tag{6}$$

Numerical calculations with a precision of at least 10^{-7} were carried out for a two-dimensional square lattice of $\Lambda = 512 \times 512$ size, and for low temperatures $\beta \equiv 1/k_B T \geqslant 1500$, emulating the $T \to 0$ limit.

Results. First, we analyze FM and PM solutions in the absence of field. In Fig. 1 we draw a phase diagram on the total filling–hybridization strength plane. For weak hybridization, FM phases are favored due to the negative balance between the increase of the kinetic and decrease of the Coulomb energies, caused by a relative shift of the spin-resolved DOS.

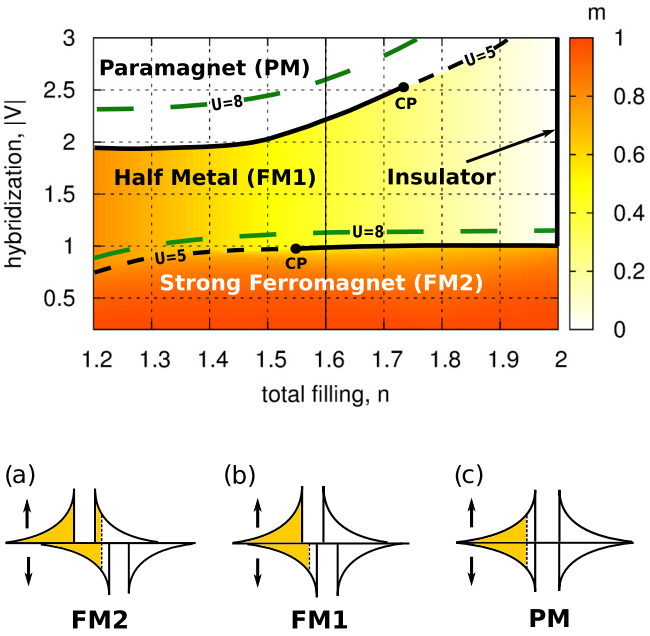

FIG. 1. (Color online) Top: Phase diagram on the plane total filling–hybridization strength for the zero field, containing both FM and PM phases for $U = 5$. The color scale denotes total spin polarization m. Phases are divided by the dashed and the solid lines. Dashed lines denote the second-order transition, whereas the solid denotes the first-order transition with the critical points, CP. Fine dashed lines mark how the phase borders would change for $U = 8$. (a)–(c) depict a schematic spin-resolved density of states corresponding to the phase sequence appearing along the solid vertical line (from bottom to top).

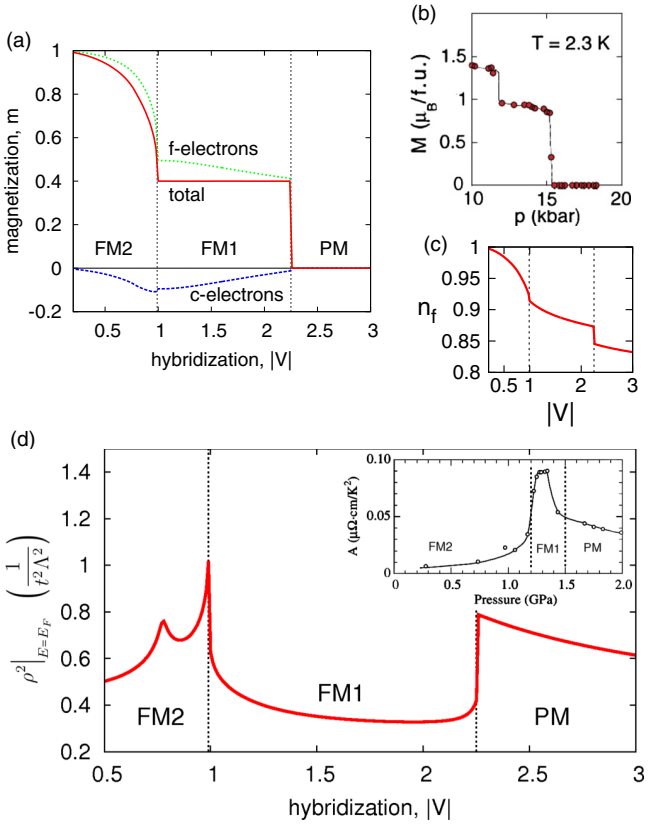

FIG. 2. (Color online) (a) Magnetization as a function of hybridization strength for the band filling $n = 1.6$, and the Coulomb repulsion $U = 5$. Both phase transitions induced by the hybridization change are of first order. (b) Corresponding experimental results from Ref. [4]. (c) f-orbital filling as a function of hybridization. (d) Square of DOS at the Fermi level vs $|V|$ through the phase sequence. Inset: Experimentally measured T^2-term coefficient A of the resistivity vs pressure from Ref. [18].

This is visualized by the diminution of the spin-subband overlap up to the FS—cf. Figs. 1(a) and 1(b). The appearance of a spontaneous polarization, as a result of a competition between the kinetic and the Coulomb energies, is in fact the feature of the Stoner mechanism for the band FM onset. In comparison to the usual single-band (e.g., Hubbard) model, we can distinguish in a natural manner between the two FM phases. The first (FM1) appears when the chemical potential is placed in the hybridization gap, between the spin subbands of the lower hybridized band, which is characterized also by magnetization equal to $m = 2 - n$ [cf. Fig. 1(b)]. In that situation, only the spin-minority carriers are present at and near the FS. The second phase (FM2) emerges when we further lower the hybridization and thus the chemical potential enters the majority spin-subband DOS [cf. Fig. 1(a)], giving rise to a step (discontinuous) increase in magnetization [cf. Fig. 2(a)]. In the limit of strong hybridization, for a fixed total filling, when the correlations weaken due to lowering of the f-orbital average occupancy [$n_f \lesssim 0.85$, cf. Fig. 2(c)], the kinetic energy gain outbalances a subsequent reduction of the average Coulomb interaction and the PM phase is energetically favorable. A similar mechanism for the formation of FM and, in particular, the characterization of phases, was studied before in Refs. [24–27].

In UGe_2 the spacing between Ge and U atoms decreases with increasing pressure, resulting in an enlargement of their orbital overlap. Even though other parameters may also be altered (e.g., ϵ_f), we presume that the main effect of the pressure exerted on the material can be modeled by a generally nonlinear concomitant strengthening of the hybridization amplitude. Thus, from Fig. 1 it can be seen that for the total filling n in the range 1.55–1.75, the sequence of phases and the order of the transitions are the same, as those found experimentally for UGe_2 by increasing the pressure [4,8]. As a representative band filling we have selected $n = 1.6$, marked by the vertical line in Fig. 1. In fact, as we compare the magnetization versus hybridization along the traced line [cf. Fig. 2(a)] with the corresponding experimental data [4] [cf. Fig. 2(b)], we find a good qualitative resemblance. Moreover, the magnetization differentiation among the orbitals [cf. Fig. 2(a)] is in agreement with the neutron scattering data [10,11] at ambient pressure (in our model $|V| \simeq 0.5$), where it was found that, almost exclusively, electrons from uranium atoms (f orbital) contribute to the ferromagnetism. In our picture it results from the fact that the competition between Coulomb repulsion and hybridization-induced itineracy concerns mainly the f electrons. Furthermore, as for low hybridization (in the FM2 phase) we obtain a small compensating polarization due to the c electrons, we suggest that the experimentally observed small negative magnetization between the uranium atoms at ambient pressure [11] may come from the delocalized cloud of conduction electrons.

Our microscopic description of the phase transitions induced by the change of the FS topology also compares favorably with the electronic-state features of UGe_2 derived from de Haas–van Alphen oscillations [18,19]. In Ref. [18] it is suggested that the majority spin FS disappears in the FM1 phase, in complete accord with the character of DOS presented in Fig. 1(b). We also reproduce the feature of an abrupt change of the FS at the FM1-PM phase transition [18,19] [cf. Fig. 2(d)]. Namely, here it corresponds to the step change of the chemical potential position merging into both bands. Furthermore, in the experimental data at the metamagnetic phase transition there is an observed significant enhancement of the quasiparticle mass renormalization [19]. As it is proportional to the DOS at Fermi level, in Fig. 2(d) we provide the corresponding behavior, which can be understood within our model by the chemical potential crossing the high hybridization peak in the majority spin subband. The transition then leads to a step change of FS only in the majority spin subband, while the minority subband evolves rather continuously, which is also seen experimentally [19].

For the sake of completeness, we have shown in the inset in Fig. 2(d) the pressure dependence of the T^2 term of resistivity [18] as it should have roughly the same dependence as the squared DOS at the FS, versus $|V|$ (we assume that the Kadowaki-Woods scaling holds). However, the jump that we obtain at the FM1-PM transition has not been observed in the resistivity measurements [18].

In the applied field, our model is also in good agreement with available experimental data for UGe_2. In Fig. 3(a) we display a phase diagram on the hybridization–applied-

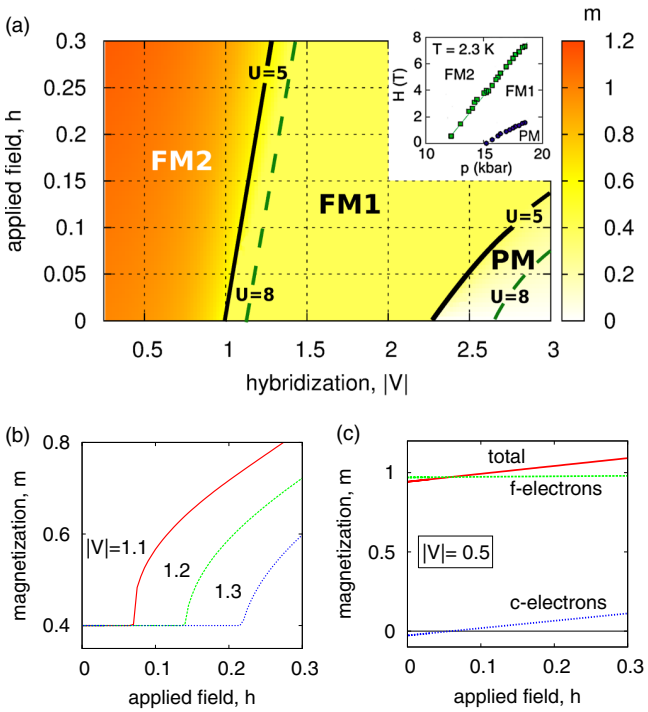

FIG. 3. (Color online) (a) Phase diagram on the applied field–hybridization strength plane for $n = 1.6$ and $U = 5$. The color scale denotes total spin polarization. The dashed lines mark the phase stability thresholds for $U = 8$. In the inset we show experimental results [4]. (b) Magnetization vs applied field for selected hybridization strengths when the system is entering into the FM1 to FM2 phase-transition regime. (c) Evolution of orbital-resolved magnetization with the field for low hybridization, $|V| = 0.5$ (mimicking ambient pressure). Note the very small c-electron polarization up to $h \simeq 0.1$.

magnetic-field plane that corresponds to that determined experimentally [4] [cf. the inset of Fig. 3(a)]. Similarly, as in Ref. [4], the magnetization at the phase transition between FM1 and FM2 triggered by the applied magnetic field starts from the same baseline, independently of the hybridization strength [cf. Fig. 3)]. However, one should note that, due to the fact that pressure not only changes the hybridization magnitude but also other microscopic parameters, we are not able to reproduce the magnetization cascade with increasing magnetic field when crossing the transitions.

The next feature found in UGe_2 at ambient pressure is an initial lack of measurable polarization on the germanium atoms with increasing magnetic field, as inferred from the neutron scattering data [10]. In our model we find a similar trend. For low hybridization ($|V| \simeq 0.5$ emulating ambient pressure), c-electron polarization increases slowly, and even up to $h \approx 0.1$ it is negligible [cf. Fig. 3(c)].

Remarks. With the simple but powerful technique based on the generalized Gutzwiller ansatz (SGA method), applied to the Anderson lattice model, we have constructed a microscopic model of FM in UGe_2. Namely, we are able to reproduce the main experimental features observed at low temperature, by applying either pressure or magnetic field [cf. Figs. 2(a) and 3(a)]. FM properties can be explained within the simplest hybridized two-orbital model, without taking into account the f-orbital degeneracy, i.e., by effectively incorporating both the Coulomb and the Hund's rule interaction into an effective interaction U, as would also be the case in the Hartree-Fock approximation [7].

To determine the stability of SC inside the FM phase, the present approach should be extended to account for the Hund's rule interaction explicitly, which can be crucial for the formation of the unconventional triplet SC [6,7,28,29]. If this is the case, it can be triggered even by a purely repulsive Coulomb interaction in conjunction with the residual Hund's rule coupling, as discussed in Refs. [28,29]. This issue requires a separate analysis. Another path for discussing the coexistence of SC with FM could be going beyond the Gutzwiller approximation, where we account also for the more distant correlations when determining the effective Hamiltonian [30,31]. Here, the central question is whether the spin-triplet pairing should be treated on the same footing as ferromagnetism, i.e., does it already appear in a direct space formulation [6,7,28,29] or is it mediated by collective spin fluctuations in the ferromagnetic phase [14,32–34] among already well defined quasiparticles. A crossover from the latter to the former approach is expected to take place with the increasing strength of the repulsive Coulomb interaction U.

Acknowledgments. The work has been partially supported by the Foundation for Polish Science (FNP) under the Grant TEAM, as well as by the National Science Centre (NCN) under the Grant MAESTRO, No. DEC-2012/04/A/ST3/00342. We would like to thank J. Kaczmarczyk for discussions and a critical reading of the manuscript.

[1] S. S. Saxena, P. Agarwal, K. Ahilan, F. M. Grosche, R. K. W. Haselwimmer, M. J. Steiner, E. Pugh, I. R. Walker, S. R. Julian, P. Monthoux, G. G. Lonzarich, A. Huxley, I. Sheikin, D. Braithwaite, and J. Flouquet, Nature (London) **406**, 587 (2000).

[2] A. J. Leggett, Rev. Mod. Phys. **47**, 331 (1975).

[3] J. F. Annett, B. L. Györffy, and K. I. Wysokiński, New J. Phys. **11**, 055063 (2009); K. I. Wysokiński, J. F. Annett, and B. L. Györffy, Phys. Rev. Lett. **108**, 077004 (2012); M. Gradhand, K. I. Wysokiński, J. F. Annett, and B. L. Györffy, Phys. Rev. B **88**, 094504 (2013).

[4] C. Pfleiderer and A. D. Huxley, Phys. Rev. Lett. **89**, 147005 (2002).

[5] V. Taufour, D. Aoki, G. Knebel, and J. Flouquet, Phys. Rev. Lett. **105**, 217201 (2010).

[6] J. Spałek, Phys. Rev. B **63**, 104513 (2001).

[7] M. Zegrodnik and J. Spałek, Phys. Rev. B **86**, 014505 (2012).

[8] C. Pfleiderer, Rev. Mod. Phys. **81**, 1551 (2009), Sec. III A.

[9] D. Aoki and J. Flouquet, J. Phys. Soc. Jpn. **81**, 011003 (2012).

[10] A. Huxley, I. Sheikin, E. Ressouche, N. Kernavanois, D. Braithwaite, R. Calemczuk, and J. Flouquet, Phys. Rev. B **63**, 144519 (2001).

[11] N. Kernavanois, B. Grenier, A. Huxley, E. Ressouche, J. P. Sanchez, and J. Flouquet, Phys. Rev. B **64**, 174509 (2001).
[12] K. Hirohashi and K. Ueda, J. Phys. Soc. Jpn. **73**, 1576 (2004).
[13] D. Belitz, T. R. Kirkpatrick, and J. Rollbühler, Phys. Rev. Lett. **94**, 247205 (2005).
[14] K. G. Sandeman, G. G. Lonzarich, and A. J. Schofield, Phys. Rev. Lett. **90**, 167005 (2003).
[15] A. B. Shick and W. E. Pickett, Phys. Rev. Lett. **86**, 300 (2001).
[16] V. H. Tran, S. Paschen, R. Troć, M. Baenitz, and F. Steglich, Phys. Rev. B **69**, 195314 (2004).
[17] Y. Onuki, I. Ukon, S. Won Yun, I. Umehara, K. Satoh, T. Fukuhara, H. Sato, S. Takayanagi, M. Shikama, and A. Ochiai, J. Phys. Soc. Jpn. **61**, 293 (1992).
[18] R. Settai, M. Nakashima, S. Araki, Y. Haga, T. C. Kobayashi, N. Tateiwa, H. Yamagami, and Y. Onuki, J. Phys.: Condens. Matter **14**, L29 (2002).
[19] T. Terashima, T. Matsumoto, C. Terakura, S. Uji, N. Kimura, M. Endo, T. Komatsubara, and H. Aoki, Phys. Rev. Lett. **87**, 166401 (2001).
[20] D. Vollhardt, Rev. Mod. Phys. **56**, 99 (1984).
[21] T. M. Rice and K. Ueda, Phys. Rev. Lett. **55**, 995 (1985).
[22] P. Fazekas and B. H. Brandow, Phys. Scr. **36**, 809 (1987).
[23] Approach derived in J. Jędrak, J. Kaczmarczyk, and J. Spałek, arXiv:1008.0021; J. Jędrak and J. Spałek, Phys. Rev. B **81**, 073108 (2010); **83**, 104512 (2011); J. Kaczmarczyk and J. Spałek, *ibid.* **84**, 125140 (2011); M. Wysokiński, J. Jędrak, J. Kaczmarczyk, and J. Spałek, in *Lectures on the Physics of Strongly Coreelated Sysytems XVI: Sixteenth Training Course in the Physics of Strongly Correlated Systems*, edited by A. Avella and F. Mancini, AIP Conf. Proc. Vol. 1485 (AIP, Melville, NY, 2012), p. 319; M. Abram, J. Kaczmarczyk, J. Jędrak, and J. Spałek, Phys. Rev. B **88**, 094502 (2013); O. Howczak, J. Kaczmarczyk, and J. Spałek, Phys. Status Solidi B **250**, 609 (2013); A. P. Kądzielawa, J. Spałek, J. Kurzyk, and W. Wójcik, Eur. Phys. J. B **86**, 252 (2013); M. M. Wysokiński and J. Spałek, J. Phys.: Condens. Matter **26**, 055601 (2014).
[24] R. Doradziński and J. Spałek, Phys. Rev. B **56**, R14239 (1997).
[25] R. Doradziński and J. Spałek, Phys. Rev. B **58**, 3293 (1998).
[26] O. Howczak and J. Spałek, J. Phys.: Condens. Matter **24**, 205602 (2012).
[27] K. Kubo, Phys. Rev. B **87**, 195127 (2013).
[28] M. Zegrodnik, J. Spałek, and J. Bünemann, New J. Phys. **15**, 073050 (2013).
[29] M. Zegrodnik, J. Bünemann, and J. Spałek, New J. Phys. **16**, 033001 (2014).
[30] J. Kaczmarczyk, J. Spałek, T. Schickling, and J. Bünemann, Phys. Rev. B **88**, 115127 (2013).
[31] J. Kaczmarczyk, J. Bünemann, and J. Spałek, New J. Phys. **16**, 073018 (2014).
[32] D. Fay and J. Appel, Phys. Rev. B **22**, 3173 (1980).
[33] T. R. Kirkpatrick, D. Belitz, T. Vojta, and R. Narayanan, Phys. Rev. Lett. **87**, 127003 (2001).
[34] R. Roussev and A. J. Millis, Phys. Rev. B **63**, 140504 (2001).

Article 4:

It is the second out of three papers, where we study the Anderson lattice model (ALM) by means of the statistically consistent Gutzwiller approximation (SGA). In this article we go beyond the $T = 0$ limit and we study the classical and quantum critical points. We find quantitative agreement with the the experiments and we predict the position of the metamagnetic critical ending point.

PHYSICAL REVIEW B **91**, 081108(R) (2015)

Criticalities in the itinerant ferromagnet UGe_2

Marcin M. Wysokiński,[1,*] Marcin Abram,[1,†] and Józef Spałek[1,2,‡]

[1]*Marian Smoluchowski Institute of Physics, Jagiellonian University, Łojasiewicza 11, PL-30-348 Kraków, Poland*

[2]*Academic Centre for Materials and Nanotechnology (ACMiN), AGH University of Science and Technology, Al. Mickiewicza 30, PL-30-059 Kraków, Poland*

(Received 28 November 2014; revised manuscript received 28 January 2015; published 20 February 2015)

We provide a microscopic description of the magnetic properties of UGe_2 and, in particular, of its both classical and quantum critical behavior. Namely, we account for all the critical points: the critical ending point (CEP) at the metamagnetic phase transition, the tricritical point, and the quantum critical end point at the ferromagnetic to paramagnetic phase transition. Their position agrees quantitatively with experiment. Additionally, we predict that the metamagnetic CEP can be traced down to zero temperature and becomes quantum critical point by a small decrease of both the total electron concentration and the external pressure. The system properties are then determined by the quantum critical fluctuations appearing near the instability point of the Fermi surface topology.

DOI: 10.1103/PhysRevB.91.081108 PACS number(s): 71.27.+a, 75.30.Kz, 71.10.−w

Introduction. Attempts to determine the quantum critical behavior and the corresponding critical points (QCPs) have attracted much attention due to the unique phenomena with singular physical properties associated with them as temperature $T \to 0$ and other parameters (pressure p, applied field H, or electron concentration n) are varied [1–3]. Additionally, in the canonical case—the heavy fermion systems—unconventional superconductivity often appears near those QCPs making the quantum critical fluctuations the primary pairing inducing factor. Also, the classical critical points (CCPs) and their evolution towards QCP provide the testing ground for study of detailed quantitative behavior of different systems [4,5].

UGe_2, in this respect, is one of the unique materials that exhibit all the above features. Therefore, the explanation of the magnetic phase diagram and intimately connected critical points within a single theoretical framework would provide a complete understanding of this remarkable quantum material [4,6–9]. The phase diagram on the pressure-temperature (p-T) plane comprises two ferromagnetic phases, of weaker (FM1) and stronger (FM2) magnetization, paramagnetic phase (PM), as well as the spin-triplet superconducting phase (SC) [4,6,10]. SC disappears at the same pressure as FM [6] and the maximum of the superconducting critical temperature T_s coincides with the critical pressure for the FM2-FM1 phase transition [7]. Thus, it is strongly suggestive that FM and SC are strongly intertwined as described by some theoretical approaches [11–15].

The p-T-H phase diagram for UGe_2 comprises the characteristic *wing shape* [8,9]. Such structure was theoretically obtained by Belitz *et al.* [16] within mean-field approach for a single-band itinerant ferromagnet. However, this approach cannot account for the two different ferromagnetic phases appearing in UGe_2, as well as for the critical ending point (CEP), separating the region with a discontinuous drop in magnetization from a crossover regime [8,17].

In this work we provide a quantitative microscopic description of all magnetic critical properties of UGe_2 within the framework of the Anderson lattice model (ALM) treated by a modified Gutzwiller approach [18], called *the statistically consistent Gutzwiller approximation* (SGA) (for a description of the method and a detailed comparison to the slave-boson approach, see Ref. [19]; for its applications, see Refs. [20]). Validity of this model in the context of UGe_2 [18] is based on earlier results: first, on band structure calculations [21,22] and second, on experimental observations [4,6,23]. The first feature is a quasi-two-dimensional topology of the Fermi surface (FS) [21,22] which justifies calculations for a two-dimensional square lattice. On the other hand, despite the circumstance that the distance between uranium atoms is above the Hill limit [4], the experimental value of the paramagnetic moment per U atom is different from that for either f^3 or f^2 configurations [6,24]. This speaks for the presence of a sizable hybridization between the initially localized f electrons and those from the conduction band. For strong enough hybridization, f electrons contribute essentially to the heavy itinerant quasiparticle states and play a dominant role in the magnetic properties [6,10,24].

We provide a coherent explanation of FM and PM phase appearances as driven by a competition between the hybridization from one side and the f-f Coulomb local repulsive interaction from the other [18]. Specifically, we obtain two different FM phases [15,18,25–28] by varying the predetermined position of the chemical potential with respect to the peaks in the quasiparticle density of states (DOS) including the spin-split subbands. Although, Gutzwiller ansatz in certain regimes favors antiferromagnetism over FM [25–27,29,30], we restrict our discussion to the latter phase, because in the considered range of electron concentration, $n \simeq 1.6$, FM phase turned out to have the lowest energy [25,26].

In Fig. 1 we draw schematically the respective DOS for considered phases. It can be seen clearly that the shape of the FS (limiting the filled parts) will be vastly different in each of the phases. Within our approach, most of the properties of UGe_2 at $T = 0$ can be explained [18] in agreement with related experiments of magnetization [7], neutron scattering [10,24], and the de Haas–van Alphen oscillations [31,32]. The character of the FM1 phase, which we obtain as a half-metallic type [cf. Fig. 1(b)], is also supported by the band-structure calculations [22].

In the present work we extend our previous approach [18] to nonzero temperature and on this basis we determine the

*marcin.wysokinski@uj.edu.pl
†marcin.abram@uj.edu.pl
‡ufspalek@if.uj.edu.pl

character of all phase transitions on the p-T-H diagram of UGe_2, as well as discuss the nature of all the classical and quantum critical points. We also show that by a small decrease of electron concentration (by $\sim$7%), the system can reach another quantum criticality via a metamagnetic transition upon changing the pressure. We also predict the corresponding change in FS topology distinguishing the two phases of significantly different magnetic susceptibility.

Model. We start from ALM with the Zeeman term included ($h \equiv \frac{1}{2} g \mu_0 \mu_B H$) in the Hamiltonian

$$\hat{\mathcal{H}} - \mu \hat{N} = {\sum_{\mathbf{i},\mathbf{j},\sigma}}' t_{\mathbf{ij}} \hat{c}^{\dagger}_{\mathbf{i},\sigma} \hat{c}_{\mathbf{j},\sigma} - \sum_{\mathbf{i},\sigma} (\mu + \sigma h) \hat{n}^{c}_{\mathbf{i},\sigma} + \sum_{\mathbf{i},\sigma} (\epsilon_f - \mu - \sigma h) \hat{n}^{f}_{\mathbf{i},\sigma} + U \sum_{\mathbf{i}} \hat{n}^{f}_{\mathbf{i},\uparrow} \hat{n}^{f}_{\mathbf{i},\downarrow} + V \sum_{\mathbf{i},\sigma} (\hat{f}^{\dagger}_{\mathbf{i},\sigma} \hat{c}_{\mathbf{i},\sigma} + \hat{c}^{\dagger}_{\mathbf{i},\sigma} \hat{f}_{\mathbf{i},\sigma}), \quad (1)$$

which comprises dispersive conduction (c) band electrons and f electrons coming from atomic f shell located at $\epsilon_f < 0$. In the model we include specifically the nearest- ($t < 0$) and the second-nearest- ($t' = 0.25|t|$) neighbor hopping amplitudes between c electrons, f level at $\epsilon_f = -3|t|$, sizable $f - f$ Coulomb repulsion $U = 5|t|$, and the $c - f$ hybridization V of the on-site form.

To obtain an effective single particle picture from the many-body Hamiltonian (1) we use the extended Gutzwiller approximation (GA) called the SGA (for details, see [19]). The method was successfully applied to a number of problems [20]. Formally, we add to the effective Hamiltonian obtained in GA [33,34], $\hat{\mathcal{H}}_{\mathrm{GA}}$, additional constraints on the number of f electrons and their magnetization by means of the Lagrange multipliers. It leads to the new effective Hamiltonian $\hat{\mathcal{H}}_{\mathrm{SGA}}$ of the form

$$\hat{\mathcal{H}}_{\mathrm{SGA}} \equiv \hat{\mathcal{H}}_{\mathrm{GA}} - \lambda^{f}_{n} \left(\sum_{\mathbf{k},\sigma} \hat{n}^{f}_{\mathbf{k},\sigma} - \Lambda n_f \right) - \lambda^{f}_{m} \left(\sum_{\mathbf{k},\sigma} \sigma \hat{n}^{f}_{\mathbf{k},\sigma} - \Lambda m_f \right) \equiv \sum_{\mathbf{k},\sigma} \hat{\Psi}^{\dagger}_{\mathbf{k}\sigma} \begin{pmatrix} \epsilon^{c}_{\mathbf{k}} - \sigma h - \mu & \sqrt{q_\sigma} V \\ \sqrt{q_\sigma} V & \epsilon_f - \sigma(h + \lambda^{f}_{m}) - \lambda^{f}_{n} - \mu \end{pmatrix} \hat{\Psi}_{\mathbf{k}\sigma} + \Lambda \left(U d^2 + \lambda^{f}_{n} n_f + \lambda^{f}_{m} m_f \right), \quad (2)$$

where $\hat{\Psi}^{\dagger}_{\mathbf{k}\sigma} \equiv (\hat{c}^{\dagger}_{\mathbf{k},\sigma}, \hat{f}^{\dagger}_{\mathbf{k},\sigma})$. Furthermore, q_σ is the hybridization narrowing factor in the standard form [18,20], and Λ is a number of lattice sites.

At nonzero temperature, one needs to minimize the generalized Landau grand-potential functional

$$\frac{\mathcal{F}}{\Lambda} = -\frac{1}{\Lambda \beta} \sum_{\mathbf{k}\sigma b} \ln \left[1 + e^{-\beta E^{b}_{\mathbf{k}\sigma}} \right] + \left(\lambda^{f}_{n} n_f + \lambda^{f}_{m} m_f + U d^2 \right), \quad (3)$$

where $E^{b}_{\mathbf{k}\sigma}$ are four eigenvalues of the effective Hamiltonian (2) labeled with the spin (σ) and band (b) indices. λ^{f}_{n} and λ^{f}_{m} are the Lagrange multipliers assuring the correct statistical consistency of equations for n_f and m_f and play the role of correlation-induced effective fields [20]. Minimization of $\mathcal{F}$ is carried out with respect to the set of all parameters $\vec{\lambda} \equiv \{d, n_f, m_f, \lambda^{f}_{n}, \lambda^{f}_{m}\}$. Additionally, as the number of particles in the system is conserved we have to determine the chemical potential and adjust it to each of the phases according to the condition $n = 1/\Lambda \sum_{\mathbf{k}b\sigma} f(E^{b}_{\mathbf{k}\sigma})$, with $f(E)$ being the Fermi-Dirac function. In effect, the model is described by set of six algebraic equations which are solved with the help of the GSL library, with typical accuracy 10^{-11}.

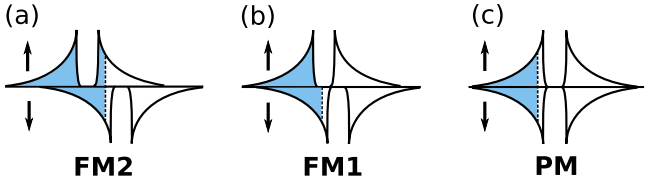

FIG. 1. (Color online) Schematic characterization of phases by their spin-resolved density of states. The arrows label the spin subbands and the dotted line marks the position of the chemical potential.

The Landau grand-potential functional for the equilibrium values of the parameters, $\mathcal{F}_0$, has the meaning of the physical grand potential Ω which is the proper quantity for studying the system at any temperature, $\mathcal{F}_0 \equiv \Omega \equiv U - TS - \mu N$. Therefore, the free energy of the system is defined by $F = \mathcal{F}_0 + \mu N$ and the ground-state energy is $E_G \equiv F(T = 0)$.

Results. We assume that the main effect of the applied pressure is emulated by an increase of the hybridization amplitude $|V|$, even though other parameters (e.g., ϵ_f) may also change. However, as our previous results indicate, hybridization change is the principal factor of the pressure dependencies observed in UGe_2 [18].

In Fig. 2 we plot the phase diagram on the $|V| - T$ plane. In the low-T regime we are able to reproduce the correct evolution of both metamagnetic (left) and ferromagnetic to paramagnetic (right) phase transitions observed in experiment (cf. inset), together with the respective critical behavior [7–9,17]. The position of the CCPs is very sensitive to the selected total band filling, $n = n_f + n_c$. Our fitting constraint is the ratio of the corresponding critical temperatures, $T_{\mathrm{CEP}}/T_{\mathrm{TCP}} \approx 7\ \mathrm{K}/24\ \mathrm{K}$ [8]. Consequently, for the band filling $n = 1.6$, selected in our previous analysis at $T = 0$ [18], we obtain agreement of our calculated ratio under the proviso that experimental values of the critical temperatures are determined with accuracy ± 0.25 K.

Our model does not account for correct curvatures of phase transitions above CCPs (cf. Fig. 2). This discrepancy can be attributed to the fact that also other microscopic parameters can alter when applying pressure, e.g., ϵ_f, and to additional

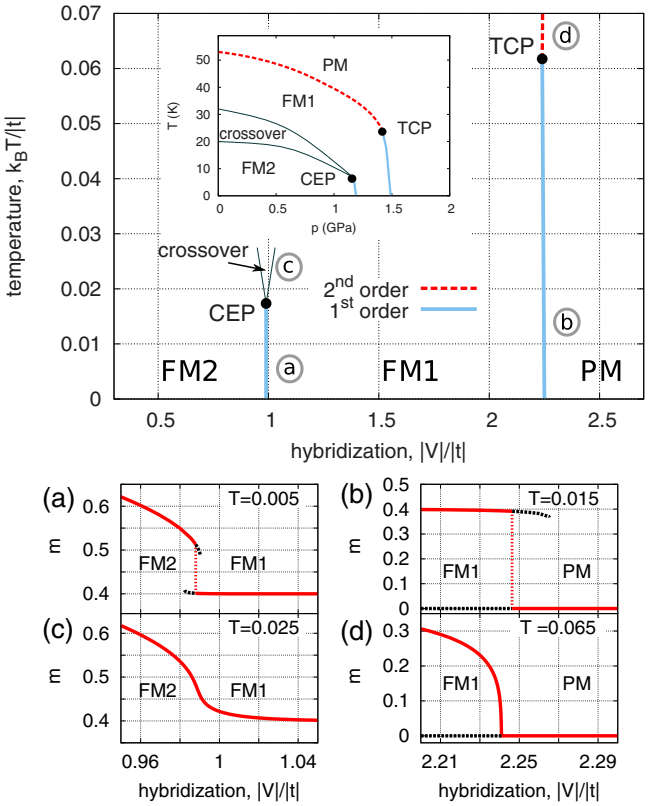

FIG. 2. (Color online) Top: Phase diagram on hybridization strength-reduced temperature plane encompassing both FM and PM phases for total band filling $n = 1.6$. The correct character of phase transitions and positions of critical points in UGe_2 [7–9,17] is reproduced. For comparison, we present in the inset the experimental p-T phase diagram of UGe_2 (cf. [7,8]). In (a)–(d) we draw the magnetization change with the increasing hybridization strength when the system undergoes phase transition at points indicated with respective encircled letters ⓐ–ⓓ. Solid red lines denote energetically favorable solution, whereas dashed black lines denote the unstable solutions.

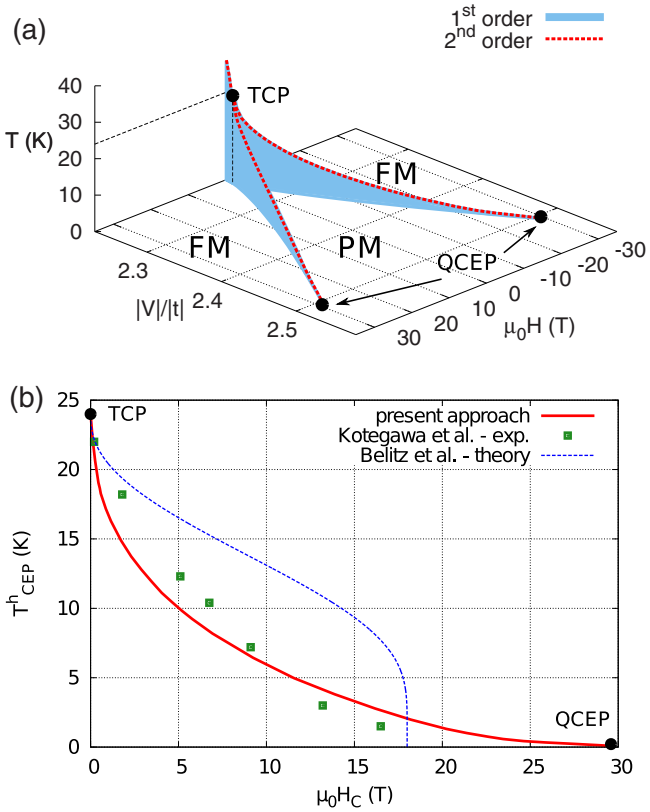

FIG. 3. (Color online) (a) Wing structure of the phase transition planes derived from our model. (b) Comparison of the calculated dependence of the temperature vs applied magnetic field at the critical end point (CEP) with the experimental points adopted from [9]. For comparison, we include also the prediction by Belitz *et al.* [16], with the fitting parameters selected on the basis [9]: $H_{\rm QCEP} = 18$ T and $T_{\rm TCP} = 24$ K.

entropic factors important in the case of $T > 0$ Gutzwiller projection [35,36].

In our calculations we have used reduced temperature $k_BT/|t|$. We rescale it to the physical units by relating it to the experimentally measured values at CCPs [7–9,17]. Accordingly, we also rescale the reduced field $\frac{1}{2}g\mu_B\mu_0H/|t|$ to Tesla units.

At the metamagnetic (FM2-FM1) phase transition we obtain CEP separating the discontinuous-transition line from the crossover regime. At low T both solutions with the weaker and the stronger magnetization coexist in the limited range of the hybridization strength [cf. Fig. 2(a)]. As the system approaches the transition from the FM1 side, FS changes drastically only in one spin subband, in which the chemical potential crosses the hybridization gap, resulting also in a discontinuous jump of the total moment $m = m_f + m_c$. With the increasing temperature, the edges of the gap are gradually smeared out. This leads to a deviation from the pure half-metallic type of the FM1 phase. The magnetization is *bending* towards the trend observed in the FM2 phase, and eventually at CEP it is changing to a crossover line [cf. Fig. 2(c)].

In the case of FM to PM transition the situation is different [cf. Figs. 2(b) and 2(d)]. At low temperature, the magnetization of this *half-metallic* FM1 phase discontinuously drops to zero [cf. Fig. 2(b)]. However, with the increasing temperature, the ferromagnetic solution departs from a sharp half-metallic type and slowly *bends* over towards the paramagnetic solution, eventually reaching the critical point by changing the transition character to that of second order [cf. Fig. 2(d)]. The just described critical point is of tricritical character (TCP). This is because its evolution can be followed by applying the magnetic field down to $T = 0$, where it turns into the quantum critical ending point (QCEP) [cf. Fig. 3(a)]. In this manner, we have achieved a full characteristic at the *wing-shape* p-T-H phase diagram [8,9]. As the detailed form of the hybridization change with applied pressure is unknown, and in principle nonlinear, we compare our predicted shape of wings by tracing the evolution of CEP on the temperature-magnetic field T^h_{CEP}-μ_0H_C plane [cf. Fig. 3(b)] and comparing it to the experimental data [9]. We obtain a satisfactory quantitative agreement with the experimental points, as well as recover its proper curvature. For comparison, the results from the

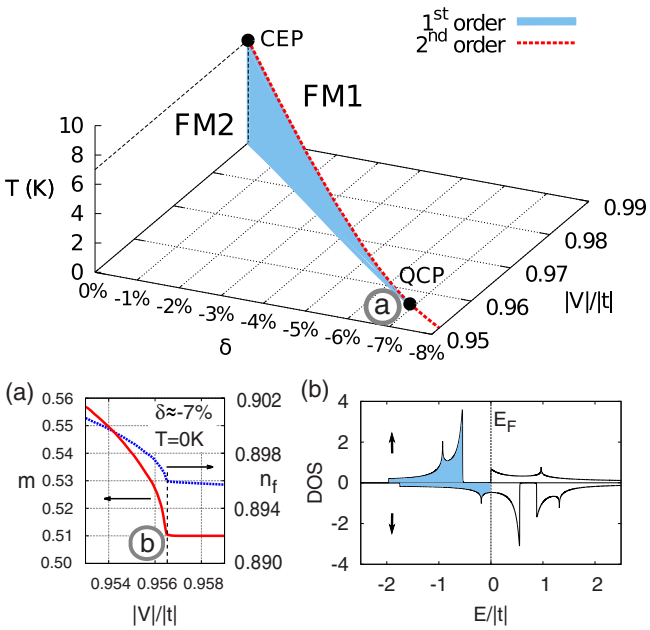

FIG. 4. (Color online) Top: Evolution of CEP on the $|V|$-T-δ plane down to $T = 0$ and QCP (see main text). Bottom: (a) Change of magnetization and f electron number as the system undergoes quantum critical transition. (b) Density of states at QCP. Note the intermediate character of FS between FM2 and FM1 of the state at QCP. Encircled letter ⓐ at top diagram refers to the position of the curves in panel (a), and respectively ⓑ at panel (a) to the position of the DOS in (b).

mean-field approach to the single-band case by Belitz *et al.* [16] are also drawn, as is universal explanation of tricritical behavior of itinerant ferromagnets. Nevertheless, as suggested by the authors in Ref. [9], the crucial element determining for UGe_2 the correct shape of the wings is the change of FS, present in our two-band ALM model. We also predict that the curve of the T^h_{CEP} vs $\mu_0 H_C$ dependence has a longer tail than that estimated in Ref. [9], i.e., that QCEP should be located at fields around 30 T. Our estimate thus calls for a more precise determination of the QCEP position.

In fitting to the data in Fig. 3 we have assumed that the g factor for f electrons $g_f = 2$ (the same as for c electrons). This assumption is based on the presumption that for itinerant electrons the crystal-field multiplet structure is washed out. Parenthetically, taking g_f significantly different provides a worse agreement, but the curvature character remains unchanged.

In Fig. 4 we draw the evolution of CEP at the metamagnetic transition with the decrease of both the hybridization and the electron concentration. The latter quantity is characterized by the parameter $\delta = \frac{n_x - n}{n} 100\%$, where $n = 1.6$ is initial and n_x is the actual concentration. On the V-T-δ phase diagram the CEP can be followed down to zero temperature, where it joins the second-order transition line [cf. Fig. 4(a)]. At this second-order transition the Fermi level for the majority spin subband is exactly at the border of the gap [cf. Fig. 4(b)]. It means that along this line quantum critical fluctuations of FS topology are present. In other terms, we have a strong indication that in the vicinity of the SC dome maximum this compound exhibits a *Lifshitz* type of quantum critical behavior. This quantum critical transition can be associated also with the specific valence change [cf. Fig. 4(a)]. However, here the average f electron number changes continuously in contrast to the discontinuous drop originating from the f-c electron repulsion [37]. The difference in the origin of *Lifshitz* type of ferromagnetic QCP with respect to that considered before [38,39] is that here it results from the two-band model and separates different FM phases.

Summary. We have described the phase diagram of UGe_2 at nonzero temperature and have determined the location of the critical points, as well as proposed an additional quantum critical point for UGe_2. With the help of the Anderson lattice model we are able to reproduce quantitatively all the principal features of the magnetism in this compound. We also have determined the location of experimentally observed critical and quantum critical points, together with a correct order of the phase transitions related to them.

Although our mean-field approach seems to capture all the features concerning details of the p-T-H phase diagram of UGe_2, we should note that, in principle, fluctuations of order parameters can bring quantitative changes to our results. However, as the phase transitions are induced by the drastic changes of the Fermi surface, the effect of the fluctuations should be minor (except near the predicted QCP—cf. Fig. 4) and may lead to a correction of the CEP and TCP positions.

It should be noted that we have employed an orbitally nondegenerate ALM. Accounting for the degenerate one would imply inclusion of the residual Hund's rule interaction present in the degenerate ALM model which could be important in inducing the spin-triplet pairing [40].

Acknowledgments. The work was partly supported by the Foundation for Polish Science (FNP) under the Grant TEAM and partly by the National Science Centre (NCN) under MAESTRO, Grant No. DEC-2012/04/A/ST3/00342. Access to the supercomputer located at Academic Centre for Materials and Nanotechnology of the AGH University of Science and Technology in Kraków is also acknowledged.

[1] H. v. Löhneysen, A. Rosch, M. Vojta, and P. Wölfle, Rev. Mod. Phys. **79**, 1015 (2007).

[2] Q. Si, P. Gegenwart, and F. Steglich, *Understanding Quantum Phase Transitions*, edited by L. D. Carr (CRC Press, Boca Raton, 2011), Chaps. 8, 18, pp. 193–216, 445–468.

[3] A. Ślebarski and J. Spałek, Phys. Rev. Lett. **95**, 046402 (2005).

[4] C. Pfleiderer, Rev. Mod. Phys. **81**, 1551 (2009) (Sec. III.A).

[5] J. Spalek, A. Datta, and J. M. Honig, Phys. Rev. Lett. **59**, 728 (1987); J. Spałek, Phys. Status Solidi B **243**, 78 (2006).

[6] S. S. Saxena, P. Agarwal, K. Ahilan, F. M. Grosche, R. K. W. Haselwimmer, M. J. Steiner, E. Pugh, I. R. Walker, S. R. Julian, P. Monthoux, G. G. Lonzarich, A. Huxley, I. Sheikin, D. Braithwaite, and J. Flouquet, Nature (London) **406**, 587 (2000).

[7] C. Pfleiderer and A. D. Huxley, Phys. Rev. Lett. **89**, 147005 (2002).
[8] V. Taufour, D. Aoki, G. Knebel, and J. Flouquet, Phys. Rev. Lett. **105**, 217201 (2010).
[9] H. Kotegawa, V. Taufour, D. Aoki, G. Knebel, and J. Flouquet, J. Phys. Soc. Jpn. **80**, 083703 (2011).
[10] A. Huxley, I. Sheikin, E. Ressouche, N. Kernavanois, D. Braithwaite, R. Calemczuk, and J. Flouquet, Phys. Rev. B **63**, 144519 (2001).
[11] T. R. Kirkpatrick, D. Belitz, T. Vojta, and R. Narayanan, Phys. Rev. Lett. **87**, 127003 (2001).
[12] K. Machida and T. Ohmi, Phys. Rev. Lett. **86**, 850 (2001).
[13] A. A. Abrikosov, J. Phys: Condens. Matter **13**, L943 (2001).
[14] D. Sa, Phys. Rev. B **66**, 140505 (2002).
[15] K. G. Sandeman, G. G. Lonzarich, and A. J. Schofield, Phys. Rev. Lett. **90**, 167005 (2003).
[16] D. Belitz, T. R. Kirkpatrick, and J. Rollbühler, Phys. Rev. Lett. **94**, 247205 (2005).
[17] F. Hardy, C. Meingast, V. Taufour, J. Flouquet, H. v. Löhneysen, R. A. Fisher, N. E. Phillips, A. Huxley, and J. C. Lashley, Phys. Rev. B **80**, 174521 (2009).
[18] M. M. Wysokiński, M. Abram, and J. Spałek, Phys. Rev. B **90**, 081114(R) (2014).
[19] J. Jędrak, J. Kaczmarczyk, and J. Spałek, arXiv:1008.0021.
[20] J. Jędrak and J. Spałek, Phys. Rev. B **83**, 104512 (2011); J. Kaczmarczyk and J. Spałek, *ibid.* **84**, 125140 (2011); O. Howczak, J. Kaczmarczyk, and J. Spałek, Phys. Status Solidi B **250**, 609 (2013); A. P. Kądzielawa, J. Spałek, J. Kurzyk, and W. Wójcik, Eur. Phys. J. B **86**, 252 (2013); M. Abram, J. Kaczmarczyk, J. Jędrak, and J. Spałek, Phys. Rev. B **88**, 094502 (2013); M. Zegrodnik, J. Spałek, and J. Bünemann, New J. Phys. **15**, 073050 (2013); M. M. Wysokiński and J. Spałek, J. Phys.: Condens. Matter **26**, 055601 (2014).
[21] A. B. Shick and W. E. Pickett, Phys. Rev. Lett. **86**, 300 (2001).
[22] M. Samsel-Czekała, M. Werwiński, A. Szajek, G. Chełkowska, and R. Troć, Intermetallics **19**, 1411 (2011).
[23] V. H. Tran, S. Paschen, R. Troć, M. Baenitz, and F. Steglich, Phys. Rev. B **69**, 195314 (2004).
[24] N. Kernavanois, B. Grenier, A. Huxley, E. Ressouche, J. P. Sanchez, and J. Flouquet, Phys. Rev. B **64**, 174509 (2001).
[25] R. Doradziński and J. Spałek, Phys. Rev. B **56**, R14239 (1997).
[26] R. Doradziński and J. Spałek, Phys. Rev. B **58**, 3293 (1998).
[27] O. Howczak and J. Spałek, J. Phys: Condens. Matter **24**, 205602 (2012).
[28] K. Kubo, Phys. Rev. B **87**, 195127 (2013).
[29] G. Kotliar and A. E. Ruckenstein, Phys. Rev. Lett. **57**, 1362 (1986).
[30] V. Dorin and P. Schlottmann, Phys. Rev. B **46**, 10800 (1992).
[31] T. Terashima, T. Matsumoto, C. Terakura, S. Uji, N. Kimura, M. Endo, T. Komatsubara, and H. Aoki, Phys. Rev. Lett. **87**, 166401 (2001).
[32] R. Settai, M. Nakashima, S. Araki, Y. Haga, T. C. Kobayashi, N. Tateiwa, H. Yamagami, and Y. Onuki, J. Phys: Condens. Matter **14**, L29 (2002).
[33] T. M. Rice and K. Ueda, Phys. Rev. Lett. **55**, 995 (1985).
[34] P. Fazekas and B. H. Brandow, Phys. Scr. **36**, 809 (1987).
[35] W.-S. Wang, X.-M. He, D. Wang, Q.-H. Wang, Z. D. Wang, and F. C. Zhang, Phys. Rev. B **82**, 125105 (2010).
[36] M. Sandri, M. Capone, and M. Fabrizio, Phys. Rev. B **87**, 205108 (2013).
[37] K. Miyake and S. Watanabe, J. Phys. Soc. Jpn. **83**, 061006 (2014).
[38] R. Roussev and A. J. Millis, Phys. Rev. B **63**, 140504 (2001).
[39] D. Fay and J. Appel, Phys. Rev. B **22**, 3173 (1980).
[40] M. Zegrodnik, J. Bünemann, and J. Spałek, New J. Phys. **16**, 033001 (2014); J. Spałek and M. Zegrodnik, J. Phys.: Condens. Matter **25**, 435601 (2013).

Article 5:

It is the third papers, where we study the Anderson lattice model (ALM) by means of the statistically consistent Gutzwiller approximation (SGA). In this paper we study the robustness of our findings that were described in the previous work (cf. Ref. [112]). We analyze the influence of the total filling n and the Landé factor g_f for f-electrons, finding that the best results are obtained when g_f is close to the value for the free electron gas. Additionally, we show how changing the value of n alters the relative position of critical ending point (CEP) and tricritical point (TCP). It allow us to precisely match the position of CEP and TCP to the experiment, calibrating the energy scale and fixing the value of n. We are finding, that for such match, the comparison with the experiment of the second-order transition line that join TCP and QCEP points gives us the best fit. It can be regarded as an argument, that ALM indeed, is a right choice to describe the magnetic phases of UGe_2.

Journal of Magnetism and Magnetic Materials 400 (2016) 27–30

Contents lists available at ScienceDirect

Journal of Magnetism and Magnetic Materials

journal homepage: www.elsevier.com/locate/jmmm

Tricritical wings in UGe_2: A microscopic interpretation

Marcin Abram*, Marcin M. Wysokiński, Józef Spałek

Marian Smoluchowski Institute of Physics, Jagiellonian University, ulica Łojasiewicza 11, PL-30-348 Kraków, Poland

ARTICLE INFO

Article history:
Received 20 June 2015
Received in revised form
3 July 2015
Accepted 10 July 2015
Available online 11 July 2015

Keywords:
Ferromagnetism
Heavy fermions
Critical points
UGe_2

PACS:
71.27.+a
75.30.kz
71.10.-w

ABSTRACT

In the present work we analyze the second order transition line that connects the tricritical point and the quantum critical ending point on the temperature–magnetic-field plane in UGe_2. For the microscopic modeling we employ the Anderson lattice model recently shown to provide a fairly complete description of the full magnetic phase diagram of UGe_2 including all the criticalities. The shape of the so-called tricritical wings, i.e. surfaces of the first-order transitions, previously reported by us to quantitatively agree with the experimental data, is investigated here with respect to the change of the total filling and the Landé factor for f electrons which can differ from the free electron value. The analysis of the total filling dependence demonstrates sensitivity of our prediction when the respective positions of the critical ending point at the metamagnetic transition and tricritical point are mismatched as compared to the experiment.

1. Motivation and overview

Quantum critical phenomena have captured general attention due to their unique singular properties observed at low temperature ($T \to 0$) and near the quantum critical point (QCP) which is frequently accompanied by the unconventional superconductivity (SC) [1]. From this perspective, f-electron compound UGe_2 is a system with phase diagram comprising coexistence of spin-triplet SC and ferromagnetism (FM) [2–6], as well as an abundance of critical points (CPs), either of quantum and classical nature [7]. Experimental studies among others have revealed existence of the two characteristic classical CPs in the absence of the field (cf. Fig. 1): (i) the critical ending point (CEP) at 7 K at the metamagnetic transition separating strong (FM2) and weak magnetization (FM1) regions [8–10], and (ii) the tricritical point (TCP) at the FM to paramagnetic (PM) phase transition located at $T=24$ K. Additionally, with the applied magnetic field the second order transition line starting from TCP can be followed to $T=0$ where it is expected to terminate in a quantum critical ending point (QCEP) [9,10]. In effect the magnetic phase boundaries in UGe_2 reflect the so-called tricritical wing shape.

Such a complex magnetic phase diagram with all the above criticalities, both classical and quantum, is particularly challenging in terms of theoretical modeling. One of the first approaches, based on the single-band model describing tricritical wings, was the work by Belitz et al. [11]. However, the microscopic description of the magnetic phase diagram with all the CPs including also CEP at the metamagnetic transition, as observed in UGe_2, has been missing until our recent works [13,14].

Our analysis is based on the (two-orbital) Anderson lattice model (ALM) [13,14], often referred to as the periodic Anderson model. Findings for UGe_2, both from first principle calculations and experiments are the following: the quasi-two-dimensional character of the Fermi surface [15], a uniaxial anisotropy for magnetization [16], U–U interatomic distance above the so-called Hill limit [1], and the paramagnetic moment per U atom different from that expected for either f^3 or f^2 atomic configurations [2,17]. We show in the following that all of these findings can be coherently explained within our two-orbital model starting with originally localized f-states and subsequently being strongly hybridized with the conduction (c) band states on a two dimensional lattice and with the applied magnetic field accounted for by the Zeeman term only.

Ferromagnetic order in our model arises from effect of competing hybridization and the f–f interatomic Coulomb repulsion. The emergence of two distinct ferromagnetic phases is in our model driven by the changing topology of the Fermi surface [18–21] which in turn is induced by a relative motion of hybridized and spin split subbands with the increasing f–c hybridization. The results obtained from such picture [13] qualitatively agree with the

* Corresponding author.
E-mail addresses: marcin.abram@uj.edu.pl (M. Abram), marcin.wysokinski@uj.edu.pl (M.M. Wysokiński), ufspalek@if.uj.edu.pl (J. Spałek).

http://dx.doi.org/10.1016/j.jmmm.2015.07.017
0304-8853/

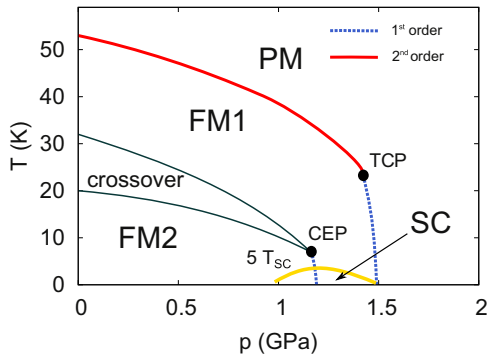

Fig. 1. Schematic magnetic phase diagram of UGe_2 on pressure–temperature plane drawn on the basis of the experimental results [9].

majority of UGe_2 magnetic and electronic properties, as seen in neutron scattering [17], de Haas–van Alphen oscillations [22,23], and magnetization measurements [8]. Also, a semi-metallic character of the weak FM1 phase is supported by the band-structure calculations [24]. A similar idea concerning the emergence of two distinct FM phases in UGe_2 was also obtained earlier within the phenomenological picture based on the Stoner theory incorporating a two-peak structure of the density of states in a single band [25]. In brief, our microscopic model extended to the case of $T>0$ [14] describes well emergence of all CPs on the magnetic phase diagram of UGe_2 [8–10] in the semiquantitative manner [14]. Here we compare in detail our results with the experimental data, namely predicted second order transition line joining the TCP with the corresponding QCEP. In particular, we determine the influence of the following factors: (i) the total band filling n, and (ii) the value of the Landé factor g_f for f states, on the position of this second-order line. The influence of factor (i) has the following importance. For exemplary filling $n=1.6$ we have shown [14] that the relative position of the TCP and CEP (cf. Fig. 1) is the same as that seen in the experiments [9,10]. The important question is whether such a mutual alignment of those two critical points is necessary to achieve a good fit and to what extent the proper curvature of the line joining TCP and QCEP is robust with respect to the selected band filling. The discussion of the dependence on (ii) has its justification in the not fully resolved nature of magnetism in heavy-fermion systems in general and UGe_2 in particular. Although it is assumed and widely accepted to be fully itinerant [2], there is evidence for a partially localized contribution [24,26]. In such a case, the influence of the orbital effects and their coupling to the spin should have an influence on g_f value.

2. Model and approach

We begin with the orbitally nondegenerate Anderson-lattice model (ALM) on square lattice and with applied magnetic field accounted for via the Zeeman splitting (i.e., with the effective field is $h \equiv \frac{1}{2} g\mu_0\mu_B H$), so that the starting Hamiltonian is

$$\begin{aligned}\hat{\mathcal{H}}_0 = &\sum_{\mathbf{i},\mathbf{j},\sigma}{}' t_{\mathbf{ij}} \hat{c}^{\dagger}_{\mathbf{i}\sigma}\hat{c}_{\mathbf{j}\sigma} - \sum_{\mathbf{i},\sigma}\sigma h \hat{n}^{c}_{\mathbf{i}\sigma} \\ &+ \sum_{\mathbf{i},\sigma}\left(\epsilon_f - \frac{g_f}{g}\sigma h\right)\hat{n}^{f}_{\mathbf{i}\sigma} + U\sum_{\mathbf{i}}\hat{n}^{f}_{\mathbf{i}\uparrow}\hat{n}^{f}_{\mathbf{i}\downarrow} \\ &+ V\sum_{\mathbf{i},\sigma}(\hat{f}^{\dagger}_{\mathbf{i}\sigma}\hat{c}_{\mathbf{i}\sigma} + \hat{c}^{\dagger}_{\mathbf{i}\sigma}\hat{f}_{\mathbf{i}\sigma}),\end{aligned} \tag{1}$$

where the onsite hybridization is of magnitude $V<0$ and the Landé factor for f electrons is g_f (the free electron value is $g=2$). The model describes a two-orbital system with the conduction (c) band arising from the nearest (t) and the second-nearest (t') neighbor hoppings, and the strong f–f Coulomb interaction is of magnitude U. If it is not stated otherwise, we set $t'=0.25|t|$, $U=5|t|$, $\epsilon_f=-3|t|$, $g_f=g=2$, and $n \equiv \sum_\sigma \langle \hat{n}^{c}_{\mathbf{i}\sigma} + \hat{n}^{f}_{\mathbf{i}\sigma}\rangle = 1.6$.

We also add to the Hamiltonian (1) the usual term with the chemical potential μ, i.e.,

$$\hat{\mathcal{H}} \equiv \hat{\mathcal{H}}_0 - \mu\sum_{\mathbf{i},\sigma}(\hat{n}^{c}_{\mathbf{i}\sigma} + \hat{n}^{f}_{\mathbf{i}\sigma}). \tag{2}$$

The model is solved here by means of *statistically consistent Gutzwiller approximation* (SGA) [27–29]. The method was successfully applied to the number of problems [30,31]. It is characterized with the physical transparency and flexibility that it could be also incorporated into other methods such as EDABI [32,33].

We introduce the Gutzwiller projection acting onto uncorrelated wave function $|\psi_0\rangle$ in the following manner:

$$\left|\psi_G\right\rangle = \prod_{\mathbf{i}} P_{G;\mathbf{i}}\left|\psi_0\right\rangle, \tag{3}$$

where $|\psi_G\rangle$ is the wave function of the correlated ground state. In effect, we map many-particle correlated Hamiltonian (1) onto an effective single-particle Hamiltonian $\hat{\mathcal{H}}_{SGA}$ acting on uncorrelated wave function $|\psi_0\rangle$, that, after taking the space Fourier transform, is as follows:

$$\begin{aligned}\hat{\mathcal{H}}_{SGA} \equiv &\hat{\Psi}^{\dagger}_{\mathbf{k}\sigma}\begin{pmatrix}\epsilon^{c}_{\mathbf{k}} - \sigma h - \mu & \sqrt{q_\sigma}V \\ \sqrt{q_\sigma}V & \epsilon_f - \sigma\dfrac{g_f}{g}h - \mu\end{pmatrix}\hat{\Psi}_{\mathbf{k}\sigma} \\ &- \lambda^{f}_{n}\left(\sum_{\mathbf{k},\sigma}\hat{n}^{f}_{\mathbf{k}\sigma} - \Lambda n_f\right) - \lambda^{f}_{m}\left(\sum_{\mathbf{k},\sigma}\sigma\hat{n}^{f}_{\mathbf{k}\sigma} - \Lambda m_f\right) + \Lambda U d^2\end{aligned} \tag{4}$$

where $\hat{\Psi}^{\dagger}_{\mathbf{k}\sigma} \equiv (\hat{c}^{\dagger}_{\mathbf{k},\sigma}, \hat{f}^{\dagger}_{\mathbf{k},\sigma})$, Λ is the number of the system sites, q_σ is the hybridization narrowing factor, and $d^2 \equiv \langle \hat{n}^{f}_{\mathbf{i}\uparrow}\hat{n}^{f}_{\mathbf{i}\downarrow}\rangle_0$ [31]. Necessary constraints for the f electron number and their magnetic moment [29] are incorporated by means of the Lagrange multipliers λ^{f}_{n} and λ^{f}_{m}, respectively. Hamiltonian (4) can be straightforwardly diagonalized with the resulting four eigenvalues $\left\{E^{b}_{\mathbf{k}\sigma}\right\}$ labeled with the spin ($\sigma=\pm1$) and hybridized-band ($b=\pm1$) indices. For $T>0$ we construct a generalized Landau grand-potential functional according to

$$\begin{aligned}\frac{\mathcal{F}}{\Lambda} = &-\frac{1}{\Lambda\beta}\sum_{\mathbf{k}\sigma b}\ln[1+e^{-\beta E^{b}_{\mathbf{k}\sigma}}] \\ &+ (\lambda^{f}_{n}n_f + \lambda^{f}_{m}m_f + Ud^2),\end{aligned} \tag{5}$$

which is next minimized with respect to the set of following parameters assembled to a vector, $\vec{\lambda} \equiv \{d, n_f, m_f, \lambda^{f}_{n}, \lambda^{f}_{m}\}$. Additionally, we adjust self-consistently the chemical potential from the condition of fixing the total number of electrons, $n = 1/\Lambda\sum_{\mathbf{k}b\sigma} f(E^{b}_{\mathbf{k}\sigma})$, where $f(E)$ is the Fermi–Dirac function. Finally the ground state energy is defined by

$$E_G = \mathcal{F}|_0 + \mu N, \tag{6}$$

where $\mathcal{F}|_0$ means that the value of $\mathcal{F}$ is taken at minimum for the parameters $\vec{\lambda}$.

3. Results and discussion

We start our analysis with the discussion on the proper assignment of the physical units to the microscopic parameters provided so far in dimensionless units (i.e. scaled by $|t|$) to make the quantitative comparison with the observed UGe_2 characteristics. To do so, we have adjusted them [14] by matching the relative positions of the two classical CPs: TCP and CEP at the ferromagnetic transition, as well as attributing the experimentally measured critical temperatures. Matching the results in physical units by fixing the position of two critical points we would call a *strong fitting*, whereas by fixing the position of just a single of them a *weak fitting*.

In our previous works [13,14] we have found that for the total filling $n=1.6$ we could coherently and quantitatively describe the UGe_2 phase diagram. Although, there is no direct experimental evidence in UGe_2 for choosing this particular filling, we have first matched for chosen n TCP and CEP temperatures according to the experiment [14] – strong fitting condition –, and second, we have verified our prediction obtaining agreement of the second-order transition line joining TCP with QCEP [10] with that measured. Additionally, the comparison has provided among others the estimate of the QCEP appearance about 30 T, i.e., higher than that suggested in Ref. [10] which is 18 T.

A natural question arises if this test is sensitive to the choice of n. We show in Fig. 2 that the second-order transition line joining TCP and QCEP determined for a slightly different total filling than $n=1.6$ deviates significantly from the trend of the experimental data [10]. Hence indeed, the comparison is very sensitive to the choice of n. Thus, together with equally sensitive adjustment of T_{TCP} and T_{CEP} with respect to the choice of n [14], it is unlikely that our excellent agreement for the single value of parameter n is fortuitous.

For the sake of completeness and reference to other related works we include in Fig. 2 the (dashed) curve predicted by the one of the most successful approaches describing the general tricritical behavior in itinerant magnetic systems [11,12]. In that procedure, the necessary inputs are the positions of the two CPs, namely TCP and QCEP, leading in fact to the *strong fitting*, but with different pairs of CPs. However, such fitting can be associated with an error as the position of the QCEP, in contrast to TCP and CEP, is not experimentally determined but only extrapolated to 18 T, following Ref. [10]. Note that this condition in our modeling is satisfied for the total filling around $n \simeq 1.55$ (cf. Fig. 2) if we take the extrapolated value of the critical field. In this case, the comparison with results for UGe_2 [10] is worse than e.g. for $n=1.6$ and the temperature of the CEP is much lower than that determined in experiments [8].

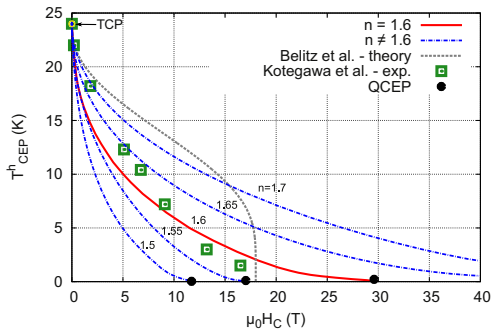

Fig. 2. The second-order transition line joining TCP and QCEP for selected values of total filling, n. Solid curve is replotted from the results reported in Ref. [14]. Experimental points are extracted from pictures in Ref. [10]. Short-dashed curve predicted by the theory formulated by Belitz et al. [11] is shown for comparison (see main text).

It is worth mentioning that the model employed by us belongs to the class discussed earlier by Kirkpatrick and Belitz [12] to reflect the generic tricriticality in the case of metallic magnets. Namely, systems in which the conduction electrons are not a source of the magnetism themselves couple to the magnetically ordered localized electrons in a second band. The origin of the first-order transition at low temperature described within the mean-field theory developed in the Refs. [11,12] is based on the effect of the soft fermionic modes coupled to the magnetization fluctuations, and thus differs from our approach. Here the mechanism for ferromagnetism is due to the coupling of the conduction electrons with localized f states by hybridizing with them and competing with the f–f Coulomb interaction. This competition in the Stoner-like manner induces phase transitions associated with the abrupt changes of the Fermi surface topology.

The simplest verification of our analysis can be carried out by means of chemical alloying, i.e., by changing the electron concentration in the system. However, the lack of known isostructural compounds to UGe_2 may be an apparent obstacle for such test. Though, the determination of the tail of the 2nd order line joining TCP and QCEP for the field larger than 16 T should provide an insight on the issue whether our model correctly predicts the appearance of QCEP around 30 T [14].

If our model is to be used to understand the magnetism of other ferromagnetic superconductors: URhGe [34] and UCoGe [35], it would provide a perfect testing ground of our model as those compounds have been frequently studied by means of the chemical substitution [1,3–6].

Finally, we provide a brief analysis of the impact of the Landé factor value for f electrons, g_f, i.e., in the situation when the z component of the total spin of the system does not commute with Hamiltonian. In Fig. 3 we present the curves for three different values of g_f. The curve for $g_f=2$ is plotted as the reference curve and is based on the results of Ref. [14]. Value of g_f is not known for UGe_2 and generally, for complex compounds has a tensor character which depends on the magnitude of the spin–orbit coupling. For that reason we restrict our discussion to the comparison when g_f is equal to the free electron value $g_f=2$, and subsequently when is lower and higher (cf. Fig. 3) [36]. Specifically, the lower value of Landé factor $g_f = 6/7$ is motivated by that for the Ce-based compounds, where it can be derived for the spin $S = 1/2$ and angular momentum $L=3$, oriented antiparallel and where, strictly speaking, our model is also generally valid, as long as we do not account for the orbital degeneracy of f states of the uranium-based materials. As presented in Fig. 3, it seems that any value of g factor for f states which deviates considerably from the free-electron value provides much worse agreement with experimental data [10]. In conclusion, due to predominantly itinerant nature of f electrons in UGe_2 [26], it is very likely that any crystal-field derived multiplet

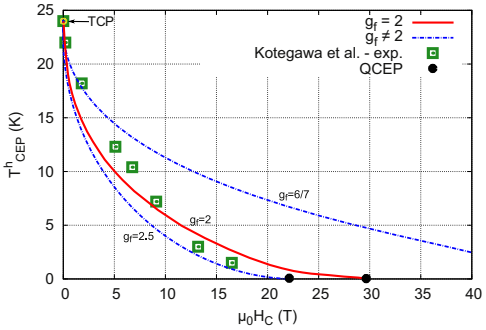

Fig. 3. The second-order transition line joining TCP and QCEP for selected values of Landé factor for f electrons, g_f. Solid curve for $g_f=2$ is replotted from the results reported in Ref. [14]. Experimental points are extracted from Ref. [10].

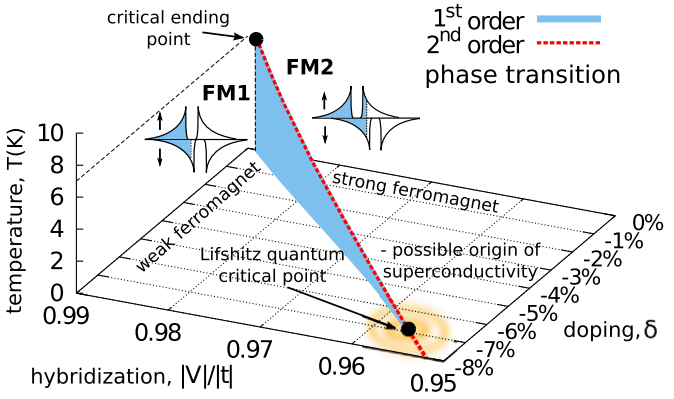

Fig. 4. Evolution of the critical temperature of CEP towards Lifshitz QCP driven by changing total filling, n, and hybridization, V, reproduced after [14].

structure is washed out and hence the value $g_f \simeq 2$ should be regarded as realistic value. Nevertheless, the problem of double localized-itinerant nature of f-electrons [24,26] may arise as the system evolves with the increasing temperature, in comparison to the pressure evolution at low temperature studied in detail here.

4. Outlook

In the present work we have employed the Anderson lattice model [13,14] to provide a fairly complete description of the magnetic phase diagram (p–T–h profiles) of UGe_2 including all the criticalities for this compound. In particular, we study the effect of the choice of the total filling on the quality of the fit, based on our model, to the experimental data [10] concerning the second-order transition line joining the critical points TCP and QCEP. We have found that our prediction is very sensitive to the change of n, which leads also to a mismatch of critical temperatures of TCP and CEP at the metamagnetic transition as compared to the experiment. We infer from this result that our excellent agreement for the single value of n is unlikely fortuitous. We have also analyzed the effect of the Landé factor g_f value for f electrons. In this case, any sizable deviation from the free electron value $g_f=2$ shifts the theoretical curves away from the experimental points. Thus treating f electrons as truly itinerant electrons in UGe_2 seems to be fully justified.

Our final remark addresses the problem of the spin-triplet superconductivity (SC) origin occurring in UGe_2 [1,2]. We have predicted in our previous work [14] the appearance of QCP in the vicinity of the SC dome. It have been proposed that CEP (cf. Fig. 1) at the metamagnetic phase boundary can be followed down to the $T=0$ by changing both the electron concentration and the hybridization magnitude $|V|$ (cf. Fig. 4). The proposed quantum critical point is of Lifshitz type as it separates states with two distinct Fermi-surface topologies. Quantum critical fluctuations or the residual f–f Hund's rule interaction (neglected here) can become the possible source of the spin-triplet superconductivity [37–41]. A detailed and quantitative discussion of the pairing requires a separate analysis.

Acknowledgements

The work was supported by the National Science Centre (NCN) under the Grant MAESTRO, no. DEC-2012/04/A/ST3/00342.

References

[1] C. Pfleiderer, Rev. Mod. Phys. 81 (2009) 1551.
[2] S.S. Saxena, P. Agarwal, K. Ahilan, F.M. Grosche, R.K.W. Haselwimmer, M. J. Steiner, E. Pugh, I.R. Walker, S.R. Julian, P. Monthoux, G.G. Lonzarich, A. Huxley, I. Sheikin, D. Braithwaite, J. Flouquet, Nature 406 (2000) 587.
[3] D. Aoki, J. Flouquet, J. Phys. Soc. Jpn. 81 (2012) 011003.
[4] D. Aoki, A. Gourgout, A. Pourret, G. Bastien, G. Knebel, J. Flouquet, C. R. Phys. 15 (2014) 630.
[5] D. Aoki, J. Flouquet, J. Phys. Soc. Jpn. 83 (2014) 051011.
[6] A.D. Huxley, Physica C 514 (2015) 368.
[7] Coexistence of FM and SC was observed for the first time by A. Kolodziejczyk for the weak itinerant ferromagnets Y_9Co_7 [42–44]. However, SC was found there to be of spin-singlet nature and strongly competing with FM, in contrast to the UGe_2 case, where it is of the spin-triplet character and its coexsitence with FM seems to be strongly cooperative as e.g. both phases disappear at the same pressure.
[8] C. Pfleiderer, A.D. Huxley, Phys. Rev. Lett. 89 (2002) 147005.
[9] V. Taufour, D. Aoki, G. Knebel, J. Flouquet, Phys. Rev. Lett. 105 (2010) 217201.
[10] H. Kotegawa, V. Taufour, D. Aoki, G. Knebel, J. Flouquet, J. Phys. Soc. Jpn. 80 (2011) 083703.
[11] D. Belitz, T.R. Kirkpatrick, J. Rollbühler, Phys. Rev. Lett. 94 (2005) 247205.
[12] T.R. Kirkpatrick, D. Belitz, Phys. Rev. B 85 (2012) 134451.
[13] M.M. Wysokiński, M. Abram, J. Spałek, Phys. Rev. B 90 (2014) 081114(R).
[14] M.M. Wysokiński, M. Abram, J. Spałek, Phys. Rev. B 91 (2015) 081108(R).
[15] A.B. Shick, W.E. Pickett, Phys. Rev. Lett. 86 (2001) 300.
[16] A. Huxley, I. Sheikin, E. Ressouche, N. Kernavanois, D. Braithwaite, R. Calemczuk, J. Flouquet, Phys. Rev. B 63 (2001) 144519.
[17] N. Kernavanois, B. Grenier, A. Huxley, E. Ressouche, J.P. Sanchez, J. Flouquet, Phys. Rev. B 64 (2001) 174509.
[18] R. Doradziński, J. Spałek, Phys. Rev. B 56 (1997) R14239.
[19] R. Doradziński, J. Spałek, Phys. Rev. B 58 (1998) 3293.
[20] O. Howczak, J. Kaczmarczyk, J. Spałek, Phys. Status Solidi B 250 (2013) 609.
[21] K. Kubo, Phys. Rev. B 87 (2013) 195127.
[22] T. Terashima, T. Matsumoto, C. Terakura, S. Uji, N. Kimura, M. Endo, T. Komatsubara, H. Aoki, Phys. Rev. Lett. 87 (2001) 166401.
[23] R. Settai, M. Nakashima, S. Araki, Y. Haga, T.C. Kobayashi, N. Tateiwa, H. Yamagami, Y. Onuki, J. Phys: Condens. Matter 14 (2002) L29.
[24] M. Samsel-Czekała, M. Werwiński, A. Szajek, G. Chełkowska, R. Troć, Intermetallics 19 (2011) 1411.
[25] K.G. Sandeman, G.G. Lonzarich, A.J. Schofield, Phys. Rev. Lett. 90 (2003) 167005.
[26] R. Troć, Z. Gajek, A. Pikul, Phys. Rev. B 86 (2012) 224403.
[27] T.M. Rice, K. Ueda, Phys. Rev. Lett. 55 (1985) 995.
[28] P. Fazekas, B.H. Brandow, Phys. Scr. 36 (1987) 809.
[29] J. Jędrak, J. Kaczmarczyk, J. Spałek, arXiv:1008.0021.
[30] M. Abram, J. Kaczmarczyk, J. Jędrak, J. Spałek, Phys. Rev. B 88 (2013) 094502.
[31] M.M. Wysokiński, J. Spałek, J. Phys.: Condens. Matter 26 (2014) 055601.
[32] A.P. Kądzielawa, J. Spałek, J. Kurzyk, W. Wójcik, Eur. Phys. J. B 86 (2013) 252.
[33] A.P. Kądzielawa, Acta Phys. Pol. A 126 (2014) A58.
[34] D. Aoki, A. Huxley, E. Ressouche, D. Braithwaite, J. Flouquet, J.-P. Brison, E. Lhotel, C. Paulsen, Nature 413 (2001) 613.
[35] N.T. Huy, A. Gasparini, D.E. de Nijs, Y. Huang, J.C.P. Klaasse, T. Gortenmulder, A. de Visser, A. Hamann, T. Görlach, H.v. Löhneysen, Phys. Rev. Lett. 99 (2007) 067006.
[36] P. Quinet, E. Biémont, At. Data Nucl. Data Tables 87 (2004) 207.
[37] M. Zegrodnik, J. Spałek, Phys. Rev. B 86 (2012) 014505.
[38] M. Zegrodnik, J. Spałek, J. Bünemann, New J. Phys. 15 (2013) 073050.
[39] J. Spałek, M. Zegrodnik, J. Phys.: Condens. Matter 25 (2013) 435601.
[40] M. Zegrodnik, J. Bünemann, J. Spałek, New J. Phys. 16 (2014) 033001.
[41] J. Spałek, Phys. Rev. B 63 (2001) 104513.
[42] A. Kołodziejczyk, B.V. Sarkissian, B.R. Coles, J. Phys. F 10 (1980) L333.
[43] A. Kołodziejczyk, Physica B 130 (1985) 189.
[44] K. Rogacki, A. Kołodziejczyk, L. Bochenek, T. Cichorek, Philos. Mag. 95 (2015) 503.

Article 6:

In this article we study the t–J–U–V model in the context of stability of superconducting (SC), antiferromagnetic (AF) and charge density wave (CDW) phases. The model is solved by means of the statistically consistent Gutzwiller approach (SGA) and the diagramatic expansion for the Gutzwiller wave function (DE-GWF). We find that the intersite Coulomb interaction term V is necessary to obtain the stability of the CDW phase. We study different CDW phase symmetries, showing that for the naive choice of the modulation vector $\mathbf{Q} = (\pi, \pi)$ no coexistence of CDW with SC can be observed. Additionally, a different methods of obtaining the Gutzwiller renormalization factors are analyzed. We point, that in the literature two different form of the Gutzwiller factors are present when AF or CDW order is analyzed. We show, that those different form of factors lead to significantly different outputs, especially regarding the stability region of AF phase. We study the origin of those difference (cf. the second Appendix of this paper).

Antiferromagnetism, charge density wave and d-wave superconductivity in the t–J–U–V model of correlated electrons

Marcin Abram,[1,*] Michał Zegrodnik,[2,†] and Jozef Spałek[1,‡]

[1] *Marian Smoluchowski Institute of Physics, Jagiellonian University, Łojasiewicza 11, 30-348 Kraków, Poland*
[2] *Academic Centre for Materials and Nanotechnology, AGH University of Science and Technology, Al. Mickiewicza 30, 30-059 Kraków, Poland*

(Dated: July 19, 2016)

We study the stability of antiferromagnetic (AF), charge density wave (CDW) and superconducting (SC) states within the extended t-J-U-V model of strongly correlated electrons using the statistically consistent Gutzwiller approximation (SGA). We concentrate on the role of the intersite Coulomb interaction term V in stabilizing the CDW phase and show that the CDW phase appears only above some critical values of V and in a limited hole doping range δ. The effect of the term V on SC and AF phases is that a stronger interaction suppresses SC, whereas the AF order is not significantly influenced by its presence. Calculations for the case of pure SC phase have been also carried out for the same model within the diagrammatic expansion for the Gutzwiller wave function (DE-GWF) in order to analyze the influence of higher-order correlations beyond the renormalized mean field approach. In the Appendix we discuss, the specific ambiguity with respect to the choice of the Gutzwiller factors when either AF or CDW orders are considered within the SGA.

PACS numbers: 71.45.Lr,71.10.Fd,71.10.-w

I. INTRODUCTION

Charge ordering (CO) was observed for the first time in 1939 in Fe_3O_4 [1, 2] and since then, it has been commonly seen in electronically correlated transition metal oxides [3]. The interest in this field grew again recently after discovering the charge density wave (CDW) state in cuprate high temperature superconductors for underdoped samples [3–5] (cf. Fig. 1 for reference). Ample evidence shows the role played by CW instability in the copper based materials [3, 6–11]. It has also been suggested that for certain materials the CDW state may have a three-dimensional character in nonzero magnetic field [12, 13]. Furthermore, it is has been argued that the CDW order parameter is characterized by the d-wave symmetry [14–16], and that there is a connection between the pseudogap phase appearance in the cuprates and the charge ordering [9, 17, 18]. Regarding theoretical analysis, various calculation schemes have been applied to the Hubbard and t-J models to investigate the stability of CO states [16, 19–21]. In this respect, the appearance of the so-called pair-density-wave state has been proposed (which can coexist with CDW state) and, as it was suggested, lead to the appearance of the pseudogap anomaly [22, 23]. Finally, it has been implied very recently [24] that the CDW solution for the t–J model has always a slightly higher energy than the generic SC+AF solution. All of this evidence means that a further analysis of CDW instability in t-J and related models is required to verify if the widely used methods of approach to this phenomena can yield the proper description of unconventional phases in the copper based materials and to what extent they cooperate or compete in those quasi-two-dimensional strongly correlated materials.

Encouraged by our recent results obtained within the t-J-U model [25, 26], which match well with experimental results for the cuprates, we concentrate here on the role of intersite Coulomb repulsion within the t-J-U-V model. In such a picture the intraatomic (Hubbard) interaction magnitude U is not regarded as extremely strong which means that the limit $U/t \to \infty$ cannot be assumed. In this situation, a straightforward decomposition of the narrow-band state into the Hubbard subbands, with upper subband being unoccupied, is not physically realized and the t-J model does not follow directly from the perturbation expansion of the Hubbard model in powers of t/U. Instead, the antiferromagnetic kinetic exchange interaction arises from the superexchange via $2p_\sigma$ states due to oxygen [27]. Consequently, nonzero double occupancies are allowed for non-half-filled band case and in such situation the Hubbard term $\sim U$ is present. This argument justifies the generalization of the t–J model to the t–J–U form. The additional term $\sim V$ is added here to analyze its importance for the CDW state stability [28].

In our analysis we have considered the three most important phases related to the cooper-based high temperature superconducting (HTS) compounds: the antiferromagnetic (AF), charge ordered (CDW), and superconducting (SC) phases. We show that the presence of the V term is necessary for CDW stability.

In the first part of this paper, the analysis is carried out with the use of the statistically consistent Gutzwiller approximation (SGA), which we can account for correlation effects in reasonable computing time (cf. derivation of SGA method in [29–31] and its various applications in

* abram.mj@gmail.com
† michal.zegrodnik@agh.edu.pl
‡ ufspalek@if.uj.edu.pl

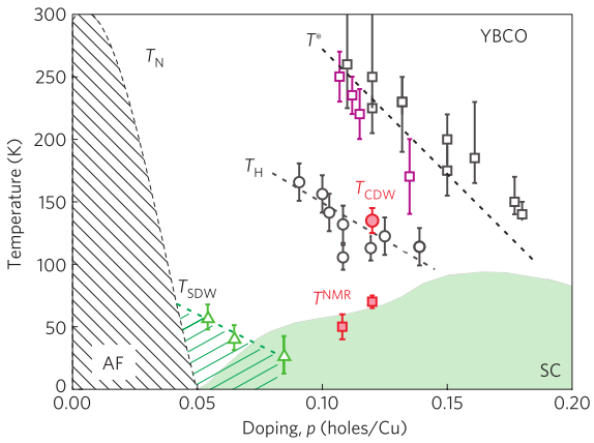

Figure 1. (Color online) Experimental phase diagram of $YBa_2Cu_3O_{6+x}$ (YBCO) on hole-doping–temperature plane. The shaded regions represent the superconducting (SC) and antiferromagnetic (AF) phases (with the Néel temperature T_N), as well as the region where the spin-density-wave (SDW) state is observed. Note, that the CDW critical temperature T_{CDW} is about twice larger than the critical temperature of SC phase. The pseudogap is marked by T^* (black squares represent the Nernst effect measurements, and the purple squares the neutron diffraction). Finally, T_H stands for the critical temperature of the large and negative Hall effect, while T^{NMR} for the temperature scale, below which the field-induced charge order is observed using NMR (Figure taken from Ref. 9).

[25, 32–39]). In the second part of the paper, we test the robustness of the pure superconducting solution, using a systematic diagrammatic expansion of the Gutzwiller-wave function (DE-GWF) method. This approach allows us to go beyond the SGA and to take into account, in higher orders, non-local correlations. The differences between SGA and DE-GWF solutions are specified there. Additionally, in the Appendix A, we discuss the ambiguity in choosing the Gutzwiller renormalization factors when either AF or CDW states are considered. Namely, we show that different calculations schemes used in the literature lead to various forms of the Gutzwiller factors, resulting in different stability regimes of the AF phase.

II. t–J–U–V MODEL

The starting Hamiltonian for the subsequent analysis has the form,

$$\hat{\mathcal{H}}_{t\text{–}J\text{–}U\text{–}V} = t \sum_{\langle i,j\rangle,\sigma} \left(\hat{c}^{\dagger}_{i\sigma}\hat{c}_{j\sigma} + H.c.\right) + t' \sum_{\langle\langle i,j\rangle\rangle,\sigma} \left(\hat{c}^{\dagger}_{i\sigma}\hat{c}_{j\sigma} + H.c.\right) + J \sum_{\langle i,j\rangle} \hat{\mathbf{S}}_i \cdot \hat{\mathbf{S}}_j + U \sum_i \hat{n}_{i\uparrow}\hat{n}_{i\downarrow} + \underbrace{\left(\tilde{V} - \frac{1}{4}J\right)}_{V} \sum_{\langle i,j\rangle,\sigma,\sigma'} \hat{n}_{i\sigma}\hat{n}_{j\sigma'}, \quad (1)$$

where t and t' are the hopping amplitudes between the nearest and the next nearest neighboring sites, J is the antiferromagnetic exchange integral, and U ($\tilde{V}$) is the on-site (intersite) Coulomb repulsion magnitude. The standard second quantization notation is used, where $\hat{c}^{\dagger}_{i\sigma}$ and $\hat{c}_{i\sigma}$ is the creation and annihilation operator, respectively, for an electron with spin quantum number $\sigma = \pm 1$ at site i. Similarly, $\hat{n}_{i\sigma} = \hat{c}^{\dagger}_{i\sigma}\hat{c}_{i\sigma}$ and $\hat{\mathbf{S}}_i = (\hat{S}^{+}_i, \hat{S}^{-}_i, \hat{S}^{z}_i)$, where $\hat{S}^{\sigma}_i \equiv \hat{c}^{\dagger}_{i\sigma}\hat{c}_{i\bar{\sigma}}$ and $\hat{S}^{z}_i \equiv \frac{1}{2}(\hat{n}_{i\uparrow} - \hat{n}_{i\downarrow})$.

As has already been mentioned, the appearance of the J term in this approach results from the superexchange via $2p_\sigma$ states due to oxygen [27]. The finite value of the Coulomb repulsion U leads to a relatively small but nonzero population of the upper Hubbard subband [40–42]. In such a situation the appearance of both the J and the U terms is admissible in the Hamiltonian. For $V = 0$ and when $U \to \infty$, the limit of the t–J model is recovered. On the other hand, for $J = V = 0$, we obtain the limit of the Hubbard model. Nevertheless, our model is not only constructed as a formal generalization of the two limits. As can be seen from the numerous estimates of the model parameters, the typical values of the parameters of the one-band model are: $t = -0.35$ eV, and $U = 8$–10 eV, so that the ratio of U to the bare bandwidth $W = 8|t|$ is $U/W \approx 2.5$, i.e., only by the factor of about two higher than typical required for Mott-Hubbard localization [43, 44]. In effect, the value of J cannot be regarded as resulting from the t/U expansion of the (extended) Hubbard model [45–51], and both J and U can be treated as independent variables. The last term comes partially from the derivation of t–J model from the Hubbard model (cf. [45–47, 49–52]) and partially represents an explicit intersite Coulomb repulsion of electrons located at neighboring sites (the term $\sim \tilde{V}$). For simplicity, we denote $V \equiv \tilde{V} - \frac{1}{4}J$.

III. METHODS

A. Statistically Consistent Gutzwiller Approximation (SGA)

To solve the Hamiltonian (1), we first use the statistically consistent Gutzwiller approximation (SGA) [29–31, 53, 54]). The main idea behind the Gutzwiller approach is to express the wave function of the system in the following form

$$|\Psi\rangle = \hat{P}\,|\Psi_0\rangle \equiv \prod_{\mathbf{k}}^{N} \hat{P}_i\,|\Psi_0\rangle, \quad (2)$$

where $\hat{P}_i$ operator weights the configuration of given occupancies $(0, \uparrow, \downarrow, \uparrow\downarrow)$ of single lattice site i and $|\Psi_0\rangle$ is the non-correlated single particle wave function, generally assumed in the broken-symmetry state of our choice. In such a situation, the expectation value of the ground-state energy of the system is

$$E = \frac{\langle\Psi|\hat{\mathcal{H}}|\Psi\rangle}{\langle\Psi|\Psi\rangle} = \frac{\langle\Psi_0|\hat{P}\hat{\mathcal{H}}\hat{P}|\Psi_0\rangle}{\langle\Psi_0|\hat{P}^2|\Psi_0\rangle} \approx \langle\Psi_0|\hat{\mathcal{H}}_{\mathit{eff}}|\Psi_0\rangle. \tag{3}$$

In other words, instead of calculating the average of the initial Hamiltonian (1) with respect to usually complicated, many-particle, wave function, we choose to modify that Hamiltonian (presumably by making it more complicated) in order to have the relatively simple task of calculating its average with respect to the single particle wave function represented by a single Slater determinant. In our case, the resultant expectation value is depended on many quantities,

$$\langle\Psi_0|\hat{\mathcal{H}}^{\mathit{eff}}_{t-J-U-V}|\Psi_0\rangle \equiv W(n, m, \delta_n, d_A, d_B, \chi, \chi_S, \chi_T, \Delta_S, \Delta_T), \tag{4}$$

where $W(\ldots)$ is a functional of a number of mean-field averages that are explained below (for the explicit form of W and the details of the calculations see Appendix A). First, n is the average number of electrons per site, m is the magnitude of staggered magnetization, and δ_n is the order parameter for CDW phase. Those three quantities can be combined together by expressing the local occupancy in the following manner,

$$n_{i\sigma} \equiv \langle\hat{c}^\dagger_{i\sigma}\hat{c}_{i\sigma}\rangle_0 \equiv \frac{1}{2}\left(n + e^{i\mathbf{Q}\cdot\mathbf{R}_i}\left(\sigma m + \delta_n\right)\right), \tag{5}$$

where for simplicity, we denote $\langle\Psi_0|\ldots|\Psi_0\rangle \equiv \langle\ldots\rangle_0$. The superlattice vector was chosen to be $\mathbf{Q} = (\pi, \pi)$, i.e., the lattice is naturally divided into two sublattices, A and B, such that one sublattice (A) has in average $\frac{1}{2}(n+m+\delta_n)$ *up* $(\uparrow)$ electrons and $\frac{1}{2}(n-m+\delta_n)$ *down* $(\downarrow)$ electrons, while the second sublattice (B) has in average $\frac{1}{2}(n-m-\delta_n)$ *up* $(\uparrow)$ and $\frac{1}{2}(n+m-\delta_n)$ *down* $(\downarrow)$ electrons. Second, the double occupancies probability on sublattices are indicated by d_A and d_B, respectively. Third, the average hopping amplitude for the first and the next nearest neighbors (1st and 2nd n.n.) are defined by

$$\chi_{ij\sigma} \equiv \langle\hat{c}^\dagger_{i\sigma}\hat{c}_{j\sigma}\rangle_0 \equiv \begin{cases} \chi_\sigma & \text{for 1st n.n.,} \\ \chi_{S,\sigma} + e^{i\mathbf{Q}\cdot\mathbf{R}_i}\chi_{T,\sigma} & \text{for 2nd n.n.,} \end{cases} \tag{6}$$

with $\chi_{S,\sigma} \equiv \frac{1}{2}(\chi_{AA\sigma} + \chi_{BB\sigma})$, $\chi_{T,\sigma} \equiv \frac{1}{2}(\chi_{AA\sigma} - \chi_{BB\sigma})$, where $\chi_{AA\sigma}$ and $\chi_{BB\sigma}$ denote respectively hopping of electron with the spin σ within sublattice A and B, and $\chi_{AB\sigma} \equiv \chi_\sigma$ is the hopping between the sublattices (cf. Fig. 2). Fourth, the electron pairing amplitude between nearest neighbors, with spin-singlet and triplet components Δ_S and Δ_T are defined by

$$\Delta_{ij\sigma} \equiv \langle\hat{c}_{i\sigma}\hat{c}_{j\bar{\sigma}}\rangle_0 = -\tau_{ij}\left(\sigma\Delta_S + e^{i\mathbf{Q}\cdot\mathbf{R}_i}\Delta_T\right), \tag{7}$$

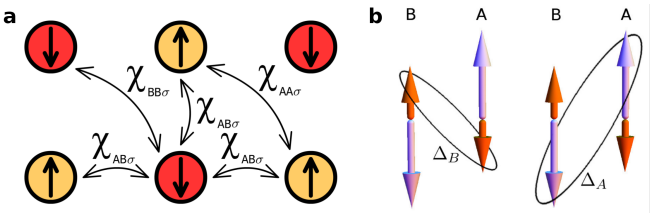

Figure 2. (Color online) Schematic interpretation of $\chi_{AB\sigma} \equiv \chi_\sigma$, $\chi_{AA\sigma}$ and $\chi_{BB\sigma}$ (panel *a*) and Δ_A and Δ_B (panel *b*). To include antiferromagnetic ordering we divide the lattice into two sublattices, A where in majority spins are *up*, and B where there are *down*. Thus, $\chi_{AB\sigma}$ denotes hopping of σ electron between the sublattices A and B, while $\chi_{AA\sigma}$ and $\chi_{BB\sigma}$ the hopping within one sublattice (A or B respectively); Δ_A denotes the pairing amplitude of majority spins *up* from sublattice A and minority spins *down* from B, and Δ_B pairing of majority spins *up* from B and minority spins *down* from A. Additionally, if CDW is present, then for site belonging to the A sublattice the average (total) number of electrons should be larger by δ_n, with respect to the neighboring site belonging to the B sublattice (for clarity, in this picture it was assumed that $\delta_n = 0$).

where $\tau_{ij} \equiv 1$ for $j = i \pm \hat{x}$, and $\tau_{ij} \equiv -1$ for $j = i \pm \hat{y}$ to ensure the d-wave symmetry of $\Delta_{ij\sigma}$, and with $\Delta_S \equiv \frac{1}{4}(\Delta_A + \Delta_B + \text{H.c.})$ and $\Delta_T \equiv \frac{1}{4}(\Delta_A - \Delta_B + \text{H.c.})$ (cf. Fig. 2).

The mean field parameter defined above is determined numerically by minimizing the system's ground-state energy. However, in order to be sure that the self-consistent conditions are also fulfilled in a variational sense, we introduce additional constraints with the help of the the Lagrange multiplier method (cf. [29–31]). Such approach leads to the effective Hamiltonian of the following form

$$\begin{aligned}\hat{K} = W(n, m, \ldots) &- \sum_{\langle i,j\rangle,\sigma}\left(\lambda^\chi_{ij\sigma}\left(\hat{c}^\dagger_{i\sigma}\hat{c}_{j\sigma} - \chi_{ij\sigma}\right) + \text{H.c.}\right) \\ &- \sum_{\langle\langle i,j\rangle\rangle,\sigma}\left(\lambda^\chi_{ij\sigma}\left(\hat{c}^\dagger_{i\sigma}\hat{c}_{j\sigma} - \chi_{ij\sigma}\right) + \text{H.c.}\right) \\ &- \sum_{\langle i,j\rangle}\left(\lambda^\Delta_{ij\sigma}\left(\hat{c}_{i\sigma}\hat{c}_{j\bar{\sigma}} - \Delta_{ij\sigma}\right) + \text{H.c.}\right) \\ &- \sum_{i\sigma}\left(\lambda^n_{i\sigma}\left(\hat{n}_{i\sigma} - n_{i\sigma}\right)\right) - \mu\sum_{i\sigma}\hat{n}_{i\sigma}.\end{aligned} \tag{8}$$

Such an approach allows us the derive the generalized grand potential function at temperature $T > 0$,

$$\mathcal{F} = -\frac{1}{\beta}\ln\mathcal{Z}, \quad \text{with} \quad \mathcal{Z} = \text{Tr}\left(e^{-\beta\hat{K}}\right), \tag{9}$$

with the Landau free energy equal to

$$F = \mathcal{F}_0 + \mu\Lambda n, \tag{10}$$

where $\mathcal{F}_0$ denotes the value of $\mathcal{F}$ obtained at the minimum, i.e. when the following conditions are fulfilled,

$$\frac{\partial\mathcal{F}}{\partial A_i} = 0, \quad \frac{\partial\mathcal{F}}{\partial\lambda_i} = 0, \quad \frac{\partial\mathcal{F}}{\partial d_A} = 0, \quad \frac{\partial\mathcal{F}}{\partial d_B} = 0, \tag{11}$$

where $\{A_i\}$ denote the mean-field averages while $\{\lambda_i\}$ refers to the Lagrange multipliers. The set of equations (11) can be subsequently solved using numerical methods. The results are presented in the Section IV.

B. Extension: DE-GWF Approach

The SGA method described in the previous Section should be considered as a more sophisticated form of the Renormalized Mean Field Theory (RMFT), with the statistical consistency conditions included explicitly. In this Section we describe the Diagrammatic Expansion Gutzwiller Wave Function (DE-GWF) [35, 55–58]. This method extend our approach beyond RMFT in a systematic manner by including the nonlocal correlations in higher orders and thus achieving the full Gutzwiller-wave-function solution step by step. It is important to note that the SGA is equivalent to the zeroth order form of the DE-GWF method. As the full approach is significantly more complicated than the SGA method, here we address the solution only for a pure superconducting phase. The determination of the full phase diagram is cumbersome within DE-GWF and must be described separately.

Similarly as before, we are looking for the ground state of the system in the form given by Eq. (2). The general form of the $\hat{P}$ operator takes the form

$$\hat{P} \equiv \prod_i \hat{P}_i = \prod_i \sum_{\Gamma} \lambda_{i,\Gamma} |\Gamma\rangle_{ii}\langle\Gamma|. \tag{12}$$

The variational parameters $\lambda_{i,\Gamma} \in \{\lambda_{i\varnothing}, \lambda_{i\uparrow}, \lambda_{i\downarrow}, \lambda_{i\uparrow\downarrow}\}$ correspond to four states from the local basis $|\varnothing\rangle_i$, $|\uparrow\rangle_i$, $|\downarrow\rangle_i$, $|\uparrow\downarrow\rangle_i$, respectively. In our analysis we assume the spatial homogeneity of the local solutions, so $\lambda_{i,\Gamma} \equiv \lambda_\Gamma$. Moreover, we also limit to the spin-isotropic case, which means that $\lambda_\uparrow = \lambda_\downarrow = \lambda$. It has been shown by Bünemann et al. [55], that it is convenient to choose the $\hat{P}_i$ operator so that it fulfills the following relation,

$$\hat{P}_i^2 = 1 + x\hat{d}_i^{\mathrm{HF}}, \tag{13}$$

where x is yet another variational parameter and $\hat{d}_i^{\mathrm{HF}} = \hat{n}_{i\uparrow}^{\mathrm{HF}}\hat{n}_{i\downarrow}^{\mathrm{HF}}$, where $\hat{n}_{i\sigma}^{\mathrm{HF}} = \hat{n}_{i\sigma} - n_0$ with $n_0 = \langle\Psi_0|\hat{n}_{i\sigma}|\Psi_0\rangle$. Eq. (13) together with the definition (12) allows us to express the variational parameters λ_Γ in terms of x (cf. Appendix A). In this manner, we are left only with one variational parameter, x, over which we minimize the ground-state energy of the form from Eq. (3).

Using the condition (13), we can write all the relevant expectation values, which appear during the evaluation of Eq. (3), in the form of a power series with respect to the parameter x. As an example, we show here the power series for the hopping probability and the intersite Coulomb interaction term (all the other terms remaining in the Hamiltonian can be expressed in analogical form, cf. Ref. 57),

$$\begin{aligned}
\langle\Psi|\hat{c}_{i\sigma}^\dagger\hat{c}_{j\sigma}|\Psi\rangle &= \sum_{k=0}^{\infty}\frac{x^k}{k!}\sum_{l_1\ldots l_k}{}' \langle\tilde{c}_{i\sigma}^\dagger\tilde{c}_{j\sigma}\hat{d}_{l_1\ldots l_k}^{\mathrm{HF}}\rangle_0, \\
\langle\Psi|\hat{n}_{i\sigma}\hat{n}_{j\sigma'}|\Psi\rangle &= \sum_{k=0}^{\infty}\frac{x^k}{k!}\sum_{l_1\ldots l_k}{}' \langle\tilde{n}_{i\sigma}^\dagger\tilde{n}_{j\sigma}\hat{d}_{l_1\ldots l_k}^{\mathrm{HF}}\rangle_0,
\end{aligned} \tag{14}$$

where $\hat{d}_{l_1\ldots l_k}^{\mathrm{HF}} \equiv \hat{d}_{l_1}^{\mathrm{HF}}\ldots\hat{d}_{l_k}^{\mathrm{HF}}$ with $\hat{d}_{\varnothing}^{\mathrm{HF}} \equiv 1$, and the primed sums have the restrictions $l_p \neq l_{p'}$ and $l_p \neq i, j$. Also, the following notation has been used $\tilde{c}_{i\sigma}^{(\dagger)} = \hat{P}_i\hat{c}_{i\sigma}^{(\dagger)}\hat{P}_i$ and $\tilde{n}_{i\sigma} = \hat{P}_i\hat{n}_{i\sigma}\hat{P}_i$. By including the first 4-6 terms of the power series we are able to calculate with sufficient accuracy the expectation value of system energy. As one can see the inclusion of higher order terms ($k > 0$) leads to the situation in which the simple expression such as, e.g.,

$$\langle\Psi|\hat{c}_{i\sigma}^\dagger\hat{c}_{j\sigma}|\Psi\rangle = q_t\langle\Psi_0|\hat{c}_{i\sigma}^\dagger\hat{c}_{j\sigma}|\Psi_0\rangle, \tag{15}$$

are no longer valid due to the inclusion of nonlocal correlations of the increased range (caused by the appearance of the $\hat{d}_{l_1\ldots l_k}^{\mathrm{HF}}$ terms inside the expectation values $\langle\ldots\rangle_0$).

By using the Wicks theorem for the averages in the non-correlated state appearing in (14), one can express the average value of the systems energy in terms of the paramagnetic and superconducting lines that connect particular lattice sites, i.e.,

$$P_{ij} \equiv \langle\hat{c}_{i\sigma}^\dagger\hat{c}_{j\sigma}\rangle_0, \quad S_{ij} \equiv \langle\hat{c}_{i\uparrow}^\dagger\hat{c}_{j\downarrow}^\dagger\rangle_0. \tag{16}$$

Such a procedure leads in a natural manner to diagrammatic representation of the energy expectation value, in which the lattice sites play the role of the vertices of the diagrams and the superconducting or paramagnetic lines are interpreted as the edges.

The minimization condition of the ground state energy, Eq. (3), can be expressed by introducing the effective single-particle Hamiltonian of the form

$$\hat{\mathcal{H}}_{\mathrm{eff}} = \sum_{ij\sigma} t_{ij}^{\mathrm{eff}}\hat{c}_{i\sigma}^\dagger\hat{c}_{i\sigma} + \sum_{ij}\left(\Delta_{ij}^{\mathrm{eff}}\hat{c}_{i\uparrow}^\dagger\hat{c}_{i\downarrow}^\dagger + H.c.\right), \tag{17}$$

where the microscopic parameters appearing in this Hamiltonian are defined as

$$t_{ij}^{\mathrm{eff}} \equiv \frac{\partial\mathcal{F}}{\partial P_{ij}}, \quad \Delta_{ij}^{\mathrm{eff}} \equiv \frac{\partial\mathcal{F}}{\partial S_{ij}}. \tag{18}$$

By using the concept of the effective Hamiltonian one can derive the self-consistent equations for P_{ij} and S_{ij}, which can be then solved numerically. Such a procedure has to be supplemented with the concomitant energy minimization with respect the variational parameter x. After determination the value of the variational parameter, together with that of the paramagnetic and superconducting lines, one can evaluate the so-called correlated superconducting gap defined as $\Delta_{G|ij} \equiv \langle\Psi_G|\hat{c}_{i\uparrow}^\dagger\hat{c}_{i\downarrow}^\dagger|\Psi_G\rangle/\langle\Psi_G|\Psi_G\rangle$, which represents the corresponding order parameter.

It should be noted that during the calculations one may limit to the terms with lines that correspond to distances smaller than $R_{\max}$, as P_{ij} and S_{ij} with increasing distance $|\Delta\mathbf{R}_{ij}| = |\mathbf{R}_i - \mathbf{R}_j|$ lead to systematically smaller contributions [58]. In our calculations we have taken $\Delta R^2_{max} = 10$ which for the case of square lattice in a spatially homogeneous state and for the d-wave pairing symmetry leads to 5 different superconducting lines. Each of those lines have their correspondent in the correlated state. The following notation is used in the subsequent discussion

$$\begin{aligned}
\Delta_G^{(10)} &\equiv \Delta_{G|ij}\ , \quad \text{for} \quad \Delta\mathbf{R}_{ij} = (1,0)a, \\
\Delta_G^{(20)} &\equiv \Delta_{G|ij}\ , \quad \text{for} \quad \Delta\mathbf{R}_{ij} = (2,0)a, \\
\Delta_G^{(30)} &\equiv \Delta_{G|ij}\ , \quad \text{for} \quad \Delta\mathbf{R}_{ij} = (3,0)a, \\
\Delta_G^{(21)} &\equiv \Delta_{G|ij}\ , \quad \text{for} \quad \Delta\mathbf{R}_{ij} = (2,1)a, \\
\Delta_G^{(31)} &\equiv \Delta_{G|ij}\ , \quad \text{for} \quad \Delta\mathbf{R}_{ij} = (3,1)a,
\end{aligned} \tag{19}$$

where a is the lattice constant.

IV. RESULTS

A. CDW stability in the Statistically Consistent Gutzwiller Approximation (SGA)

The numerical calculations were carried out for the two dimensional, square lattice. Unless stated otherwise, $t = -1$, $J = |t|/3$, $U = 20|t|$ and $\beta = 1500/|t|$, where $\beta \equiv 1/k_BT$. It was checked that for such choose of β, we reproduce the $T = 0$ limit. To obtain the results in physical units, all the quantities must be multiplied by the corresponding physical value of $|t|$ that is 0.35 eV.

In Figure 3, we present the order parameters of the phases AF, CDW and SC respectively, as well as the double occupancy, d (or d_A and d_B if such value depends on the sublattice), all as a function of doping, $\delta \equiv 1 - n$. The order parameters for AF and CDW phases are the staggered magnetization m and the difference of the average number of electrons between the sublattices A and B, δ_n, respectively. In case of SC, there are two order parameters (cf. [59, 60]), singlet Δ_S and triplet Δ_T. Note, that $\Delta_T \neq 0$ only if $m \neq 0$ and d splits to $d_A \neq d_B$ only if $\delta_n \neq 0$.

In the Figure 3 a), we display the situation in the absence of the intersite Coulomb interaction term ($V = 0$), while in the panels b) and c), the effect of the nonzero value of V ranging from 0 to $1.5|t|$. One can see, that with the increasing value of V, the SC order parameters are suppressed and in the underdoped region only a pure AF phase remains [61]. In the Figure 3 d), the CDW order parameter, δ_n is presented. For $V < 1.85|t|$, no stable CDW phase is observed, but when V reaches the critical value around $1.85|t|$, a region of stable CDW order appears near $\delta \approx 0.47$. With further increasing value of V, the CDW phase regime broadens up. Note, that here

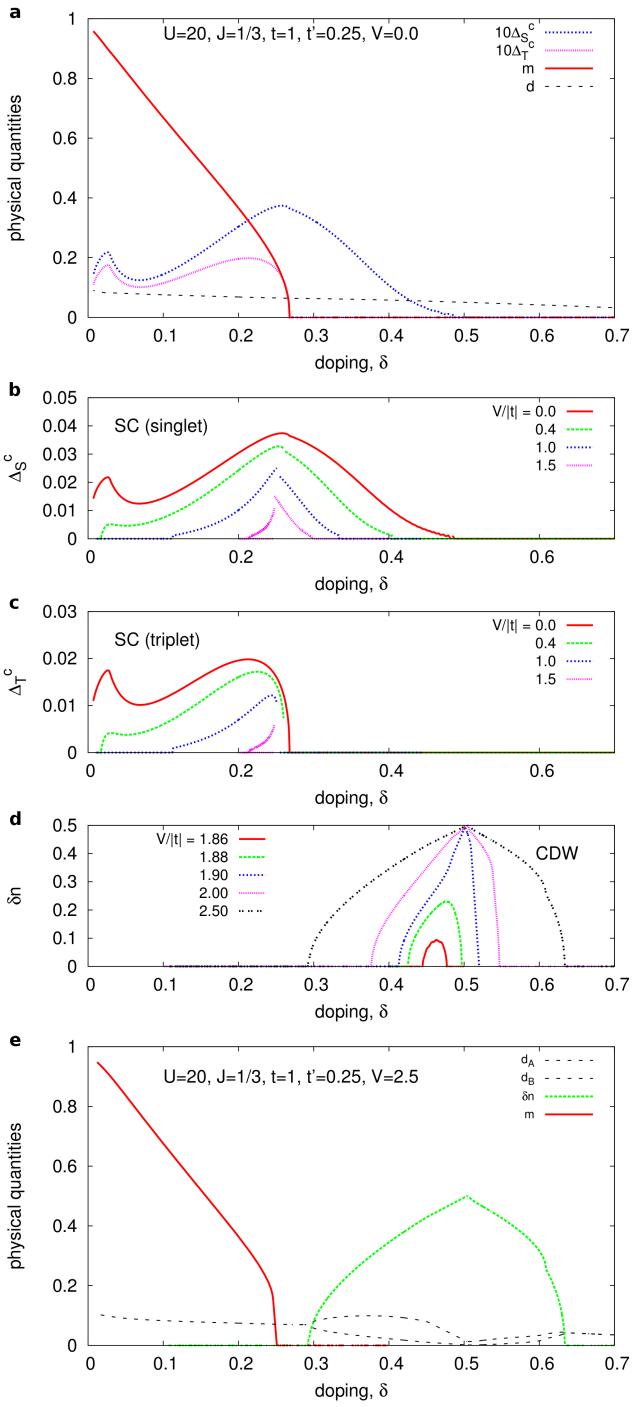

Figure 3. (Color online) Phase diagrams as a function of doping δ for different values of parameters, as specified. a) AF and SC phases as well as the proportion of the double occupied sites d^2 for $V = 0$ (note, that in the plot d instead of d^2 is shown). b) and c) superconducting order parameters Δ_S^c and Δ_T^c, respectively, for selected values of $V/|t|$. d) CDW order parameter as a function of $V/|t|$. e) the phase diagram for $V/|t| = 2.5$. Note that there is no stable SC phase for such a large value of V.

both AF and CDW states have the same modulation vector $\mathbf{Q} = (\pi, \pi)$.

The Figure 3 *e*) shows the phase diagram for $V/|t| = 2.5$. For such relatively large values of V the SC order is no longer observed and the CDW phase regime is broad. Note also, that the AF region is barely affected by the change of the V value in presented range.

We see that the regime of CDW stability with the vector $\mathbf{Q}$, commensurate with that of AF, order does not reflect properly the observed regime of coexistence depicted in Fig. 1. This question requires a more subtle analysis, as we show next. It is not strange that the CDW state is robust around $\delta = n = 0.5$, as then every second site has a surcharge and thus the intersite interaction is diminished for $\delta_n \approx n$, which is the case of large V. Small values of $V \lesssim |t|$ acts positively in the sense that it both reduces the upper concentration of superconductivity disappearance (from $\delta = 0.45$ to 0.3, as required for HTS), as well as makes the SC phase disappear for $\delta < 0.1$, where AF phase becomes the only stable phase. On the other hand, CDW state is not yet stable then. Hence, we have to discuss the CDW state onset for a realistic value of $\mathbf{Q}$ (cf. next Section).

B. Extension: SC vs. CDW stability

In this subsection we discuss first the robustness of the pure superconducting phase within the DE-GWF method, i.e., when going beyond SGA (RMFT form). First, we show the differences between the SGA and the DE-GWF for the selected set of the model parameters. The SC gap parameters obtained in the diagrammatic approach are displayed in Fig. 4 *a*). As one can see, the nearest neighboring pairing amplitude $\Delta_G^{(10)}$ is the dominant one. Nonetheless, the remaining larger-distance contributions are also significant. It should be also noted that in some doping regions different contributions can be of opposite sign. For example in the underdoped regime both $\Delta_G^{(10)}$ and $\Delta_G^{(30)}$ obey exactly the *d*-wave symmetry, but with the opposite phase. The situation is different in SGA method, where the only nonzero pairing contribution taken into account is the nearest neighboring one. In Fig. 4 *b*) we present the evolution of the $\Delta_G^{(10)}$ gap with increasing order of calculations. The lowest dotted–dashed line corresponds to the SGA method which is also equivalent to the zeroth order of the DE-GWF approach. The differences between the green dotted line (the fourth order) and the black solid line (the fifth order) are very small which means that we have achieved a convergence with the assumed accuracy. As one can see, the two methods, SGA and DE-GWF, are qualitatively similar, but the correlations increase the pairing amplitude by 30%–40%.

In Figure 5 we show the influence of the intersite Coulomb repulsion term on the stability of the paired phase within the DE-GWF method. As one can see, the

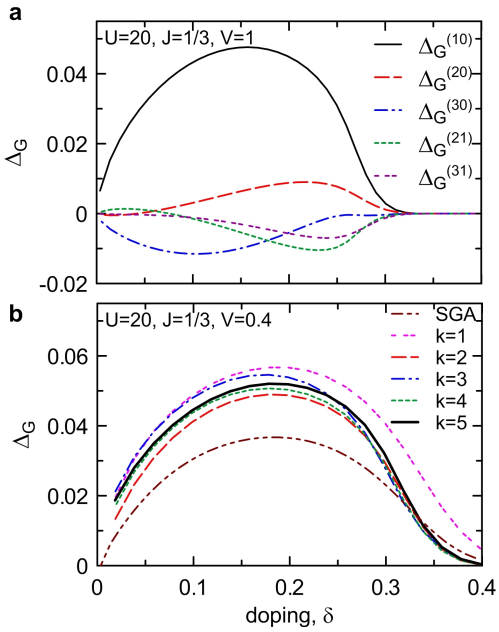

Figure 4. (Color online) *a*) the magnitudes of correlated gaps $\Delta_G^{(mn)}$ (cf. Eq. (19)) between different atomic sites as a function of doping for a selected set of microscopic parameters. *b*) evolution of the nearest neighbor correlated gap Δ_G^{10} with the increasing order k of computations. The zeroth-order (SGA) results (the lowest line) are equivalent to the zeroth order DE-GWF approach. Note, that the lower critical concentration of the SC order is shown here to be 0 even for $V > 0$. This was not the case in the previous Section. The difference is related to whenever AF order is or is not considered. For $V > 0$ the AF order compete with the SC order in underdoped regions and a pure AF phase wins, as it was shown in Fig. 3, but if the AF order is not considered, the SC solution can survive, as it is shown here.

upper critical doping for the disappearance of the superconducting phase decreases again significantly when the term V is included, as in the SGA. One of the differences between the two considered methods is that inclusion of the higher order contributions leads to the appearance of the so-called non-BCS region which is manifested by the kinetic energy gain at the transition to the SC phase. The kinetic energy gain is defined by

$$\Delta E_{\rm kin} \equiv E_G^{SC} - E_G^{PM}, \quad E_G \equiv \frac{1}{N} \sum_{ij\sigma}{}' t_{ij} \langle \hat{c}_{i\sigma}^{\dagger} \hat{c}_{j\sigma} \rangle_G, \quad (20)$$

where E_G^{SC} and E_G^{PM} correspond to the kinetic energies in the SC and normal (paramagnetic, PM) phases, respectively. For the BCS-like region $\Delta E_{\rm kin} > 0$, which is also true for the BCS theory of the phonon-mediated superconductors, whereas $\Delta E_{\rm kin} < 0$ for the non-BCS region. The appearance of the non-BCS regime is purely attributed to the higher-order correlation effects, taken into account within the DE-GWF method, and cannot be accounted for within SGA or any other form of RMFT. It should be noted that the non-BCS behavior has been

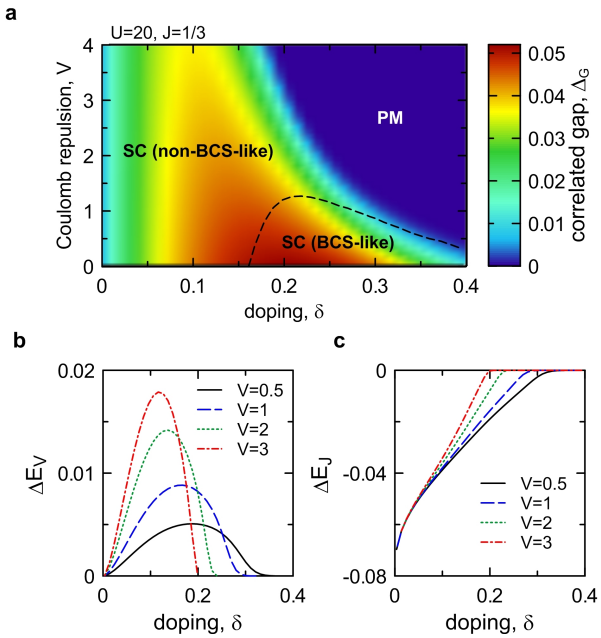

Figure 5. (Color online) *a*) correlated gap as a function of both doping (δ) and the intersite Coulomb repulsion (V). One can distinguish between two superconducting regimes, BCS-like and non-BCS which are defined in the main text. *b*) and *c*) contribution to the condensation energy coming from the intersite Coulomb term $\sim V$ and the exchange term $\sim J$, respectively. While the Coulomb repulsion $\sim V$ increases the energy of SC with respect to the normal (PM) state, the opposite is true for the exchange term. In this sense, the Coulomb interactions $\sim V$ play a destructive role for the pairing, whereas those $\sim J$ provide the main role in it, together with the kinetic-energy gain in the underdoped regime.

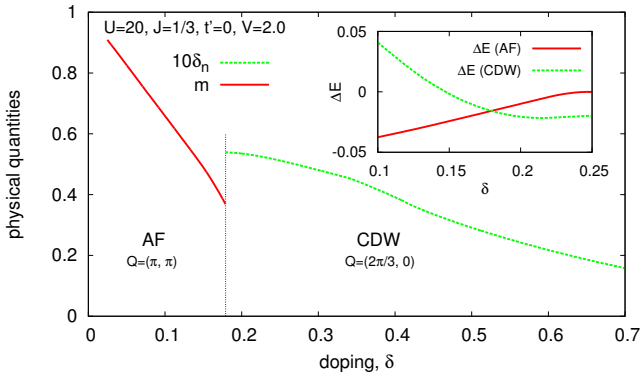

Figure 6. (Color online) Phase diagram with the inclusion of the AF and CDW orders. AF modulation vector is $\mathbf{Q}_{AF} = (\pi, \pi)$ while the one corresponding to the CDW is $\mathbf{Q}_{CDW} = (\frac{2}{3}\pi, 0)$. Such form of CDW symmetry is close to the observed in the experiment. Neither SC order or hopping between the second neighboring sites ($t' = 0$) was included here. In the inset, a difference between the energy of the two considered solutions and the plain paramagnetic one is presented. Note, that the energy of AF and CDW solution intersect, indicating the appearance of the first order transition.

detected experimentally [62, 63] for the underdoped samples, which shows the necessity of including the higher orders to describe some important aspects of cuprate physics. We show here also that the intersite Coulomb repulsion promotes the non-BCS behavior by pushing it to higher doping values (cf. Fig. 5). So even though the intersite Coulomb interaction has a destructive effect on diminishing the condensation energy (cf. Fig. 5 *b*), it extends the region of the non-BCS state. In Figures 5 *b*) and *c*) we plot explicitly the contributions to the condensation energy that originate from the intersite Coulomb repulsion term (V) and the exchange interaction term (J), respectively. The Coulomb repulsion term increases the energy of SC phase with respect to the normal (PM) state which means that it has a negative influence on the pairing strength. The opposite is true for the effect of the exchange term.

Finally, we discuss the effect of symmetry choice for the CDW ordering. Namely, so far we have assumed the simplest form of symmetry, with the modulation vector $\mathbf{Q} = (\pi, \pi)$, whereas in experiments, the CDW modulation vector is closer to $\mathbf{Q}_{CDW} = (\frac{2}{3}\pi, 0)$ [9, 12]. Such a more realistic situation has been considered here as well, without the inclusion of the SC phase so far, as the calculation of all considered phases is difficult and should be studied separately. From Fig. 6 we see, that in this altered scenario the maximum of the CDW order parameter is shifted towards smaller dopings with respect to the previous situation. It is an important result since it is observed that CDW appears in the underdoped regime, close to the boundary of AF phase (cf. Fig. 1 and [9, 10]). This suggests, that the full description including all phases (and their possible coexistence) with such choice of the CDW modulation vector might bring the theory closer to the experiment. It is an interesting starting point for further investigations, including the stability of the SC and AF states. Such a study may constitute a firm test for the one-band minimal model of HTS.

V. DISCUSSION

We have analyzed stability of AF, SC, CDW (and some of the possible coexistent phases) within the t–J–U–V model. For this purpose we have used both SGA and DE-GWF methods. By using the former approach we have shown that CDW phase with $\mathbf{Q} = (\pi, \pi)$ stabilizes only above certain value of V (the intersite Coulomb repulsion), which is detrimental to SC phase stability. With the increasing V, the CDW stability range broadens, while the SC phase is gradually suppressed. It is consistent with the experimental findings, according to which CDW and SC compete with each other. However, it should be mentioned that according to our calculations the CDW phase becomes stable in the overdoped regime, while in the experiment this phase is observed for much

smaller doping values.

In the second half of the article we analyzed the influence of the higher order terms on the pure SC phase withing the DE-GWF method. One of the differences between the DE-GWF and SGA is that in the former approach, the larger distance contributions to the pairing in real space appear (cf. Fig. 4), whereas in the SGA only the nearest neighbor SC gap parameter is present. The second result is that the magnitude of the SC order parameter in DE-GWF is enhanced by about 40% compared to the zero order calculations (SGA). It is observed, that CDW and SC phases coexist [3, 6–11]. However, in SGA the increase of the V parameter suppresses SC before CDW appears. Therefore, the inclusion of the higher order terms that can lead to stability of the coexistent SC-CDW phase might be necessary.

Regarding the DE-GWF approach, the correlation effects taken into account through higher-order terms allow us to reproduce the appearance of the non-BCS behavior in the underdoped regime seen in the experiment [64–67].

Acknowledgments

We would like to acknowledge the financial support from the Grant MAESTRO, No. DEC-2012/04/A/ST3/00342 from the National Science Centre (NCN) of Poland.

Appendix A: Form of the W function

Using the SGA method, we need to calculate the full average of the Hamiltonian $\langle\psi\,|\,\hat{\mathcal{H}}_{t\text{–}J\text{–}U\text{–}V}\,|\,\psi\rangle$ (cf. Eq. 3), namely

$$\begin{aligned} W = \langle\hat{\mathcal{H}}_{t\text{–}J\text{–}U\text{–}V}\rangle &= t\sum_{\langle i,j\rangle,\sigma}\left(\langle\hat{c}^{\dagger}_{i\sigma}\hat{c}_{j\sigma}\rangle + H.c.\right) \\ &+ t'\sum_{\langle\langle i,j\rangle\rangle,\sigma}\left(\langle\hat{c}^{\dagger}_{i\sigma}\hat{c}_{j\sigma}\rangle + H.c.\right) + J\sum_{\langle i,j\rangle}\langle\hat{\mathbf{S}}_i\cdot\hat{\mathbf{S}}_j\rangle \\ &+ U\sum_i\langle\hat{n}_{i\uparrow}\hat{n}_{i\downarrow}\rangle + \underbrace{\left(\tilde{V}-\frac{1}{4}J\right)}_{V}\sum_{\langle i,j\rangle,\sigma,\sigma'}\langle\hat{n}_{i\sigma}\hat{n}_{j\sigma'}\rangle, \end{aligned} \tag{A1}$$

where for simplicity we denote $\langle\Psi|\ldots|\Psi\rangle \equiv \langle\ldots\rangle$. However, this task is non-trivial, since the $|\psi\rangle$ wave function is unknown. The standard Gutzwiller procedure in such cases [53, 54] is to assume, that $\Psi = \hat{P}\,\Psi_0$, where Ψ_0 is a simple, non-correlated wave function, and $\hat{P} = \prod_i \hat{P}_i$ is the operator, which changes the likelihood of sites to be occupied by certain states. In general form,

$$\begin{aligned} \hat{P}_i = \sum_j \lambda_{ij}|\Gamma_j\rangle_{ii}\langle\Gamma_j| = \lambda_{i,0}(1-\hat{n}_{i\uparrow})(1-\hat{n}_{i\downarrow}) + \\ \lambda_{i,\uparrow}\hat{n}_{i\uparrow}(1-\hat{n}_{i\downarrow}) + \lambda_{i,\downarrow}(1-\hat{n}_{i\uparrow})\hat{n}_{i\downarrow} + \lambda_{i,d}\hat{n}_{i\uparrow}\hat{n}_{i\downarrow}. \end{aligned} \tag{A2}$$

Following [55], we assume that $\hat{P}_i^2 = 1 + x_i\,\hat{n}^{HF}_{i\uparrow}\hat{n}^{HF}_{i\downarrow}$, with $\hat{n}^{HF}_{i\sigma} \equiv \hat{n}_{i\sigma} - n_{i\sigma}$. Next, $\hat{P}_i^2$ acting on the local basis, $|\varnothing\rangle_i$, $|\uparrow\rangle_i$, $|\downarrow\rangle_i$, $|\uparrow\downarrow\rangle_i$), one can yields:

$$\lambda^2_{i,0} = 1 + x_i\,n_{i\sigma}n_{i\bar{\sigma}}, \tag{A3}$$

$$\lambda^2_{i,\sigma} = 1 - x_i\,(1-n_{i\sigma})n_{i\bar{\sigma}}, \tag{A4}$$

$$\lambda^2_{i,d} = 1 + x_i\,(1-n_{i\sigma})(1-n_{i\bar{\sigma}}), \tag{A5}$$

where x_i is a variational parameter. When $\forall_i\, x_i = 0$, then the operator $\hat{P} = \mathbb{1}$ and $|\Psi\rangle = |\Psi_0\rangle$, but when $\exists_i\, x_i < 0$, then the likelihood that the site i has two electrons is reduced. Since the the average number of electrons in the system should remain constant, $x_i < 0$ requires, that the number of the single occupied sites is increased and the number of empty sites is reduced at the same times.

The meaning of parameter x_i is not easy to provide, therefore we introduce d_i^2 as the likelihood of double occupancy at site i, namely,

$$\langle\Psi|\hat{n}_{i\uparrow}\hat{n}_{i\downarrow}|\Psi\rangle \equiv d_i^2. \tag{A6}$$

We can relate d_i^2 to the x_i parameter, since

$$d_i^2 = \langle\Psi|\hat{n}_{i\uparrow}\hat{n}_{i\downarrow}|\Psi\rangle = \langle\Psi_0|\hat{P}_i\hat{n}_{i\uparrow}\hat{n}_{i\downarrow}\hat{P}_i|\Psi_0\rangle = \lambda^2_{id}n_{i\uparrow}n_{i\downarrow}, \tag{A7}$$

where we assumed that $\langle\Psi_0|\hat{n}_{i\uparrow}\hat{n}_{i\downarrow}|\Psi_0\rangle \equiv \langle\hat{n}_{i\uparrow}\hat{n}_{i\downarrow}\rangle_0 = n_{i\uparrow}n_{i\downarrow}$, i.e., that the following averages $\langle\hat{c}_{i\uparrow}\hat{c}_{i\downarrow}\rangle_0$ and $\langle\hat{c}^{\dagger}_{i\uparrow}\hat{c}_{i\downarrow}\rangle_0$ are zero. Using Eqs. (A5)–(A7), we can show, that

$$x_i \equiv \frac{d^2 - n_{i\uparrow}n_{i\downarrow}}{n_{i\uparrow}n_{i\downarrow}(1-n_{i\uparrow})(1-n_{i\downarrow})}, \tag{A8}$$

and as a result, we can rewrite the expressions (A3)–(A5) in the form:

$$\lambda^2_{i0} = \frac{1 + d^2 - n_\sigma - n_{\bar{\sigma}}}{(1-n_\sigma)(1-n_{\bar{\sigma}})}, \tag{A9}$$

$$\lambda^2_{i\sigma} = \frac{n_\sigma - d^2}{n_\sigma(1-n_{\bar{\sigma}})}, \tag{A10}$$

$$\lambda^2_{id} = \frac{d^2}{n_\sigma n_{\bar{\sigma}}}. \tag{A11}$$

To calculate the averages, that are present in Eq. (A1), we need one more (partial) result,

$$\hat{P}_i\hat{c}^\dagger_{i\sigma}\hat{P}_i = (\lambda_\sigma \hat{n}_{i\sigma}(1-\hat{n}_{i\bar{\sigma}}) + \lambda_d \hat{n}_{i\sigma}\hat{n}_{i\bar{\sigma}})\,\hat{c}^\dagger_{i\sigma}\,(\lambda_{\bar{\sigma}}\hat{n}_{i\bar{\sigma}}(1-\hat{n}_{i\sigma}) + \lambda_0(1-\hat{n}_{i\sigma})(1-\hat{n}_{i\bar{\sigma}})) = (\alpha_{i\sigma} + \beta_{i\sigma}\hat{n}^{HF}_{i\bar{\sigma}})\hat{c}^\dagger_{i\sigma}, \tag{A12}$$

where

$$\alpha_{i\sigma} = \sqrt{\frac{(n_{i\sigma}-d_i^2)(1-n+d_i^2)}{n_{i\sigma}(1-n_{i\sigma})}} + |d_i|\sqrt{\frac{n_{i\bar{\sigma}}-d_i^2}{n_{i\sigma}(1-n_{i\sigma})}}, \tag{A13}$$

$$\beta_{i\sigma} = -\sqrt{\frac{(n_{i\sigma}-d_i^2)(1-n+d_i^2)}{n_{i\sigma}(1-n_{i\sigma})(1-n_{i\bar{\sigma}})^2}} + |d_i|\sqrt{\frac{n_{i\bar{\sigma}}-d_i^2}{n_\sigma n_{\bar{\sigma}}^2(1-n_\sigma)}}. \tag{A14}$$

Note, that for $\hat{P}_i\hat{c}_{i\sigma}\hat{P}_i$ we would obtain the same result as above. Now, using above expressions, one can calculate any average. For example, the average of the hopping term is

$$\begin{aligned}\langle \hat{c}^\dagger_{i\sigma}\hat{c}_{j\sigma}\rangle &= \langle \hat{P}_i\hat{P}_j\hat{c}^\dagger_{i\sigma}\hat{c}_{j\sigma}\hat{P}_i\hat{P}_j\rangle_0 = \langle \hat{P}_i\hat{c}^\dagger_{i\sigma}\hat{P}_i\,\hat{P}_j\hat{c}_{j\sigma}\hat{P}_j\rangle_0 \\ &= \alpha_{i\sigma}\alpha_{j\sigma}\langle \hat{c}^\dagger_{i\sigma}\hat{c}_{j\sigma}\rangle_0 + \alpha_{i\sigma}\beta_{j\sigma}\langle \hat{n}^{HF}_{i\bar{\sigma}}\hat{c}^\dagger_{i\sigma}\hat{c}_{j\sigma}\rangle_0 \\ &+ \alpha_{j\sigma}\beta_{i\sigma}\langle \hat{n}^{HF}_{j\bar{\sigma}}\hat{c}^\dagger_{i\sigma}\hat{c}_{j\sigma}\rangle_0 + \beta_{i\sigma}\beta_{j\sigma}\langle \hat{n}^{HF}_{i\bar{\sigma}}\hat{n}^{HF}_{j\bar{\sigma}}\hat{c}^\dagger_{i\sigma}\hat{c}_{j\sigma}\rangle_0.\end{aligned} \tag{A15}$$

Using the Wick theorem, we can check that $\langle \hat{n}^{HF}_{i\bar{\sigma}}\hat{c}^\dagger_{i\sigma}\hat{c}_{j\sigma}\rangle_0 = 0$ and $\alpha_{j\sigma}\beta_{i\sigma}\langle \hat{n}^{HF}_{j\bar{\sigma}}\hat{c}^\dagger_{i\sigma}\hat{c}_{j\sigma}\rangle_0 = 0$, as far as we assume that $\langle \hat{c}^\dagger_{i\sigma}\hat{c}^\dagger_{i\bar{\sigma}}\rangle_0 = 0$ and $\langle \hat{c}^\dagger_{i\sigma}\hat{c}_{j\bar{\sigma}}\rangle_0 = 0$. The last average is usually non-zero, but small, therefore it can be neglected here. We are left with,

$$\langle \hat{c}^\dagger_{i\sigma}\hat{c}_{j\sigma}\rangle \approx \alpha_{i\sigma}\alpha_{j\sigma}\langle \hat{c}^\dagger_{i\sigma}\hat{c}_{j\sigma}\rangle_0. \tag{A16}$$

In the simplest case, where neither AF nor CDW order is considered, we have $\alpha_{i\sigma} = \alpha_{j\sigma} = \alpha$ and

$$\alpha^2 = g_t \equiv \frac{n-2d^2}{n(1-n/2)}\left(\sqrt{1-n+d^2}+|d|\right)^2, \tag{A17}$$

what is the Gutzwiller factor for hopping part, well known from the literature [40, 68–70].

In the similar manner, other averages from Eq. (A1) can be calculated. To give, one more example, we show here how to calculate the last term, $\langle \hat{n}_{i\sigma}\hat{n}_{j\sigma'}\rangle$, that is perhaps the most non-trivial (and rarely discussed in the literature). To shorten the length of the expressions, we will assume here for moment, that we are interested only in AF order. The generalization for the CDW order (or others) is not difficult, and it can be left to the reader. Note, that AF symmetry requires, that n_σ from A sublattice is equal to $n_{\bar{\sigma}}$ from the B sublattice.

In such case,

$$\begin{aligned}\Lambda^{-1}&\sum_{\langle i,j\rangle,\sigma,\sigma'}\langle \hat{n}_{i\sigma}\hat{n}_{j\sigma'}\rangle = \Lambda^{-1}\sum_{\langle i,j\rangle,\sigma,\sigma'}\langle \hat{P}_i\hat{n}_{i\sigma}\hat{P}_i\hat{P}_j\hat{n}_{j\sigma'}\hat{P}_j\rangle_0 = \\ &= \Lambda^{-1}\sum_{\langle i,j\rangle,\sigma,\sigma'}\left\langle\left(\hat{n}_{i\sigma}+(\lambda_d^2-\lambda_\sigma^2)\hat{n}_{i\sigma}\hat{n}^{HF}_{i\bar{\sigma}}\right)\left(\hat{n}_{j\sigma'}+(\lambda_d^2-\lambda_{\bar{\sigma}'}^2)\hat{n}_{j\sigma'}\hat{n}^{HF}_{j\bar{\sigma}'}\right)\right\rangle_0 \\ &\approx \Lambda^{-1}\sum_{\langle i,j\rangle,\sigma}\langle n_{i\sigma}n_{j\sigma}\rangle_0 + \langle n_{i\sigma}n_{j\bar{\sigma}}\rangle_0 \\ &\quad+\left(\langle \hat{n}_{j\bar{\sigma}}\rangle_0\langle \hat{n}_{i\bar{\sigma}}\hat{n}^{HF}_{j\sigma}\rangle_0 + \langle \hat{n}_{j\bar{\sigma}}\rangle_0\langle \hat{n}_{i\sigma}\hat{n}^{HF}_{j\sigma}\rangle_0 + \langle \hat{n}_{i\sigma}\rangle_0\langle \hat{n}_{j\sigma}\hat{n}^{HF}_{i\bar{\sigma}}\rangle_0 + \langle \hat{n}_{i\sigma}\rangle_0\langle \hat{n}_{j\bar{\sigma}}\hat{n}^{HF}_{i\bar{\sigma}}\rangle_0\right)(\lambda_d^2-\lambda_\sigma^2) \\ &\quad+(\lambda_d^2-\lambda_\sigma^2)(\lambda_d^2-\lambda_{\bar{\sigma}}^2)\langle \hat{n}_{i\sigma}\rangle_0\langle \hat{n}_{j\sigma}\rangle_0\langle \hat{n}^{HF}_{i\bar{\sigma}}\hat{n}^{HF}_{j\bar{\sigma}}\rangle_0 + (\lambda_d^2-\lambda_\sigma^2)(\lambda_d^2-\lambda_\sigma^2)\langle \hat{n}_{i\sigma}\rangle_0\langle \hat{n}_{j\bar{\sigma}}\rangle_0\langle \hat{n}^{HF}_{i\bar{\sigma}}\hat{n}^{HF}_{j\sigma}\rangle_0 \\ &= 2n^2 + (-4\chi^2+4\Delta_S^2+4\Delta_T^2)\left(1+n_\sigma(\lambda_d^2-\lambda_\sigma^2)+n_{\bar{\sigma}}(\lambda_d^2-\lambda_{\bar{\sigma}}^2)\right) \\ &\quad+4n_\sigma(\lambda_d^2-\lambda_\sigma^2)n_{\bar{\sigma}}(\lambda_d^2-\lambda_{\bar{\sigma}}^2)(-\chi^2) + 2\left(\left[n_\sigma(\lambda_d^2-\lambda_\sigma^2)\right]^2+\left[n_{\bar{\sigma}}(\lambda_d^2-\lambda_{\bar{\sigma}}^2)\right]^2\right)(\Delta_S^2+\Delta_T^2) \\ &= 2n^2 + 4g_v^\chi(-\chi^2) + 4g_v^\Delta(\Delta_S^2+\Delta_T^2),\end{aligned} \tag{A18}$$

where

$$g_v^\chi \equiv \left(1+n_\sigma(\lambda_d^2-\lambda_\sigma^2)+n_{\bar{\sigma}}(\lambda_d^2-\lambda_{\bar{\sigma}}^2)+n_\sigma(\lambda_d^2-\lambda_\sigma^2)n_{\bar{\sigma}}(\lambda_d^2-\lambda_{\bar{\sigma}}^2)\right), \tag{A19}$$

$$g_v^\Delta \equiv \left(1+n_\sigma(\lambda_d^2-\lambda_\sigma^2)+n_{\bar{\sigma}}(\lambda_d^2-\lambda_{\bar{\sigma}}^2)+\frac{1}{2}\left(\left[n_\sigma(\lambda_d^2-\lambda_\sigma^2)\right]^2+\left[n_{\bar{\sigma}}(\lambda_d^2-\lambda_{\bar{\sigma}}^2)\right]^2\right)\right). \tag{A20}$$

The approximate sign in Eq. (A18) results from the fact, that we neglected terms proportional to χ^4, Δ_S^4, Δ_T^4 or

$n_\sigma n_{\bar\sigma}\chi^2$. Note, that if no AF order is considered ($m = 0$), then $n_\sigma = n_{\bar\sigma} = n/2$ and then

$$g_v^\chi = g_v^\Delta = \left(\frac{2d^2 + n(1-n)}{n(1-n/2)}\right)^2. \tag{A21}$$

Appendix B: Two ways of defining the Gutzwiller factor in the presence of extra symmetries

In this Section we show, that introducing extra ordering, such as AF or CDW, can lead to a specific ambiguity in determining the final form of the Gutzwiller factors. We will explain also, how we decided to choose which of the form was used in the main text.

For simplicity, we assume in this Section, that in our model $U \to \infty$, resulting in $d \to 0$. In other words, we consider the case where the correlated state $|\Psi\rangle$ has no double occupancies. Additionally, to make our arguments easy to follow, we consider only AF order (no CDW) and we focus on example of the Gutzwiller factor for the hopping term, that has been already discussed to some extent in the previous Section (cf. Eq. (A17)). The generalization to other states and for another averages should be straightforward.

In the previous appendix, one of our our objective was to find an operator $\hat{P}$, that makes the following approximation as close, as possible,

$$\langle\Psi|\hat{c}^\dagger_{i\sigma}\hat{c}_{j\sigma}|\Psi\rangle \approx \langle\Psi_0|\hat{P}_i\hat{c}^\dagger_{i\sigma}\hat{P}_i\,\hat{P}_j\hat{c}_{j\sigma}\hat{P}_j|\Psi_0\rangle \tag{B1}$$

From the other hand, we can find such function $g_t(n_{i\sigma}, n_{i\bar\sigma}, d, \ldots)$ (called the Gutzwiller renormalization factor), that

$$\langle\Psi_0|\hat{P}_i\hat{c}^\dagger_{i\sigma}\hat{P}_i\,\hat{P}_j\hat{c}_{j\sigma}\hat{P}_j|\Psi_0\rangle = g_t\langle\Psi_0|\hat{c}^\dagger_{i\sigma}\hat{c}_{j\sigma}|\Psi_0\rangle. \tag{B2}$$

Therefore, the Gutzwiller renormalization factor can be obtained, by comparison of the likelihood of a specific process (in this example hopping) in the correlated $|\Psi\rangle$, and in the uncorrelated $|\Psi_0\rangle$ states, namely

$$g_t(n_{i\sigma}, n_{i\bar\sigma}, d, \ldots) \approx \frac{\langle\Psi|\hat{c}^\dagger_{i\sigma}\hat{c}_{j\sigma}|\Psi\rangle}{\langle\Psi_0|\hat{c}^\dagger_{i\sigma}\hat{c}_{j\sigma}|\Psi_0\rangle}. \tag{B3}$$

Let us assume, that there are on average n electrons per site and the staggered magnetization is equal to m. For the non correlated case ($U = 0$), there is in average $n_{A\sigma} = \frac{1}{2}(n + \sigma m)$ electrons with spin σ per site for the A sublattice and $n_{B\sigma} = \frac{1}{2}(n - \sigma m)$ for the B sublattice. Additionally, in average $n_{\uparrow\downarrow} = n_{A\uparrow}n_{A\downarrow} = n_{B\uparrow}n_{B\downarrow}$ sites are double occupied and consequently, $n_\varnothing = (1 - n_{A\uparrow})(1 - n_{A\downarrow}) = (1 - n_{B\uparrow})(1 - n_{B\downarrow})$ sites are empty (cf. Table I).

In the correlated state $|\Psi\rangle$ ($U \neq 0$) the likelihood of the double occupancy should be smaller than that determined for $|\Psi_0\rangle$. The appropriate adjustment is made by choosing the proper form of the $\hat{P}$ operator (cf. [53, 54]). In the specific case of $U \to \infty$, no double occupancies should be allowed in the correlated state, what results in $\forall_i\ \lambda_{i,d} \equiv 0$ (cf. the general form of $\hat{P}$ operator, Eq. (A2)). However, by changing the probability of states to be doubly occupied, we change also the average number of the electrons in the system. To avoid this, other lambdas, $\lambda_{i,0}$, $\lambda_{i,\uparrow}$ and $\lambda_{i,\downarrow}$, need to be modified as well.

Table I. Likelihood of a site being in the certain state (uncorrelated case $|\Psi_0\rangle$).

state	for A sublattice	for B sublattice
$\|\uparrow\rangle$ or $\|\uparrow\downarrow\rangle$	$n_{A\uparrow} = \frac{1}{2}(n+m)$	$n_{B\uparrow} = \frac{1}{2}(n-m)$
$\|\downarrow\rangle$ or $\|\uparrow\downarrow\rangle$	$n_{A\downarrow} = \frac{1}{2}(n-m)$	$n_{B\downarrow} = \frac{1}{2}(n+m)$
$\|\uparrow\rangle$	$n_{A\uparrow}(1-n_{A\downarrow})$	$n_{B\uparrow}(1-n_{B\downarrow})$
$\|\downarrow\rangle$	$n_{A\downarrow}(1-n_{A\uparrow})$	$n_{B\downarrow}(1-n_{B\uparrow})$
$\|\varnothing\rangle$	$(1-n_{A\uparrow})(1-n_{A\downarrow})$	$(1-n_{B\uparrow})(1-n_{B\downarrow})$
$\|\uparrow\downarrow\rangle$	$n_{A\uparrow}n_{A\downarrow}$	$n_{B\uparrow}n_{B\downarrow}$

There are two intuitive ways how it can be achieved:

1. We can "split" every double occupancy, separating the electrons (one $\uparrow$ and one $\downarrow$) to different, previously empty sites. Such operation would not change the global magnetization of the system (the difference between the *up* and *down* electrons, $m \equiv n_\uparrow - n_\downarrow$) but it would modify the proportion of the number of the single occupied states $|\uparrow\rangle$ to the number of $|\downarrow\rangle$ states.

2. We can "erase" the double occupancies. However, such action would change the number of electrons in the system. Therefore, to restore the previous number of electrons, we can *proportionally* add *up* and *down* electrons to previously empty sites. This operation would keep the proportion of the number of single occupied states with spin *up* to those with spin *down*, but it would modify the global magnetization of the system.

Each of the presented schemes, leads to the different probability of sites to be in certain states, as it is presented in the Table II. Note, that in the first scheme, the proportion of $|\uparrow\rangle$ states is the same as "$|\uparrow\rangle$ or $|\uparrow\downarrow\rangle$" states in the Table I. In the second scheme, after erasing the doubly occupied states, the number of the electrons has changed from n to $n - n_{A\sigma}n_{A\bar\sigma}$ in the A sublattice and to $n - n_{B\sigma}n_{B\bar\sigma}$ in the B sublattice. Therefore, to restore the previous number of electron in the system, the probability that the state will have single electron σ was renormalized by the factor $n/(n-2n_{A\uparrow}n_{A\downarrow}) \equiv n/(n-2n_{B\uparrow}n_{B\downarrow})$.

Now, it is possible to derive the g_t Gutzwiller factor for the hopping term in both schemes. For the hopping to occur in the correlated state, in one site (for example belonging to the A sublattice) there need to be a single electron with the spin σ, while the neighboring site (that belongs the the B sublattice) needs to be empty (or vice versa). Therefore, by comparing the amplitudes of the bra and the ket contributions of $\langle\Psi|\hat{c}^\dagger_{i\sigma}\hat{c}_{j\sigma}|\Psi\rangle$, with the

Table II. Likelihood of a site being in the certain state (correlated case $|\Psi\rangle$). In the table, only the results for the A sublattice were shown. For the B sublattice simply $n_{B\sigma} = n_{A\bar{\sigma}}$.

state	scheme 1. ("splitting")	scheme 2. ("erasing")
$\|\uparrow\rangle$	$n_{A\uparrow} = \frac{1}{2}(n+m)$	$n_{A\uparrow}(1-n_{A\downarrow})\frac{n}{n-2n_{A\uparrow}n_{A\downarrow}}$
$\|\downarrow\rangle$	$n_{A\downarrow} = \frac{1}{2}(n-m)$	$n_{A\downarrow}(1-n_{A\uparrow})\frac{n}{n-2n_{A\uparrow}n_{A\downarrow}}$
$\|\varnothing\rangle$	$1-n_{A\uparrow}-n_{A\downarrow}$	$1-n_{A\uparrow}-n_{A\downarrow}$
$\|\uparrow\downarrow\rangle$	0	0

help of Table II, we can write that in the first scheme,

$$\langle\Psi|\hat{c}^{\dagger}_{i\sigma}\hat{c}_{j\sigma}|\Psi\rangle \overset{(1)}{=} \sqrt{n_{A\sigma}n_{B\sigma}}(1-n). \tag{B4}$$

while in the second,

$$\langle\Psi|\hat{c}^{\dagger}_{i\sigma}\hat{c}_{j\sigma}|\Psi\rangle \overset{(2)}{=} \sqrt{\frac{n_{A\sigma}(1-n_{A\bar{\sigma}})n_{B\sigma}(1-n_{B\bar{\sigma}})}{(n-2n_{A\uparrow}n_{A\downarrow})(n-2n_{B\uparrow}n_{B\downarrow})}}n(1-n). \tag{B5}$$

Analogically, we can calculate the hopping probability in the uncorrelated state. Namely, the hopping can occur when either one site has electron with the spin σ or is double occupied, and when either the neighboring site is empty or has one electron with the spin $\bar{\sigma}$ (cf. also [71]). Using Table I, we get

$$\langle\Psi_0|\hat{c}^{\dagger}_{i\sigma}\hat{c}_{j\sigma}|\Psi_0\rangle = \sqrt{n_{A\sigma}(1-n_{B\sigma})n_{B\sigma}(1-n_{A\sigma})}. \tag{B6}$$

This leads to (cf. Eq. (B3)) to either

$$g_t^{(1)} = \frac{1-n}{\sqrt{(1-n_{A\uparrow})(1-n_{B\uparrow})}}, \tag{B7}$$

or

$$g_t^{(2)} = \frac{\sqrt{\frac{(1-n_{A\bar{\sigma}})(1-n_{B\bar{\sigma}})}{(1-n_{A\sigma})(1-n_{B\sigma})}}(1-n)}{\sqrt{(1-\frac{2n_{A\uparrow}n_{A\downarrow}}{n})(1-\frac{2n_{B\uparrow}n_{B\downarrow}}{n})}}, \tag{B8}$$

depending on the scheme chosen. Note, that if only AF order is considered (no CDW), then $n_{A\uparrow} = n_{B\downarrow}$, and the last equation has simpler form,

$$g_t^{(2)} = \frac{1-n}{1-\frac{2n_{A\uparrow}n_{A\downarrow}}{n}} \equiv \frac{1-n}{1-\frac{2n_{B\uparrow}n_{B\downarrow}}{n}}. \tag{B9}$$

Both $g_t^{(1)}$ and $g_t^{(2)}$ are present in the literature, for example $g_t^{(2)}$ in [28, 40, 68, 70], whereas $g_t^{(1)}$ is identical with the zero-order renormalization factors of the DE-GWF method [55–58, 72].

Note, that if no AF order is present,

$$g_t^{(1)} = g_t^{(2)} = \frac{1-n}{1-n/2}, \tag{B10}$$

and there is no difference between $g_t^{(1)}$ and $g_t^{(2)}$ anymore (cf. also Eq. (A17) and take $d = 0$).

If instead, CDW and no AF order were considered, we would simply take in Eqs. (B7) and (B7) $n_{A\sigma} = n_A$ and $n_{B\sigma} = n_B$ such, that $n_A \neq n_B$. In such case also $g_t^{(1)} \neq g_t^{(2)}$.

The above discussion, can be easily caried out for other Gutzwiller factors, that renormalize other averages than hopping.

It was checked, that the two schemes lead to substantially different outputs, especially regarding the stability of the AF phase. In the first scheme (used in the main text of this paper) the AF phase is stable in the wide range of doping, from 0 to about $\delta_{max} = 0.27$ (cf. Fig. 3). Using the second scheme, the AF phase is stable only very close to the half-filling with $\delta_{max} < 0.006$ (cf. our previous paper [25]).

In this paper, we decided to use the first scheme, since we wanted to compare our results to those obtained within the DE-GWF approach. And, as it was mentioned, in the zeroth-order of DE-GWF method, the renormalization factors for averages are identical to those from the first scheme.

[1] E. J. W. Verwey, Nature **144**, 327 (1939).
[2] E. J. W. Verwey and P. W. Haayman, Physica **8**, 979 (1941).
[3] B. Keimer, S. A. Kivelson, M. R. Norman, S. Uchida, and J. Zaanen, Nature **518**, 179 (2015).
[4] J. M. Tranquada, B. J. Sternlieb, J. D. Axe, Y. Nakamura, and S. Uchida, Nature **375**, 561 (1995).
[5] J. P. Attfield, Solid State Sciences **8**, 861 (2006).
[6] G. Ghiringhelli, M. Le Tacon, M. Minola, S. Blanco-Canosa, C. Mazzoli, N. B. Brookes, G. M. De Luca, A. Frano, D. G. Hawthorn, F. He, T. Loew, M. M. Sala, D. C. Peets, M. Salluzzo, E. Schierle, R. Sutarto, G. A. Sawatzky, E. Weschke, B. Keimer, and L. Braicovich, Science **337**, 821 (2012).
[7] R. Comin, A. Frano, M. M. Yee, Y. Yoshida, H. Eisaki, E. Schierle, E. Weschke, R. Sutarto, F. He, A. Soumyanarayanan, Y. He, M. Le Tacon, I. S. Elfimov, J. E. Hoffman, G. A. Sawatzky, B. Keimer, and A. Damascelli,

Science **343**, 390 (2014).
[8] E. H. da Silva Neto, P. Aynajian, A. Frano, R. Comin, E. Schierle, E. Weschke, A. Gyenis, J. Wen, J. Schneeloch, Z. Xu, S. Ono, G. Gu, M. Le Tacon, and A. Yazdani, Science **343**, 393 (2014).
[9] J. Chang, E. Blackburn, A. T. Holmes, N. B. Christensen, J. Larsen, J. Mesot, R. Liang, D. A. Bonn, W. N. Hardy, A. Watenphul, M. v. Zimmermann, E. M. Forgan, and S. M. Hayden, Nature Physics **8**, 871 (2012).
[10] M. Hücker, N. B. Christensen, A. T. Holmes, E. Blackburn, E. M. Forgan, R. Liang, D. A. Bonn, W. N. Hardy, O. Gutowski, M. v. Zimmermann, S. M. Hayden, and J. Chang, Phys. Rev. B **90**, 054514 (2014).
[11] S. Blanco-Canosa, A. Frano, E. Schierle, J. Porras, T. Loew, M. Minola, M. Bluschke, E. Weschke, B. Keimer, and M. Le Tacon, Phys. Rev. B **90**, 054513 (2014).
[12] S. Gerber, H. Jang, H. Nojiri, S. Matsuzawa, H. Yasumura, D. A. Bonn, R. Liang, W. N. Hardy, Z. Islam, A. Mehta, S. Song, M. Sikorski, D. Stefanescu, Y. Feng, S. A. Kivelson, T. P. Devereaux, Z.-X. Shen, C.-C. Kao, W.-S. Lee, D. Zhu, and J.-S. Lee, Science **350**, 949 (2015).
[13] M.-H. Julien, Science **350**, 914 (2015).
[14] K. Fujita, M. H. Hamidian, S. D. Edkins, C. K. Kim, Y. Kohsaka, M. Azuma, M. Takano, H. Takagi, H. Eisaki, S.-i. Uchida, A. Allais, M. J. Lawler, E.-A. Kim, S. Sachdev, and J. C. S. Davis, Proceedings of the National Academy of Sciences **111**, E3026 (2014).
[15] E. Fradkin, S. A. Kivelson, and J. M. Tranquada, Rev. Mod. Phys. **87**, 457 (2015).
[16] A. Allais, J. Bauer, and S. Sachdev, Phys. Rev. B **90**, 155114 (2014).
[17] W. D. Wise, M. C. Boyer, E. Chatterjee, T. Kondo, T. Takeuchi, H. Ikuta, Y. Wang, and E. W. Hudson, Nature Physics **4**, 696 (2008).
[18] K. M. Shen, F. Ronning, D. H. Lu, F. Baumberger, N. J. C. Ingle, W. S. Lee, W. Meevasana, Y. Kohsaka, M. Azuma, M. Takano, H. Takagi, and Z.-X. Shen, Science **307**, 901 (2005).
[19] A. Amaricci, A. Camjayi, K. Haule, and G. Kotliar, Phys. Rev. B **82**, 155102 (2010).
[20] S. Sachdev and R. La Placa, Phys. Rev. Lett. **111**, 027202 (2013).
[21] P. Corboz, T. M. Rice, and M. Troyer, Phys. Rev. Lett. **113**, 046402 (2014).
[22] P. A. Lee, Phys. Rev. X **4**, 031017 (2014).
[23] Y. Wang, D. F. Agterberg, and A. Chubukov, Phys. Rev. Lett. **114**, 197001 (2015).
[24] W.-L. Tu and T.-K. Lee, Scientific Reports **6** (2016), 10.1038/srep18675.
[25] M. Abram, J. Kaczmarczyk, J. Jędrak, and J. Spałek, Phys. Rev. B **88**, 094502 (2013).
[26] J. Spalek, M. Zegrodnik, and J. Kaczmarczyk, arxiv:1606.03247 [cond-mat].
[27] N. Plakida, *High-Temperature Cuprate Superconductors* (Springer, 2010) chapters 5, 7.
[28] R. Eder, J. van den Brink, and G. A. Sawatzky, Phys. Rev. B **54**, R732 (1996).
[29] J. Jędrak, J. Kaczmarczyk, and J. Spałek, arxiv:1008.0021 [cond-mat].
[30] J. Jędrak and J. Spałek, Phys. Rev. B **81**, 073108 (2010).
[31] J. Jędrak and J. Spałek, Phys. Rev. B **83**, 104512 (2011).
[32] J. Kaczmarczyk and J. Spałek, Phys. Rev. B **84**, 125140 (2011).
[33] O. Howczak, J. Kaczmarczyk, and J. Spałek, Phys. Stat. Solidi (b) **250**, 609 (2013).
[34] A. P. Kądzielawa, J. Spałek, J. Kurzyk, and W. Wójcik, Eur. Phys. J. B **86**, 252 (2013).
[35] M. M. Wysokiński and J. Spałek, J. Phys.: Condens. Matter **26**, 055601 (2014).
[36] M. M. Wysokiński, M. Abram, and J. Spałek, Phys. Rev. B **90**, 081114 (2014).
[37] M. Abram, Acta Phys. Pol. A **126**, A (2014).
[38] M. M. Wysokiński, M. Abram, and J. Spałek, Phys. Rev. B **91**, 081108 (2015).
[39] M. Abram, M. M. Wysokiński, and J. Spałek, J. Magn. Magn. Mater. **400**, 27 (2016).
[40] F. C. Zhang and T. M. Rice, Phys. Rev. B **37**, 3759 (1988).
[41] F. C. Zhang, Phys. Rev. Lett. **90**, 207002 (2003).
[42] R. B. Laughlin, Phil. Mag. , 1165 (2006).
[43] N. F. Mott, Proceedings of the Physical Society. Section A **62**, 416 (1949).
[44] N. F. Mott, *Metal-Insulator Transitions* (CRC Press; 2 Sub edition, 1990).
[45] K. A. Chao, J. Spalek, and A. M. Oles, Journal of Physics C: Solid State Physics **10**, L271 (1977).
[46] K. A. Chao, J. Spałek, and A. M. Oleś, Phys. Rev. B **18**, 3453 (1978).
[47] J. Spatek and A. M. Oles, Physica B+C **86-88**, 375 (1977), (the jurnal made a a mistake in the authors names; it should be "Spałek" and "Oleś").
[48] J. Spałek, A. M. Oleś, and K. A. Chao, Phys. Status Solidi B **87**, 625 (1978).
[49] J. Spalek, A. M. Oleś, and K. A. Chao, Phys. Status Solidi B **108**, 329 (1981).
[50] J. Spalek, Acta. Phys. Pol. A **111**, 409 (2007).
[51] J. Spałek and J. M. Honig, "Metal-Insulator Transitions, Exchange Interactions, and Real Space Pairing," (Nova Science Publishers, editor A. Narlikar, Vol. 8, 1991) pp. 1–67.
[52] J. Spałek, Phys. Rev. B **37**, 533 (1988).
[53] M. C. Gutzwiller, Phys. Rev. Lett. **10**, 159 (1963).
[54] M. C. Gutzwiller, Phys. Rev. **137**, A1726 (1965).
[55] J. Bünemann, T. Schickling, and F. Gebhard, EPL (Europhysics Letters) **98**, 27006 (2012).
[56] J. Kaczmarczyk, J. Spałek, T. Schickling, and J. Bünemann, Phys. Rev. B **88**, 115127 (2013).
[57] J. Kaczmarczyk, J. Bünemann, and J. Spałek, New Journal of Physics **16**, 073018 (2014).
[58] J. Kaczmarczyk, T. Schickling, and J. Bünemann, Phys. Status Solidi B **252**, 2059 (2015).
[59] S. Tsonis, P. Kotetes, G. Varelogiannis, and P. B. Littlewood, J. Phys.: Condens. Matter **20**, 434234 (2008).
[60] A. Aperis, G. Varelogiannis, and P. B. Littlewood, Phys. Rev. Lett. **104**, 216403 (2010).
[61] For completeness, we have tested the influence of t' parameter. For $t' = 0$, while increasing the value of V, the SC dome both shrinks and moves towards $\delta = 0$. Therefore for $t' = 0$, the pure AF phase (for $V > 0$) appears on the right side of the SC dome, not on the left, as it was described in the main text (for $t' = 0.25$).
[62] G. Deutscher, A. F. Santander-Syro, and N. Bontemps, Phys. Rev. B **72**, 092504 (2005).
[63] C. Giannetti, F. Cilento, S. Dal Conte, G. Coslovich, G. Ferrini, H. Molegraaf, M. Raichle, R. Liang, H. Eisaki, M. Greven, A. Damascelli, D. van der Marel, and

F. Parmigiani, Nat. Commun. **1**, 353 (2011).
[64] H. J. A. Molegraaf, C. Presura, D. van der Marel, P. H. Kes, and M. Li, Science **295**, 2239 (2002).
[65] G. Deutscher, A. F. Santander-Syro, and N. Bontemps, Phys. Rev. B **72**, 092504 (2005).
[66] F. Carbone, A. B. Kuzmenko, H. J. A. Molegraaf, E. van Heumen, V. Lukovac, F. Marsiglio, D. van der Marel, K. Haule, G. Kotliar, H. Berger, S. Courjault, P. H. Kes, and M. Li, Phys. Rev. B **74**, 064510 (2006).
[67] C. Giannetti, F. Cilento, S. Dal Conte, G. Coslovich, G. Ferrini, H. Molegraaf, M. Raichle, R. Liang, H. Eisaki, M. Greven, A. Damascelli, D. van der Marel, and F. Parmigiani, Nat. Commun. **2**, 353 (2011).
[68] T. Ogawa, K. Kanda, and T. Matsubara, Prog. Theor. Phys. **53**, 614 (1975).
[69] D. Vollhardt, Rev. Mod. Phys. **56**, 99 (1984).
[70] M. Ogata and H. Fukuyama, Reports on Progress in Physics **71**, 036501 (2008).
[71] B. Edegger, V. N. Muthukumar, and C. Gros, Advances in Physics **56**, 927 (2007).
[72] M. M. Wysokiński, J. Kaczmarczyk, and J. Spałek, Phys. Rev. B **92**, 125135 (2015).

Article 7

Topic of this article goes beyond the scope of this Thesis. However, it is included here to show that the analytic and numerical methods I have learned during my PhD study are applicable in various contexts, not only in case of strongly correlated electronic systems.

In this work we analyze a system of hard spheroplatelets near a hard wall. The main research question was to predict the orientation of the molecules near the wall, as the transition from the isotropic to the biaxal nematic phase occurs. The main findings are that the preferred orientation of the short molecule axes is perpendicular to the wall and that the biaxality close to the wall can appear only if the phase is biaxal in the bulk.

Model of hard spheroplatelets near a hard wall

A. Kapanowski and M. Abram
Institute of Physics, Jagiellonian University, ulica Reymonta 4, 30-059 Kraków, Poland
(Received 3 July 2013; revised manuscript received 14 April 2014; published 10 June 2014)

A system of hard spheroplatelets near an impenetrable wall is studied in the low-density Onsager approximation. Spheroplatelets have optimal shape between rods and plates, and the direct transition from the isotropic to biaxial nematic phase is present. A simple local approximation for the one-particle distribution function is used. Analytical results for the surface tension and the entropy contributions are derived. The density and the order-parameter profiles near the wall are calculated. The preferred orientation of the short molecule axes is perpendicular to the wall. Biaxiality close to the wall can appear only if the phase is biaxial in the bulk.

DOI: 10.1103/PhysRevE.89.062503 PACS number(s): 61.30.Cz, 77.84.Nh

I. INTRODUCTION

Biaxial nematic phases attracting experimental, theoretical, and computer simulation research since its first prediction by Freiser [1]. There phases are characterized by an orientational order along three perpendicular directions and by the existence of three distinct optical axes. They are very interesting from both the fundamental and the technological points of view [2,3]. Biaxial materials could offer a possibility of fast switching of the second director and better viewing characteristics.

In practical applications liquid crystals are always placed in limited space and even a weak interaction with a limiting surface can change the structure of a liquid crystal near the boundary. A basic model for a phase boundary is the smooth hard planar wall. Despite its simplicity it can induce interesting phenomena.

The behavior of hard biaxial molecule fluids near a hard surface is poorly understood. In this paper we study the nematic-wall and the isotropic-wall interfaces assuming that biaxial molecules interact with one another and with the wall only via hard-core repulsion. Analytical results for the surface tension and the entropy contributions are derived. We find the preferred orientation of the phase composed of the most biaxial spheroplatelets with the optimal shape between rods and plates. For such molecules there is the direct transition from the isotropic phase to the biaxial nematic phase on increasing the density. The preferred phase orientation minimize the nematic-wall surface tension. The density and order-parameter profiles are calculated in the case of the isotropic and the biaxial nematic phase.

The paper is organized as follows. In Sec. II interfacial phenomena and biaxial molecules studies are briefly reviewed in order to provide the background for our studies. In Sec. III the statistical theory of the phase ordering is provided for the case of the hard molecules at the hard wall in the low-density limit. In Sec. IV the theory is applied to the system of hard spheroplatelets where the direct transition from the isotropic phase to the biaxial nematic phase is present in the bulk. Section V contains a summary.

II. BACKGROUND

In order to make the paper self-contained, we collect the relevant definitions and facts concerning interfacial phenomena and biaxial molecule studies.

A. Fluid interfacial phenomena

There are many fluid interfacial phenomena, such as anchoring, critical adsorption, prewetting, and wetting transitions [4]. The possible structural rearrangements in the vicinity of the interface are (1) periodic modulations of density, (2) polar ordering of molecular dipoles, and (3) modifications of the scalar order parameter [5]. Anchoring is a fixing of the phase orientation by the surface with lifting the orientation in the bulk via the elastic forces. In confined geometry, phase transitions are usually shifted with respect to the transitions observed in infinite geometry.

Let us consider the case of a second-order transition from a disordered to an ordered phase. The order parameter fluctuations appear in the bulk with a correlation length which diverges at the transition. The correlation length at the surface becomes infinite in a direction parallel to the surface plane. This creates an ordered layer at the surface in which the order parameter decreases exponentially to zero in the bulk over a penetration length. The penetration length is equal to the correlation length and thus diverges at the transition. This phenomenon is called critical adsorption [4].

When the transition is first order, the situation is more complex. Partial or complete wetting can appear depending on the values of a contact angle. When one explores the coexistence curve between phases, one can go from a partial wetting regime to a complete wetting regime via a wetting transition.

B. Studies of hard biaxial molecules

Computer simulations studies of anisotropic hard molecules have confirmed that hard-core interactions are essential for liquid crystal phase behavior [6]. Over the years a variety of hard-particle models have been studied theoretically and by using computer simulations. These investigations have shown that hard-particle fluids can exhibit many liquid-crystalline phases, such as uniaxial and biaxial nematic [7], smectic, crystal, and plastic solid phases [8,9].

Several types of biaxial molecule fluids were investigated: ellipsoids with three different axes [7,10–13], biaxial Gay-Berne particles [14–18], rectangular parallelepipeds [19,20], spheroplatelets, and spherocuboids [21]. Singh and Kumar developed a theory with a general convex-body coordinate system that can be used to describe any hard convex body [22,23]. The results can be utilized in the study of

structural, thermodynamic, and transport properties of ellipsoidal fluids.

The hard spheroplatelet is a natural generalization of the spherocylinder. In 1986 Mulder expressed the pair-excluded volume at fixed orientation in closed form [24]. Later the phase diagram of the hard spheroplatelet fluid was proposed as a result of bifurcation analysis in the low-density Onsager approximation [25]. The density versus particle biaxiality phase diagram displays a cusp-shaped biaxial nematic phase intervening between two uniaxial nematic phases. Holyst and Poniewierski studied the Landau bicritical point at which a direct transition from the isotropic phase to the biaxial nematic phase occurs [26]. A dense system of hard biaxial molecules (spheroplatelets and ellipsoids) was considered using a density functional theory. They found that the density of the isotropic phase at the Landau bicritical point was always higher than that at the isotropic-nematic transition in the limit of uniaxial molecules.

In 1991 Taylor extended the pair-excluded volume to the case of nonidentical spheroplatelets [27]. In the same year Taylor and Herzfeld studied nematic and smectic order in a fluid of hard biaxial spheroplatelets [28]. They used scaled particle theory for the fluid configurational entropy, in conjunction with a cell description of translational order. When the possibility of translational order was considered, the phase diagram displayed three distinct smectic A phases, columnar and crystalline ordering for higher densities (packing greater then 0.6). For low and intermediate densities the diagram was identical with previous findings (the isotropic phase, the two uniaxial nematic phases separated by the biaxial nematic phase). The necessity of further studies of the Landau point region was noted.

In 2009 van der Pol *et al.* found biaxial nematic and biaxial smectic phases in a colloidal model system of mineral goethite particles with a simple boardlike shape and short-range repulsive interaction [29]. The biaxial nematic phase was stable over a large concentration range, and the uniaxial nematic phase was not found. Other studies showed that shape polidispersity of particles can stabilize the biaxial nematic phase, and it can induce a novel topology in the phase diagram [30,31]. Another stabilizing factor is a small tetrahedral deformation of particles as was shown within the extended Straley model [32].

Recently Peroukidis *et al.* calculated the full phase diagram of hard biaxial spheroplatelets by means of Monte Carlo simulations [33,34]. New classes of phase sequences were identified: $I - [N_+] - \text{Sm-}A$, $I - [N_{b-} - N_{b+}] - \text{Sm-}A$ (crossover), $I - [N_-] - \text{Sm-}A$, $I - [N_-] - \text{Col}_x$ (columnar phases), $I - \text{Cub}$ (cubatic phases). The brackets indicate phases that may be absent. The most interesting finding was the crossover between two distinct biaxial nematic states. The formation of anisotropic supramolecular assemblies was demonstrated.

C. Hard molecules at the interface

Properties of liquid crystal phases in the bulk and at the surface generally are not the same. Different physical systems were studied in the past: fluids with uniaxial molecules in contact with a single (hard or attractive) wall, confined by two walls (thin cells) or curved surfaces [35]. Let us recall the main results concerning solid-fluid interfaces. We will not discuss nematic free surfaces and thin films.

In 1984 Telo da Gama studied wetting transitions at a solid-fluid interface using attractive walls and the attractive forces with a hard core for molecular interactions [36]. The wetting transitions were always weakly first order. In 1988 Poniewierski and Holyst studied a system of hard spherocylinders in contact with a single hard wall [37]. They used a simple local approximation for the one-particle distribution function and showed that the preferred orientation of the nematic director is parallel to the wall. The density and order-parameter profiles were calculated. The nematic main order parameter was enhanced near the wall even though the density was reduced. The wall-induced biaxiality was small in the interfacial region. Wetting by the nematic phase occurred at the nematic-isotropic coexistence. Later the stability of the uniaxial solution close to the wall was investigated in the limit of very long molecules [38], and the bifurcation point was found. The nematic-phase–isotropic-phase interface for hard spherocylinders was studied in Ref. [39].

A hard-rod fluid confined by two parallel wall was studied by Mao *et al.* [40]. The aim of this work was to calculate the depletion force between the plates due to confinement of the rods. Van Roij *et al.* investigated the phase behavior of colloidal hard-rod fluids ($L/D = 15$) near a single wall and confined in a slit pore [41–44]. They obtained (1) a wall-induced surface transition from uniaxial to biaxial symmetry, (2) complete orientational wetting of the wall-isotropic fluid interface by a nematic film, and (3) capillary nematization, with a capillary critical point, induced by confinement in the slit pore.

The properties of a model suspension of hard colloidal platelets with continuous orientations and vanishing thickness were studied using several methods by Reich *et al.* [45]. It is interesting that this system is not described well by the Onsager theory, and a scaling argument known from thin rods does not hold. The fundamental measure theory density functional was used, which includes contributions to the free energy that are of the third order in density.

III. THEORY

The aim of this section is to develop the statistical theory of the phase ordering for the case of the hard molecules at the hard wall in the low-density limit. The expressions for the density, the order parameters, and the surface tension will be derived.

A. Description of the system

The system of hard spheroplatelets in the presence of a hard wall is considered. A spheroplatelet can be described as a rectangular block with dimensions $2a \times b \times c$, capped with quarter spheres of radius a and half-cylinders with radius a and lengths b and c such as to produce a piecewise smooth convex body; see Fig. 1. The position and the orientation of a spheroplatelet are determined by $\vec{r}$ and the three Euler angles $R = (\phi,\theta,\psi)$, respectively. Alternatively, the orientation can be described by the three orthonormal vectors $(\vec{l},\vec{m},\vec{n})$. The z

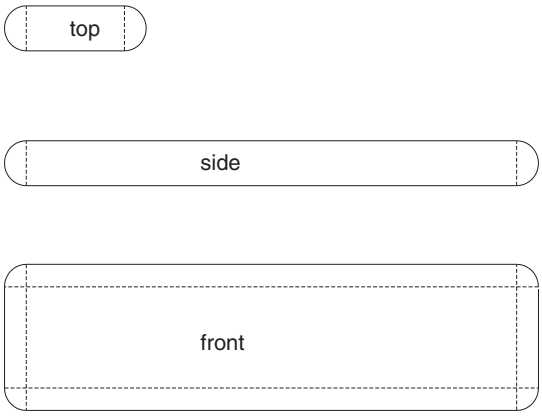

FIG. 1. Front, side, and top view of a spheroplatelet.

axis is chosen to be perpendicular to the wall. The density of the fluid at $z = +\infty$ is ρ_0.

The grand thermodynamical potential Ω as a functional of the one-particle distribution function $\rho(\vec{r},R)$ has the following form:

$$\beta\Omega\{\rho\} = \beta F_{\rm id}\{\rho\} + \beta F_{\rm ex}\{\rho\} + \beta \int d\vec{r}\, dR \rho(\vec{r},R)[V_{\rm ext}(\vec{r},R) - \mu], \quad (1)$$

where the ideal gas contribution is

$$\beta F_{\rm id}\{\rho\} = \int d\vec{r}\, dR \rho(\vec{r},R)\{\ln[\Lambda\rho(\vec{r},R)] - 1\}, \quad (2)$$

μ is the chemical potential, $\beta = 1/k_BT$ is the Boltzmann factor, $V_{\rm ext}$ stands for the external potential, and Λ is the (irrelevant) thermal volume of molecules. $F_{\rm ex}$ is the excess part of the free energy corresponding to the interactions between molecules. We assume the low-density Onsager approximation for $F_{\rm ex}$, i.e.,

$$\beta F_{\rm ex} = -\frac{1}{2}\int d\vec{r}_1\, dR_1\, d\vec{r}_2\, dR_2 \rho(\vec{r}_1,R_1)\rho(\vec{r}_2,R_2) f_{12}, \quad (3)$$

where f_{12} stands for the Mayer function, which is equal to -1 when two molecules overlap and 0 otherwise. The one-particle distribution function has the normalization

$$\int d\vec{r}\, dR \rho(\vec{r},R) = N. \quad (4)$$

The expression for the external potential exerted on a molecule by the hard wall reads as follows:

$$V_{\rm ext}(z,R) = \begin{cases} +\infty & \text{for} \quad z < z_m(R), \\ 0 & \text{for} \quad z > z_m(R), \end{cases} \quad (5)$$

where $z_m(R) = a + (b|m_z| + c|n_z|)/2$ stands for the minimal distance between the wall and a molecule of orientation R. The minimization of $\Omega\{\rho\}$ with respect to $\rho(\vec{r},R)$ leads to the integral equation for $\rho(\vec{r},R)$:

$$\ln[\Lambda\rho(\vec{r}_1,R_1)] + \beta V_{\rm ext}(\vec{r}_1,R_1) - \int d\vec{r}_2\, dR_2 \rho(\vec{r}_2,R_2) f_{12} = \beta\mu. \quad (6)$$

In the absence of an external potential Eq. (6) has a spatially uniform solution $\rho(\vec{r}_1,R_1) = \rho_0 f(R)$, where $f(R)$ is the orientational distribution function normalized to unity. For the isotropic phase $f(R) = 1/8\pi^2$, for the uniaxial nematic phase $f(R) = f(\vec{l}\cdot\vec{N},\vec{n}\cdot\vec{N})$, and for the biaxial nematic phase $f(R) = f(\vec{l}\cdot\vec{L},\vec{l}\cdot\vec{N},\vec{n}\cdot\vec{L},\vec{n}\cdot\vec{N})$. The unit orthogonal vectors $(\vec{L},\vec{M},\vec{N})$ determine three axes of the D_{2h} symmetry of the biaxial nematic phase. In the uniaxial nematic phase with $D_{\infty h}$ symmetry only the $\vec{N}$ vector survives.

B. The liquid crystal-wall surface tension

When the wall is present, instead of solving Eq. (6), we approximate $\rho(z,R)$ as follows [37]:

$$\rho(z,R) = \rho_0 f(R)\exp[-\beta V_{\rm ext}(z,R)]. \quad (7)$$

Let us note that the density profiles obtained from (7) will not exhibit the short-range oscillatory behavior that is expected close to the wall. It is assumed that the directors $(\vec{L},\vec{M},\vec{N})$ do not change throughout the sample. Substitution of (7) into (1) and subtraction of the bulk term leads to the expression for the liquid crystal-wall surface tension γ [37],

$$\beta\gamma = -(S_{\rm rot} + S_{\rm tr,id} + S_{\rm tr,ex})/k_B - \beta\Delta\mu\Gamma, \quad (8)$$

where $S_{\rm rot}$, $S_{\rm tr,id}$, and $S_{\rm tr,ex}$ are the surface entropies per unit area,

$$\beta\Delta\mu = \beta\mu - \ln[\Lambda\rho_0/(8\pi^2)]; \quad (9)$$

$$\Gamma = \int_0^\infty dz\, dR[\rho(z,R) - \rho_0 f(R)] = -\rho_0 \int dR f(R) z_m(R) \quad (10)$$

stands for the adsorption [37]. The rotational entropy $S_{\rm rot}$ comes only from the ideal term in the free energy. According to the usual convention, the rotational entropy is defined in such a way that it vanishes for the isotropic phase

$$S_{\rm rot}/k_B = \rho_0 \int dR f(R) z_m(R) \ln[8\pi^2 f(R)]. \quad (11)$$

The translational entropy have two contributions: $S_{\rm tr,id}$ from the ideal term and $S_{\rm tr,ex}$ from the excess term:

$$S_{\rm tr,id}/k_B = -\rho_0 \int dR f(R) z_m(R), \quad (12)$$

$$S_{\rm tr,ex}/k_B = \frac{1}{2}\rho_0^2 \int dR_1\, dR_2 f(R_1) f(R_2) z_m(R_1) K(R_1,R_2) + \frac{1}{2}\rho_0^2 \int dR_1\, dR_2 f(R_1) f(R_2) L(R_1,R_2), \quad (13)$$

where

$$L(R_1,R_2)=\int_{z_m(R_1)-z_m(R_2)}^{\infty} dz_{12}\times[z_{12}-z_m(R_1)+z_m(R_2)]V(|z_{12}|,R_1,R_2), \quad (14)$$

$$V(|z_{12}|,R_1,R_2)=-\int dx_{12}\,dy_{12}\,f_{12}, \quad (15)$$

$$K(R_1,R_2)=-\int dr_{12}\,f_{12}. \quad (16)$$

$K(R_1,R_2)$ is the excluded volume for two spheroplatelets. $V(|z_{12}|,R_1,R_2)$ is the intersection of the excluded volume for two spheroplatelets of orientations R_1 and R_2 with a plane parallel to the wall and distant from the center of the excluded volume by $|z_{12}|$. The entropy $S_{\mathrm{tr,id}}$ is negative because the wall restricts the translational freedom of molecules. The first (positive) term in $S_{\mathrm{tr,ex}}$ takes into account the pairs of molecules, one of which interacts directly with the wall whereas the other does not. The second (positive) term takes into account all pairs in which both molecules interact directly with the wall [37].

The nematic-wall surface tension γ is a function of directors through the distribution function $f(R)$. The tension should be minimized with respect to the phase orientation in order to find the equilibrium value of the phase orientation.

C. The density and the order parameter profiles

In the approximation (7) for the one-particle distribution function $\rho(z,R)$, the thickness of the interfacial region is equal to the range of V_{ext}. Outside, the density and the order parameters are equal to their bulk values. Thus only the range $a\leqslant z\leqslant a+\sqrt{b^2+c^2}/2$ is interesting. For $z<a$, $\rho(z)=0$ and the order parameters are undefined. Integrating $\rho(z,R)$ over the angular variables, we find that

$$\rho(z)=\rho_0\int dR f(R)\exp[-\beta V_{\mathrm{ext}}(z,R)]. \quad (17)$$

The orientational distribution function is equal to $f(z,R)=\rho(z,R)/\rho(z)$ in the interfacial region. The average of any function $A(R)$ can be calculated as

$$\langle A\rangle(z)=\int dR f(z,R)A(R). \quad (18)$$

The formula (18) will be used to calculate the order parameters.

IV. RESULTS

The spheroplatelets are useful objects because many calculations can be done analytically. In this section the most important results from the literature are recalled and an exemplary calculations for the spheroplatelets at the hard wall are presented.

A. Spheroplatelets

The volume of a spheroplatelet is equal to

$$V_{\mathrm{mol}}=4\pi a^3/3+\pi a^2(b+c)+2abc. \quad (19)$$

The pair-excluded volume is given by [25]

$$\begin{aligned}K(R_1,R_2)=&\,32\pi a^3/3+8\pi a^2(b+c)+8abc\\&+4abc\{|\vec{m}_1\times\vec{n}_2|+|\vec{n}_1\times\vec{m}_2|\}\\&+4ab^2|\vec{m}_1\times\vec{m}_2|+4ac^2|\vec{n}_1\times\vec{n}_2|\\&+b^2c\{|\vec{l}_1\cdot\vec{m}_2|+|\vec{m}_1\cdot\vec{l}_2|\}\\&+bc^2\{|\vec{l}_1\cdot\vec{n}_2|+|\vec{n}_1\cdot\vec{l}_2|\}.\end{aligned} \quad (20)$$

The expansion of the excluded volume $K(R_1,R_2)$ can be given as

$$\begin{aligned}K(R_1,R_2)&=\sum_j\sum_{\mu\nu}K^{(j)}_{\mu\nu}F^{(j)}_{\mu\nu}\left(R_2^{-1}R_1\right)\\&=\sum_{[I]}K^{[I]}F^{[I]}\left(R_2^{-1}R_1\right),\end{aligned} \quad (21)$$

where the coefficients $K^{(j)}_{\mu\nu}$ are symmetric in the indices μ and ν due to the particle interchange symmetry. The invariants $F^{(j)}_{\mu\nu}=F^{[I]}$ are defined in Ref. [46], where the indicator $[I]=(j,\mu,\nu)$ is explained. First indices are $[1]=(0,0,0)$, $[2]=(2,0,0)$, $[3]=(2,0,2)$, $[4]=(2,2,0)$, and $[5]=(2,2,2)$. The invariants are related to Wigner functions $D^{(j)}_{\mu\nu}$. If j is even, then $0\leqslant\mu,\nu\leqslant j$,

$$F^{(j)}_{00}(R)=D^{(j)}_{00}(R), \quad (22)$$

$$F^{(j)}_{0\nu}(R)=\frac{1}{\sqrt{2}}\left[D^{(j)}_{0\nu}(R)+D^{(j)}_{0-\nu}(R)\right], \quad (23)$$

$$F^{(j)}_{\mu 0}(R)=\frac{1}{\sqrt{2}}\left[D^{(j)}_{\mu 0}(R)+D^{(j)}_{-\mu 0}(R)\right], \quad (24)$$

$$\begin{aligned}F^{(j)}_{\mu\nu}(R)=&\,\tfrac{1}{2}\left[D^{(j)}_{\mu\nu}(R)+D^{(j)}_{\mu-\nu}(R)\right.\\&\left.+D^{(j)}_{-\mu\nu}(R)+D^{(j)}_{-\mu-\nu}(R)\right].\end{aligned} \quad (25)$$

If j is odd, then $2\leqslant\mu,\nu\leqslant j$,

$$\begin{aligned}F^{(j)}_{\mu\nu}(R)=&\,\tfrac{1}{2}\left[D^{(j)}_{\mu\nu}(R)-D^{(j)}_{\mu-\nu}(R)\right.\\&\left.-D^{(j)}_{-\mu\nu}(R)+D^{(j)}_{-\mu-\nu}(R)\right].\end{aligned} \quad (26)$$

The most important excluded volume coefficients have the form

$$\begin{aligned}K^{(0)}_{00}=&\,32\pi a^3/3+8\pi a^2(b+c)+(8+2\pi)abc\\&+\pi a(b^2+c^2)+b^2c+bc^2,\end{aligned} \quad (27)$$

$$K^{(2)}_{00}=(5/16)(b^2c-2bc^2+2\pi abc-2\pi ac^2-\pi ab^2/2), \quad (28)$$

$$K^{(2)}_{02}=K^{(2)}_{20}=(5\sqrt{3}/16)(bc^2+\pi abc-\pi ab^2/2), \quad (29)$$

$$K^{(2)}_{22}=(-15/16)(b^2c+\pi ab^2/2). \quad (30)$$

For molecules intermediate between rods and plates, called the most biaxial molecules, the direct transition from the isotropic to the biaxial nematic phase is present. In that case

$K_{02}^{(2)} = K_{20}^{(2)} = 0$, $K_{00}^{(2)} > 0$, $K_{22}^{(2)} < 0$, and

$$c^2 + \pi ac - \pi ab/2 = 0 \quad \text{for} \quad b > c. \tag{31}$$

From the analysis of isotropic-symmetry-breaking bifurcations [25] it is possible to find the transition point from the isotropic phase to the biaxial nematic phase

$$\rho_C = -5/K_{22}^{(2)} \quad \text{for} \quad b > c. \tag{32}$$

We will study physically equivalent systems with $b < c$ because then it is easier to discuss the values of the order parameters. The condition for the most biaxial molecules has the form

$$b^2 + \pi ab - \pi ac/2 = 0 \quad \text{for} \quad b < c. \tag{33}$$

Let us define packing $y = \rho V_{\text{mol}}$. We studied two systems with $b < c$ in order to check that our results do not depend qualitatively on the molecule elongations (this is important in the context of the Onsager approximation):

$$b = 1.5\pi a, \quad c = 7.5\pi a, \quad y_C = 0.48174 \text{ (system A)}, \tag{34}$$

$$b = 2\pi a, \quad c = 12\pi a, \quad y_C = 0.29437 \text{ (system B)}. \tag{35}$$

This choice corresponds to the following sets of parameters from Ref. [33]: $(l^*, w^*) \approx (12.78, 3.36)$ for system A; $(l^*, w^*) \approx (19.85, 4.14)$ for system B.

B. The phase in the bulk

The phase in the bulk is described by a spatially uniform solution of the form

$$\ln f(R) = \sum_j \sum_{\mu\nu} S_{\mu\nu}^{(j)} F_{\mu\nu}^{(j)}(R), \tag{36}$$

$$S_{\mu\nu}^{(j)} = -\rho_0 \sum_\sigma K_{\sigma\nu}^{(j)} \langle F_{\mu\sigma}^{(j)} \rangle \quad \text{for} \quad j > 0, \tag{37}$$

$$\langle F_{00}^{(0)} \rangle = 1 \text{ (the normalization condition)}. \tag{38}$$

According to Mulder [25] and others [47], we can focus on the $j = 2$ subspace with four independent parameters $S_{\mu\nu}^{(2)}$,

$$f \sim \exp(S^{[2]} F^{[2]} + S^{[3]} F^{[3]} + S^{[4]} F^{[4]} + S^{[5]} F^{[5]}). \tag{39}$$

The solution of Eq. (37) should have the orientation minimizing the surface tension γ. Equation (37) was solved numerically for systems A and B by means of the C program. Multidimensional minimization was done by the downhill simplex method, implemented in the function *amoeba* [48]. The dependence of the order parameters on the packing are presented in Fig. 2 (system A) and in Fig. 3 (system B).

Let us recall the meaning of the order parameters $\langle F_{\mu\nu}^{(2)} \rangle$. The $\langle F_{00}^{(2)} \rangle$ order parameter is a measure of the alignment of the $\vec{n}$ molecule axis along the Z axis of the reference frame. The $\langle F_{02}^{(2)} \rangle$ order parameter describes the relative distribution of the $\vec{l}$ and the $\vec{m}$ axes along the Z axis. Both $\langle F_{00}^{(2)} \rangle$ and $\langle F_{02}^{(2)} \rangle$ can be nonzero in the uniaxial nematic phase. The $\langle F_{20}^{(2)} \rangle$ order parameter describes the relative distribution of the $\vec{n}$ axis along the X and the Y axes. The $\langle F_{22}^{(2)} \rangle$ order parameter is related to the distribution of the $\vec{l}$ axis along the X axis and the distribution of the $\vec{m}$ axis along the Y axis.

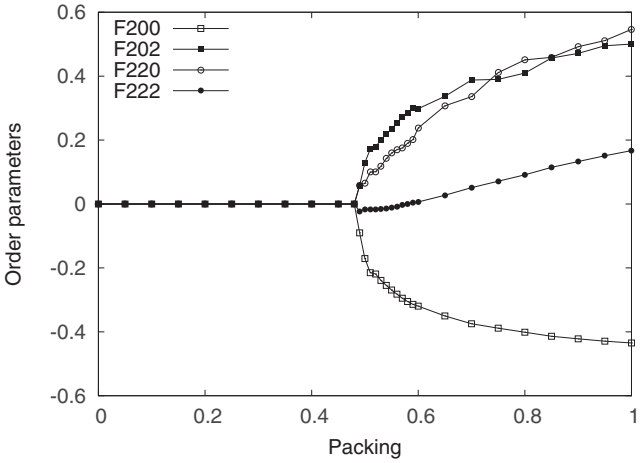

FIG. 2. Order parameters $\langle F_{\mu\nu}^{(2)} \rangle$ ($F2\mu\nu$ in the picture) vs packing in the bulk for system A. The phase orientation for $y > y_C$ is described by the vectors $(\vec{L}, \vec{M}, \vec{N}) = (\vec{e}_z, -\vec{e}_y, \vec{e}_x)$. This is the solution minimizing the surface tension.

C. Isotropic phase in the bulk

The system is in the isotropic phase ($S_{\mu\nu}^{(j)} = 0$) for $\rho < \rho_C$. Near the wall the order parameter $\langle F_{00}^{(2)} \rangle$ decreases from 0 to $-1/2$, whereas the order parameter $\langle F_{02}^{(2)} \rangle$ increases from 0 to $\sqrt{3}/2$. The long molecule axes $\vec{n}$ tend to be parallel to the wall, and the short molecule axes $\vec{l}$ tend to be perpendicular to the wall. The symmetry in the xy plane is not broken, and the phase is uniaxial. In the interfacial region the density is reduced and decreases to zero as $z \to a$. The density and the order parameters profiles for system A are plotted in Fig. 4. In the case of system B the results are similar. The same profiles for the uniaxial order parameter $\langle F_{00}^{(2)} \rangle$ were obtained in the case of hard spherocylinders by means of Monte Carlo simulations

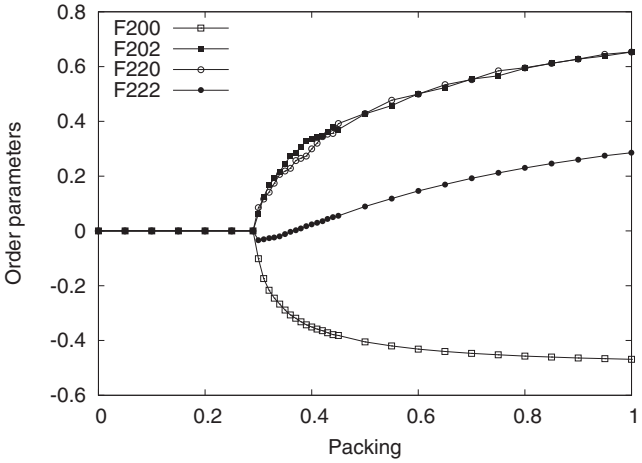

FIG. 3. Order parameters $\langle F_{\mu\nu}^{(2)} \rangle$ ($F2\mu\nu$ in the picture) vs packing in the bulk for system B. The phase orientation is the same as in Fig. 2.

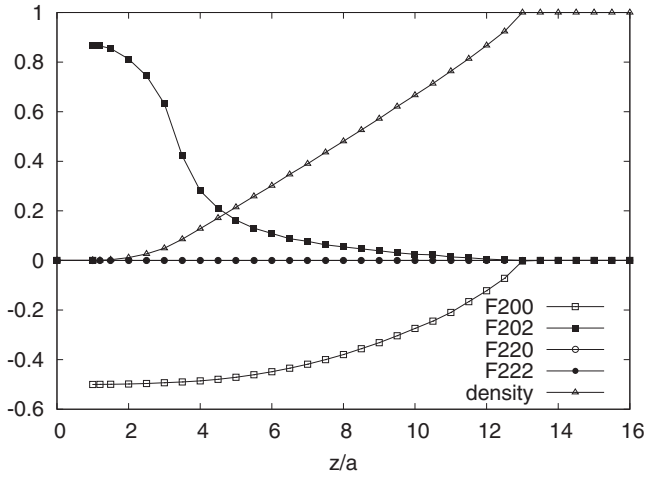

FIG. 4. Density profile $\rho(z)/\rho_0$ and order parameters $\langle F^{(2)}_{\mu\nu}\rangle$ ($F2\mu\nu$ in the picture) for the isotropic phase in the bulk (system A). In the interfacial region the phase is uniaxial, $\langle F^{(2)}_{20}\rangle = \langle F^{(2)}_{22}\rangle = 0$. The density decreases to zero near the wall. The molecule positions are in the range $z > a$.

[43]. We have the additional nonzero order parameter $\langle F^{(2)}_{02}\rangle$ indicating that our particles are biaxial. The density profiles of a hard-spherocylinder fluid suggest that a small kink (a density maximum) at $z = a + c/2$ is possible for the spheroplatelets.

The surface tension for the isotropic phase is positive and has the form

$$\beta\gamma = \rho_0(a + b/4 + c/4) + \tfrac{1}{2}\rho_0^2[K^{[1]}(a + b/4 + c/4) - L^{[1][1]}]. \quad (40)$$

The relation between μ and ρ_0 in our model, for the case of the isotropic phase and the weak biaxial nematic phase, is

$$\beta\Delta\mu = \rho_0 K^{[1]} > 0. \quad (41)$$

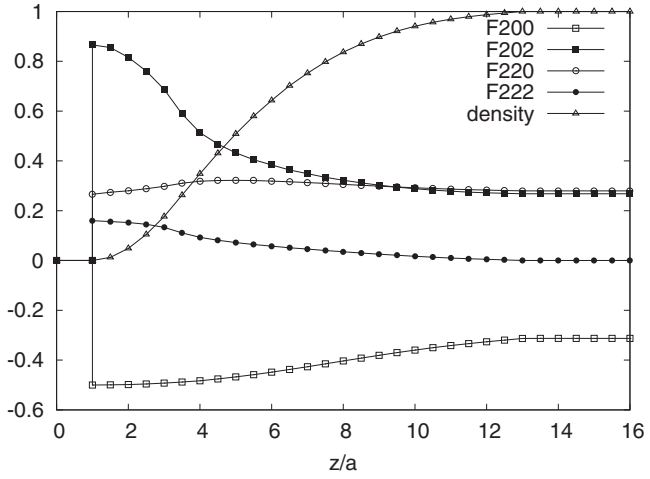

FIG. 5. Density profile $\rho(z)/\rho_0$ and order parameters $\langle F^{(2)}_{\mu\nu}\rangle$ ($F2\mu\nu$ in the picture) for the biaxial nematic phase in the bulk at packing $y = 0.6$ (system A). In the interfacial region the phase is biaxial. The density decreases to zero near the wall. The phase orientation is $(\vec{L},\vec{M},\vec{N}) = (\vec{e}_z, -\vec{e}_y, \vec{e}_x)$.

D. Weak biaxial nematic phase

Let us consider a weak biaxial nematic phase near the transition point from the isotropic to the biaxial nematic phase:

$$S^{(j)}_{\mu\nu} \ll 1 \text{ for } j > 0, \quad S^{(0)}_{00} = -\ln(8\pi^2). \quad (42)$$

The orientational distribution function $f(R)$ and the order parameters have a simplified form

$$f(R) = \frac{1}{8\pi^2}\left[1 + \sum_{j>0} S^{(j)}_{\mu\nu} F^{(j)}_{\mu\nu}(R)\right], \quad (43)$$

$$\langle F^{(j)}_{\mu\nu}\rangle = \frac{S^{(j)}_{\mu\nu}}{2j+1}. \quad (44)$$

For the case of the weak biaxial nematic phase, it is possible to calculate many physical quantities analytically.

E. Alignment close to the wall

Disregarding the problem of the equilibrium phase orientation we can study the alignment close to the wall ($z = a$) in the case of the weak biaxial nematic phase in the bulk. The restrictions imposed on the Euler angles are as follows: $\theta = \pi/2$, $\psi = 0$ or $\psi = \pi$, or $\psi = 2\pi$. We assume that the most important are the parameters $S^{(2)}_{\mu\nu}$ and the order parameters $\langle F^{(2)}_{\mu\nu}\rangle$:

$$F^{(2)}_{00}(R)|_{\text{wall}} = -1/2, \quad (45)$$

$$F^{(2)}_{02}(R)|_{\text{wall}} = \sqrt{3}/2, \quad (46)$$

$$F^{(2)}_{20}(R)|_{\text{wall}} = \cos(2\phi)\sqrt{3}/2, \quad (47)$$

$$F^{(2)}_{22}(R)|_{\text{wall}} = \cos(2\phi)/2. \quad (48)$$

$$f(a,\phi) = \frac{1}{2\pi}\left[1 + \sum_{\mu\nu} S^{(2)}_{\mu\nu} F^{(2)}_{\mu\nu}(R)|_{\text{wall}}\right], \quad (49)$$

$$\left\langle F^{(2)}_{\mu\nu}\right\rangle\Big|_{\text{wall}} = \int_0^{2\pi} d\phi f(a,\phi) F^{(2)}_{\mu\nu}(R)|_{\text{wall}}, \quad (50)$$

$$\left\langle F^{(2)}_{00}\right\rangle\Big|_{\text{wall}} = -1/2, \quad (51)$$

$$\left\langle F^{(2)}_{02}\right\rangle\Big|_{\text{wall}} = \sqrt{3}/2, \quad (52)$$

$$\left\langle F^{(2)}_{20}\right\rangle\Big|_{\text{wall}} = \left[S^{(2)}_{20}\sqrt{3} + S^{(2)}_{22}\right]\sqrt{3}\pi/4, \quad (53)$$

$$\left\langle F^{(2)}_{22}\right\rangle\Big|_{\text{wall}} = \left[S^{(2)}_{20}\sqrt{3} + S^{(2)}_{22}\right]\pi/4. \quad (54)$$

The order parameters close to the wall can be expressed by the bulk order parameters by means of Eq. (44):

$$\left\langle F^{(2)}_{20}\right\rangle\Big|_{\text{wall}} = \left[\left\langle F^{(2)}_{20}\right\rangle\sqrt{3} + \left\langle F^{(2)}_{22}\right\rangle\right]5\sqrt{3}\pi/4, \quad (55)$$

$$\left\langle F^{(2)}_{22}\right\rangle\Big|_{\text{wall}} = \left[\left\langle F^{(2)}_{20}\right\rangle\sqrt{3} + \left\langle F^{(2)}_{22}\right\rangle\right]5\pi/4. \quad (56)$$

We conclude that biaxiality close to the wall can appear only if the phase is biaxial in the bulk. Note that the equality $\langle F_{20}^{(2)}\rangle|_{\text{wall}} = \sqrt{3}\langle F_{22}^{(2)}\rangle|_{\text{wall}}$ is valid also for the strong biaxial nematic phase.

F. Alignment in the interfacial region

The weak biaxial phase is now considered. It is possible to calculate almost all parts of the surface tension analytically:

$$\Gamma = -\rho_0[(a + b/4 + c/4) + S^{[2]}(-b/32 + c/16) + S^{[3]}(-\sqrt{3}b/32)], \tag{57}$$

$$\begin{aligned} S_{\text{rot}}/(\rho_0 k_B) = {} & S^{[2]}(-b/32 + c/16) + S^{[3]}(-\sqrt{3}b/32) \\ & + S^{[2]}S^{[2]}(a/5 + 5b/128 + c/16) \\ & + S^{[2]}S^{[3]}(\sqrt{3}b/64) \\ & + S^{[3]}S^{[3]}(a/5 + 7b/128 + c/32) \\ & + S^{[4]}S^{[4]}(a/5 + 15b/256 + c/32) \\ & + S^{[4]}S^{[5]}(-7\sqrt{3}b/384) \\ & + S^{[5]}S^{[5]}(a/5 + 31b/768 + 13c/24), \end{aligned} \tag{58}$$

$$S_{\text{tr,id}}/k_B = \Gamma, \tag{59}$$

$$A_{\mu\sigma}^{(j)} = \frac{1}{2j+1}\sum_{\nu} S_{\mu\nu}^{(j)} K_{\sigma\nu}^{(j)}, \tag{60}$$

$$L^{[I][J]} = \int dR_1\, dR_2 \frac{1}{(8\pi^2)^2} F^{[I]}(R_1) F^{[J]}(R_2) L(R_1, R_2), \tag{61}$$

$$\begin{aligned} 2S_{\text{tr,ex}}/\left(\rho_0^2 k_B\right) = {} & K^{[1]}(a + b/4 + c/4) \\ & + A^{[2]}(-b/32 + c/16) + A^{[3]}(-b\sqrt{3}/32) \\ & + K^{[1]}S^{[2]}(-b/32 + c/16) \\ & + K^{[1]}S^{[3]}(-b\sqrt{3}/32) \\ & + S^{[2]}A^{[2]}(a/5 + 5b/128 + c/16) \\ & + \left(S^{[2]}A^{[3]} + S^{[3]}A^{[2]}\right)(b\sqrt{3}/128) \\ & + S^{[3]}A^{[3]}(a/5 + 7b/128 + c/32) \\ & + S^{[4]}A^{[4]}(a/5 + 15b/256 + c/32) \\ & + \left(S^{[4]}A^{[5]} + S^{[5]}A^{[4]}\right)(-7\sqrt{3}b/768) \\ & + S^{[5]}A^{[5]}(a/5 + 31b/768 + 13c/24) \\ & + L^{[1][1]} + \sum_{[I]=2}^{5} S^{[I]}\left(L^{[1][I]} + L^{[I][1]}\right) \\ & + \sum_{[I]=2}^{5}\sum_{[J]=2}^{5} S^{[I]}S^{[J]}L^{[I][J]}. \end{aligned} \tag{62}$$

TABLE I. Table reporting the values of the coefficients $L^{[I][J]}$ in a^4 units for system A. Errors estimated are less then 10% . The dagger symbol (†) points to values that probably go to zero (according to our tests).

$L^{[I][J]}/a^4$	$[J]=[1]$	$[J]=[2]$	$[J]=[3]$	$[J]=[4]$	$[J]=[5]$
$[I]=[1]$	26 209	7294	−112	5.16†	−4.97†
$[I]=[2]$	−3415	−1027	214	−0.247†	0.256†
$[I]=[3]$	1211	415	−84.4	0.061†	0.214†
$[I]=[4]$	11.4†	3.68†	−0.622†	−213	355
$[I]=[5]$	−3.16†	−0.921†	0.154†	85.5	−94.0

TABLE II. Table reporting the values of the coefficients $L^{[I][J]}$ in a^4 units for system B. Errors estimated are less then 10% . The dagger symbol (†) points to values that probably go to zero (according to our tests).

$L^{[I][J]}/a^4$	$[J]=[1]$	$[J]=[2]$	$[J]=[3]$	$[J]=[4]$	$[J]=[5]$
$[I]=[1]$	110 826	32 921	−4264	14.5†	−13.9†
$[I]=[2]$	−15 975	−5075	960	−0.317†	0.002†
$[I]=[3]$	5355	2149	−370	−0.094†	−0.996†
$[I]=[4]$	36.0†	13.2†	−1.4†	−1026	1911
$[I]=[5]$	−5.63†	−2.55†	0.02†	432	−456

Let us note that in the case of hard ellipsoids the hard Gaussian overlap (HGO) model [15,49] is often used, because it is computationally simple and shares some similarities with

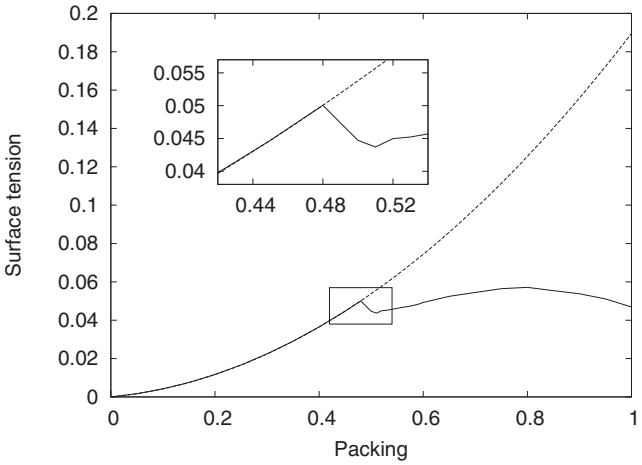

FIG. 6. Surface tension $\beta\gamma a^2$ vs packing (system A). The dashed line describes values calculated for the isotropic phase. The inset shows the neighborhood of the point $y_C = 0.48174$ with the transition from the isotropic phase to the biaxial nematic phase.

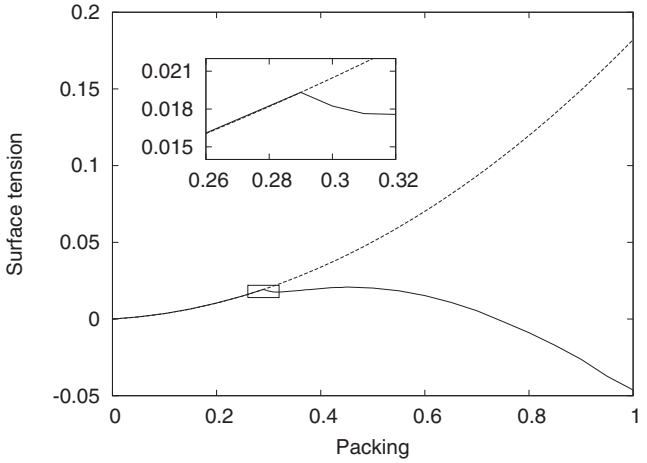

FIG. 7. Surface tension $\beta\gamma a^2$ vs packing (system B). The dashed line describes values calculated for the isotropic phase. The inset shows the neighborhood of the point $y_C = 0.29437$ with the transition from the isotropic phase to the biaxial nematic phase.

the hard ellipsoid fluid. However, it was shown [50] that the HGO model turns out to be inappropriate for elongated molecules (length to breadth ratio above 5). In the case of spheroplatelets we used known expressions for the excluded volume and the $K^{[I]}$ coefficients, but the coefficients $L^{[I][J]}$ were calculated numerically. Inside the formula for the surface tension there are no terms with $K^{[I]}$ that mix $(S^{[2]}, S^{[3]})$ with $(S^{[4]}, S^{[5]})$. Numerical calculations suggest that the same is true for the terms with $L^{[I][J]}$. The biaxial order parameters are separated from the uniaxial ones.

The density and the order parameters profiles for system A, for the biaxial nematic phase in the bulk, are plotted in Fig. 5. The biaxiality is present also in the interfacial region. The surface tension for systems A and B is shown in Figs. 6 and 7, respectively. On increasing density, the surface tension increases, and there is the maximum at the transition (in the bulk) from the isotropic to the biaxial nematic phase.

For high density, the surface tension decreases, but it can be attributed to the fact that the low-density approximation is no longer valid and the order parameters $\langle F^{(j)}_{\mu\nu} \rangle$ with $j > 2$

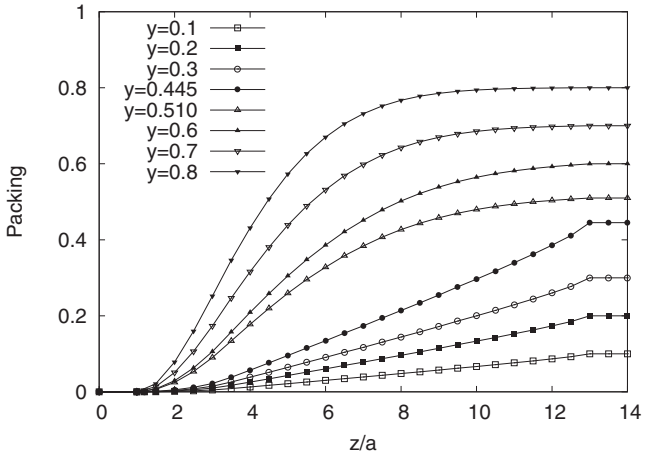

FIG. 8. Comparison of the packing profiles $y(z)$ in the interfacial region for different phase packing in the bulk (system A).

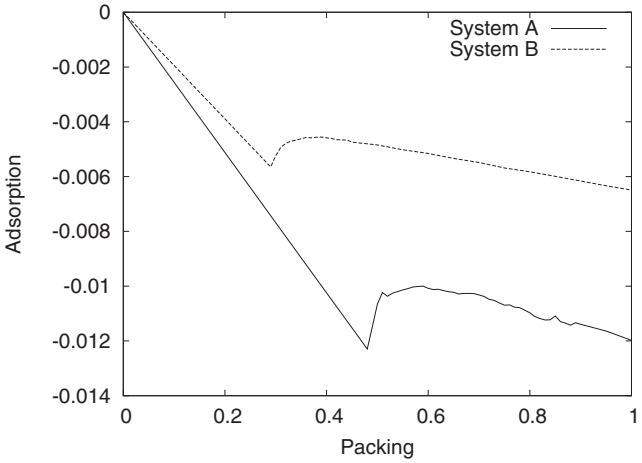

FIG. 9. Adsorption Γa^2 vs packing for systems A and B.

are needed. Note that the closest packing of spheroplatelets in both systems is greater than 0.9. The density profiles in the interfacial region for system A are shown in Fig. 8.

The density dependence of the adsorption is shown in Fig. 9. In the case of the isotropic phase, the adsorption decreases according to a simple linear formula $\Gamma = -\rho_0(a + b/4 + c/4)$. After the transition to the biaxial nematic phase the adsorption first increases and then again decreases. The adsorption is finite, and this suggests lack of the wall wetting [45].

V. SUMMARY

In this paper we presented the statistical theory of hard molecules near a hard wall in the low-density Onsager approximation. A simple local approximation for the one-particle distribution function was applied. The theory was used to study two systems composed of the most biaxial hard spheroplatelets, where the direct transition from the isotropic phase to the biaxial nematic phase occurs in the bulk. The density and the order-parameter profiles near the wall were calculated.

The main result is the description of the phase near a wall at the transition from the isotropic to the biaxial nematic phase. Analytical results for the surface tension and the entropy contributions were presented. The results should not depend on the low-density approximation because they are the same for systems with different molecule elongations. The preferred orientation $(\vec{L}, \vec{M}, \vec{N})$ of the biaxial nematic phase is described by the condition $\vec{L} = \vec{e}_z$, where the short molecule axes tend to be perpendicular to the wall. The uniaxial symmetry along the axis perpendicular to the wall must be broken spontaneously in order to set the vectors $\vec{M}$ and $\vec{N}$. The phase orientation imposed by the wall extends into the bulk via the elastic forces.

For the case of the isotropic phase in the bulk, the phase near the wall is uniaxial because some orientations are excluded by the presence of the wall. The density profile of the phase in the interfacial region changes at the transition. If the phase is biaxial in the bulk, then more molecules can enter the interfacial region. The complete wetting of the wall by a nematic film is not expected because the transition from the isotropic to the biaxial nematic phase is second order and the adsorption remains finite.

In order to confirm our predictions computer simulations of hard spheroplatelets near the wall are needed. It would be interesting to check the density profiles in the interfacial region. The validity of the local approximation for the one-particle distribution function could be also tested. We expect the short range density oscillations close to the wall.

Another interesting problem is the behavior of the system composed of less biaxial molecules where, on increasing the density, the following sequence of transitions is present: the first-order transition from the isotropic phase to the uniaxial nematic phase and, next, the second-order transition to the biaxial nematic phase.

ACKNOWLEDGMENTS

The authors are grateful to J. Spałek for his support. M.A. was supported by the Foundation for Polish Science (FNP) through Grant TEAM.

[1] M. J. Freiser, Phys. Rev. Lett. **24**, 1041 (1970).
[2] R. Berardi, L. Muccioli, S. Orlandi, M. Ricci, and C. Zannoni, J. Phys.: Condens. Matter **20**, 463101 (2008).
[3] C. Tschierske and D. J. Photinos, J. Mater. Chem. **20**, 4263 (2010).
[4] B. Jerome, Rep. Prog. Phys. **54**, 391 (1991).
[5] M. Kleman and O. D. Lavrentovich, *Soft Matter Physics: An Introduction* (Springer-Verlag, New York, 2003).
[6] M. P. Allen, G. T. Evans, D. Frenkel, and B. M. Mulder, Adv. Chem. Phys. **86**, 1 (1993).
[7] M. P. Allen, Liq. Cryst. **8**, 499 (1990).
[8] D. Frenkel and B. M. Mulder, Mol. Phys. **55**, 1171 (1985).
[9] A. Stroobants, H. N. W. Lekkerkerker, and D. Frenkel, Phys. Rev. A **36**, 2929 (1987).
[10] P. J. Camp and M. P. Allen, J. Chem. Phys. **106**, 6681 (1997).
[11] C. Vega, Mol. Phys. **92**, 651 (1997).
[12] A. N. Zakhlevnykh and P. A. Sosnin, Mol. Cryst. Liq. Cryst. **293**, 135 (1997).
[13] C. McBride and E. Lomba, Fluid Phase Equilib. **255**, 37 (2007).
[14] R. Berardi, C. Fava, and C. Zannoni, Chem. Phys. Lett. **236**, 462 (1995).
[15] R. Berardi, C. Fava, and C. Zannoni, Chem. Phys. Lett. **297**, 8 (1998).
[16] R. Berardi and C. Zannoni, J. Chem. Phys. **113**, 5971 (2000).
[17] C. Zannoni, J. Mater. Chem. **11**, 2637 (2001).
[18] R. Berardi, L. Muccioli, and C. Zannoni, J. Chem. Phys. **128**, 024905 (2008).
[19] B. S. John, C. Juhlin, and F. A. Escobedo, J. Chem. Phys. **128**, 044909 (2008).
[20] Y. Martínez-Ratón, S. Varga, and E. Velasco, Phys. Chem. Chem. Phys. **13**, 13247 (2011).
[21] B. M. Mulder, Mol. Phys. **103**, 1411 (2005).
[22] G. S. Singh and B. Kumar, J. Chem. Phys. **105**, 2429 (1996).
[23] G. S. Singh and B. Kumar, Ann. Phys. (NY) **294**, 24 (2001).
[24] B. M. Mulder, Liq. Cryst. **1**, 539 (1986).
[25] B. Mulder, Phys. Rev. A **39**, 360 (1989).
[26] R. Holyst and A. Poniewierski, Mol. Phys. **69**, 193 (1990).
[27] M. P. Taylor, Liq. Cryst. **9**, 141 (1991).
[28] M. P. Taylor and J. Herzfeld, Phys. Rev. A **44**, 3742 (1991).
[29] E. van den Pol, A. V. Petukhov, D. M. E. Thies-Weesie, D. V. Byelov, and G. J. Vroege, Phys. Rev. Lett. **103**, 258301 (2009).
[30] A. G. Vanakaras, M. A. Bates, and D. J. Photinos, Phys. Chem. Chem. Phys. **5**, 3700 (2003).
[31] S. Belli, A. Patti, M. Dijkstra, and R. van Roij, Phys. Rev. Lett. **107**, 148303 (2011).
[32] A. Kapanowski, Mol. Cryst. Liq. Cryst. **540**, 50 (2011).
[33] S. D. Peroukidis and A. G. Vanakaras, Soft Matter **9**, 7419 (2013).
[34] S. D. Peroukidis, A. G. Vanakaras, and D. J. Photinos, Phys. Rev. E **88**, 062508 (2013).
[35] W.-Y. Zhang, Y. Jiang, and J. Z. Y. Chen, Phys. Rev. Lett. **108**, 057801 (2012).
[36] M. M. Telo da Gama, Mol. Phys. **52**, 585 (1984); **52**, 611 (1984).
[37] A. Poniewierski and R. Holyst, Phys. Rev. A **38**, 3721 (1988).
[38] A. Poniewierski, Phys. Rev. E **47**, 3396 (1993).
[39] R. Holyst and A. Poniewierski, Phys. Rev. A **38**, 1527 (1988).
[40] Y. Mao, P. Bladon, H. N. W. Lekkerkerker, and M. E. Cates, Mol. Phys. **92**, 151 (1997).
[41] R. van Roij, M. Dijkstra, and R. Evans, Europhys. Lett. **49**, 350 (2000).
[42] R. van Roij, M. Dijkstra, and R. Evans, J. Chem. Phys. **113**, 7689 (2000).
[43] M. Dijkstra, R. van Roij, and R. Evans, Phys. Rev. E **63**, 051703 (2001).
[44] M. Dijkstra and R. van Roij, J. Phys.: Condens. Matter **17**, S3507 (2005).
[45] H. Reich, M. Dijkstra, R. van Roij, and M. Schmidt, J. Phys. Chem. B **111**, 7825 (2007).
[46] A. Kapanowski, Phys. Rev. E **55**, 7090 (1997).
[47] R. Rosso and E. G. Virga, Phys. Rev. E **74**, 021712 (2006).
[48] W. H. Press, B. P. Flannery, S. A. Teukolsky, and W. T. Vetterling, *Numerical Recipes in C: The Art of Scientific Computing* (Cambridge University Press, Cambridge, 1988).
[49] B. J. Berne and P. Pechukas, J. Chem. Phys. **56**, 4213 (1972).
[50] E. de Miguel and E. M. del Rio, J. Chem. Phys. **115**, 9072 (2001).

Brief summary and conclusions

The central focus of our work in this Thesis was to analyze the applicability of:

- the single-band models (extended t–J model) of strongly correlated electrons to the description of high-temperature superconductors (on example of the cuprates); and
- the two-orbital model (Anderson Lattice Model, ALM) to the description of heavy-fermion systems with application to the UGe_2 compounds.

In the first series of articles [51, 53, 91] we have shown that both the t–J–U and t–J–U–V models reproduce qualitatively the position of antiferromagnetic (AF), superconducting (SC) and paramagnetic (PM) phases observed in experiment. We analyzed the problem of the coexistence of AF and SC phases taking different possible versions of the Gutzwiller renormalization scheme [53,91]. Additionally, we have shown that the charge density wave (CDW) phase is stabilized in the presence of the intersite Coulomb repulsion [91].

The second series of articles [111–113] was devoted to the analysis of the applicability of ALM to the description of magnetic phases of UGe_2. We have presented [111], that the phase sequence observed in the experiment can be explained as an effect of competition between the f–f electron Coulomb interaction energy and the hybridization between the f electrons and the electrons from the conduction band. Additionally, we have have shown [112,113] that the positions of classical and quantum critical points on the phase diagram of UGe_2 obtained within statistically consistent Gutzwiller approximation (SGA) is in semi-quantitative agreement with the experiment.

Our last article [91], where the analysis of the stability of CDW phase was included, provides a number of ideas as to what can be addressed in the near future, namely:

- We have checked, that when the CDW modulation vector is $\mathbf{Q} = (\pi, \pi)$, then with the increasing value of intersite repulsion V, the SC phase disappears before the CDW phase becomes stable. Therefore, there is no SC+CDW coexistence for such choice of $\mathbf{Q}$. We have presented, that the choice of $\mathbf{Q} = (\frac{2}{3}\pi, 0)$, makes the CDW phase stable in wider region of parameters. So far, due to the complexity of calculations, no SC phase was included in this case. We expect that SC phase could still become stable in such a situation, and possibly SC+CDW coexistence may be observed. The calculations seems to be quite tedious, but could be worked out withing a few-month period.
- We have checked, that withing DE-GWF approach the SC order parameter is about 40% larger than that obtained for SGA. However, again due to the complexity of such task, neither AF nor CDW phase was considered in the full DE-GWF calculations. Nevertheless, it is possible to extend our solver to include all (SC, AF and CDW) types of ordering at the same time.